Investigations into the Rab Family of Genes and Their Roles in Signalling during Vertebrate Early Development

Emma Jane Kenyon

September 2006

Thesis submitted to the University of London for the degree of Doctor of Philosophy

National Institute for Medical Research,
Wellcome Trust Sanger Institute
And University College London

ProQuest LLC
789 East Eisenhower Parkway
P.O. Box 1346
Ann Arbor, MI 48106-1346

Abstract

The mammalian Rab family consists of between 60-70 members, making it the largest sub family of the Ras superfamily. Rabs are responsible for vesicle trafficking within cells, acting as molecular switches cycling between the GDP inactive and GTP bound active forms. Far from being just cellular housekeeping genes, these genes have been shown to have specific functions which, when disrupted, can lead to clinical disorders and interesting developmental defects.

This thesis therefore seeks to investigate this interesting family of genes and their roles in zebrafish development. Using antisense morpholino oligonuleotides in a loss of function screen, this thesis identifies the function of 13 zebrafish *rabs.* Three of these, *rab1a3, rab3c1* and *rab28* have specific and interesting phenotypes, with pigmentation defects seen in *rab1a3* and *rab3c1* and behavioural defects seen in *rab28.* In particular, the pigmentation defect in *rab3c1* resulted in the discovery that the embryos were blind.

This thesis also shows an essential role for *rab5a2* in zebrafish development and Nodal signalling. Disruption of this *rab* causes a dramatic early phenotype, with 100% mortality in embryos prior to 24 hours post fertilization. *rab5a2* morpholino injected embryos show no visable organizer and have reduced nodal target gene expression. Overexpression of *rab5a2* shows embryos with additional expression of Nodal target genes *no tail* and *goosecoid* in the animal pole of the embryos but not the dorsal marker *chd.* Microarray analysis of *rab5a2* morpholino injected embryos showed reduction and upregulation of expression of many genes involved in dorsal ventral patterning. This suggests a complex role for *rab5a2* in patterning the early embryo, as both dorsalizing and ventralizing genes such as *chd, bmp4* and *wnt8* were down regulated while, ventralizing genes such as *bmp2b* were upregulated.

Contents

Abbreviations

ADMP - anti-dorsalizing morphogenic protein

AP – anterior posterior

Bmp – Bone Morphogenic Protein

Bmpr - Bone Morphogenic Protein Receptor

Boz - Bozozok

COP 1 - Coatomer complex

Cyc – Cyclops

Dkk - Dickkopf

Dpp - decapentaplegic

DV – Dorsal-Ventral

ER – Endoplasmic Reticulum

EVL – Enveloping Layer

Fgf – Fibroblast Growth Factor

FYVE – named after four proteins Fab1, YOTB/ZK632.12, Vac1, and EEA1

GTPase – guanosine triphosphate hydrolyze enzyme

Hh – Hedgehog

Hpf – hours post fertilization

HSPG - heparin sulphate proteoglycans

MBT- Mid Blastula Transition

MO - Morpholino

NSF - *N*-ethylmaleimide Sensitive Fusion protein

Oep – One eyed pinhead

ORF – Open Reading Frame

PtdIns(3)P - phosphatidylinositol-3-phosphate

SFRP - secreted frizzled-related protein

SNARE - Soluble NSF Attachment Protein REceptor

Sqt - Squint

TAE - Tris, acetate, EDTA

TE - Tris EDTA

TGF - Transforming growth factor

VAMP - Vesicle –Associated Membrane Protein

Wg - Wingless

Wnt – combined from the *Drosophila* gene *wingless* and the mouse gene *int*

YSL – Yolk Syncytial Layer

ZMD – Zygotic Maternal Dominant

Glossary

Glypicans - the main cell-surface heparin sulphate proteoglycans,

Mid Blastula Transition – The stage where cell cycles lengthen and become asynchronous this begins at the 512-cell stage

Non- cell-autonomous - genotypically mutant cells cause other cells (regardless of their genotype) to exhibit a mutant phenotype

Prenylation - addition of hydrophobic molecules to facilitate protein attachment to the cell membrane.

Zygotic Maternal Dominant – effect that is expressed when both zygotic and maternal genomes are heterozygous for the mutant locus.

Homophilic cell adhesion - The attachment of an adhesion molecule in one cell to an identical molecule in an adjacent cell

List of Figures

List of Tables

Acknowledgements

Firstly I would like to thank the four people without whom this thesis would not have been possible. I would like to thank Derek for taking me on as his PhD student for reading my thesis and for never having a cross word to say. Secondly I would like to thank Matthew Clark and Huw Williams who have helped me with and through my experimental work and who volunteered (ok Matt you were volunteered) to read drafts of my thesis and because of whom Thursday night has returned to being chip and pub night. Lastly I would like to thank James Bull for being well James Bull, for feeding me, washing my clothes and for undertaking the rather ominous task of trying to spell check my thesis after Word had a nervous breakdown trying to cope with my spelling errors.

In addition to these people I would like to thank Isabel Campos for getting me started on this project and her invaluable help when I arrived, the rest of the lab and for discussions, cake, help and general gossiping and Mark Bushel for offering to read my thesis and random diving discussions.

Lastly I would like to thank the fish without whom quite literally this project and many others like it would not be possible.

Thank you

Chapter 1

Introduction

1.1 Zebrafish Development

Zebrafish (*Danio rerio*) are small, fresh water fish, which as adults are approximately two centimetres in length. They produce small, transparent eggs, which are fertilized shortly after laying. Once fertilized, the zebrafish embryos develop rapidly with the embryo, being recognisable as a fish by 24 hours post fertilization (hpf). By 48 hpf, the juvenile pigment has become apparent and they have started to hatch from their protective membrane, known as the chorion. Following three days of development the swim bladder has developed and after five days the eyes have become fully functional and the young are capable of independent feeding. Sexual maturity is reached between three and six months (Westerfield 2000).

1.1.1 From Fertilization to Gastrulation: An overview of morphological characteristics

Shortly after fertilization, yolk platelets separate from cytoplasm, which collects around the point of sperm entry at the animal pole (Kimmel et al., 1995). This animal pole cytoplasm cleaves approximately every 20 minutes to form a clump of cells, the blastoderm, situated on top of the large yolk cell (Kimmel et al., 1995). When the blastoderm reaches 512 cells the cell cycles lengthen and become asynchronous, and *de novo* transcription of the zygotic genome begins in a process called the mid-blastula transition (MBT) (Kane and Kimmel, 1993). At approximately four hpf the blastoderm cells move over the yolk cell and cover it, in a process called epiboly. When the cells have migrated to cover half the yolk - 50% epiboly – other gastrulation movements begin. Blastoderm cells internalise to form two cell layers; the outer epiblast and inner hypoblast (Kimmel et al., 1989). Concomitantly, a thickened marginal region, termed the germ ring, appears at the margin between the blastoderm and the yolk cell. This is followed by a local accumulation of cells in a structure called the embryonic shield which corresponds to the Spemann's organizer identified in amphibian development (Schier and Talbot, 2001; Spemann and Mangold, 1924). The appearance of the shield is the earliest visual marker of the

dorsal ventral axis in the embryo (Figure 1.1.1). During germ ring formation, epiboly temporarily arrests, but after shield formation, epiboly continues and the margin of the blastoderm eventually advances around the yolk cell to cover it completely (Houart et al., 1998; Kimmel et al., 1989)

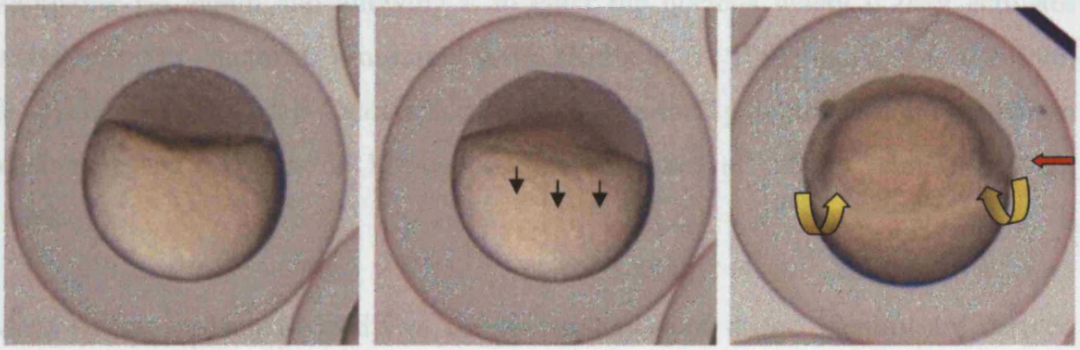

Figure 1.1.1: Figure showing movement of blastoderm cells during early zebrafish development.

Black arrows indicate the movement of cells during epiboly. Yellow arrows indicate the movement of cells during involution. Red arrow identifies the dorsal organizer (shield)

1.1.2 Dorsal Establishment.

Our understanding of the establishment of the dorsal axis remains incomplete. It has been shown however, that the yolk is an important early source of dorsal-ventral (DV) patterning signals (Piccolo et al., 1999). Dorsal identity in the embryo is established by a dorsal determinant, or determinants, that are initially located at the vegetal pole and translocated along microtubules to the future dorsal side before the first cleavage division occurs (Aanstad and Whitaker, 1999; Jesuthasan and Stahle, 1997). Experimental evidence for the presence of maternally inherited dorsal determinants has been shown by removal of the vegetal most part of the yolk shortly after fertilisation, which resulted in strongly ventralized embryos (Mizuno et al., 1996). This result suggests that the vegetal part of the yolk contains a dorsalizing factor, which is transferred to the future dorsal side early in development (Piccolo et al., 1999). Prior to shield formation β-Catenin, is seen to translocate to dorsal nuclei. It is thought that an unknown dorsalizing factor may bring about the stabilisation and nuclear translocation of β-Catenin and the activation of many dorsally associated

genes (Kelly et al., 2000; Kelly et al., 1995; Schneider et al., 1996). Cytoplasmic β-Catenin is targeted for degradation by a complex containing APC, axin, Glycogen synthase kinase-β (GSKβ) and other components which allow only low levels of β-Catenin to accumulate (Hinck et al., 1994; Papkoff et al., 1996). Activation of the canonical Wnt signalling pathway inhibits the β-Catenin degradation complex, stabilizing β-Catenin and allowing it to enter the nucleus where it then activates transcription of canonical Wnt target genes (Kelly et al., 1995; Papkoff et al., 1996; Schneider et al., 1996). β-Catenin accumulates specifically in nuclei of dorsal margin blastomeres as early as the 128-cell stage (Dougan et al., 2003; Schneider et al., 1996).

Many of the molecular details of the establishment of dorsal identity are derived from experiments done with the amphibian *Xenopus laevis*. Many of these results have been replicated in zebrafish embryos. In zebrafish when β-catenin is activated outside the dorsal region, a second dorsal axis is induced (Kelly et al., 1995) and, in *Xenopus laevis* if maternal *β-catenin* mRNA is inhibited using antisense oligonucleotides, then dorsal cell fates are inhibited (Tao et al., 2005). In zebrafish, the maternal effect loci *ichabod* and *tokkaebi* disrupt the nuclear localization of β-Catenin and lead to ventralized embryos (Kelly et al., 2000; Nojima et al., 2004). Indeed *ichabod* has been recently shown to encode *β-catenin-2* (Bellipanni et al., 2006). In *Xenopus laevis* one target of β-Catenin activation, is the transcription factor *siamois* (Wylie et al., 1996). In zebrafish, *dharma,* the gene mutated in *bozozok (boz)* mutants, is also a member of the hox family, as is *siamois* and although probably not performing exactly the same function *dharma* may also encode an important mediator of β-Catenin function (Nelson and Gumbiner, 1998). Mutant *boz* embryos often have no notochord or prechordal mesoderm and exhibit cyclopia and deficiencies in ventral regions of the CNS. Earlier in development, the shield does not form and the expression of several organizer genes is strongly reduced or eliminated at late blastula. The Dharma protein is thought to act downstream of β-catenin since injection of *β-catenin* into *boz* mutants does not rescue the mutant. Mutants develop some dorsal tissue, suggesting that Dharma is only essential for a portion of organizer functions (Kodjabachian et al., 1999). Both *siamois,* in frog, and *dharma,* in fish, have been shown to induce the formation of an ectopic body axis when overexpressed (Fekany et al., 1999; Nelson and Gumbiner, 1998).

In *Xenopus laevis*, β-Catenin has been shown to act on Vg1 (a transforming growth factor-β (TGF-β)) and VegT (a T-box transcription factor) (Nielsen et al., 2000; Tao et al., 2005; Zhang et al., 1998). Both Vg1 and VegT are localised to the vegetal pole. Vg1 is synthesized as an inactive precursor protein from maternally supplied mRNA and activated dorsally during cortical rotation (Melton, 1987; Yisraeli and Melton, 1988; Zhang and King, 1996). Absence of Vg1 leads to an absence of mesoderm (Melton, 1987; Zhang et al., 1998). VegT, on the other hand, can regulate generation of endoderm, in both a cell-autonomous manner and by inducing expression of the TGF-β family of secreted cytokines. In addition, the induction of TGF-βs means that VegT is also upstream of the induction of mesoderm (Clements et al., 1999). When maternal *vegT* mRNA is depleted in early embryos it results in the loss of the vegetal mesoderm-inducing signals and the loss of endodermal markers. Therefore, maternal *vegT* is essential for mesoderm and endoderm development (Clements and Woodland, 2003). The lack of mesoderm and endoderm, caused by Vg1 and VegT inhibition, can be rescued by injection of RNA encoding nodal proteins which are members of the TGF-β family which act downstream of β-Catenin, Vg1 and VegT (Melton, 1987; Zhang et al., 1998; Zhang and King, 1996). In zebrafish, the factors with functional homology to Vg1 and VegT are unknown as loss of function studies of the closest known orthologues do not produce similar phenotypes.

At MBT in zebrafish, the embryo switches from control by the inherited maternal products to control by the zygotic genome (Kane and Kimmel, 1993). Soon after this, other zygotic genes are activated by β-Catenin. Amongst these genes are *chordin*, *dickkopf1 (dkk1)*, *squint (sqt)* and *fibroblast growth factors* (*fgf*s). These genes act to inhibit the action of ventralizing factors or, in the case of *sqt*, to induce mesendodermal fates around the margin (Tao et al., 2005). The establishment of correct DV patterning is a balancing act between these dorsal associated genes antagonising ventral genes such as *wnt8* and *bone morphogenetic proteins (bmp)* (This is discussed in more detail in section 1.1.3.3).

Recent research has suggested that DV asymmetry in zebrafish can be identified experimentally as early as the two cell stage (Gore et al., 2005). Map kinase p38

antibody staining localises to the region of the embryo that will eventually become the dorsal side (Fujii et al., 2000). P38 has been shown not to specify dorsal fates since expression of dorsal genes still occurs in embryos expressing a dominant negative version of the gene (Fujii et al., 2000) It is thought, however, that p38 controls the rate of cell division in the dorsal blastomeres since, when dominant negative versions are overexpressed, there are larger, fewer blastomeres on the dorsal side (Fujii et al., 2000). Disruption of microtubules, which are thought to participate in the specification of dorsal, results in no activation of p38, suggesting that p38 may be regulated by the same factors that establish DV asymmetry (Fujii et al., 2000). Direct evidence for early asymmetry is provided in recent work that demonstrated that maternal transcripts of *sqt* are localized to two blastomeres of the four cell embryo (Gore et al., 2005). Removal of cells containing these transcripts from four-to-eight-cell embryos, or oocyte injection of antisense MO oligonucleotides (MOs) targeted to *sqt*, cause a loss of dorsal structures (Gore et al., 2005).

1.1.3 Dorsoventral Patterning and the Organizer.

Formation of the zebrafish embryonic shield is the first morphological indication of the DV axis although it is clear that the DV axis has been established prior to shield formation. The shield consists of two layers of cells - the epiblast and the hypoblast - and is covered by a tight epithelium the enveloping layer (EVL). Despite members of the *TGF-β* and *wnt* families having been implicated in the formation of the organizer (Feldman et al., 1998; Smith and Harland, 1991), no endogenous signalling molecule has been identified that results in the direct formation of the organizer. The function of the organizer during gastrulation is to inhibit ventral signals, differentiate axial structures and facilitate morphogenesis. Many of these organizer functions are mediated through the secretion of signalling factors (Feldman et al., 1998; Knecht et al., 1995). Amongst the first of the signalling factors to be secreted are members of the FGF, Wnt and TGF-β families (Feldman et al., 1998). The organizer is known to induce dorsal fates within mesoderm, anterior fates within endoderm and neural fates within ectoderm, achieved through opposing morphogenic activities, emanating from the ventrolateral regions of the embryo (Kodjabachian et al., 1999).

1.1.3.1 TGF-β signals.

TGF-β was identified in 1978 by de Larco *et al* due to its ability to induce phenotypic transformation of fibroblasts into diverse mouse cell types (de Larco and Todaro, 1978). Subsequently, many more TGF-β-related factors were identified resulting in a large family of TGF-βs, present in all metazoa. In humans, the TGF-β family contains at least 35 family members, including BMPs and Nodals (Derynck and Miyazono, 2006) which are also found in zebrafish. This section is concerned with the BMPs and their role in DV patterning, with the Nodals covered in greater detail in section 1.3.

The BMP family of growth factors were named for their ability to induce the formation of bone and cartilage. The BMPs induce ventral fates within the embryo and they accomplish this by binding to the extracellular domains of type I and type II BMP receptors (BMPRs) (Koenig et al., 1994; ten Dijke et al., 1994). These are transmembrane proteins, which contain intracellular serine/threonine kinase domains (Lin et al., 1992). Signal transduction through BMPRs results in mobilization of members of the Smad family of proteins, especially Smad1, Smad5 and Smad8 (Hild et al., 1999; Nakayama et al., 1998; Xu et al., 1998). These Smads are transcription factors, that are phosphorylated by ligand bound receptors, allowing them to translocate to the nucleus and, together with the non-receptor-regulated Smad protein Smad4, regulate target gene expression (Zhang et al., 1997). Secreted antagonists of this pathway include Chordin, Noggin and Follistatin, while the transmembrane protein Bambi functions as a decoy receptor (Fainsod et al., 1997; Onichtchouk et al., 1999). In addition to this, there are inhibitory Smads, Smad6/7, which are thought to interfere with Smad1/5/8 phosphorylation (Heldin et al., 1997; Nakao et al., 1997). The inhibitory Smads also recruit ubiquitin ligases, known as Smad ubiquitination regulatory factor 1 (Smurf1) and Smurf2, to the activated type I receptor, resulting in receptor ubiquitination and degradation, and termination of signalling (Ebisawa et al., 2001; Zhang et al., 2001)

In zebrafish, a number of BMP pathway components are essential for the formation of ventral cell types, including BMP2b and BMP7. These are widely expressed soon after MBT but become restricted to the ventral half of the embryo by the onset of

gastrulation (Dick et al., 2000; Schier and Talbot, 2005). Both of these genes have zebrafish mutants, (the *bmp2b* mutant *swirl* and the *bmp7* mutant *snailhouse*) that are strongly dorsalized. It is thought that the ventralizing signal *in vivo* is a BMP2b-BMP7 heterodimer (Schmid et al., 2000). Previous studies in *Drosophila, Xenopus laevis* and zebrafish have shown that BMP signalling is required for global DV patterning decisions during early gastrulation (Gelbart, 1989; Graff et al., 1994; Pyati et al., 2005). In DV patterning, the effect of the BMP pathway in zebrafish is a balancing act between many factors. The major modifiers in this pathway include Alk8, a type I BMP receptor required for the specification of ventral cell fates (Bauer et al., 2001; Connors et al., 1999; Mintzer et al., 2001), Smad5 (Hild et al., 1999), Chordin, Ogon/Sizzled and the protease Tolloid (Connors et al., 1999). *chordin* mutants have a ventralized phenotype (Schulte-Merker et al., 1997) whereas *bmp2b;chordin* double mutants are dorsalized, suggesting that *chordin* is not needed for dorsal development if BMPs are inactivated (Hammerschmidt et al., 1996b; Miller-Bertoglio et al., 1999; Piccolo et al., 1996). The sizzled gene is mutated in *ogon* mutants (Martyn and Schulte-Merker, 2003; Yabe et al., 2003) which have a ventralized phenotype similar to *chordin* mutants. This phenotype can be suppressed by overexpression of Chordin (Miller-Bertoglio et al., 1999; Wagner and Mullins, 2002). Tolloid promotes BMP signalling by cleaving and inactivating Chordin (Blader et al., 1997). The antidorsalizing morphogenic protein (ADMP) is a divergent member of the BMP family expressed on the dorsal side of the late blastula as well as in the axial mesoderm and anterior neuroectoderm during gastrulation (Lele et al., 2001; Lin et al., 1997). Overexpression of ADMP causes ventralization and a reduction of the organizer. Embryos injected with MOs (MO injected embryos) knocking down ADMP show moderate expansion of dorsal mesoderm. ADMP may be part of a negative feedback system which limits the size of the organizer region, possibly with the aid of *bmp2b* and *bmp7* (Lele et al., 2001; Willot et al., 2002).

1.1.3.2 Wnt Signalling

The Wnt pathway is essential for ventral and posterior fates within the embryo. Early in zebrafish development, maternal signalling divides nascent mesoderm into axial (dorsal) and non-axial (ventral) domains. Subsequently, subdivision of non-axial mesoderm into multiple DV fate domains involves zygotic Wnt8 and BMP signalling

as well as the Vent/Vox/Ved family of transcriptional repressors (Erter et al., 2001). Deletion or inhibition of both ORFs of the bicistronic (two non-overlapping open reading frames of *wnt8* produces a loss of ventroposterior structures and expansion of dorsal fates (Lekven et al., 2001). A reduction of Wnt3a and Wnt8 activity results in stronger expansion of dorsoanterior fates, suggesting that these genes have overlapping functions (Shimizu et al., 2005a); (Ramel et al., 2005).

The Wnt family of proteins signal through Frizzled-Lrp receptor complexes and employ a number of cytoplasmic proteins to stabilize β-Catenin (Cong et al., 2004; Sheldahl et al., 1999; Yang-Snyder et al., 1996) . These proteins enable β-Catenin to accumulate in the nucleus and activate target gene expression. Secreted antagonists of this pathway include secreted frizzled-related protein (SFRP), Cerberus and Wnt inhibitory factor (WIF), which act by binding to Wnt proteins. The Wnt antagonist, Dkk, acts by binding the LRP subunit of the receptor (Bafico et al., 2001; Brott and Sokol, 2002; Li et al., 2002) counteracting the ventralizing and posteriorizing effects of Wnt signalling (Hashimoto et al., 2000). *ddk* is an early target of maternal β-Catenin and is expressed early in the dorsal margin and dorsal yolk syncytial layer (YSL – see section 1.1.4.1) as well as later during gastrulation in the developing prechordal plate (Gonzalez-Sancho et al., 2005).

Genes that may be modified by Wnt signalling include *vox*, *vent* and *ved*. Inactivation of the redundant homeodomain transcriptional repressors Vox (also known as Vega1) and Vent (Vega2) leads to severe loss of ventroposterior structures (Kawahara et al., 2000a; Kawahara et al., 2000b). This loss of function phenotype in zebrafish is strain dependent, AB strain fish lacking *vox/vent* are essentially wild type (Imai et al., 2001) whereas inactivation of a third gene encoding a homeodomain transcriptional repressor *ved* strongly dorsalizes all strains of embryos, including the AB strain (Shimizu et al., 2002). This dorsalized phenotype is similar to that seen in zebrafish *wnt8* mutants and there is evidence that *wnt8* activates *vox* and *vent* expression repressing dorsal genes (Ramel et al., 2005). *chordin* is a key target of Vox and Vent and these proteins also repress other dorsal genes including *boz*, *goosecoid*, *floating head* and *dkk1* (Imai et al., 2001; Melby et al., 2000).

1.1.3.3 FGF signalling

The FGF family has been implicated in mesoderm formation, neural induction, DV patterning, and anterior-posterior (AP) patterning of the embryo (Furthauer et al., 2004; Kimelman and Kirschner, 1987; Lamb and Harland, 1995). In early zebrafish development, as soon as the zygotic genes become activcated, FGF has a role in restricting *bmp* RNAs to the ventral side of the embryo (Furthauer et al., 2004). The FGF signal is initiated on the dorsal side of the embryo by the expression of *fgf3*, *fgf8* (a mutation in which is responsible for the zebrafish mutant *acerebellar* (Reifers et al., 1998) and *fgf24,* and this expression then spreads progressively to lateral and ventral domains. The restriction of BMP signalling shows an important role for FGFs in DV patterning. The FGF pathway is first active at the dorsal blastoderm margin, along the entire margin and, finally, in the tail bud (Furthauer et al., 2004; Ulrich et al., 2003). FGFs bind and activate receptor tyrosine kinases, the dimerization of the receptor results in *trans*-phosphorylation, as well as the recruitment and activation of downstream effectors (Bellot et al., 1991; Kornbluth et al., 1988). Downstream targets of FGF include *pea3*, *erm*, and *sprouty4* which are induced over broad domains in neighbouring cells (Furthauer et al., 2004; Ulrich et al., 2003). These genes are activated at different thresholds of FGF. In zebrafish wild type embryos, it has been shown that *erm* is activated furthest from the source of FGF, followed by *pea3* and, finally, *sprouty4* is activated closest to the source (Scholpp and Brand, 2004).

In zebrafish, FGF signals may effect mesoderm formation via interactions with the Nodal signalling pathway (Furthauer et al., 2004), possibly relaying the action of TGF-β ligands over long distances. FGF is required downstream of Nodal signalling to induce the co-receptor One-Eyed Pinhead (Oep) in cells distant from the source of Nodal (Griffin and Kimelman, 2003; Mathieu et al., 2004). This mechanism contributes to the amplification and propagation of Nodal signals (Mathieu et al., 2004). Partial inhibition of FGF signalling, and blocking of Oep, disrupts posterior development and leads to the death of dorsal mesoderm cells by the end of gastrulation (Griffin and Kimelman, 2003; Mathieu et al., 2004). The FGF and BMP pathways have also recently been shown to have a repressive effect on endodermal precursors induced by Nodal signalling (Poulain et al., 2006).

1.1.3.4 Convergence Extension movements

The term convergent extension is used in the context of the developing zebrafish embryo to describe the movements that lead to the accumulation of cells at the dorsal side of the embryo followed by the anterior-posterior (AP) extension of the body axis (Warga and Kimmel, 1990) (Figure 1.1.2). Convergence and extension allows the thinning and spreading of the germ layers during epiboly. When Nodal signalling is lost both mesoderm formation and extension of the embryonic axis are inhibited. This loss does not, however, prevent the dorsal accumulation of cells suggesting that convergence and extension are not mutually exclusive (Feldman et al., 1998). It is thought that during convergence and extension, the cells move as a cohesive group as molecules that mediate cell polarity, sorting and adhesion have also been shown to be required for convergence and extension movements (Heisenberg et al., 2000; Ulrich et al., 2003; Wallingford et al., 2000). A mutation in zebrafish Wnt11 (*slb*) - which has been shown to control cell cohesion through E-cadherin - results in embryos with compromised convergence and extension movements during gastrulation (Heisenberg et al., 2000; Ulrich et al., 2005).

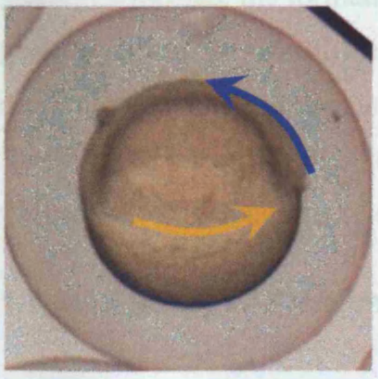

Figure 1.1.2: Photo of an embryo undergoing convergence and extession movements.

Yellow arrow indicates convergence movements as cells move towards the dorsal side of the embryo. Blue arrow indicates extension movements as cells extend along the AP axis.

1.1.4 The Yolk Cell

1.1.4.1 The Yolk Syncytial Layer (YSL) and its role in patterning

The YSL is an extra embryonic region, produced in zebrafish at the midblastula stage, when deep marginal blastoderm cells collapse and release their nuclei into the underlying yolk cell (Kimmel and Law, 1985). The YSL is a source of mesoderm and endoderm inducers (Chen and Kimelman, 2000; Hsu et al., 2006; Mizuno et al., 1996). Transplantation experiments have shown that when the YSL is transplanted into the animal-pole region of the host after MBT, the yolk cell and the YSL can induce mesoderm and organizer gene expression in the blastoderm (Mizuno et al., 1996). The YSL has been compared to the Nieuwkoop centre in *Xenopus*, a group of cells located in the dorsal-vegetal region of the blastula that are thought to induce the Spemann organizer in the overlying marginal zone in a non-cell-autonomous manner (Bischof and Driever, 2004; Gimlich and Gerhart, 1984). An important early step in the formation of the Nieuwkoop centre in *Xenopus* is the nuclear localization of β-Catenin in an area that will become dorsal (Guger and Gumbiner, 1995). In zebrafish, β-Catenin accumulates in the nuclei of dorsal blastomeres and the dorsal YSL, where, with the Tcf/Lef family proteins, it activates the expression of zygotic genes that mediate the formation of dorsal structures. One of the first of these zygotic genes activated in zebrafish is *boz,* which is expressed shortly before MBT within dorsal blastomeres and then at late blastula/early gastrula in the dorsal YSL (Solnica-Krezel and Driever, 2001). It has been suggested that *boz* is a direct target of β-Catenin-Tcf/Lef signalling (Geng et al., 2003; Leung et al., 2003).

1.1.4.2 Epiboly and the importance of the yolk cell

At the start of epiboly, the cells of the blastoderm sit on top of the yolk cell. The yolk itself is surrounded by a thin anuclear yolk cytoplasmic layer. Between the blastoderm and the yolk are the YSL and the blastoderm rim. The YSL is divided into two sections both of which contain yolk syncytial nuclei. These are the external YSL, a relatively thick belt of cytoplasm, and the internal YSL, a thinner layer (Betchaku and Trinkaus, 1986; Kimmel and Law, 1985). In the killifish, *Fundulus*

heteroclitus, the mechanism of epiboly has been more extensively researched (Trinkaus, 1963) but a similar process has been observed in zebrafish (Warga and Kimmel, 1990). Early work in *Fundulus* showed that epiboly begins with the contraction of the external YSL an autonomous process which can occur in the absence of the blastoderm. As epiboly progresses, the EVL, which tightly covers the blastoderm ensuring the correct physiological environment for the developing cells, moves down the yolk (Keller and Trinkaus, 1987). The underlying blastoderm cells link tightly with the YSL at the margin and are driven down the yolk by the YSL's epiboly movements, which are, in turn, driven by an intercrossing network of microtubules (Trinkaus, 1984). In zebrafish changes in configuration of the yolk microtubules are strictly correlated with epibolic movements, with disruption of microtubules blocking the vegetal movement of the YSL but only partially disrupting the epiboly of the EVL and deep cells (Solnica-Krezel and Driever, 1994). Recent evidence in zebrafish has shown that pregnenolone, a steroid in the yolk cell, is required to maintain an adequate level of polymerized microtubules and so normal epiboly (Hsu et al., 2006).

In addition to the movements of microtubules in the yolk, epiboly is driven by endocytosis (Betchaku and Trinkaus, 1986; Solnica-Krezel and Driever, 1994). In the external YSL, immediately beneath the EVL attachment region, endocytosis removes sections of the external YSL membrane reducing it and pulling the EVL vegetaly. The external YSL membrane is then fused with the internal YSL membrane to expand the internal YSL and drive further epibolic movement (Betchaku and Trinkaus, 1986). At approximately 50% epiboly an actin band forms in the external YSL, beneath the EVL margin - the region of active endocytosis (Cheng et al., 2004). This actin band is vital for epiboly, as shown by experiments in zebrafish inhibiting the formation of the actin cytoskeleton which result in a slowing of, and failure to complete, epiboly (Cheng et al., 2004; Zalik et al., 1999). *betty boop* the zebrafish homologue of MAPKAPK2 (a regulator of actin filament formation) displays premature constriction of the margin and is thought to regulate epiboly (Holloway, unpublished data, 2006; Wagner et al., 2004).

A further important factor in epiboly is the requirement for the intracellular adhesion molecule E-cadherin. Whilst a reduction in E-cadherin in zebrafish impairs epiboly, a

stronger loss-of-function interferes with early cells divisions and halts development completely (Babb and Marrs, 2004). Interestingly, the first zebrafish epiboly mutant identified, *half baked (hab)* (Kane et al., 1996), has a defect in the *E-cadherin* (*cdh1*) gene. In the *hab* mutant, the deep cells cease movement at mid-gastrulation, whilst epiboly of EVL and YSL proceeds further (Kane et al., 2005; Shimizu et al., 2005b).

1.1.5 Morphogen Gradients in the Developing Embryo

A morphogen can initially be described as a substance which governs the pattern of tissue development in an organism, where different concentrations of morphgen can induce different cell fates. In the early 20th century, biological morphogen gradients were first suggested by Child and Boveri from their work in *Hydra* and nematode respectively (Child, 1915; Child, 1941; Gilbert, 1997; Slack, 1994; Tsikolia, 2006), with the discovery of their importance in developmental biology being accredited to the work done in *Drosophila* by geneticist Thomas Hunt Morgan (Lawrence, 2004; Lawrence, 2001; Oppenheimer, 1983; Yucel and Small, 2006). These ideas were later refined in the 1960's by Lewis Wolpert with his 'French flag' model that described how morphogens could subdivide a tissue into discrete domains of different target gene expression (Figure 1.1.3) (Wolpert, 1996). Wolport's work in chick limb development demonstrated that grafting the region with morphogenic properties to successive positions along the antero-posterior axis could modify the positional information along the axis and so modify the pattern of digits obtained. He concluded that the interpretation of positional information can provide the basis for pattern formation in limb morphogenesis and that this pattern was consistent with a model based on diffusion of a labile morphogen (Tickle et al., 1975), similar to that proposed for the development of pattern in invertebrates (Wolpert, 1996).

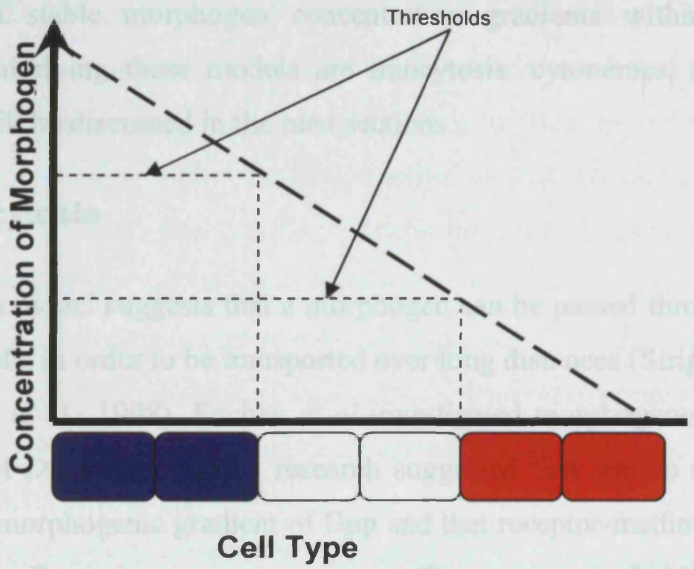

Figure 1.1.3: Diagram of Wolperts "French flag" model
Showing how morphogens could subdivide a tissue into discrete domains of different target gene expression (reproduced from (Wolpert, 1996).

In developmental biology, following the work of researchers such as Wolpert, morphogens can be described as signalling molecules which form spatial extracellular concentration gradients emanating from a restricted source of production. Cells receive a different concentration of morphogen depending on their distance from the source and this elicits a concentration-specific response. A more solid understanding of morphogens was obtained when Gurdon and collaborators used the animal cap assay in *Xenopus laevis* (Gurdon et al., 1985). This exogenous model system showed that the selection of genes expressed by animal cap cells is determined by the distance from a source of Activin - a peptide growth factor of the TGF-β family contained in vegetal cells and capable of inducing other cells to form mesoderm. Activin's long-range signal spreads over at least ten cell diameters in a few hours and does so by passive diffusion by-passing cells that do not respond to the signal or synthesize protein themselves. These results provided support for the operation of morphogen concentration gradients in vertebrate development as well as for a diffusion based model of these concentration gradients (Gurdon et al., 1994).

Following the general acceptance of morphogen gradients as a potential mechanism for patterning naïve tissue, four models have been proposed for the establishment and

maintenance of stable morphogen concentration gradients within tissues. The mechanisms underlying these models are trancytosis, cytonemes, argosomes and diffusion and will be discussed in the next sections.

1.1.5.1 Transcytosis

The transcytosis model suggests that a morphogen can be passed through a series of neighbouring cells in order to be transported over long distances (Strigini and Cohen, 1997; Bellaiche et al., 1998). Enchev *et al* investigated morphogenesis in the wing imaginal disk of *Drosophila.* Their research suggested that simple diffusion could not explain the morphogenic gradient of Dpp and that receptor-mediated endocytosis was essential for Dpp's long range movement (Entchev et al., 2000). Enchev *et al* proposed that Dpp was transported by transcytosis and suggested a role for Rabs, small GTPases of the Ras superfamily (Entchev et al., 2000). The transcytosis model will be expanded on in section 1.2 where the Rab family will be looked at in greater detail alongside the roles of Rabs in this method of morphogen movement.

1.1.5.2 Cytonemes

Cytonemes ('cell threads' neme = thread) is a term coined by Ramı´rez-Weber *et al* who discovered very thin projections from fluorescently labelled cells in the *Drosophila* imaginal disc emanating from the lateral flank towards the disc centre. These projections were shown to represent cytoplasmic extensions and were designated cytonemes. The cytonemes extend from disc cells toward the AP compartment border, but not from AP border cells outward. Ramı´rez-Weber *et al* (Ramirez-Weber and Kornberg, 1999) hypothesized that the cytoplasmic extensions grow in response to a chemoattractant. Different parts of the imaginal disc were placed next to anterior or posterior fragments to ascertain which parts of the disc could act as an attractant. The results showed that the anterior or posterior fragments only grew projections if placed next to the excised boundary region from between the anterior and posterior. Branchless – the drosophila homologue of FGF (dFGF) - was identified as a chemoattractant for these projections suggesting that activated FGF protein could be produced at the compartment border or that dFGF could function as a growth factor and stimulate non-polarized cell growth of cytonemes. Ramı´rez-

Weber *et al* (Ramirez-Weber and Kornberg, 1999) also showed that projections similar to cytonemes could be seen in cultures from mouse limb bud as well as those from chick. The authors suggested that cytonemes might play a role in disc cells defining their relationship with signalling centres so that cytonemes link outlying cells directly to signalling cells. This mechanism has been suggested as an efficient long distance transport for morphogens such as Hh and Dpp whose movement is said to be inconsistent with simple diffusion in the imaginal disc. The hypothesis is that Hh and Dpp are released at sites of cytoneme contact delivering the morphogens efficiently to target cells and limiting their spread (Ramirez-Weber and Kornberg, 1999) (Figure 1.1.4). Recently Hsiung *et al* has shown evidence for cytonemes involvment in Dpp signalling with the Dpp receptor, Thickveins, present in punctae that move along cytonemes (Hsiung et al., 2005).

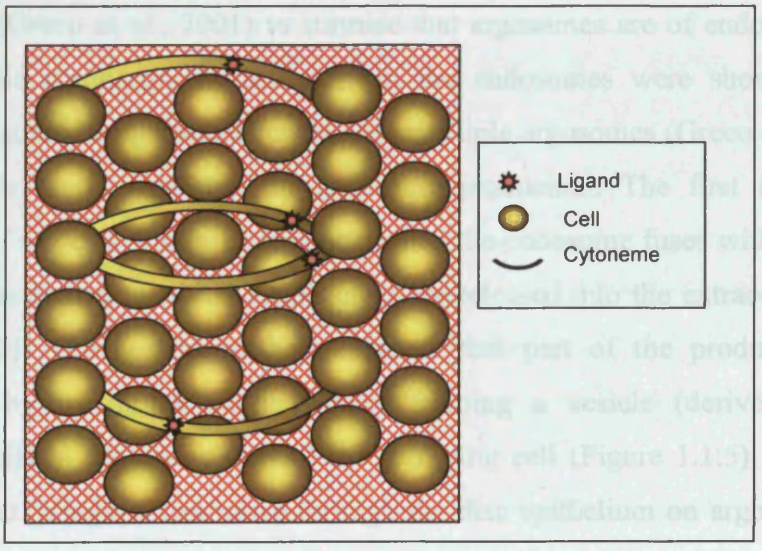

Figure 1.1.4: Diagramatic representation of cytonemes possible role in morphogen gradient formation.

Diagram shows cytonemes projectiong from distant to expressing cells (adapted from (Williams et al., 2004).

1.1.5.3 Argosomes

Many morphogens have been found to be tightly associated with membranes; the Wnt family bind heparin sulphate proteoglycans (HSPG) whilst hedgehog binds to membranes via covalently attached cholesterol and palmitate (Hashimoto et al.,

2000; Mann and Beachy, 2000; Nakato et al., 1995; Pepinsky et al., 1998). Greco *et al* observed that all hypotheses for the spread of morphogens assumed the release of the molecule from the membrane of the producing cells (Greco et al., 2001). Greco *et al* set out to investigate whether for the spread of morphogens might include their transport in vesicles at every stage of transport. This hypothesis was tested using fluorescent labelled markers (CFP-GPI) on the cytoplasmic and external faces of the membranes of the *Drosophila* imaginal disc. The expression of these markers was specifically driven in certain populations of cells within the wing disk but not others allowing the visualisation of vesicles derived from these populations in the non-expressing tissue. These 'exovesicles', found distant from the tissue expressing the membrane marker, were termed argosomes presumably from the mythical Greek ship, *Argo*, captained by Jason. Argosomes were shown to consist mainly of membrane with a fraction present in the early endocytic compartment. This led Greco *et al* (Greco et al., 2001) to surmise that argosomes are of endocytic origin. The endocytic compartments that contain the endosomes were shown to move rapidly with some compartments containing multiple argosomes (Greco et al., 2001). Two methods were suggested for argosome production. The first involves the production of vesicles within endosomes, when the endosome fuses with the plasma membrane the internal vesicles (exosomes) are released into the extracellular space (Figure 1.1.5). The second method suggests that part of the producing cell is internalised by its immediate neighbour forming a vesicle (derived from the producing cell) in the endosomes of the receiving cell (Figure 1.1.5). Greco *et al* suggested that Wingless can move through the disc epithelium on argosomes since Wingless in receiving cells colocalizes with argosomes derived from cells that synthesize wingless (Greco et al., 2001). Further, the rate of Wingless spread is consistent with the spread of argosomes. As removal of HSPG results in Wingless not associating with argosomes the authors propose that one function for the interaction of Wingless with HSPG might be to allow the incorporation of Wingless into argosomes (Greco et al., 2001).

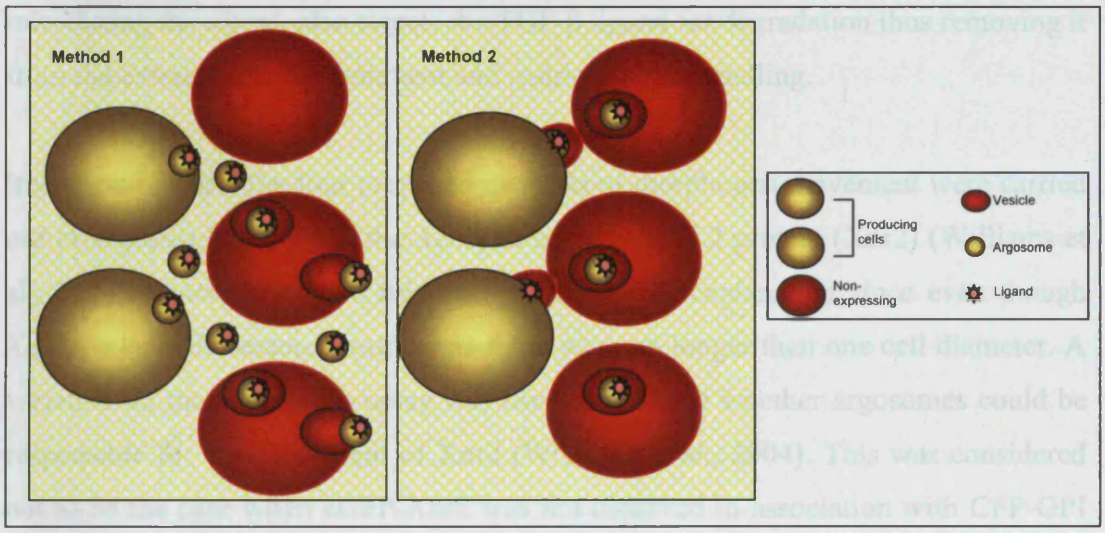

Figure 1.1.5: Diagramatic representation of argosomes possible role in morphogen gradient formation.

Diagram showing membranes from producing cells transporting ligands through reciving tissue in "exovesicles" (adapted from (Williams et al., 2004))

1.1.5.4 Diffusion

The original and simplest model for the movement of morphogens in a tissue has been by extracellular free diffusion. The diffusion model implies that intermediate cells do not play any role during the movement of the morphogen. Support for this is seen in *Xenopus laevis* animal caps, when endocytosis is blocked but TGF-β1 still spreads through the tissue (McDowell et al., 2001). Since morphogens signal over long distances doubt has been cast on the ability of free diffusion to form stable long-range concentration gradients with much of this stemming from the nature of the morphogen (Belenkaya et al., 2004; Entchev et al., 2000). The ideal morphogen to fit the diffusion model would need to be a small ligand which did not adhere to anything other than the receptor. Often this is not the case, both Wnt and Hh have been shown to adhere to proteoglycans in *Drosophila* and mouse cell culture, with Hh showing a high affinity for membranes (Blitzer and Nusse, 2006; Rietveld et al., 1999). This would result in their diffusion being hindered by extracellular binding proteins and proteoglycans (Kerszberg and Wolpert, 1998; Piek et al., 1999). TGF-β is a small ligand but its movement in *Xenopus laevis* is limited by the expression of the TGF-β type 2 receptor (McDowell et al., 2001), which in addition to its role in

transducing the signal, also targets the TGF-β ligand for degradation thus removing it from the extracellular environment and restricting its signalling.

Investigations into the four proposed methods of morphogen movement were carried out in *Xenopus laevis* using the *Xenopus* nodal-related 2 protein (Xnr2) (Williams et al., 2004). Cytonemes were ruled out as a possible explanation since even though *Xenopus* cells did extend protrusions these were no longer than one cell diameter. A variation on the animal cap assay was used to examine whether argosomes could be responsible for the movement of Xnr2 (Williams et al., 2004). This was considered not to be the case when eGFP-Xnr2 was not observed in association with CFP-GPI positive vesicles in receiving cells. Transcytosis was also ruled out, since affecting endocytosis using constitutively active or dominantly negative Rab5 had no effect on the expression domain or level of activation of endogenous *Xbra* a target gene of Xnr2. *Williams et al* showed that eGFP-Xnr2 in the receiving cells was extracellular and confined to interstices between cells. They therefore, proposed that eGFP-Xnr2 exerts its effects by diffusion. Time lapse corroborates this notion and shows that Xnr2 can travel ten cells within two hours on the exogenous animal cap assay. The authors admit the limitations of the animal cap assay and suggest that different morphogens in different developmental contexts use different means of transport (Williams et al., 2004).

1.2 Cell Trafficking and Transport

Embryonic development relies on many different cell biological processes including cell signalling and cell adhesion. These would not be possible, however, without the cells ability to traffic and transport substances into, around and out of the cell. Eukaryotic cells routinely traffic substances, not only between organelles but also across the outer cell membrane, using vesicles - microscopic fluid filled sacs surrounded by a lipid membrane. Vesicles are involved in secretion, endocytosis and various recycling processes within the cell (Armstrong, 2000). There are four main stages to vesicle trafficking: formation - the vesicle must be formed and packed with its cargo; targeting – the vesicle is released from its membrane and directed towards the target membrane; tethering/docking – the vesicle aligns and attaches with the target membrane; and finally fusion - allowing the vesicle to release the cargo at its destination (Armstrong, 2000; Zerial and McBride, 2001). Each stage of the vesicle trafficking process requires specialized protein machinery, many of which belong to the Ras superfamily of guanosine triphosphatases (GTPases).

1.2.1 Introduction to Rabs

In 1983, the accidental discovery of Ypt1p, in *Saccharomyces cerevisiae* by Gallwitz et al (Gallwitz et al., 1983) showed that vesicular transport is governed by conserved monomeric GTPases. Subsequently, Salminen and Novick (Salminen and Novick, 1987) provided the first evidence that a Ras-like GTPase (Sec4) was directly involved in vesicular transport whilst Tavitian and colleagues (1987) cloned the first mammalian homologs of SEC4/YPT termed *rab* (*ras*-like in rat brain) genes (Touchot et al., 1987). Ypt1p was shown to be necessary for the docking process of vesicles with the Golgi. Yeast cells lacking functional Ypt1p showed accumulation of endoplasmic reticulum (ER) membranes, vesicles and ER core glycosylated proteins before they died (Schmitt et al., 1988). The *ypt1p* gene showed 70% sequence homology to the *rab1* gene found in mammalian cells and, furthermore, *rab1* could replace the essential function of *ypt1p* in yeast, suggesting that these genes are orthologous (Touchot et al., 1987). Continuing studies in yeast and

mammalian cells showed that different Ypt/Rab-GTPases were performing the same function, however, each localized to different parts of the secretory and endocytic pathways (Lazar et al., 1997). The localization of these proteins and their effectors, aided by SNARE proteins, help determine the specificity of the vesicle, ensuring they are transported, docked and fused with the correct target (Hammer and Wu, 2002; Ossig et al., 1995; Price et al., 2000a). The complete sequencing of the *Saccharomyces cerevisiae* genome has revealed the total number of *ytp* genes to be 11, some of which are phenotypically redundant (Lazar et al., 1997). Only those *ytp* genes involved in the biosynthetic pathway are essential for cell viability. Loss of the Ytp proteins Ypt1p, Ypt51p , Yptp6, Ypt7p, Sec4p and Ypt31p/Ypt32p (Benli et al., 1996; Haubruck et al., 1989; Schmitt et al., 1986; Singer-Kruger et al., 1994; Wichmann et al., 1992), proved fatal for the cell and demonstrated their essential nature. These essential Ytp proteins correspond to Rab1, Rab5, Rab6, Rab7 Rab8 and Rab11 in mammalian cells and are now considered 'core' Rabs (Lazar et al., 1997; Singer-Kruger et al., 1995; Ullrich et al., 1996).

The Rabs are now known to be the largest sub family in the Ras superfamily. The Ras-superfamily comprises of over 150 human members (with evolutionarily conserved orthologs found in *Drosophila*, *Caenorhabditis elegans*, *S. cerevisiae*, *Saccharomyces pombe* and *Dictyostelium* as well as in plants (Bush et al., 1993; Garrett et al., 1993; Haubruck et al., 1990; Nonet et al., 1997). The Ras superfamily is divided into five major branches on the basis of sequence and functional similarities: Ras, Rho/Rac, Rab, Ran and Arf. (Colicelli, 2004; Pereira-Leal and Seabra, 2000; Wennerberg et al., 2005). The Rab family is found in all eukaryotes, with over 60 *rab* genes uncovered in the human genome (Colicelli, 2004; Zerial and McBride, 2001) and over 80 in zebrafish (Clark, MD, pers. com.). Rab proteins localize to specific intracellular compartments, consistent with their function in distinct vesicular transport processes (Zerial and McBride, 2001). This localization is dependent on prenylation (addition of hydrophobic molecules to facilitate protein attachment to the cell membrane) and specificity is dictated by divergent C-terminal sequences (Khosravi-Far et al., 1991). For example, Rab1 is found in the intermediate compartment of the *cis*-Golgi network and is involved in ER to Golgi transport (Ayala et al., 1989), while Rab5 is located in early endosomes (vesicles

involved in endocytosis) and regulates clathrin-mediated vesicle transport from the plasma membrane to early endosomes (Gorvel et al., 1991).

Although Rab proteins are localized within individual cells, at the level of the whole organism many of the *rab* transcripts identified to date have ubiquitous distribution, although their level of expression may vary from one cell type to another. This is surprising given the high degree of regulation at the protein level (see section 1.2.3). However, there are exceptions with some Rabs being cell type- or tissue-specific. For example, in mammals Rab3A is only expressed in neurons and neuro-endocrine cells (Fischer von Mollard et al., 1990; Johnston et al., 1991) while Rab17 has only been detected in epithelial cells (Lutcke et al., 1993).

1.2.2 Rab Homology and Classification.

The similarities between the members of the Ras-superfamily make them difficult to classify. All of the Ras family contain the conserved regions referred to as G1–G3 and PM1–PM3. These regions are involved in binding guanine nucleotide and phosphate/$Mg2^{+}$ respectively (Valencia et al., 1991). There are two regions that undergo a significant conformational change upon GTP binding and hydrolysis: the switch I (Ras residues 30-38) domain and the switch II (59-67) domain (Figure 1.2.1). Although the GTP-bound and GDP-bound state of the Rabs (as with rest of the Ras family) have similar conformations they also have pronounced differences. Critically the GTP-bound conformation has higher affinity for effector targets (Bishop and Hall, 2000; Milburn et al., 1990). This difference corresponds to the changes in the switch I and switch II regions. It is mainly through the conformational changes in these two switch regions that regulatory proteins and effectors distinguish the nucleotide status of the GTPases (Dumas et al., 1999). Although the GTP-bound form is the active form for all Ras superfamily GTPases it is the cycling between the two states, in which distinct functions are associated with each nucleotide-bound form, that is also critical for the activities of Rabs (Geyer et al., 1996; Pereira-Leal and Seabra, 2000).

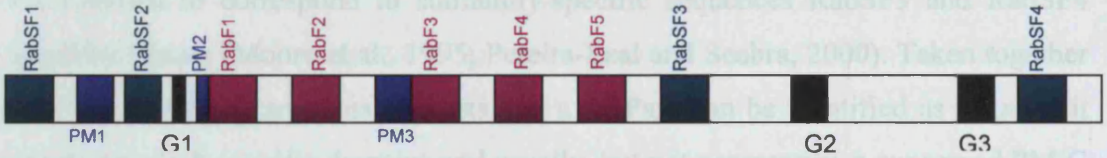

Figure 1.2.1: Diagram representing the structure of *rab* GTPases

G1-3 (black) are regions involved in guanine nucleotide binding, PM1-3 (blue) are regions involved in phosphate/$Mg2^{+}$ binding, RabF1-5 (pink) are Rab family motifs and RabSF1-4 (green) are subfamily-specific sequences. Adapted from (Bucci et al., 1995).

Studies undertaken by Pereira-Leal and Seabra (2000) facilitated the classification of Rabs. They showed the existence of five short conserved stretches of residues which appear to be diagnostic for the Rab family (Pereira-Leal and Seabra, 2000). These are termed Rab family motifs (RabF), with the section termed RabF1 localising to the effector domain. Most, though not all Rabs, also have a double-cysteine motif in the C-terminus which is regarded as a good diagnostic of a Rab protein. Rab8 and Rab13 are the exceptions as they contain only a single cysteine residue. Therefore the double-cysteine motif may confirm that a given small GTPase is a Rab, but it's absence should not be used to prove it is not (Pereira-Leal and Seabra, 2000).

The *rab* genes can also be placed into sub groups (such as Rab1a and Rab1b) in which the genes share over 70% amino acid identity to one another. It could be assumed that these genes are functionally related and interact with the same type of effector but this is not necessarily the case. For example, the Rab3 subgroup has at least 4 members in humans showing 77-85% amino acide identity with the greatest variance evident within the N- and C-terminal regions. Although they have high sequence homology their subcelluar targets and functional roles are distinct (Pavlos et al., 2001). Rab3a is expressed in neurons and neuroendocrine cells and together with Rab3c regulates neurotransmitter release, Rab3b is specifically expressed in polarized epithelial cells, while Rab3d is mainly expressed in adipocytes and is possibly involved in glucose transporter trafficking in response to insulin stimulation (Bucci et al., 1995). While working on Rab3a Ostermeier and Brunger (1999) identified three regions that contribute to an effector region pocket that mediates binding to the effector. These regions were named Rab complementary-determining regions (RabCDR's) with the individual regions called RabCDRI-III. These regions

were shown to correspond to subfamily-specific sequences RabSF3 and RabSF4 found by Moore (Moore et al., 1995; Pereira-Leal and Seabra, 2000). Taken together these bioinformatic analyses suggests that a GTPase can be identified as a Rab if it has the five Rab specific domains and usually, but not necessarily, a conserved PM/G (GTPase binding region) motif and a double-cystine C-terminal motif. Sub-families can be classified as such if they have 70% identity and conservation at the RabSF and RabF motifs (Pereira-Leal and Seabra, 2000).

Lastly, alternative splicing of a gene can result in different forms or a protein. *rab6a* is the only know *rab* to do this. The gene has a duplicated exon, and incorporation of either of the two exons by alternative splicing is shown to generate the isoforms named Rab6a and Rab6a' in human, which differ in only three amino acid residues (Echard et al., 2000). Interestingly this is conserved in zebrafish where two isoforms of Rab6a have also been found (Clark, MD, pers. com.).

1.2.3 Rab Regulators

Rabs are described as molecular switches, able to cycle between GTP bound (active) and GDP bound (inactive) forms and thus, recruiting a diverse group of "effector proteins" to the cytoplasmic leaflet of vesicular membranes (Zerial and McBride, 2001). When a Rab switches conformation to the inactive form, the effectors dissociate, the Rab is removed from the membrane and recycled back to a donor compartment. Rab function is promoted by the following factors: 1) guanine-exchange factors (GEFs) which accelerate guanine-nucleotide exchange and promote formation of the active, GTP-bound form on targeting to a donor membrane (Camus et al., 1995; Schmidt and Hall, 2002). 2) GTPase activation factors (GAPs) which stimulate guanine-nucleotide hydrolysis to promote formation of the inactive GDP-bound form (Settleman et al., 1992) and 3) GDP-dissociation inhibitors (GDIs) which prevent nucleotide dissociation, extracting the Rab from the target membranes and recycling it back to the donor membranes by binding it only in its GDP rather than GTP state (Fischer von Mollard et al., 1994; Sasaki et al., 1991; Seabra et al., 2002). GDI's transport the Rab back to the donor compartment for recycling without the Rab becoming active (Figure 1.2.2).

All members of the Ras superfamily of proteins undergo protein prenylation, a post-translational lipid modification that involves the attachment of a farnesyl (15-carbon) or geranylgeranyl (20-carbon) group to cysteine or serine residues at or near the C-terminus. These modifications are essential for the GTPases to associate tightly with cell membranes. Without this lipid modification, the proteins remain in the cytosol and are unable to associate with membranes or localise subcellularly, processes which are critical for their biological activities (Wennerberg et al., 2005, Casey and Seabra, 1996). Three different protein prenyltransferases have been identified which perform this role, protein farnesyl transferase (PFT or FTase), protein geranylgeranyl transferase type-I (PGGT or GGTase-I) and Rab geranylgeranyl transferase (RGGT or GGTase-II). These proteins have a heterodimeric structure and consist of distinct α- and β-subunits (Leung et al., 2006). FTase and GGTase-I recognise only substrates containing a CAAX motif at the C-terminus and these are found in the Ras sub familys of Rac and Rho. GGTase-II recognises only Rab substrates of which there are six different C-terminal motifs -CC, -CXC, -CCX, -CCXX, -CCXXX and –CXXX (Pereira-Leal and Seabra, 2000).

There are two conditions in which prenylation can occur. In the first, a newly synthesized Rab must form a stable complex with Rab escort protein (REP) to enable its recognition by GGTase-II. In the second, a newly synthesized Rab can associate with a preformed REP:GGTase-II complex (Mruk et al., 2005). The first scenario suggests association of an unprenylated Rab protein with REP where the interaction relies mostly on ionic bonds and does not involve the two C-terminal cysteine residues (Anant et al., 1998). This complex is then presented to GGTase-II, which adds two geranylgeranyl moieties to the Rab protein without prior dissociation of REP (Thoma et al., 2001b; Thoma et al., 2001c). After the transfer of the isoprenoids onto C-terminal cysteines, the complex remains associated until the binding of a new geranylgeranyl diphosphate (GGpp) molecule, which stimulates the release of the Rab-GG:REP complex. The REP then delivers the Rab to the target membrane (Leung et al., 2006). The second scenario implies that REP-1 and RGGT can form a tight complex in the presence of GGpp. This complex can associate with a Rab protein, but this occurs ten times more slowly than in the first scenario (Thoma et al., 2001a). This model depends on the *in vivo* concentrations of the proteins involved.

At high concentrations of all the components the second scenario maybe preferred whereas at low concentrations, the first scenario may be preferred.

Upon completion of its function at the target membrane the Rab/REP complex must then be returned to its membrane of origin. This is mediated by the cytosolic protein Rab GDP dissociation inhibitor (GDI). Rab-GDI interacts promiscuously with the GDP-bound Rab extracting it from membranes to the cytosolic reservoir for re-use (Wu et al., 1996). GDI/Rab forms a soluble complex in the cytoplasm which then delivers the Rab to the donor membrane. Once there, the GDI is released to the cytosol and the Rab remains membrane-associated. As GDI has a strong binding affinity for GDP bound Rabs the less well-characterized GDI-dissociation factor (GDF) catalyses the dissociation of Rab GDI complexes in order to enable transfer of Rabs from GDI onto membranes. Work in mammalian cells has shown that the integral membrane protein Yip3 acts catalytically to dissociate complexes of endosomal Rabs bound to GDI and to deliver them onto the membranes (Sivars et al., 2003). Rab-GDI's share homology with REP, but are thought to bind only prenylated Ypt/Rab proteins, preferentially in their GDP-bound form, inhibiting GDP dissociation and masking the prenyl modification (Seabra and Wasmeier, 2004). Once at the membrane the Rab is activated to the GTP-bound form by GEF and is ready to transport vesicles from the donor membrane to the target membrane. At this point the Rab is hydrolysed back to its GDP bound state with the help of GAP. The Rab is then ready to be recycled back to the donor compartment by GDI and the whole process starts again. All of the Ras superfamily of small GTPases exhibit high-affinity binding for GDP and GTP, and possess low intrinsic GTP hydrolysis and GDP/GTP exchange activities. GTPases within a family branch use shared GAPs and GEFs whereas GTPases in different branches exhibit structurally distinct but mechanistically similar GAPs and GEFs (Bernards and Settleman, 2004; Pan and Wessling-Resnick, 1998).

1.2.4 Rab Effectors and SNARES

Rab effectors are a soluble and diverse collection of proteins that transduce the Rab signal. A Rab effector preferentially binds to the GTP-bound conformation of Rab and competes for interaction with GAP proteins (Nakafuku et al., 1993; Schimmoller et al., 1998). They can be described as a protein - or protein complex - which binds the GTPase directly in a GTP-dependent manner and is required for the Rab-specific downstream function (Grosshans et al., 2006; Nakafuku et al., 1993). These Rab effectors perform diverse functions including vesicle budding, tethering and docking, vesicle transport by way of the cytoskeleton and vesicle motility. The Rab effectors show structural heterogeneity with some effectors sharing structural features. For example, p115/Uso1p, Rabaptin-5 and early endosome antigen 1 (EEA1), all contain predicted coiled-coil regions, Rab3-interacting molecule (Rim1), EEA1 and Rabenosyn-5 contain FYVE zinc-fingers (named after four proteins Fab1, YOTB/ZK632.12, Vac1, and EEA1) (Christoforidis et al., 1999a; McBride et al., 1999; Stenmark et al., 1996). The best characterized Rab effectors have been shown to mediate tethering and docking of a Rab-bearing vesicle with the target membrane to which it will fuse (McBride et al., 1999; Zerial and McBride, 2001). Other well characterised effectors are involved in vesicle motility while in recent work interesting insights into cell adhesion and cell signalling have been identified (Eggenschwiler et al., 2001; Eggenschwiler et al., 2006; Gibbs et al., 2004; Lock and Stow, 2005; Pellinen et al., 2006; Scholpp and Brand, 2004).

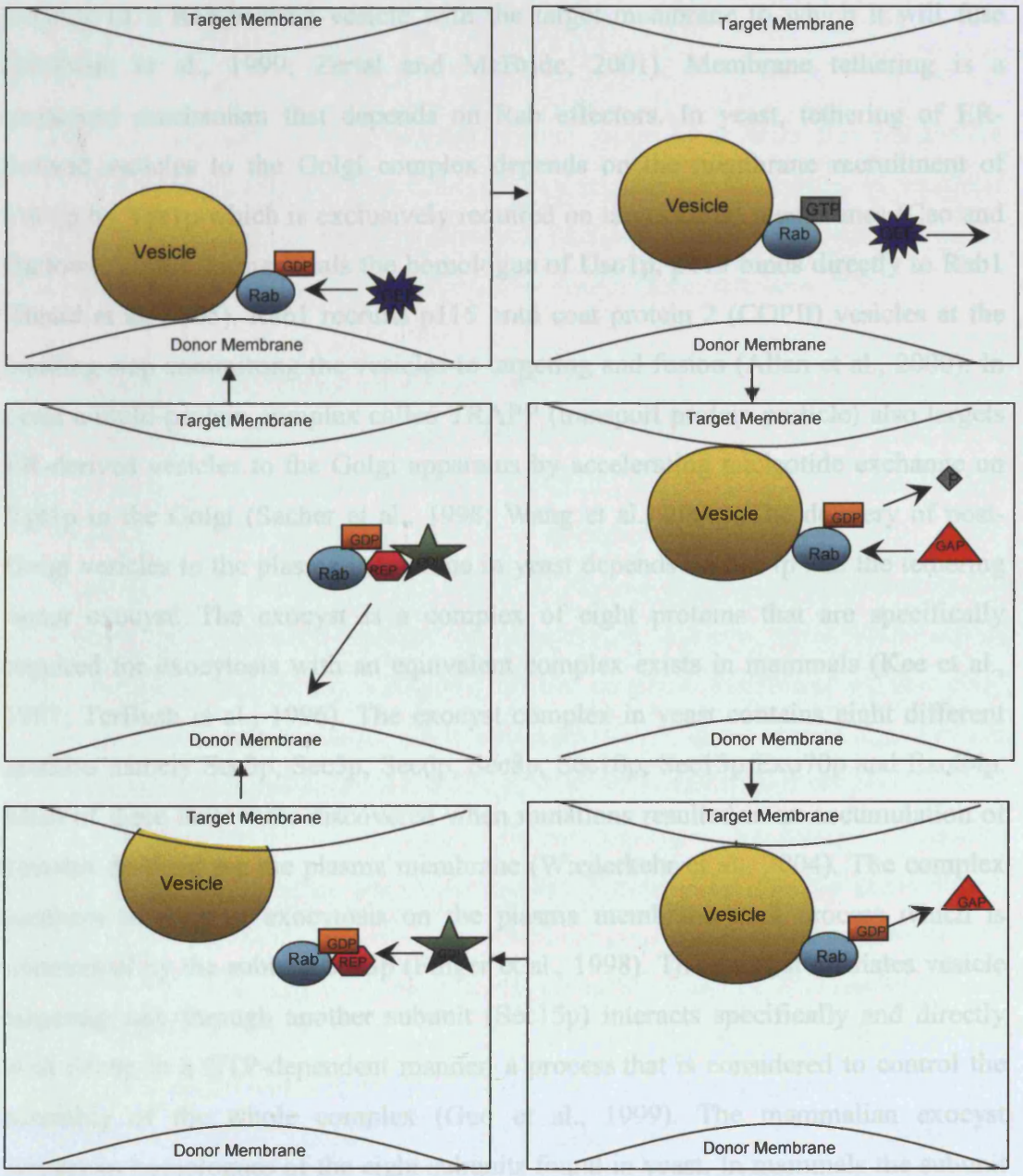

Figure 1.2.2: Diagram showing the regulation of Rab GTPases during vesicle trafficking.

1.2.4.2 Tethering Effectors

The best characterized Rab effectors have been shown to mediate tethering and docking of a Rab-bearing vesicle with the target membrane to which it will fuse (McBride et al., 1999; Zerial and McBride, 2001). Membrane tethering is a conserved mechanism that depends on Rab effectors. In yeast, tethering of ER-derived vesicles to the Golgi complex depends on the membrane recruitment of Uso1p by Ypt1p which is exclusively required on target Golgi membranes (Cao and Barlowe, 2000). In mammals the homologue of Uso1p, p115 binds directly to Rab1 (Beard et al, 2005). Rab1 recruits p115 onto coat protein 2 (COPII) vesicles at the budding step committing the vesicles to targeting and fusion (Allan et al., 2000). In yeast a multi-protein complex called TRAPP (transport protein particle) also targets ER-derived vesicles to the Golgi apparatus by accelerating nucleotide exchange on Ypt1p in the Golgi (Sacher et al., 1998; Wang et al., 2000). The delivery of post-Golgi vesicles to the plasma membrane in yeast depends on Sec4p and the tethering factor exocyst. The exocyst is a complex of eight proteins that are specifically required for exocytosis with an equivalent complex exists in mammals (Kee et al., 1997; TerBush et al., 1996). The exocyst complex in yeast contains eight different proteins namely Sec3p, Sec5p, Sec6p, Sec8p, Sec10p, Sec15p Exo70p and Exo84p. Most of these units were discovered when mutations resulted in an accumulation of vesicles destined for the plasma membrane (Wiederkehr et al., 2004). The complex localizes to sites of exocytosis on the plasma membrane in a process which is determined by the subunit Sec3p (Finger et al., 1998). The exocyst mediates vesicle targeting and, through another subunit (Sec15p) interacts specifically and directly with Sec4p in a GTP-dependent manner, a process that is considered to control the assembly of the whole complex (Guo et al., 1999). The mammalian exocyst comprises homologues of the eight subunits found in yeast. In mammals the subunit responsible for association with Rabs is Sec5, rather than Sec15 in yeast. Another difference between the yeast and mammalian exocyst is that the mammalian complex associates with a protein called RaIA instead of a Rab (Brymora et al., 2001).

In early endocytosis, mammalian Rab5 regulates both clathrin-coated vesicle-mediated transport from the plasma membrane to the early endosomes and homotypic early endosome fusion (Bucci et al., 1992; Gorvel et al., 1991). Early

endosomal autoantigen 1 (EEA1) is the Rab5 effector that mediates tethering/docking of early endosomes (Christoforidis et al., 1999a). This will be discussed in further detail in Chapter 5.

1.2.4.1 SNAREs

Vesicle tethering and docking requires another group of proteins for completion. Once the vesicle reaches its target, the effector triggers the interaction of vesicular (v-SNARE) and target (t-SNARE) proteins. This brings the vesicle and the target membranes into close apposition and mediates fusion (Kierszenbaum, 2000).

SNARE (Soluble NSF Attachment Protein REceptor) proteins have been proposed to mediate all intracellular fusion events (Sollner et al., 1993). The first of these to be discovered were the synaptic proteins; SNAP-25, syntaxin (STX1), and VAMP (Vesicle –Associated Membrane Protein or synaptobrevin) (Bennett et al., 1992; Oyler et al., 1989; Trimble et al., 1988). STX1 and VAMP are anchored to the membrane by a carboxyl-terminal transmembrane domain while SNAP-25 is peripherally attached to the membrane by the covalent attachment of 16-carbon saturated fatty acids (palmitate) to four cysteine residues in the central region of the protein (Chen and Scheller, 2001). It was thought that each type of transport vesicle had a distinct v-SNARE, which paired with an unique complementary t-SNARE at the appropriate target membrane (Rothman and Warren, 1994; Sollner et al., 1993). This interaction enabled the vesicle to dock at the appropriate membrane, leading to the subsequent dissociation of the SNARE complex, with the ATPase activity of NSF (*N*-ethylmaleimide Sensitive Fusion protein) driving the fusion. This view has since been modified and it is now thought that NSF acts as a chaperone to reactivate SNAREs after fusion instead of directly driving fusion (Morgan and Burgoyne, 1995). The specificity of targeting is brought about by the Rab protein family, with assembly of the SNARE complex driving the lipid fusion (Chen and Scheller, 2001).

Rabs and SNAREs interact via intermediate proteins the nature and number of which can be quite diverse between different steps of membrane traffic (Armstrong, 2000; Tall et al., 1999). The active form of the Rab protein generally nucleates the assembly of a protein complex that can ultimately bind to or tether the target

membrane and then a SNARE complex can form (Armstrong, 2000). Certain organelles are enriched in SNAREs which helps them to identify the correct target and to limit non-specific fusion events. During vesicle transport a given SNARE will spread throughout many cellular compartments such that organelles will contain SNARE complexes which must remain inactive until they return to their place of specific function. This is where the Rabs provide their additional layer of regulation (Zerial and McBride, 2001).

1.2.4.3 Budding effectors

It is thought that Rab proteins influence vesicle budding, in a transport event-specific manner (Allan et al., 2000; Bucci et al., 1992; Riederer et al., 1994). *in vivo* studies in mammals have indicated a possible role for Rab1 in budding of vesicles from the ER (Allan et al., 2000; Nuoffer et al., 1994). While Rab9 has been implicated in budding from endosomes directed to the *trans*-Golgi network (TGN) (Riederer et al., 1994). In yeast a component (Vam2p/Vps41p) of the Ypt7p (Rab7)-tethering complex HOPS has been implicated in the budding of vesicles from the Golgi (Price et al., 2000a). HOPS stands for homotypic fusion and vacuole protein sorting and is also referred to as Class C Vps protein complex (Rieder and Emr, 1997). Components of this complex include as mentioned the Vam2p/Vps41p proteins as well as Vam6p/Vps39p proteins (Price et al., 2000a; Seals et al., 2000). It should be noted that Ytp7p has not been shown to be directly implicated in Golgi budding (Price et al., 2000b). *in vivo* mammalian Rab5 has been shown to modulate the half-life of clathrin-coated pits on the plasma membrane during vesicle formation (Bucci et al., 1992). *in vitro* mammalian Rab5 is required for vesicle formation with the suggested Rab5 GAP, RN-Tre, downregulating Rab5 and inhibiting receptor internalization (Lanzetti et al., 2000; McLauchlan et al., 1998).

1.2.4.4 Motility Effectors

Rabs have been shown to determine the distribution of cellular compartments by regulating the movement of vesicles and organelles along cytoskeletal filaments (Cheney and Rodriguez, 2001). Probably the best charachterized of these is the Rab motility effector myosin Va. In collaboration with Rab27a and melanophilin (another Rab effector), myosin Va has been shown to be involved in correct pigment

patterning in both mice and humans as defects in any of these genes is responsible for the human disorder Griscelli's syndrome (see section 1.2.6.4) (Bahadoran et al., 2001; Matesic et al., 2001; Menasche et al., 2000). In yeast, interactions have been found between Sec4p and the myosin heavy chain Myo2p (Pruyne et al., 1998) suggesting that vesicles are propelled by motor proteins along polarized actin cables towards the site of exocytosis (Pruyne et al., 1998; Schott et al., 1999). In a screen looking for mammalian Rab effectors it was found that Rab6 interacts with a kinesin-like protein (Echard et al., 1998), Rabkinesin-6, which has since been shown to be important for cytokinesis (Echard et al., 1998; Hill et al., 2000). Rab5 has been shown to regulate the attachment of early endosomes to microtubules and their motility along those microtubules (Nielsen et al., 1999).

1.2.4.5 Cell Adhesion Effectors

Recent papers have shown a role for Rabs in cell adhesion (Kohler and Zahraoui, 2005; Ulrich et al., 2005). Small GTPases, such as Rab3b, Rab8 and Rab13 have been shown to localize to tight junctions between cells (Lutcke et al., 1993). These tight junctions are multifunctional complexes involved in various signalling events controlling cell–cell adhesion, differentiation and polarity. Kohler et al (2004) demonstrated that mammalian Rab13 directly interacts with PKA and inhibits PKA-dependent phosphorylation of the actin-remodelling protein VASP resulting in the recruitment of VASP, ZO-1 and claudin1 to cell–cell junctions to be inhibited (Kohler et al., 2004). Kohler also suggested a link between Rab13 and protein kinase A signalling during tight junction assembly in epithelial cells (Kohler et al., 2004).

Pellinen has shown an association, in both yeast and mammalian cells, of Rab21 and Rab5 with integrins (Pellinen et al., 2006). Continual trafficking of integrin cell adhesion molecules to and from the cell surface is vital to cell migration. Rab21 and Rab5 associate with the cytoplasmic domains of α-integrin chains, and their expression influences the endo/exocytic traffic of the integrins (Pellinen et al., 2006). Knock down of Rab21 impairs integrin-mediated cell adhesion and motility, whereas its overexpression stimulates cell migration and cancer cell adhesion to collagen and human bone (Pellinen et al., 2006). If there is a point mutation in the integrin in the region where the integrin associates with Rab21, when Rab21 is overexpressed, it

fails to induce cell adhesion (Pellinen et al., 2006). It is thought that these Rabs target the integrins to intracellular compartments and this regulates cell adhesion. (Pellinen et al., 2006).

1.2.5 Disorders caused by Mutations in Rabs

Although there are now over 60 Rabs uncovered in the human genome only a small number of mammalian Rabs have been show to be directly linked with specific disorders: These Rabs are Rab3a, Rab7, Rab23, Rab27a and Rab38 (Eggenschwiler et al., 2001; Kapfhamer et al., 2002; Loftus et al., 2002; Menasche et al., 2000; Verhoeven et al., 2003).

1.2.5.1 Rab3a and the earlybird mouse.

In a screen for mouse mutants with abnormal rest–activity and sleep patterns, a "semidominant" mutation called earlybird - which shortens the circadian period of locomotor activity and homeostatic response to sleep loss was - identified (Kapfhamer et al., 2002). Sequence analysis of *rab3a* identified a point mutation in a conserved amino acid (Asp77Gly) within the GTP-binding domain resulting in significantly reduced levels of Rab3a protein suggesting that the Asp77Gly change may affect the overall stability of the protein. Phenotypic assessment of earlybird mice and mice with a null allele of *rab3a* revealed anomalies in circadian period and sleep homeostasis, providing evidence that Rab3a-mediated synaptic transmission is involved in these behaviours (Kapfhamer et al., 2002). Rab3s are known to be the most abundant Rab proteins in the brain and have a regulatory role in synaptic vesicle trafficking. Mice with a targeted loss-of-function mutation in *rab3a* have defects in Ca2+-dependent synaptic transmission which lead to an increased number of vesicles released in response to an action potential in the mutant mice (Kapfhamer et al., 2002).

1.2.5.2 Rab7 in Charcot-Marie-Tooth type 2B Neuropathy

Charcot-Marie-Tooth type 2B (CMT2B) neuropathy is a clinical disorder characterized by distal muscle weakness and wasting and a high frequency of foot ulcers, which results in the need for amputations of the toes due to recurrent infections. The gene responsible has been mapped to chromosome 3q13-q22 where two mis-sense mutations (Leu129Phe and Val162Met) were found in Rab7. The alignment of Rab7 orthologues shows that both missense mutations target highly conserved amino acid residues. Rab7 is a late endosomal protein with expression found in sensory and motor neurons (Verhoeven et al., 2003). Later work showed a further mutation a heterozygous A to C mutation, changing asparagine to threonine at codon 161 whose phenotype lacked the motor features of the other mutations. This mutation is situated adjacent to one of the previous mutations suggesting hotspot for mutations in the highly conserved C terminus of Rab7 (Houlden et al., 2004).

1.2.5.3 Rab23 and the openbrain mouse

Sonic hedgehog (Shh) is essential for many aspects of mammalian embryogenesis including the patterning of the neural tube and limbs (Chandrasekhar et al., 1998; Couve-Privat et al., 2004; Tsukazaki et al., 1998). Hedgehog acts as an extracellular ligand which binds the trans-membrane receptor Patched (Ptc). In the absence of Hedgehog, Patched represses the activity of a second transmembrane protein, Smoothened (Smo), thereby blocking the downstream signalling pathway (Murone et al., 1999).

The mouse *open brain (opb)* gene product has been shown to have an opposing role to Shh (Gunther et al., 1994). In neural patterning *opb* is required for dorsal cell types and Shh is required for ventral cell types in the spinal cord (Eggenschwiler and Anderson, 2000). Mutations in *opb* causes the embryos to die during the second half of gestation with an open neural tube in the head and spinal cord, abnormal somites, polydactyly and poorly developed eyes (Gunther et al., 1994). *opb* mutants lack dorsal cell types specifically in the caudal spinal cord while Shh mutants lack ventral cell types throughout the spinal cord (Eggenschwiler and Anderson, 2000). The *opb* mutant phenotypes resemble those produced by partial loss of function of Ptc which acts as a negative regulator of the Shh pathway (Eggenschwiler et al., 2001). The *opb* mutant phenotype could be the result of partial activation of the Shh signalling

pathway in dorsal and lateral neural cells. When *opb* was cloned it was found to encode for Rab23 (Eggenschwiler et al., 2001). Dorsalizing signals are thought to activate transcription of *rab23* in order to silence the Shh pathway in dorsal neural cells. (Eggenschwiler et al., 2001). More recent research using Rab23-GFP showed that Rab23 co-localizes in endosomes with Ptc but it was thought that it may act more distally in regulating Shh (Evans et al., 2003).

Additional proteins which influence Shh signalling and whose cellular trafficking could be regulated by Rab23 have been uncovered (May et al., 2005). A forward genetic approach in mice identified a role for intraflagellar transport (IFT) genes in Shh signal transduction, downstream of Ptc and Rab23 (May et al., 2005). IFT proteins are essential for cilia assembly and have recently been associated with a number of developmental processes, such as left-right axis specification and limb and neural tube patterning (Haycraft et al., 2005; May et al., 2005) (Wang et al., 2006).

Work this year (Eggenschwiler et al., 2006) has shown that, contrary to initial speculations suggesting that Ptc and Smo are the targets of Rab23 action, Rab23 mutants do not appear to affect the localization and dynamics of either protein. Genetic analyses have now shown that Rab23 actually functions downstream of Smo and affects the function of the Shh-regulated Gli family of transcription factors (Eggenschwiler et al., 2006). Double mutant analysis has shown that the primary target of Rab23 is the Gli2 activator and that Rab23 and Gli3 repressor have additive effects on patterning (Eggenschwiler et al., 2006). Analysis of Gli3 protein suggests that Rab23 also has a role in promoting the production of Gli3 repressor (Eggenschwiler et al., 2006). Antibodies generated against Rab23 showed that the protein is highly enriched in the adult rodent brain and present in low levels in multiple tissues of the adult rodent. This suggested a role for Rab23 not only in the embryo but also in the adult (Guo et al., 2006).

1.2.5.4 Rab27a in Griscelli syndrome and Ashen mice

Griscelli's syndrome (GS) is a rare autosomal recessive disease characterized by an immune deficiency. Patients have uncontrolled T-lymphocyte and macrophage

activation (haemophagocytic syndrome, HS) leading to death in the absence of bone-marrow transplantation. In addition, patients show partial albinism with striking silvery-metallic hair sheen and mild cutaneous depigmentation (Griscelli et al., 1978). The disease has been attributed to an abnormal melanosome distribution (Griscelli et al., 1978). Melanosomes are melanin-containing vesicles in the epidermis the uniform distribution of which leads to normal pigmentation.

Originally the mutation responsible for this syndrome was mapped to 15q21 and the myosin-V gene (Pastural et al., 1997). However a mutation in the *rab27a* gene can also cause GS (Pastural et al., 2000). Studies have shown that in normal melanocytes Rab27a colocalizes with melanosomes but in melanocytes isolated from a patient with GS, there is abnormal melanosome distribution and a lack of *rab27a* expression. Re-expression of *rab27a* in GS melanocytes restores melanosome transport to dendrite tips, leading to a phenotypic reversion of the diseased cells implicating Rab27a as a key component of vesicle transport machinery in melanocytes (Bahadoran et al., 2001). Unlike the GS patients with the *myosin-V* gene mutation GS patients with the *Rab27a* mutation exhibited reduced T cell cytotoxicity and cytolytic granule exocytosis (Menasche et al., 2000).

The pigmentation defect mutants *dilute* (*d*), *leaden* (*ln*), and *ashen* (*ash*) in mice show mutations in *myosin Va*, *melanophillin* and *rab27a* respectively, with defects in *myosin V* and *rab27a* and more recently melanophilin corresponding to genes shown to be defective in GS (Matesic et al., 2001; Menasche et al., 2003; Mercer et al., 1991; Wilson et al., 2000). All three mouse mutations produce a lightened coat colour due to defects in pigment vesicle transport (Wilson et al., 2000) in addition *ash* mice show platelet defects resulting in increased bleeding times and a reduction in the number of platelet dense granules.

Melanosomes are transported by microtubules to the dendrite tips and then are retained there by MyoVa-mediated interaction with the cortical actin cytoskeleton (Wu et al., 1998). It is thought that Rab27a, melanophilin, and myosin Va form a ternary complex in the human melanocyte cells where melanophilin has a role in bridging Rab27a on melanosomes and myosin Va on actin filaments during

melanosome transport. (Costa et al., 1999; Karcher et al., 2001; Nagashima et al., 2002).

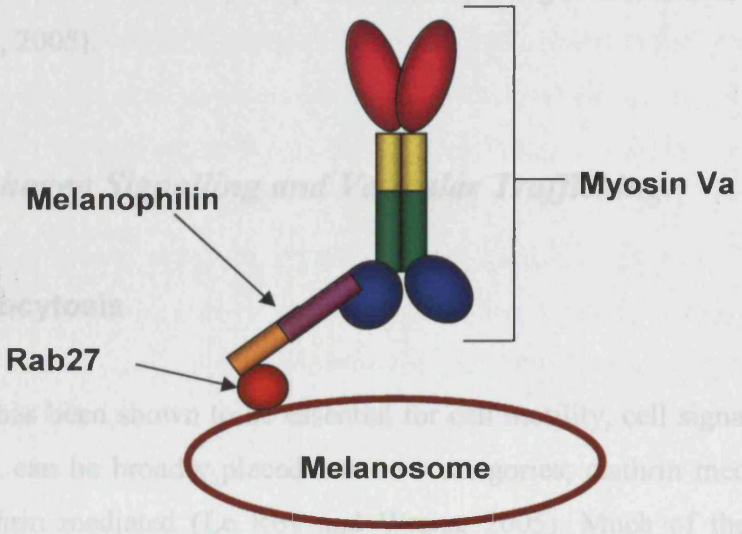

Figure 1.2.3: Diagram of myosin Va attachment to melanosomes via melanophilin.

(Adapted from Cheney and Rodriguez, 2001; Costa et al., 1999; Karcher et al., 2001; Maciver, 2006)

1.2.5.5 Rab 38 and the chocolate mouse.

Disorders with reduced pigmentation can be placed into two groups according to whether they affect melanocyte differentiation or melanosome function. Those that affect melanocyte differentiation are characterized by a localized absence of melanocytes resulting in ''white patch'' patterns. Disorders with affected melanosome function include Oculocutaneous albinism (OCA) I-IV and Griscelli syndrome (GS). Microarray analysis has revealed that *rab38* demonstrates a similar expression profile to melanocytic genes and further comparative genomic analysis has linked human *rab38* to the mouse chocolate (*cht*) locus (Loftus et al., 2002). Mutant mice exhibit a brown coat similar in colour to mice with a mutation in tyrosinase-related protein 1 (*Tyrp1*). This forms a mouse model for OCA (Loftus et al., 2002; Suzuki et al., 2003). In the melanocytes of these mice the targeting of TYRP1 protein to the melanosome is impaired, suggesting that Rab38 plays a role in the sorting of TYRP1 (Loftus et al., 2002). More recent work has also shown that *rab38* mRNA and native protein are expressed in a tissue-specific manner in the lung, skin, stomach, liver, and kidney. Cellular analysis has shown Rab38 mainly

colocalized with endoplasmic reticulum-resident proteins and also partly with intermittent vesicles between the endoplasmic reticulum and the Golgi complex. This implies that Rab38 abnormality may cause multiple organ diseases as well as OCA (Osanai et al., 2005).

1.2.6 Morphogen Signalling and Vesicular Trafficking.

1.2.6.1 Endocytosis

Endocytosis has been shown to be essential for cell motility, cell signalling and cell adhesion and can be broadly placed into two categories; clathrin mediated (CME) and non-clathrin mediated (Le Roy and Wrana, 2005). Much of the literature is concerned with CME which is of particular interest in development, as a possible route by which TGF-β receptors, such as those for the Nodals, are internalized (Anders et al., 1998). Clathrin independent endocytosis is used to describe any endocytic process that does not involve clathrin (Le Roy and Wrana, 2005). One form which is suggested to also play a role in development relies on cholesterol-rich membrane domains such as lipid rafts and caveolae (raft/caveolae endocytosis)(Polo and Di Fiore, 2006). In this form of endocytosis receptors are internalized and thought to be delivered for degradation (Le and Nabi, 2003; Pelkmans et al., 2005). Investigations using epiderimal growth factor receptors have suggested that during signalling a choice is made between CME and raft/caveolae endocytosis (Polo and Di Fiore, 2006). If low doses of receptor are internalized then endocytosis progresses via CME. High doses of receptor internalization have been shown to correlate with the monoubiquitination of EGFR and so are probably destined for degradation via raft/caveolae endocytosis. It has therefore been suggested that CME is preferred at low doses for prolonged endosomal signalling but some of the receptors are routed through the raft/caveolae endocytosis pathway for degradation at higher does. Such routing avoids excess stimulation with signalling considered as the ratio of CME to raft/caveolae endocytosis (Polo and Di Fiore, 2006). This view, however, has been recently challenged by the suggestion that clathrin coated vesicles may play a part in the degradative endocytic pathway (Lakadamyali et al., 2006).

The correct sorting of endocytic ligands and receptors is essential for proper cell function. Early endosomes are considered to be the initial sorting station, where cargos for degradation are separated from those for recycling (Lakadamyali et al., 2006). Live mammalian cell imaging used to monitor individual endosomes and ligands has shown that a sorting mechanism takes place prior to early endosome entry and that endosomes are comprised of two distinct populations. The first of these endosomes are highly mobile on microtubules and mature rapidly toward late endosomes. The second are static endosomes that mature much more slowly. Those cargos destined for degredation are targeted to the dynamic endosomes whereas those destined for recycling are enriched in the larger, static population (Lakadamyali et al., 2006). This pre-early endosome sorting process is thought to be dependent on microtubule motility, involve endocytic adaptors and interestingly begin at clathrin-coated vesicles (Lakadamyali et al., 2006).

In metazoans, CME requires dynamin, a member of a family of self assembling GTPases. During endocytosis, dynamin forms an oligomeric 'collar', in a GTP-dependent manner, which is thought to induce fission of vesicles from the plasma membrane (Takei et al., 1995), in addition to recruiting effectors such as actin-binding proteins (Elde et al., 2005). The actin cytoskeleton is important in endocytosis as demonastrated by interference with actin turnover in mammalian cells by pharmacological agents which inhibits endocytic uptake and the formation of coated vesicles (Lamaze et al., 1997). However, this block in endocytosis in mammalian cells seems to be partial (Fujimoto et al., 2000; Moskowitz et al., 2003).

1.2.6.2 Evidence for vesicle trafficking in morphogen movement

The trancytosis model of morphogen movement proposes that morphogens use vesicular trafficking through the cells to reach their target cells. Much of the evidence for this comes from work in *Drosophila* other investigations, however, suggest a role for this mechanism in vertebrates.

The *Drosophila* Dpp protein, the orthologue of Bmp2/4, has been shown to act as a morphogen, patterning the early embryo including well characterised roles in specifying cell fates along the AP axis of the wing (Eldar et al., 2002; Lecuit et al.,

1996; Weigmann and Cohen, 1999). Functional GFP-Dpp fusions have enabled visualisation of Dpp showing that it forms a long-range dose gradient across 30 cells (Entchev et al., 2000; Teleman and Cohen, 2000) travelling at a rate of more than four cells per hour in all directions. This is not unusual for signalling factors and is consistent with diffusion, however Dpp cannot form a stable gradient by diffusion (Entchev et al., 2000; Teleman and Cohen, 2000). It is possible this is due to the mature Dpp peptide binding to the extracellular matrix components and so restricting its extracellular movement. The binding of Dpp to the receptor may also decrease the range of Dpp. Additionally Dpp signalling range may be reduced by internalized Dpp being degraded in receiving cells upon targeting to the late endosome/lysosome. Labelled GFP-Dpp disappears within 3h and is considered to be actively degraded (Entchev and Gonzalez-Gaitan, 2002).

Dpp has been show to be targeted towards degradation by a sorting mechanism which depends on the small GTPase Rab7 (Entchev et al., 2000). Dpp's signalling range has been shown to be determined by Rab7-dependent rates of degradation (Entchev et al., 2000). Entchev *et al* have shown that Dpp is internalized by the receiving cells where it localizes in endosomes and is then excised with the help of dynamin in clathrin-coated pits to form endocytic vesicles (Entchev et al., 2000). In the dynamin mutant (*shibire*) Dpp is not internalized and can only be observed extracellularly adjacent to its source (Entchev et al., 2000). In endocytic and endosomal-defective tissue Dpp has a range which, Entchev *et al* propose is consistent with their estimated range - less than five cells - of Dpp in the absence of transcytosis (Entchev et al., 2000). They proposed that receiving cells are required to perform transcytosis in order to form a long-range Dpp gradient (Figure 1.2.4). Their transcytosis model implies that Dpp is internalized in the receiving cell, traffics through the endocytic pathway and is re-secreted allowing it to signal in adjacent cells. Consistent with this is the observation that Rab5 activity can alter the signalling range of Dpp (Entchev et al., 2000). Rab5 controls endocytic trafficking by directing the budding of endocytic vesicles from the plasma membrane (McLauchlan et al., 1998) to their fusion with the early endosome (Bucci et al., 1992). Cells expressing a dominant negative Rab5 showed reduced range of expression of the Dpp target gene *spalt,* whilst cells overexpressing Rab5 showed increased expression range of *spalt* (Entchev et al., 2000). Enchev *et al* suggested

that once Dpp enters the endocytic pathway, it can be sorted towards degradation or recycling (Entchev et al., 2000). Recycled Dpp is re-secreted and moves forward into the target tissue. Dpp transcytosis is considered to be controlled by endocytic Rab proteins which include Rab5 and Rab7.

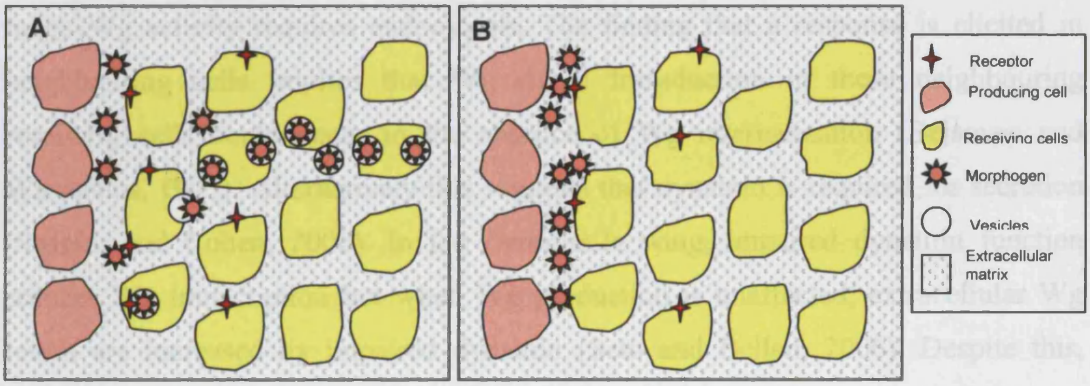

Figure 1.2.4: Diagramatic representation of planar transcytosis possible role in morphogen gradient formation.
Diagram A shows morphogens moving through receiving cells in vesicles. Diagram B shows planar transcytosis impeded by a reduction in endocytosis (i.e.*rab5* deficient cells).

Teleman and Cohen (2000) have an alternative explanation to transcytosis. They agree that Dpp-GFP forms an unstable extracelluar gradient which can travel over long distances. However, they show with the slow spread of target gene induction that this extracellular gradient differs from the activity gradient. They propose that the activity gradient is shaped at the level of receptor activation possibly by the need to downregulate a Dpp repressor (Teleman and Cohen, 2000). A subsequent paper by Belenkaya et al (2004) contradicted earlier studies and showed that Dpp is mainly extracellular with its extracellular gradient coinciding with its activity gradient. They demonstrated that blocking endocytosis using *shibire* does not block Dpp movement but inhibits Dpp signal transduction suggesting endocytosis is needed but not essential for transport. They suggest a model where Dpp moves along the cell surface by restriced extracellular diffusion involving glypicans Dally and Dally-like (Belenkaya et al., 2004).

The *Drosophila* Wnt homolog Wingless (Wg), has been found in vesicular structures at the target tissue (Gonzalez et al., 1991). It has therefore been suggested that it

spreads throughout the target tissue by trafficking through the receiving cells during patterning of the epidermis in the Drosophila embryo (Bejsovec and Wieschaus, 1995). Wg is thought to be internalized by Dynamin-dependent endocytosis, since in dynamin mutant embryos Wg is only able to elicit signalling in the cells neighbouring the source (Bejsovec and Wieschaus, 1995). This indicates that long-range Wg activity requires endocytosis. The finding that a response is elicited in neighbouring cells implies that Wg signal transduction in these neighbouring receiving cells could occur in the absence of Wg internalization (Bejsovec and Wieschaus, 1995). Alternatively this suggests that dynamin is required for secretion (Strigini and Cohen, 2000). In the *Drosophila* wing, impaired dynamin function reduces Wg transcription but when Wg production is unaffected, extracellular Wg levels are increased by impaired dynamin (Seto and Bellen, 2006). Despite this, target gene expression is reduced, suggesting that internalization at the target is also required for efficient Wg signalling *in vivo*. Rab5 deficient cultured cells showed a reduction of the activity of the Wg reporter Super8XTOPflash suggesting that internalization and endosomal transport facilitate Wg signalling (Seto and Bellen, 2006). When endosomal transport is impaired, Wg signalling is reduced however, when transport to endosomes is increased expression of Wg targets is enhanced. This increased signalling correlates with greater colocalization of Wg, Arrow, and Dishevelled on endosomes (Seto and Bellen, 2006). Regulation of endocytosis is the mechanism through which Wg signalling levels are determined (Seto and Bellen, 2006).

Hedgehog (Hh) has been shown to restrict the propagation of Wg signalling suggesting that this signalling pathway sets a barrier for the spreading of Wg (Sanson et al., 1999). It has been suggested that it does this by vesicular trafficking (Dubois et al., 2001). Wg degradation is specifically enhanced posteriorly by a mechanism thought to be initiated by Hedgehog activating EGF receptor signalling (Scott, 2001). Sequentially EGF receptor signalling is thought to activate the transcription of an unknown factor in posterior cells and this in turn enhances Wingless degradation (Dubois et al., 2001). In the absence of the Hh ligand, Patched (Ptc) antagonizes Hh signalling by binding Smoothened and blocking its signalling activity and possibly destabilizing it (Chen and Struhl, 1996; Denef et al., 2000). When Hh is present it binds to Ptc triggering its internalization, followed by phosphorylation of

Smoothened which becomes stabilized and accumulates at the surface and signals (Denef et al., 2000). There is the possibility that Hh elicits signalling by diverting Ptc into a distinct trafficking route releasing Smoothened from its repression (Chen and Struhl, 1996; Denef et al., 2000) and implying a role for Hh in vesicular trafficking. Vesicle trafficking may have an additional role in the movement of Nodal and Lefty. In chick embryos Nodal-GFP and Lefty-GFP fusion proteins are localized in the endosome (Sakuma et al., 2002) suggesting the possibility that Nodal and Lefty dispersal occurs by intracellular trafficking. Vesicular trafficking has been suggested to play one of two roles depending on the morphogen (Entchev and Gonzalez-Gaitan, 2002). Intracellular trafficking could push forward the ligands when the extracellular space restricts its movement as seems to be the case for Dpp in the wing. Alternatively, internalization and degradation of the morphogens could restrict the range of the morphogen if the extracellular matrix permits its long-range diffusion as appears to apply to Wg in the Drosophila embryo (Entchev and Gonzalez-Gaitan, 2002).

1.3 Nodal signalling

Zygotic Nodal signalling is essential for mesoderm and endoderm formation in the developing embryo (Feldman et al., 1998) with evidence in chick suggesting a possible role for endocytosis in its movement (Sakuma et al., 2002). Recently maternal transcripts of the zebrafish nodal Squint have been shown to be localized to cells that may form the dorsal side of the embryo (Gore et al., 2005) suggesting a role for maternal transcripts of Nodal protein in DV patterning. Nodal proteins are therefore considered to be of great importance in the study of zebrafish development

1.3.1 Introduction to Nodal Signalling

Nodal is a gene found to be essential for the establishment of the primitive streak, in mice, from which mesoderm and endoderm are derived. *nodal* encodes a TGF-β superfamily ligand (Zhou et al., 1993) identified by an insertional mutagenesis screen in mouse. Mutant embryos, lacking a functional *nodal* gene fail to gastrulate and the expression of mesoderm markers such as *brachyury* is severely inhibited (Rebagliatia et al., 1998). Zebrafish have 3 homologues of this gene *squint* (*sqt*), *cyclops* (*cyc*) and *southpaw*. Squint and Cyclops are expressed at the blastoderm margin and are required for prechordal plate and notochord formation. In their absence there is a lack of mesoderm and endoderm formation (Dougan et al., 2003; Feldman et al., 1998) (Figure 1.3.1). An additional role for Nodal signalling has been observed in patterning axial mesoderm precursors in the organizer along the anterioposterior axis (Gritsman et al., 2000). This patterning occurs by differential activation of the Nodal signalling pathway (Gritsman et al., 2000). Embryos mutant for both *squint* and *cyclops* do not develop a shield and, in addition markers for dorsal mesoderm such as *goosecoid* and *floating head* are not expressed at the onset of gastrulation (Feldman et al., 1998). The nodal related gene *southpaw (spaw)* has been shown to regulate left-right asymmetry in the visceral organs and brain of the developing embryo. *spaw* is expressed bilaterally in paraxial mesoderm precursors then subsequently within the left lateral plate mesoderm (Long et al., 2003) but is not detected prior to

somitogenesis. Since much of this thesis is concerned with events preceding somitogenesis, the actions of *spaw* will not be fully discussed.

The *nodal* related genes encode a pro and mature region that once transcribed are cleaved to produce a mature ligand which is a covalently disulfide-linked dimer. All TGF-β related ligands show a conserved cysteine this is essential for the secretion and biological function of the protein (Sampath et al., 1998). A mutation of this cysteine is thought to disrupt the formation of disulphide bonds and possibly ligand dimerization.

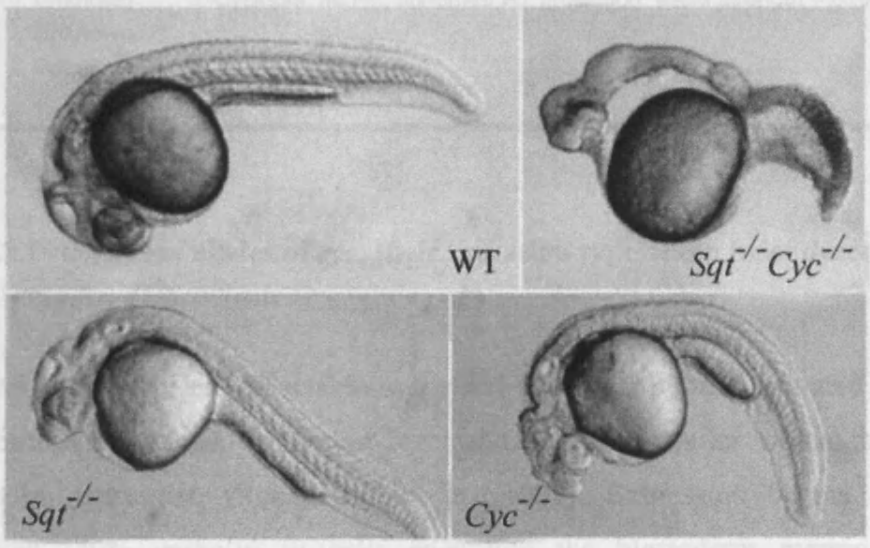

Figure 1.3.1: The zebrafish nodal mutants.
Comparing wild type embryos to ***squint*** homozygous mutants, ***cyclops*** homozygous mutants and both ***sqt*** and ***cyc*** homozygous mutants (Feldman et al., 1998).

1.3.2 Cyclops

cyclops muatants have a variety of alleles of differing types and strengths most derived from ENU mutagenesis (Table 13.1) (www.zfin.org) The *cyclops (cyc)* gene product is required for the formation of ventrally located cells in the neuroectoderm, both in the forebrain and more posteriorly in the floor plate (Solnica-Krezel et al., 1996). *cyclops* mutants have been shown to have a failure in specification of cells

that come to occupy the ventral midline of the neural tube (Hatta et al., 1991) giving a cyclopean phenotype (Figure 1.3.1).

Allele	Mut. Type	Brief Description
b16	Deficiency	Strong cyclopia, interrupted floor plate.
m101	Unknown	Cyclopia; CNS and floor plate defects.
m122	Unknown	Cyclopia; CNS and floor plate defects.
m294	Point	Cyclopia; CNS and floor plate defects; null allele.
sg1	Point	Temperature-sensitive allele. Incompletely penetrant at 22 deg. C, completely penetrant at 28.5 deg C.
st5	Deficiency	
te262c	Unknown	Patchy floor plate; weak allele.
tf219	Unknown	Cyclopia, no FP, abnormal RT projection; allele strength = *b16*.
tu43x	Unknown	
B299	Deletion	
B213	Translocation	

Table 1.3.1: Different alleles of *cyc*, their mutation type and a brief description
Adapted from the Zfin website (*www.zfin.org*)

cyclops transcripts are not detectable in the fertilized egg, but are activated after the MBT, reaching maximal expression level at shield stage, after which there is a decrease in expression (Rebagliatia et al., 1998). Expression begins in early gastrulation (30% epiboly) in cells encircling the blastoderm margin and is progressively restricted to the dorsal organizer. Mid-gastrulation expression extends along the midline mesendoderm and by the end of gastrulation *cyclops* is expressed in the prechordal mesendoderm and posterior tail bud mesoderm but disappears from both regions by the 2-3 somite stage. In *cyclops* mutants the expression is initially indistinguishable from WT but declines thereafter and is absent in the prechordal plate. *cyclops* expression is initially normal in the mutant *oep* (see Chapter 3.4), but decreases during gastrulation contributing to the cyclopia and floorplate defects of *oep* mutants. This suggests that *cyclops* and *oep* are necessary for maintenance rather than activation of *cyclops* expression (Rebagliati et al., 1998). Subsequently it was found that *oep* is a co-receptor required for nodal signalling (Gritsman et al., 1999). In *bozozok (boz)* mutants which show a loss of chordomesoderm (Fekany et al., 1999) dorsal *cyclops* expression is greatly reduced or absent throughout gastrulation

resembles that of *cyc,* but is usually less severe. The range of phenotypes varies from mild phenotypes such as eyes being to close together (hence the name) to more severe phenotypes including complete cyclopia (Figure 1.3.1). This is, again, due a failure to specify prechordal mesendoderm and subsequent failure to specify the midline of the anterior neural plate.

Although very similar and partially functionally redundant, Sqt has been shown to differ from Cyc in a number of important ways. While Cyc only has short range activity, Sqt can act as morphogen (Chen and Schier, 2001) capable of acting in a dose dependent manner directly at a distance. Sqt producing cells can induce expression of *gsc* - a nodal target gene - at the source and in its immediate neighbours where there are high levels of nodal signalling. Further away Sqt induces first *flh* and then at a greater distance *ntl* and *bik* where the levels of nodal signalling are lower. At reduced levels of Sqt, *gsc* is not induced and *ntl* is only induced close to the source (Chen and Schier, 2001). This long range signalling was not seen in cells producing Cyclops (Chen and Schier, 2001).

1.3.4 Receptors, Co-receptors, Extracellular Inhibitors

The TGF-β superfamily ligands signal by binding to transmembrane serine-threonine kinase receptors. Two sets of receptors have been identified, which are assembled into a receptor complex (Dougan et al., 2003). Type I receptors are predominantly involved in the activation of downstream transducers while type II receptors phosphorylate and activate type I receptors in response to ligand binding (Whitman, 2001). In addition to these receptors there is a class of factors specifically required for signalling by Nodal related ligands. These are EGF-CFC factors; a family of membrane attached extracellular glycoproteins that include OEP in zebrafish and Cripto in mice. Maternal and zygotic loss of *oep* function phenocopies the loss of both Sqt and Cyc. Loss of *oep* function renders cells unable to respond to ectopic *cyc* or *sqt* but does not alter responsiveness to activin (Whitman, 2001) another TGF-β family member that signals through the same receptors as the Nodals (Reissmann et al., 2001; Sun et al., 2006). This suggests that the requirement for EGF-CFC factors is specific to the Nodal superfamily of TGF-β ligands (Gritsman et al., 1999).

The best characterized Nodal antagonists in zebrafish are the Lefties (Goering et al., 2003; Parsons et al., 2002a; Schmid et al., 2000). There are at least two zebrafish lefties, *lefty 1* and *lefty 2*. Overexpression of these in zebrafish induces phenotypes strongly resembling *cyclops;squint* double mutants or maternal-zygotic *one-eyed pinhead* mutants (Sakuma et al., 2002). Loss of Lefty function leads to enhanced Nodal signalling during mesoderm induction with expansion of mesendoderm and loss of ectoderm in addition to left-right pattern defects (Parsons et al., 2002a; Sakuma et al., 2002). Individually, loss of Lefty1 causes aberration during somitogeneseis stages including left-right pattern defects, while Lefty2 depletion has no obvious consequences. The gastrulation defects of embryos depleted of Lefty1 and Lefty2 have been shown to result from the deregulation of Sqt signalling (Parsons et al., 2002a). In contrast, de-regulation of *cyclops* does not affect morphology or the transcription of Nodal target genes during gastrulation. Cyclops is thought to be specifically required for the maintenance of *lefty 1* and *lefty 2* transcription. Severe gastrulation defects do not arise in zebrafish unless two Nodals or two Leftys are removed (Parsons et al., 2002a). This suggests that the activity of Leftys is controlled at the level of transcription with Lefty expression being dependent on Nodal signalling in most tissues.

identifying *boz* as an early-acting upstream regulator of *cyclops* (Sampath et al., 1998).

1.3.3 Squint

There are two known mutant alleles of the *squint* both of which are insertion mutations (Table 1.3.2) (www.zfin.org). Expression of *sqt* is both maternal and zygotic with *sqt* RNA found to be uniformly expressed in oocytes at all stages of oogenesis (Gore and Sampath, 2002). Five minutes after egg activation *sqt* RNA aggregates in clusters throughout the yolk and is detected in the emerging blastoderm. At the one cell stage RNA is restricted to the blastoderm and excluded from the yolk cell (Gore and Sampath, 2002). This movement from yolk to blastoderm is microtubule dependent (Gore and Sampath, 2002). At the four cell stage *sqt* localizes to two blastomeres that may become the dorsal region of the embryo. Removal of these blastomeres can result in loss of dorsal structures. This localization requires a highly conserved sequence of the 3' untranslated region (UTR) (Gore et al., 2005).

Allele	Mut. Type	Brief Description
Cz35 (z1)	Insertion	Cyclopia; prechordal plate, ventral nervous system defects; null allele.
hi975	Insertion	Mild eye cyclopia, u-shaped somites.

Table 1.3.2: Different alleles of *squint*, their mutation type and a brief description.
Adapted from Zfin (*www.zfin.org*)

Subsequently in the developing embryo the *sqt* gene has been shown to be expressed in the dorsal region of the blastula including the embryonic YSL which has been implicated as a source of signals that induce organizer development and mesendoderm formation. Mis-expression of *sqt* RNA within the embryo or specifically in the YSL induces ectopic or expanded dorsal mesoderm (Feldman et al., 1998). The expression of Sqt is shown to be at peak abundance around sphere stage and declines sharply after shield stage. Loss of *sqt* results in a phenotype that

1.4 Thesis aims

With the publication of the zebrafish genome, Dr Matthew Clark has undertaken to identify all the Rabs in the genome and classify them according to sequence homology to their mammalian counterparts. To date, there are estimated to be over 80 zebrafish rabs (Clark, MD, pers. com.), compared to over 60 in mammals (Colicelli, 2004). This thesis aims to characterise the function of specific members of the extensive *rab* family. To achieve this anti-sense MO oligonucleotides will be used to knock-down individual *rabs* with further analysis including overexpression assays and microarrays

This thesis aims to uncover new roles for the *rab* family in zebrafish development with the ultimate aim of identifying the function of all the zebrafish *rabs*. This thesis presents the results obtained when 13 *rab* genes were knocked-down, bringing the total number of genes screened to 37 with a small number of these genes exhibiting specific and fascinating defects when knocked-down. In mammalian development a small minority of *rab* genes have been implicated in disorders such as Griscelli's syndrome or the *openbrain* mutant in mice. Investigations into *rabs* in zebrafish have shown that sequence homology does not necessarily translate to functional homology (Campos, 2004).

In addition to screening the zebrafish *rabs*, this thesis further characterizes the function of *rab5a2*: the only *rab* gene screened to date which resulted in mortality before the completion of epiboly. The essential nature of this *rab* is not surprising, since *rab5* has been identified as one of the core *rab* genes. What is surprising is that, although many of the other core *rabs* have also been screened, none of them have shown such a dramatic early phenotype. In addition, there are four *rab5* genes in zebrafish, however, none of the other *rab5s* display such early morbidity. Recent experiments in zebrafish have shown the zebrafish *rab5* family to be important in cell signalling and cell migration during early development. This research, coupled with results from Dr Campos showing a lack of organizer and *nodal* responsive

markers in *rab5a2* MO injected embryos, has suggested a role for *rab5a2* in Nodal signalling.

It is therefore the aim of this thesis to further characterise *rab5a2* and in particular its effect on Nodal signalling by using antisense morpholino oligonucleotides and overexpression of RNA analysis. This thesis also looks at the contribution of maternal and zygotic transcripts of *rab5a2* in nodal signalling in addition to analysing the effect of *rab5a2* on exogenously supplied *nodal* RNA. Finally this thesis uses microarray analysis to identify other genes and possible pathways affected by the knocking down of *rab5a2.* The results show a complex and vital role for *rab5a2* in cell signalling and zebrafish development and that its loss of function impacts on many hundreds of genes.

Chapter 2

Materials and Methods

2.1 Embryology methods

2.1.1 Embryo Fixation

At different stages of embryo development 10 embryos were placed in Eppendorf tubes and the water replaced with 4% PFA in PBS. These were stored overnight at 4°C. If embryos were over 20 somites the chorions were removed before fixing in PFA. If the embryos were younger than 20 somites the chorions were removed after fixing. Fixed embryos were dehydrated by washing 3 times with 100% MeOH. They were then stored in 100% MeOH at -20°C.

2.1.2 In Situ Hybridization Analysis.

The embryos were rehydrated by serial incubations of PBT and methanol (75% MeOH /25% PBT for 5 min, 50% MeOH -/50% PBT for 5 min, 25% MeOH /75% PBT for 5 min, 100% PBT for 5 min twice). They were then placed in hybridisation mix (HM) for 5 min, the HM was changed and the embryos placed in the incubator at 68°C for no less than 1 hour. The HM was then removed and replaced with 200µl of HM containing 1 µg/ml of probe and left to hybridise overnight at 68°C.

The embryos were washed in 50% HM/50% 2×SSC for 5 min, 2×SSC for 15 min, and 0.2×SSC for 2 x 30 min at 68°C. They were then washed with 50% 0.2×SSC/50% PBT for 10 min and PBT for 10 min at room temberature (RT). The embryos were finally washed in fresh PBT/2% goat serum/2mg:ml BSA and left for several hours at RT. The PBT was then replaced with PBT/2% goat serum/2mg:ml BSA containing 1:2500 dilution of anti-dig solution (Roche) and left at 4°C overnight.

The PBT antibody solution was removed and the embryos washed with PBT (PBT quick wash, PBT for 3×5 min, PBT for 4×15 min all at RT). The embryos were then washed with staining buffer (2×5 min) incubated in staining solution (NBT/BCIP (Roche)) in the dark and monitored for expression. The staining reaction was stopped

by removing the staining solution and washing the embryos in PBS pH 5.5/2mM EDTA for 3 min. The embryos were then fixed in PFA for 20 min at RT.

2.1.3 Designing UTR or ATG Morphlino's

Antisense MO-modified oligonucleotides or MOs will be used for loss of function anlysis. In zebrafish these are both effective and specific translation inhibitors (Nasevicius and Ekker, 2000). The MOs were designed using the known sequences for each zebrafish *rab* and 25 bases of sequence unique to that gene designed either against the start codon (ATG) of the open reading frame or against the 5' UTR region. These were then sent for synthesis to Genetools (www.gene-tools.com). The MOs arrived back in a powdered form that was re-hydrated in distilled water. The MOs were quantified and the working doses achived by dilution with phenol red and MO buffer (see section 2.1.5). Phenol red was used as it is pH sensitive and therefore enables visualization of those embryos that were not correctly injected.

2.1.4 Designing Splice MO's

Splice MOs were designed by identifying an intron exon boundary of the gene of interest. A MO was then designed against 25 bases of this region with at least 10 bases in the intonic region and at least 10 bases in the exonic region. The sequence was then sent to Genetools for synthesis. The MO was then diluted as in section 2.1.5.

2.1.5 Resuspension, cleaning and dilution of MOs

The powdered MO was dissolved in 60µl of distilled water. 1µl of MO was diluted in 800µl of HCl 0.1M and quantified using a spectrophotometer. The concentration of MO was calculated as follows:

$$C(\mu g/\mu l) = (A \times 800 \times MW) / \text{molar absorbency}(\varepsilon)$$

Where A was the value from the spectrophotometer. The stocks were diluted in phenol red at 2ng, 4ng and 8ng per 1.4nl.

2.1.6 Microinjection of embryos at the 1- 8 cell stage

The embryos were injected using a pneumatic picopump (World Precision Instruments inc.) attached to nitrogen-filled tubing and holder. This was mounted on a Narishigne micro manipulator which was in turn mounted on a Kanetec stand. The injection needles used were filamented borosilicate glass capillaries (World Precision Instruments inc 1B00F-4) pulled using a Kopf needle puller (model 720 at solenoid level 3 and heat level 15) and the edge cut with a razor blade, and calibrated under the microscope with a millimetre ruler. The embryos were aligned for injection along a glass slide placed in a glass petri dish. 1.4nl of the desired solution was injected into the yolk of the embryo at the 1-4 cell stage under a Leica dissecting microscope.

2.1.7 Microinjection of embryos for 1 cell in 128

Embryos were de-chorionated on agarose in 1x danieau solution at the four cell stage. A ramp was made by placing a glass slide at a slight angle into a small petri dish containing 2% molten agarose (Sigma) in 1x Danieau solution. When the agarose was set the slide was removed and the dish filled with 1x Danieau solution. A filamented borosilicate glass capillarie (World Precision Instruments inc 1B00F-4) was pulled into a needle and the end cut with a razor blade. The needle was filled with the desired solution and calibrated to inject 100pl. When the embryos reached the 64 cell stage they were lined up on the ramp, when they reached the 128 cell stage a single cell in the animal pole was injected (see section 2.1.6 for apparatus used).

2.1.8 Visualizing biotinylated-dextran.

Embryos were fixed (see section 2.1.1), rehydrated (see section 2.1.2) and incubated for 30 minutes in 1:5000 avin in PBT. The embryos were then washed 3 times with PBT and soak for 30mins in 0.4mg/ml DAB/PBT (Sigma). The solution was then changed for DAB/PBT with 0.003% H_2O_2 and watched for 30mins. Once the desired staining was achieved the reaction was stopped by rinsing with PBT. The embryos were then fixed in PFA for 20 mins at RT.

2.1.9 Fixing Embryos for Protein and/or RNA extraction.

Embryos were transferred into a clean Petri dish and washed once in 1x Danieau solution. The required number of embryos were placed in a 1.5ml Eppendorf and washed again. All the Danieau solution was removed leaving. The tubes were then flicked so the embryos are arranged along the side of the tubes. The tubes were then snap frozen in dry ice and stored at -80.

2.1.10 Assaying epiboly movements

The embryos were de-chorinated at dome stage, 30% epiboly and shield stage in a petri dish containing 1% agarose and filled with 1x Danieau solution. The embryos were then placed in glass dishes contaning 5mg/ml of biotinylated-dextran (Molecular probes 10,000mw lysine fixable) in 1x Danieau solution for 20 minutes. The embryos were then washed 3 times over 15 minutes and fixed in 4% PFA.

2.1.11 Staging embryos

During the Rab screen in Chapter 3 the embryos were staged according to time post fertilization. Therefore, both the control MO injected embryos and the *rab* morpholino injected embryos are the same age but not necessarily the same developmental stage. This enables any developmental delay to be visualized. In contrast during both the characterization- and microarray analysis of *rab5a2* (Chapters 5 and 6) the experimental and control embryos were analyzed at the same developmental stage. Here, the time post fertilization differed due to the developmental delay seen in the experimental embryos. Staging in this way was necessary to compare the pathways affected by *rab5a2* at set developmental stages.

2.2 Molecular Methods

2.2.1 Synthesis of Probe

2µg of plasmid was linearised by digesting with the appropriate enzyme for 2hrs at 37°C. The total volume was then made up to 100µl. 100µl of phenol/chloroform/isoamylalcohol solution was added to the linearised DNA vortexed briefly and centrifuged for 2 minutes at 13000rpm. The top layer was removed and put in a clean Eppendorf. 100µl of chloroform/isoamylalcohol solution was added vortexed and centrifuged for a further 2 minutes. The top layer was again removed and put in a clean Eppendorf. 10ul of NaAc (3M pH 5.2) and 3x100% ethanol was added. This was left at –20°C for 1hour and then centrifuged at 13000rpm for 30 minutes. The ethanol was removed and 300µl of ice cold 70% ethanol added and then centrifuge at 13000rpm for 10 minutes. The ethanol was removed and the DNA pellet dried at 37°C. The DNA was then resuspended in 8.5µl of water.

The RNA was synthesized by adding 4µl of 5x transcription buffer (NEB), 2µl of 0.1M DTT, 2µl of NTP-DIG-RNA (Roche), 1.5µl of RNAse inhibitor (NEB) and 2µl of polymerase (NEB) to the resuspended DNA. This was incubated at 37°C for 2hrs. A 1µl aliquot of the RNA was removed and run on a 1% agarose/TAE gel to estimate the amount of RNA synthesized. The volume of the reaction was then increased to 50µl and 2µl of DNase I (ribonuclease-free) (Promega) was added. The reaction was then incubated at 37°C for 30 minutes to remove the DNA template and leave only RNA.

The RNA was recovered by centrifuge using a Chroma spin-100 column (Clontech). The column was first centrifuged to remove the water. The volume of RNA was increased to 100µl and added to the column which was spun at 3000rpm for 5 min to recover the RNA. The RNA was quantified in a spectophotometer and diluted to the desired concentration using RNAse free water.

2.2.2 PCR amplification of DNA

5µl of template DNA, 5µl of forward primer (10µM), 5µl reverse primer (10µM), 0.5µl polymerase (eg. Taq), 10µl 5x PCR buffer and 24.5µl H_2O were mixed together in a 0.2ml PCR tube. The tube was placed in the thermal cycler (MJ Research inc) at:

1) 94°C for 2min
2) 94°C for 15 seconds
3) Annealing temperature of primers for 30seconds
4) 72°C for 30 seconds
5) Goto 2 29 times more

To check the size of the PCR product 1µl of the reaction was run on a 2% agrose (Sigma) gel with an appropriate DNA ladder.

2.2.3 Cloning

2µl of PCR product, 1µl of salt solution, 1µl of TOPO cloning vector and 1µl of sterile water were mixed together in and Eppendorf tube and left to incubate at room temperature for 20 minutes. They were then placed on ice.

2.2.4 Transformation

2ul of the TOPO Cloning reaction was added to 20µl of One Shot TOPO 10 chemically competent E.Coli and mixed gently. The mixture was incubated on ice for 20minutes and then heat-shocked for 30 seconds at 42°C. The tubes were immediately transfered on to ice and left for 2 minutes. 250µl of room temperature SOC medium was added to the reaction, the tubes were caped tightly and shake horizontally (200rpm) at 37°C for 1 hour. Pre-warmed selective plates were spread with either 25µl or 200µl of the transformation reaction and incubated overnight at 37°C. Finally 3-5 colonies were picked and cultured in L-broth with a suitable selective antibiotic over night at 37°C. The culture was then centrifuged and the supernatant drained. The plasmid DNA was then recovered from the remaining pellet by the use of a Qiagen miniprep kit.

2.2.5 Recovery of Plasmid DNA from E.Coli.

This was done using a Qiagen mini prep kit using the protocol set out by the manufacturer.

2.2.6 5' capped RNA synthesis

5µl of linearised DNA, 10µl of 5x transcription buffer, 5µl of 0.1M DTT, 5µl of 5mM CAP (NEB), 5µl of 1mM GTP (NEB), 5µl of 5mM UTP (NEB), 5µl of 5mM ATP (NEB), 5µl of 5mM CTP (NEB), 2µl of RNAse inhibitor (NEB) and 3µl of polymerase (NEB) were mixed together in a 1.5ml Eppendof tube and incubateed at 37°C for 20mins. 4µl of 10mM GTP was added to the reaction which was incubate at 37°C for a further 2 hours. 1µl of the reaction was then run on a 1% agarose gel (Sigma) to check whether the RNA was synthesized. 3µl of RNAse free DNAse (Promega) was added and the reaction incubated at 37°C for a further 20 mins. 1µl of the reaction was then run on a 1% agarose gel. The volume of the reaction was increase to 100µl and the RNA recovered using chroma-100 spin columns (see section 2.2.1).

2.2.7 Agarose Gel Electrophoresis.

A 1% agarose gel was prepared by dissolving agarose in TAE and adding 5µl of ethidium bromide per 100ml. The gel was poured into a gel tray and combs placed in until set. Once set the combs were removed and the gel placed in the gel tank with TAE poured to the fill line on the tank. 10µl of ladder was loaded into the first lane with 1µl of the sample mixed with 9µl of orangeG load buffer loaded into subsequent lanes.

2.2.8 Extracting RNA from injected embryos

30 embryos were prepared as described in section 2.1.9. 100µl of Trizol was added to the frozen samples which were then homogenised (blue pestles from Eppendof). 20ul of chloroform was added and the tubes shaken vigorously for 15 seconds. The tubes were left at room temperature for 2-3minutes then centrifuged at 1200xg for 15minutes at 4°C. 70µl of the clear supernatant was removed and place in a clean 1.5

ml Eppendorf tube with 70µl of isopropanol. The samples remained at room temperature for 10 minutes and were then spun for 10minutes at 4°C. The isopropanol was removed leaving a pellet.The pellet was washed with 120µl of 70% ethanol and vortexed briefly. The pellet and ethanol were spun at 7,500xg for 10 minutes. The ethanol was removed and the pellet dried. The pellet was resuspended in 30µl of H_20 and 1µl run on a 1% agarose gel.

2.2.9 Making cDNA

1.5µg of RNA was placed in a clean Eppendorf and the volume made up to 12µl with water. 1µl of 0.5µM random primers were added to the RNA and the tube spun briefly. The samples were then incubated at 70°C for 10 minutes. 4µl of (5x) 1st strand buffer, 1µl of (10uM) DNTP's and 2µl of (0.1M) DTT was added and incubated at 42°C for 2minutes. 1µl Superscript RT (200U/ul) was added and the reaction incubated at 42°C for 1 hour. The reaction was heated to 70°C for 15 minutes and spun briefly. Finally the reaction was placed on ice for 10 minutes and stored at -20

2.2.10 Taqman RT-PCR

Using cDNA made from the protocol in section 2.2.9 a dilution plate was made. A control sample was diluted 1/10, 1/100 and 1/1000. All other samples were diluted 1/10.

2µl of the undiluted control was placed in the first well of a 96 well of an Applied Biosystems ABI optical plate, 2µl of 1/10 control dilution was placed in the second well, 2µl of of the 1/100 control dilution was placed in the third well and 2µl of the 1/1000 dilution placed in the fourth well. 2µl of all other samples were placed in the remaining wells. To each sample (including control dilutions) was added 10µl of Applied Biosystems TaqMan Universal PCR Master Mix, 1µl of TaqMan primer and 7µl of water. This was repeated using all the required primers and control primers

Each plate was then sealed with Applied Biosystems ABI optical adhesive covers (4311971). The plates were then placed in the RT-PCR (ABI prism) machine. Using the 7000system software the programme was set to absolute quantification for a 96 well plate and set for a 20µl reaction. The programme was then run and results saved for analysis.

2.2.11 Producing GFP-Nodal Fusion constructs

The cleavage sites for both Sqt and Cyc were identified (Figure 2.2.1) (Squint –$^{5'}$-CGGCGCCACAGAAGG$^{-3'}$,Cyclops–$^{5'}$-CTCAGGAGCCGCAGG$^{-3'}$) (Rebagliatia et al., 1998) and primers designed to isolate the pro and mature regions (Table 2.4.2)

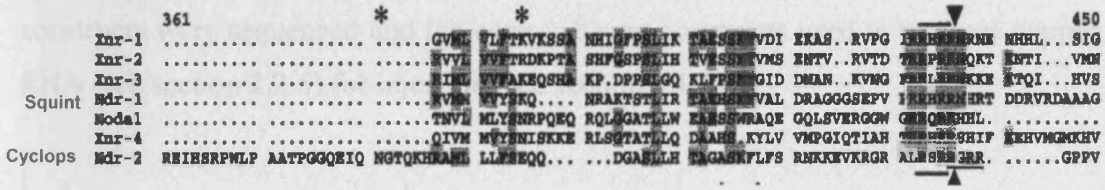

Figure 2.2.1: Cleavage site of Nodals in *Xenopus laevis* and zebrafish.
The yellow blocks identifiy the cleavage regions in zebrafish squint and cyclops.

The pro and mature regions of *sqt* and *cyc* were amplified from cDNA by PCR using KOD polymerase. A one percent agarose gel was run to check for the correct size product. The PCR products were cleaned using a Qiagen MinElute kit.1µl of Taq was added to 10µl of PCR product and 5µl of buffer and incubated at 72°C for 10 minutes. The products were cloned into the Invitrogen GFP cloning vectors (pcDNA3.1/CT-GFP TOPO and pcDNA3.1/NT-GFP TOPO) according to the Invitrogen protocol with the pro regions in the C-terminal linked GFP vector (pro-GFP) and the ligand regions in the N-terminal linked GFP vector (GFP-ligand).The clones were sent away for sequencing for conformation of correct insert.

The pro-GFP and GFP mature constructs were digested using the restriction enzymes BsrG1 and Xma1. The digests were then run on a gel and the large fragment from the pro-GFP construct cut from the gel and cleaned using a Qiagen gel extraction kit. This process was repeated for the smaller fragment of the GFP-ligand construct. The

large pro-GFP fragment was treated with SAP (Promega) as described by the manufacturer. The large pro-GFP fragments and the small GFP-ligand fragments were then ligated together (Figure 2.2.2) using T4 DNA ligase (Promega) as described by the manufacturer. The constructs were then transformed as described in section 2.2.4 and the DNA recovered using a Qiagen minprep kit.

The DNA was sequenced and the correct fusion constructs amplified using primers from Table 2.4.2 which add restriction sites to the amplified products. The amplified products and the insertion vector (pCS2+) were digested using EcoR1 and BamH1 and the products run on a gel. These were cleaned and ligated using T4 DNA ligase (Promega) as described by the manufacturer. The constructs were then transformed as described in section 2.2.4 and the DNA recovered using a Qiagen minprep kit. The constructs were sequenced and the correct fusion constructs used to produce capped RNA (see section 2.2.6) for injection (see section 2.1.6).

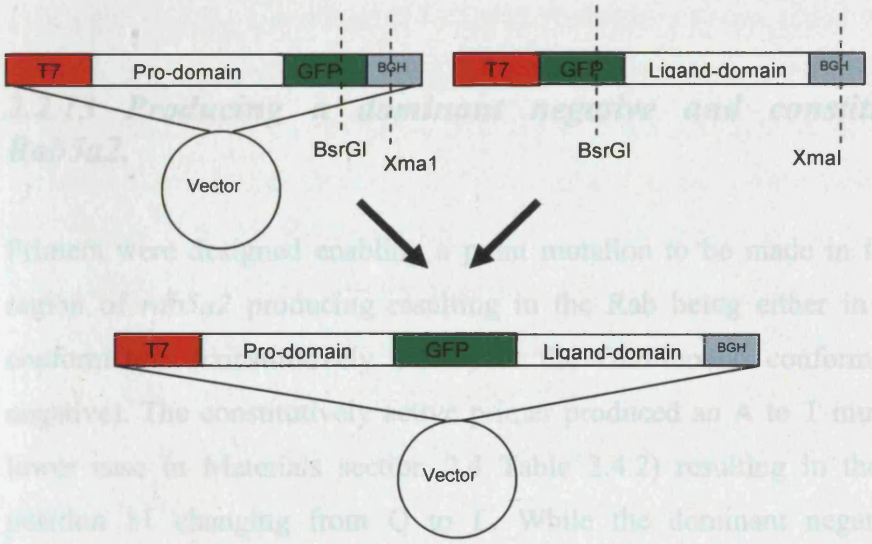

Figure 2.2.2: A diagrammatic representation of the methods used to make a GFP-nodal fusion construct

Showing the promoter domains and the restriction enzymes used and where they cut.

2.2.12 β-catenin stain

Embryos were fixed in 4% paraformaldehyde in phosphate-buffered saline (PBS) for four hours at 4°C. The embryos were then dechorionated and washed with PBS/ 0.1% Triton X-100 (PBS-Tr) five times. The embryos were then washed with

PBS/0.1% Triton X-100/% DMSO (PBS-DT) and blocked with 5% bovine serum in PBS-DT for one hour. After one hour the embryos were incubated with anti-β-catenin antibodies (1/500 dilution, Sigma C2206) overnight at 4°C. The embryos were then washed four times with PBS-Tr and incubated with secondary anti- rabbit antibody at 1/500 dilution, from the VECTASTIN ABC kit, for six hours at room temperature. The embryos were washed four times with PBS-Tr. Two drops of solution A and two drops of solution B (vectastain ABC kit) were added to PBT and left for 30min at RT after which time they were added to the embryos and left at RT for one hour. At the end of the hour the embryos were washed six times over the period of one hour. A diaminobenzidine (DAB, Sigma) tablet was dissolved in 33ml of PBT and any particulate spin out. 1ml of this was added to each of the goups of sample embryos which were left to incubate for 10minutes in the dark on glass. 1μ of 30% H_2O_2 is then added to the DAB and embryos these were then left in the dark and observed for staining. When it was time to stop the reaction the embryos were wahed in PBT.

2.2.13 Producing a dominant negative and constitutively active Rab5a2.

Primers were designed enabling a point mutation to be made in the GTP binding region of *rab5a2* producing resulting in the Rab being either in the GTP-bound conformation (constitutively active) or the GDP-bound conformation (dominant negative). The constitutively active primer produced an A to T mutation (shown in lower case in Materials section 2.4 Table 2.4.2) resulting in the amino acid at position 81 changing from Q to L. While the dominant negative primer also produced an A-T mutation (shown in lower case in Materials section Table 2.4.2) resulting in the amino acid at position 133 changing from N to L.

Using the Stratagene QuikChange Site-Directed Mutagenesis Kit 1μl of ds-DNA template (50ng) was added to a PCR tube containing 2.5μl of 10X QuickChange Multi reaction buffer (Stratagene), 18.3μl of double-distilled H_2O, 1.2μl of 10μM mutagenic primers, 1μl of dNTP mix (Stratagene) and 1μl of QuickChange Multi

enzyme blend (Stratagene). The reaction was placed in the thermal cycler (MJ Research inc) at:

1: 95°C for 1minute
2: 95°C for 1minute
3: 55°C for1minute
4: 65°C for 4minutes 45 seconds
5: Repeat from step 2 29 more times

The reaction was placed on ice for 2 minutes.1ul of *Dpn* I (Stratagene) restriction enzyme (10U/ µl) was added to the reaction which was pipetted up and down several times to mix the reaction. The reaction was spun for 1 minute then incubated at 37°C for 1hour.

45µl of the XL10-Gold (Stratagene) ultracompetent cells were transferred to a prechilled 14ml BD Falcon polypropylene round-bottom tube (BD biosciences Catalog 352059). 2µl of the β-ME mix (Stratagene) was added to the cells. The contents were swirled and incubated on ice for 10minutes swirling every 2 minutes. 1.5µl of the *Dpn* I –treated DNA was added to the ultracompetent cells which were then incubated on ice for a further 30 minutes. The cells were then heat pulsed in a 42°C water bath for 30 seconds and then incubateed on ice for 2 minutes.0.5ml of preheated (42°C) NZY+ broth was added to the reaction. The reaction was incubated at 37°C for 1 hour shaking at 225-250rpm. The DNA was then recovered using a Qiagen miniprep kit and sequenced to check for only the required mutation. All controls were performed as described in the Stratagene QuikChange Site-Directed Mutagenesis Kit

2.3 Expression Array

2.3.1 Total RNA extraction from tissue using Trizol.

The embryos were homogenised in 1.5ml Eppendorf tubes in 10 volumes of Trizol per embryo with a pestle (Eppendorf). The homogenate was then triturated six times with a 1ml filtered pipette tip then six times with a 200µl filtered pipette tip. The embryos were incubated for 5 minutes at room temperature. Phase Lock Gel-Heavy tubes were prespun at 1500rpm for 30seconds. The cell lysate was added to the Phase Lock Gel-Heavy and incubate at room temperature for 4 minutes. 0.2 ml of chloroform per 1 ml of TRIzol reagent initially used was added to the tubes. The tubes were capped and shaken vigorously for 15 seconds after which they were centrifuged at 12,000xg for 10 minutes at 2–8°C. The clear aqueous phase containing the RNA was transferred to a fresh 1.5ml Eppendorf tube. The RNA was precipitated by adding 0.5 mlof Isopropyl alcohol per 1ml Trizol reagent initially used. The samples were mixed by repeated inversion and allowed to incubate at room temperature for 10 minutes. The samples were centrifuged for 10 minutes at 12,000xg at 2–8°C. The supernatant was removed and the RNA pellet washed by adding 1ml of 75% ethanol per 1ml Trizol reagent initially used. The samples were vortexed and centrifuged at 7,500xg for 5 minutes at 2–8°C. The supernatant was removed and the pellet briefly air-dried. The RNA pellet was dissolved in 20µl of RNase free water and incubated at 55–60°C for 10 minutes. The RNA was quantitated using a Nano drop and 1 µl of each sample run on a 1% gel.

2.3.2 Generation of Amino Allyl-modified Amplified RNA (aRNA)

This protocol uses the Ambion Amino Allyl MessageAmp™ II aRNA Amplification Kit all reagents were from this kit unless otherwise stated.

2µg of RNA was prepared in 10µl of RNase-free water in a 0.5ml tube and placed on ice.1µl of T7 Oligo (dT) Primer (Ambion) and 1µl of 0.1X bacterial mRNA cocktail were added. The RNA oligo mixture was incubated at 70°C for 10 min and snap-chilled on ice. 2µlof 10x First Strand Buffer (Ambion), 4µl of dNTP mix (Ambion),

1µl of Rnase inhibitor (Ambion) and 1µl of ArrayScript (Ambion) were added to the mixture.The reaction mixture was spun briefly and incubated at 42°C for 2 hours and then chilled on ice for 2 minutes. 63µl of Nuclease-free water, 10µlof 10X Second Strand Buffer, 4µl of dNTP Mix, 2µl of DNA Polymerase and 1µl of Rnase H was added on ice to the reaction mixture and mixed gently. The samples were spun briefly and incubated at 16°C for 2 hours. 250µl of cDNA Binding Buffer was added to the samples and mixed by pipetting up and down 3-4times. The samples were transferred to a Filter Cartridge (Ambion kit) and centrifuge for 1 minute at 10,000xg. The flow-through was discarded. 500µl of wash buffer (Ambion kit) was added to the cDNA filter cartridge and centrifuged for 1 minutes at 10,000xg. The flow through was discarded. The cDNA Filter Cartridge was spun for an additional minute to remove trace amounts of buffer. 9µl of nuclease-free water (pre-heated to 55C) was added to the centre of the filter in the cDNA Filter Cartridge, left at room temperature for 2 minutes and then centrifuged for 1 minute at 10,000xg. A second 9µl of preheated nuclease-free water was added to the cartridge and spun as previously.

3µl of aaUTP (50mM), 12µl of ATP, CTP, GTP mix (25mM), 3µl of UTP Solution (50mM), 4µl of T7 10X Reaction Buffer and 4µl of T7 Enzyme Mix were added to the double-stranded cDNA at room temperature and mixed gently. The reaction mixture was spun briefly and incubated for 16 hours at 37°C. 60µl of room temperature nuclease-free water was added to the in vitro transcription reaction. 350µl of aRNA Binding Buffer and 250µl of 100% ethanol was added to each aRNA sample and mixed by pipetting the mixture up and down 3-4 times. The sample was pipetteed onto the centre of the filter in an aRNA filter Cartridge and centrifuged for 1minute at 10,000xg. The flow through was discarded. 650µl of wash Buffer was added to each aRNA Filter Cartridge and centrifuged for 1 minute at 10,000xg. The flow-through was disgarded and the aRNA Filter Cartridge spun for an additional 1 minute to remove trace amounts of wash buffer. 100µl of nuclease-free water preheated to 60°C was added to the centre of the filter. The filter cartridge was left at room temperature for 2 minutes and then centrifuged for 1 minute at 10,000xg. The aRNA in the elute was then quantitated.

2.3.3 Dye Coupling Amino Allyl-modified aRNA

Dye Coupling Reaction

The aRNA was spun for 5 minutes at 13000rpm. For each labelling reaction (2 per sample cy3 and cy5) 15µg of aRNA was removed and placed in a fresh tube. To this $1/10^{th}$ volume of 3M NaAc pH5.2 and 2.5 volumes of 100% ethanol was added and the mixture incubateed at -20°C for 30 minutes to precipitate. The precipitated aRNA was spun at 13000rpm for 5minutes. The pellet was washed with 500µl of 80% ethanol and spun at 13000rpm for 2-5minutes. The ethanol was removed and the pellet was resuspended thoroughly in 9µl of coupling buffer (Amino Allyl MessageAmp II aRNA Amplification Kit, Ambion). Light levels were reduced and activated CyDyes (CyDye Post-Labelling Reactive Dye Packs, Amersham) packs were left to equilibriate to room temperature. 11µl of DMSO (Amino Allyl MessageAmp II aRNA Amplification Kit, Ambion) was added per vial of dye pack. The resuspended CyDye was added to the aRNA in coupling buffer, mixed and incubate at room temperature in the dark for 45 minutes. 4.5ul of 4M hydroxylamine was added to the reaction mixture and incubated at room temperature for 15 minutes.

Purification of dye couples aRNA.

To each labelling reaction was added 75µl of RNase-free water and 350µl of buffer RLT from RNeasy mini kit (Qiagen). This was mixed thoroughly. 250µl of 100% ethanol was added and mixed thoroughly by pipetting. The sample was transfered to a RNeasy Mini column and spun for 1 minutes at 8000rpm. The column was removed to a fresh collection tube and 500µl of buffer RPE was added. The column was spun for 1 minute at 8000rpm.This was repeated twice. The column was placed in an elution tube and 50µl of water added. The column was incubated at room temperature for 2 minutes then spun at 8000rpm for 1 minute. Another 50µl of water was added to the column and incubated at room temperature for 2 minutes. The column was spun at 8000rpm for 1 minutes and the column discarded. The dye coupled aRNA was then quantified.

2.3.4 Competitive Hybridisation of labelled aRNA to Microarrays.

The labelled aRNA is spun for 5 minutes at 13000rpm. 2µg of labelled aRNA is removed and combined with those aRNAs to be compared on the array. 8µl of Cot-1 DNA (1ug/ul, Invitrogen), 4µl of polyA DNA (2ug/ul, Sigma), 25µl of salmon sperm DNA (10mg/ml, Ambion), 1/10th volume 3M NaAc pH5.2, 2.5 volumes of 100% ethanol were added to the combined aRNAs. The sample was incubated at 20°C for 30minutes and spun for 5 minutes at 13000rpm. The pellet was washed with 500µl 80% ethanol. The ethanol was removed and the pelley was dried for a few minutes at 70°C to remove any remaining ethanol. 10µl of water was then added and the sample incubated at 70°C for 5 minutes to dissolve the pellet. 50µl of RNA hybridisation buffer was added and mixed. The sample was the incubated at 70°C for 5 minutes and at room temperature for 10 minutes. The sample was then spun briefly, mixed and spun for 5 minutes at 13000rpm. 55µl of the hybridisation sample mixture was applied to a coverslip (25 x 60mm) placed on a flat surface. A microarray slide was gently lower onto the coverslip and placed DNA side up in the humid chamber to incubate at 47°C for 12-24 hours.

Array washes

The microarray was removed from the humid chamber and quickly placed in a slide rack submerged in 200ml of room temperature wash solution 1 (See Materials section 2.4). The slide was washed at room temperature for 5 minutes with gentle shaking. The slide rack was transfered to wash solution 2 and wash at room temperature for 15 minutes with vigorous shaking. This step was repeated with clean solution 2. The slide rack was then transfered to wash solution 3 and wash at room temperature for 5 minutes with vigorous shaking. This step was repeated with clean solution 3. After a final rinse in fresh wash solution 3, the slide rack is quickly transfered to a centrifuge and spun at 1000rpm for 1-2 minutes to dry the slides. The slides were then scanned using a laser-based scanner by PerkinElmer (ScanArray ExpressHT). The slides were analysed using image analysis software by PerkinElmer (version 3) which aligns the oligo spots and analyses the intensity of each of the dyes for each oligo spot on the array. The intensity data for each slide was then transferred into Agilent's Genespring software for analysis the difference in intensities between both dyes. This data was then grouped with the other replicates including the dye

swapped slides and analysed for differences between experimental and controls samples. The data was normalized using LOWESS (see Methods section 2.6) and finally the threshold for the fold change of gene expression between the experimental and control genes was set. For example only those genes that showed a 1.5 fold change in expression between the control samples and the experimental samples are listed to have changed. From the normalized data set those genes that show a significant change ($p<=0.05$) in a t-test were also listed to have changed. Therefore the genes that were finally selected to have changed were those that showed both a three fold change in expression and that were statistically significant. This ensures the minimum of false positive.

2.4 Materials

Phenol/chlorophorm/isoamylalcohol solution:

phenol:chloroform:isoamylalcohol = 25:24:1

Hybridisation Mix (HM):

	For 500 ml:
50% formamide	250 ml formamide
5×SSC	125 ml 20×SSC
0.1% Tween 20	500 µl Tween 20
pH adjusted to 6 with citric acid	4.6 ml citric acid 1M, pH6
50 µg/ml heparin	500 µl heparin 50 mg/ml 4×SSC
500 µg/ml Torula RNA	0.25 g Torula RNA

Staining buffer (NTMT):

	For 50 ml
100 mM tris HCl pH 9.5	5 ml 1M tris HCl pH 9.5
50 mM $MgCl_2$	2.5 ml 1M $MgCl_2$
100 mM NaCl	1 ml NaCl 5M
0.1% Tween 20	50 µl Tween 20

Staining solution:

NBT 100mg/ml - 112.5 µl

BCIP 50 mg/ml - 175 µl

Staining buffer - 50 ml

PCR buffer (5x):

2.5ml 2M KCL
1ml 1M Tris pH8.4
0.25ml 1M $MgCl_2$
200µl dATP 100µM
200µl dTTP 100µM
200µl dCTP 100µM
200µl dGTP 100µM
1.7ml BSA 10µg/ml

Phenol Red MO buffer:

1:4 25mg/ml phenol red : 5mM HEPES (pH7.2), 200mM KCl

Danieau Solution:

	30x
5M NaCl	1740mM
KCl	21mM
1M MgSO4	12mM
Ca(NO3)2	18mM
HEPES pH7.6	150mM

Expression Array:

Wash solution 1: 2X SSC filter sterilised
Wash solution 2: 0.1X SSC, 0.1% SDS, filter sterilised
Wash solution 3: 0.1X SSC, filter sterilised

RNA hybridisation Buffer:

50% formamide
5X SSC
0.1% SDS
0.1mg/ml BSA

Agarose gel for embryo manipulation

2% Agarose gel with 1x daneaus.

NZy+ Broth

10g of NZ amine (casein hydrolsate)

5g of yeast extract

5g of NaCl

Deionized H2O to a final volume of 1 liter

pH7.5

Autoclave then to 50mls of above was added:

625µl 1M MgCl2

625µl 1M MgSo4

1ml of 20% glucose (or 500µl of 2M glucose)

Gene name	MO Name	Type	Sequence	Clone
Rab3c1	zRab3c1	Splice	TGACATCAACTTACCAGTCCTGTAC	
Rab3c1	zRab3c1	ATG	TTGTCTTGCGTAGCAGCCATCTTCC	IMAGp998O1811847
Rab5a1	zrab5a1	ATG	GACAGTTGTCAATCACCCCGTCTTC	IMAGp998J226597
Rab5a2	zrab5a2	ATG	TCGTTGCTCCACCTCTTCCTGCCAT	IRAKp961M19104
Rab5b	zrab5b	ATG	CCTGCCTGTCCCACGGGTACTCATG	CHBOp575A2123
Rab5c	zrab5c	ATG	CGCTGGTCCACCTCGCCCCGCCATG	IRAKp961I04102
Rab1a3	MC14	UTR	GATTCATCGTGGACTGGACACTG	IRAKp961G04102
Rab11a1	MC3	UTR	TACGAACTCCGTGTTTTCAAATGTA	IMAGp998H109110
Rab20	MC5	UTR	AGACTCAACTCTCACAGGTAAACTC	IMAGp998N1514300
Rab3c1	MC7	UTR	CGTATAACTCCATTTGCTTTAGACA	IMAGp998O1811847
Rab11b1	MC9	UTR	ATTTTAGACAAGCCGCCCCGTCCTG	IMAGp998P2011849
Rab1a2	MC11	UTR	GTTCAGCAGGAGATCGGACTCTTTT	IRAKp961C23103
Rab11b2	MC13	UTR	ACCGCACTGAAATGTTGTTATTTAG	IRAKp961G01102
Rab6a	MC15	UTR	CAGACATGCTGCCGGTTCCACT	IRAKp961H19102
Rab28	MC17	UTR	GCTTCAGCTCGGCAGCGCGACAC	IRAKp961N08101
Rab11a2	MC19	UTR	ATCTCGATCAAAACAAAAGCGCAAA	LLKMp964G0315
Rab18(2)	MC21	UTR	ACCGGAAAATGCCTCTATGAGCAAA	MPMGp637E1023
Rab1a4	MC23	UTR	CATGACGGACAGCACGCGAAAATCC	Singapore 58G07
Rab1a1	MC25	UTR	AAAGGGCTTGTTATTGTTTGTCCAG	
Rab5a2	zRab5a2	Splice	ATGAAGCGTTTGTCTTACCTCCTAT	

Table 2.4.1 Experimental MOs showing sequence, type of MO, target gene and corresponding gene clone.

Primer Name	Sequence
Rab5a2 forward	CGGGATCCCGGTCATGGCAGGAAGAGG
Rab5a2 reverse	GGAATTCCGAGGAGCGTGGTTTAGGT
Constitutively active Rab5a2 forward	GGATACAGCTGGCCtGGAGCGCTACCACAG
Constitutively active Rab5a2 reverse	CTGTGGTAGCGCTCCaGGCCAGCTGTATCC
Dominant negative Rab5a2 forward	AGCTTTGGCTGGGAtCAAGGCAGACCTTGC
Dominant negative Rab5a2 reverse	GCAAGGTCTGCCTTGaTCCCAGCCAAAGCT
Forward Squint pro primer	ATGTTTTCCTGCGGGCTCCTGA
Reverse Squint pro Primer	TCCTTCTGTGGCGCCGA
Forward Squint ligand primer	AACCACAGAACTGATGATAG
Reverse Squint ligand primer	TCAGTGGCAGCCGCATTCT
Forward Cyclops pro primer	ATGCACGCGCTCGGAGT
Reverse Cyclops pro primer	CCCTGCGGCTCCTGA
Forward Cyclops ligand primer	GGCCGCCGGGGGCCA
Reverse Cyclops ligand primer	TCACAGGCATCCGCACT
pCs2 Cyc F	GGAATTCCATGCACGCGCTCGGAGT
pCs2 Cyc R	AAGGCCTTTCACAGGCATCCGCACT
pCs2 Sqt F	GGAATTCCATGTTTTCCTGCGGGCTCCTGA
pCs2 Sqt R	AAGGCCTTTCAGTGGCAGCCGCATTCT

Table 2.4.2: Experimental primers showing sequence, direction and target gene.

2.5 Equipment

2.5.1 Photography

Photographs were acquired using either a Zeiss Axioplan 2 compound microscope with the Axioplan camera and Axiovision 4 software or on a Leica dissecting scope with the Zeiss Axioplan camera and Axiovision 4 software.

2.5.2 Microscopy

General microscope work was done on a Leica (M295) dissecting microscope. For live embryos the microscopes own light was used. For *in situ*'s an external light source was used.

2.5.3 Confocal Microscopy

Embryos were placed in a depression slide in 1x danieau solution and covered with a 22mm x 40mm coverslip. The embryos were then viewed under a Biorad confocal microscope.

2.5.4 Optokinetic response apparatus

The optokinetic response apparatus consists of a spinning cylinder of alternating black and white colour. Inside this cylinder is a stable immobile platform on which the petri dish containing fish imobalised in methyl cellulose (Sigma) were placed (Figure 2.5.1 inset). The spinning cylinder is controlled by a dial which dictates the direction of cylinder movement and the speed (Figure 2.5.1). The apparatus was made by Loyd Stemple from technical Lego.

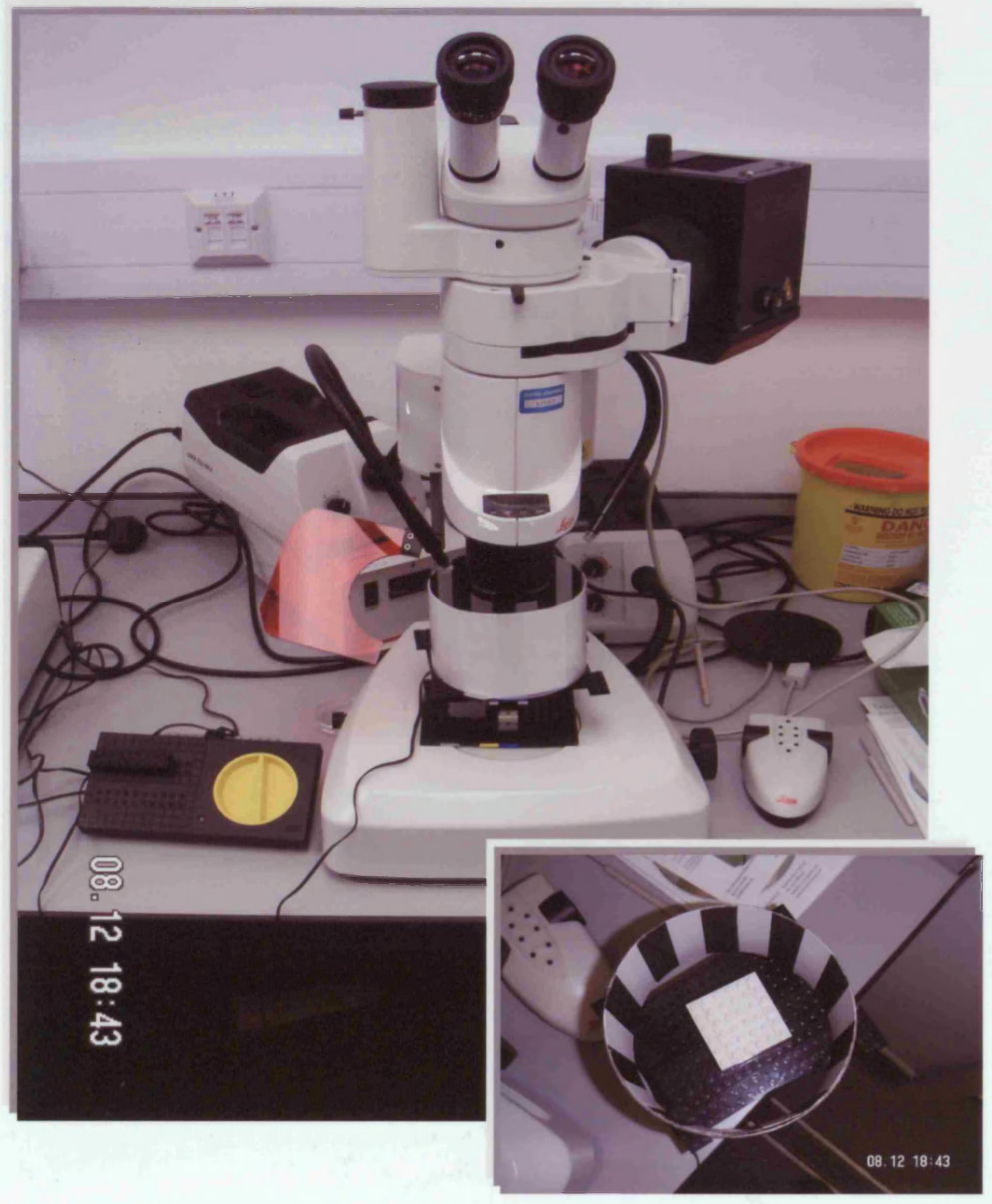

Figure 2.5.1: The optokinetic response apparatus for assaying embryos for blindness. Apparatus is seen placed under a under a Leica (M295) dissecting microscope. Inset picture shows white platform on which embryos in dish are placed and alternating white and black pattern of the spinning disk.

2.6 Statistical Analysis

The microarray data was analysed using Genespring (Agilent Technologies) which uses a standard t-test for analysis. The data is normalized to try and correct for systematic bias and remove non-biological influences. Genespring uses locally weighted scatterplot smoothing (LOWESS) for for global normaliztion. This adjusts for overall dye bias

Chapter 3

Screening the Zebrafish Rabs

3.1 Introduction

This study is a continuation of work by Dr. Isabel Campos, a former PhD student in the Stemple laboratory (Campos, 2004). With the sequencing of the zebrafish genome, more Rabs have been uncovered and there are now estimated to be over 80 *rab* genes (Clark, MD, pers. com.). cDNA clones for many of these genes have either been cloned by PCR and/or 5' and 3' RACE, or were obtained from outside sources (RZPD) and confirmed by sequencing. Design of the morpholinos (MO) for the first pass of this screen was primarily undertaken by Dr. Matthew Clark, with any additional MOs, for more in depth studies, designed by the author.

3.1.1 Loss of Function Screen

The MO for the initial pass of the loss of function screen are designed against 25 bases of the UTR region immediately 5' of the ATG start codon. There are three reasonsfor this: The first is that the UTR is considered to be more unique to the gene, a MO designed against this area is unlikely to bind any other gene, but to be sure each MO was checked by both Dr Clark and the author. Secondly, a MO in this area allows more efficient rescue by the injection of RNA encoding solely the open reading frame, as this does not contain sequence complementary to the MO. Lastly in our hands UTR MOs are usually more subtle than ATG MOs. An ATG MO, that would normally be lethal at a low dose, could show a distinct phenotype at higher does if a UTR MO were used.

In the initial pass of the Rab MO screen the embryos were injected with three different doses of MO: 8ng, 4ng or 2ng producing a dose response curve. The embryos were checked for a phenotype at gastrulation, 24 hours post fertilisation (hpf), and then each day until 5 days post fertilization (dpf). If all the embryos died then a lower dose was used, until the embryos no longer showed a phenotype. If the embryos show an abnormal phenotype, they were re-injected to check for reproducibility and photographed at shield stage if there was a gastrulation phenotype, 24hpf, 48hpf and, in some cases, later, up to 5 dpf. All *rab* MO injected

embryos were compared against embryos injected with a standard control MO supplied by Genetools at a dose 2ng higher than that of the highest does of *rab* MO.

This chapter concentrates on the Rabs screened solely by the author and shows the diverse range of phenotypes observed when *rab* expression is disrupted. These include heart phenotypes, pigmentation phenotypes, hatching phenotypes and some less specific phenotypes, such as greying of the brain indicative of cell death or tail abnormalities. Although, the Rabs do not typically exhibit a single phenotype but, rather, a host of malformations, this chapter has grouped the Rabs based on the common phenotypic features.

3.2 Pigmentation defects following knockdown of zebrafish rabs

This section focuses on those Rabs which following MO knockdown resulted in pigmentation defects. Stripe formation and colour patterning in zebrafish is an interesting system in which to study how spatial patterns form. It is also an interesting and visual way of examining at neural crest function. Most pigmented cells of vertebrates are derived from the neural crest, a transient population of cells that arises during neurulation along the dorsal neural tube and then migrates throughout the embryo (Kelsh et al., 1996). The neural crest also specifies many other cell types including neurons and glia of the peripheral and enteric nervous systems and cartilage of the head and neck (Eisen and Weston, 1993; Raible et al., 1992).

There are three types of pigment cells in zebrafish: the black melanin-containing melanophores; the yellow or orange pteridines and carotenoids containing xanthophores and the silvery guanine-rich reflecting platelets – iridophores (Parichy, 2003). Melanophores in zebrafish start to appear at 24hpf, increasing in number until around 60hpf (Yang et al., 2004), at which point, the embryo has approximately 400 melanophores. This number remains constant until approximately two weeks post fertilization, at which time the juvenile fish starts to develop its adult pigment (Milos et al., 1983; Parichy et al., 1999). A melanophore cell contains hundreds of melanin-

filled pigment vesicles, known as melanosomes. These melanosomes can be aggregated in the centre of the cell or dispersed through the cytoplasm. This pigment movement takes place in response to extracellular cues such as neurotransmitters (Levina and Gordon, 1983). The melanosome dispersion is induced by elevation of intracellular cAMP levels, while aggregation is triggered by depression of cAMP (Horowitz et al., 1980). Melanosomes are known to be associated with the microtubule based motors, dynein and kinesin (Lambert et al., 1999). Movement of the melanosome towards the centre of the cell is believed to involve the activation of the associated dynein motors (Skold et al., 2002). Movement towards the cell periphery is believed to involve the associated kinesin motors. Kinesin-2 is thought to mediate the long-range transport of melanosomes on microtubules, while myosin V, on actin filaments, is considered to be required for uniform distribution (Levi et al., 2006; Rogers and Gelfand, 1998; Wu et al., 1997). Interestingly two mammalian disorders casued by mutations in *rab27a* and *rab38* result in pigmentation defects (section 1.2.6.4 and 1.2.6.5).

3.2.1 Rab3c1

3.2.1.1 Initial Screening

Embryos injected with the *rab3c1* MO initially appeared normal and underwent successful gastrulation. By 24h hpf, about 80% of the 2ng *rab3c1* embryos had survived as the dose of *rab3c1* morpholino increased the number of embryos that survived decreased (2ng n = 31/38, 4ng n = 25/38, 8ng n = 22/43). While the 2ng embryos looked phenotypically normal many of the embryos that had been injected with either 8ng or 4ng of the *rab3c1* MO had small heads and brains (4ng n = 10/25, 8ng n = 22/22) (Figure 3.2.1 C), compared to control MO injected embryos (controls) (n = 40) (Figure 3.2.1 A). The MO injected embryos had poorly defined brain structures with the fore-, mid-, and hindbrain being disrupted (Figure 3.2.1 D). Some of these embryos also displayed heart oedema sometimes with no discernable heart tube (not shown).

At 48hpf, many of the embryos appeared normal, with the remainder possessing smaller brains, which appeared to be tinged yellow (2ng n= 2/31, 4ng n = 10/25, 8ng n = 22/22). In addition, some showed curved tails and malformed, oedematous hearts and had no circulation (2ng n= 2/31, 4ng n = 10/25, 8ng n = 12/22).

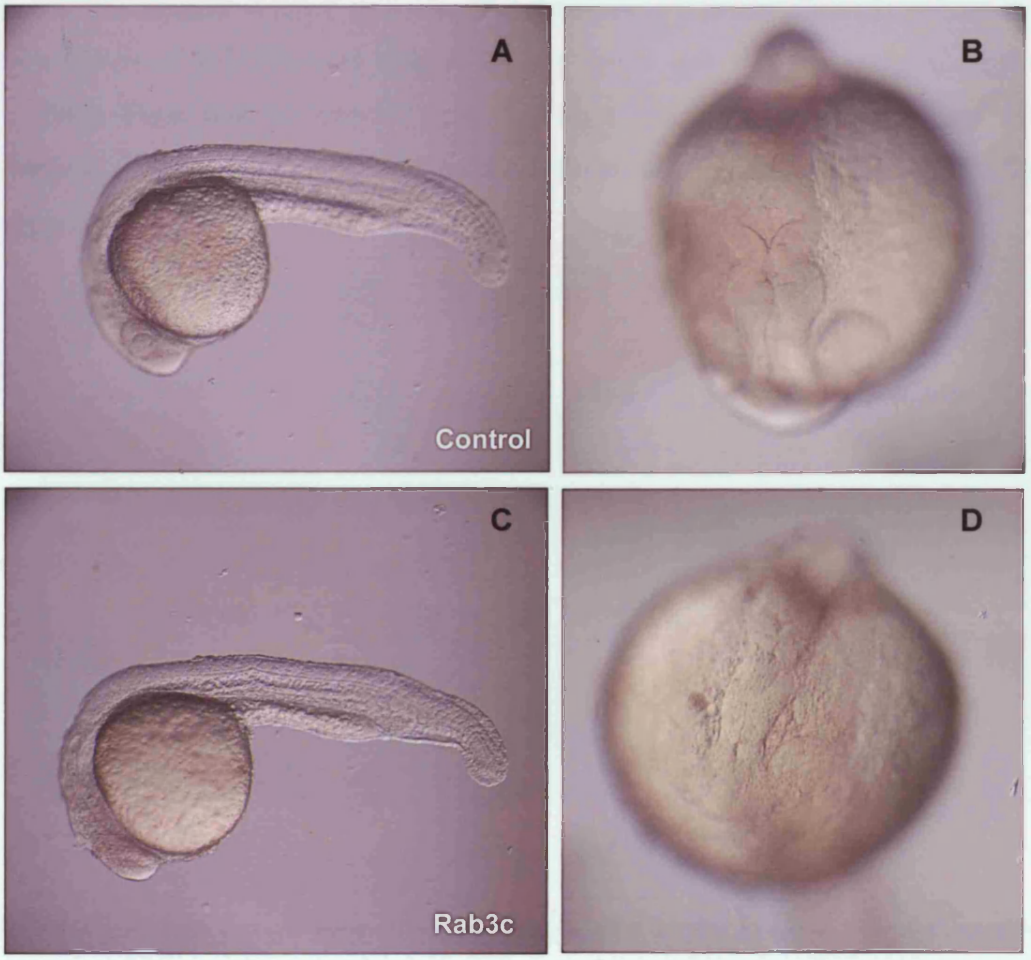

Figure 3.2.1: Lateral view of 24hpf embryos: control MO injected embryo (A) compared to 8ng *rab3c1* MO injected embryo (C). Dorsal anterior view of 24hpf embryos: control MO injected embryo (B) compared to 8ng *rab3c1* MO injected embryo (D).

By day five, the surviving embryos, were either normal or showed either defects in the distribution of melanophores, with thicker blotches of pigment being laid down on the head (2ng n = 7/31, 4ng n = 5/25, 8ng n = 10/22) (Figure 3.2.2 B and A) or a

shorter body, a smaller brain and pericardial oedema (2ng n = 2/31, 4ng n = 10/25, 8ng n = 12/22) (Figure 3.2.2 D and C). A closer look at the milder pigmentation phenotype revealed several aspects: Firstly, it showed a tight packing of melanophores on the head of the MO injected embryos (Figure 3.2.3 D and A). Secondly, the eyes of the MO injected embryos were smaller and the lens appears to be protruding (Figure 3.2.3 E and B). Finally, the swim bladder was either absent or not inflated (Figure 3.2.3 F and C). This interesting pigmentation phenotype is a characteristic of fish that have adapted themselves to darker surroundings (Logan et al., 2006). These observations led to the hypothes that the embryos were blind with constantly dark adapted pigment pattern, consistent with the defects observed in eye morphology.

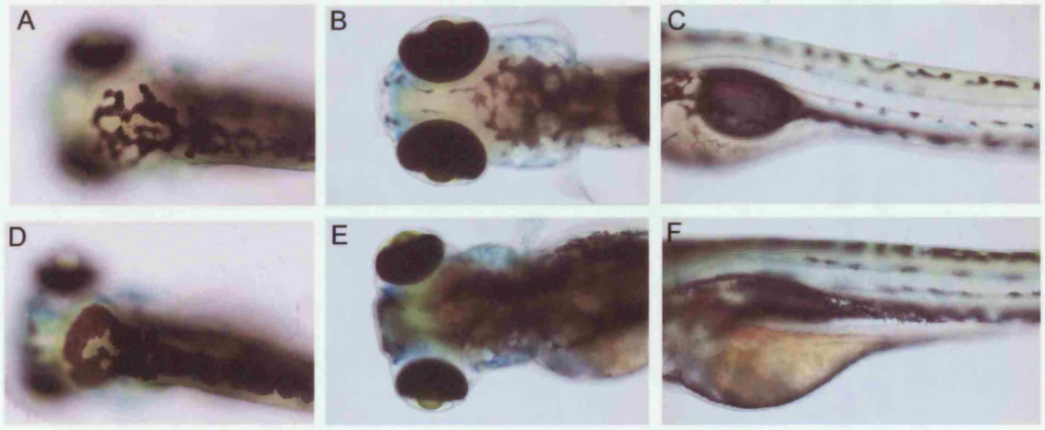

Figure 3.2.3: The dorsal view of pigment patterns in the head of five dpf control injected embryos (A) compared to five dpf *rab3c1* MO injected embryos (D). The dorsal view of eye morphology in 5 dpf control MO injected embryos (B) compared to *rab3c1* injected MO embryos (E). Side view of swim bladder in five dpf control MO injected embryos (C) compared to five dpf *rab3c1* MO injected embryos (F).

Figure 3.2.2: Dorsal view of 5dpf embryos: control MO injected embryo (A) compared to mild phenotype in *rab3c1* MO injected embryo (B) Lateral view of 5dpf embryos: control MO injected embryo (C) compared to severe phenotype in *rab3c1* MO injected embryo (D)

3.2.1.2 Assaying for blindness

To establish whether the embryos were blind, an optokinetic response apparatus was constructed (see Figure 2.5.1 Materials and Methods section 2.5.4). Each embryo was assayed individually so that movements from one embryo did not affect any other embryo. Both the control and the MO injected embryos were assayed for their ability to follow the clockwise and anti-clockwise motion of an alternating back and white spinning cylinder (see inset Figure 2.5.1 section 2.5.4). The control embryos followed the movement of the cylinder in both the anti-clockwise and clockwise directions (Figure 3.2.4 A and B see supplemental disk Mov 3.2.1A and Mov 3.2.1B). Conversely, the *rab3c1* MO injected embryos showed no response to the spinning cylinder, in either direction (Figure 3.2.4 C and D see supplemental disk Mov 3.2.1C and Mov 3.2.1D). The embryos were lightly touch-stimulated using a pair of forceps, resulting in eye movement in both control injected and *rab3c1* MO injected embryos.

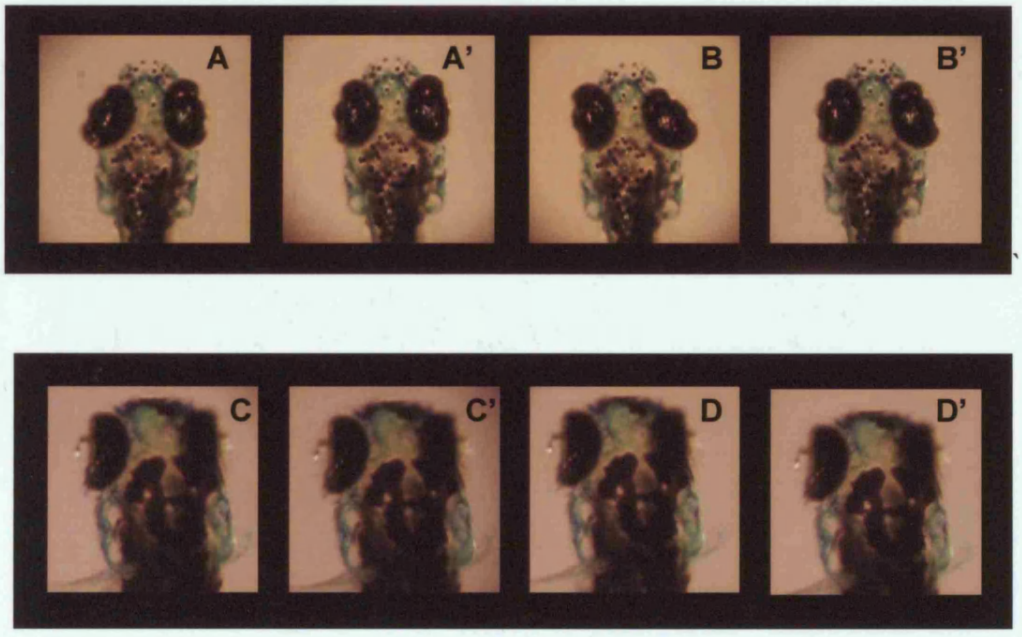

Figure 3.2.4: Still images taken from a short movie (see supplemental disk Mov 3.2.1). The stills at the top of the figure show the dorsal view of a five dpf control embryo following the spinning cylinder first in a clockwise direction (A), compared to no cylinder movement (A'), and then in an anticlockwise direction (B) compared to no cylinder movement (B'). The stills at the bottom of the figure show a five dpf *rab3c1* MO injected embryo not responding to cylinder movement in any of the directions (C, C' D and D').

3.2.1.3 Penetrance of phenotype

None of the three doses of the *rab3c1* MO produced a fully penetrant mild or severe phenotype. Therefore, the dose was increased until it became fully penetrant, or all the embryos died. The pigment phenotype increased in penetrance in a dose dependent manner (Figure 3.2.5) until 16ng. At 16ng, it was still not fully penetrant but at 19ng, all embryos displayed a phenotype far more severe. These embryos had very small brains and eyes, a short body axis and curved tail. These individuals were not assayed for blindness, since the eyes were so small that they appeared virtually absent.

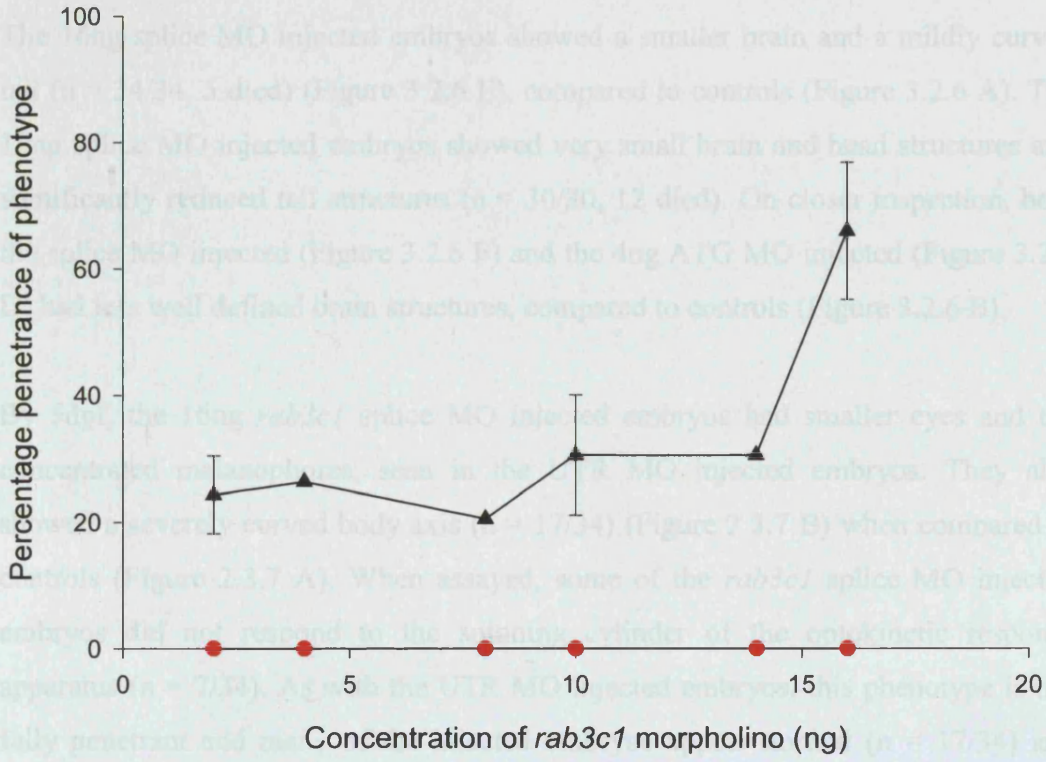

Figure 3.2.5: Graph showing the penetrance of *rab3c1* (black triangles) in a dose dependent manner (points with no error bars *n*=1 clutch, points with error bars *n*=2 or more clutches) compared to control embryos (red circles). The number of *rab3c1* injected embryos showing a phenotype at 2ng: n=7/23, 2/11 4ng: 5/19, 8ng: 10/39, 10ng: 4/19, 10/25, 14ng: 18/41 and 16ng: 35/48, 12/19, 35/39, 33/87. The number of control injected embryos showing a phenotype 2ng: 0/29, 0/15 4ng: 0/20 8ng: 0/44 10ng: 0/32, 0/30 14ng: 0/45 and 16ng: 0/45, 0/23, 0/41, 0/44.

3.2.1.4 Confirmation of *rab3c1* MO injected phenotype using alternative MOs.

To ascertain whether the phenotype observed due to the *rab3c1* MO, was a verifiable effect, two additional MOs were designed. The first was designed against the start codon of the open reading frame of the *rab3c1* gene and the second is a splice MO, designed to bind part of an intron and an exon. Either 16ng or 18ng of the splice MO was injected, as a comparison with the UTR MO. The 3 standard doses (2ng, 4ng, 8ng) of the ATG MO were injected for the screen.

At 24hpf, the 4ng ATG MO injected embryos showed smaller brains and eyes and a curved tail (Figure 3.2.6 D) (n = 35/35, 7 died), compared with controls (Figure 3.2.6 A). The 8ng ATG MO injected embryos showed a more severe phenotype, with very little brain, massively reduced eyes and reduced tail structures (n = 22/22, 17 died). The 16ng splice MO injected embryos showed a smaller brain and a mildly curved tail (n = 34/34, 5 died) (Figure 3.2.6 E), compared to controls (Figure 3.2.6 A). The 18ng splice MO injected embryos showed very small brain and head structures and significantly reduced tail structures (n = 30/30, 12 died). On closer inspection, both the splice MO injected (Figure 3.2.6 F) and the 4ng ATG MO injected (Figure 3.2.6 D) had less well defined brain structures, compared to controls (Figure 3.2.6 B).

By 5dpf, the 16ng *rab3c1* splice MO injected embryos had smaller eyes and the concentrated melanophores, seen in the UTR MO injected embryos. They also showed a severely curved body axis (n = 17/34) (Figure 2.3.7 B) when compared to controls (Figure 2.3.7 A). When assayed, some of the *rab3c1* splice MO injected embryos did not respond to the spinning cylinder of the optokinetic response apparatus (n = 7/34). As with the UTR MO injected embryos, this phenotype is not fully penetrant and many of the injected embryos appear normal (n = 17/34) and respond to the optokinetic response assay. By 5dpf, the 18ng splice MO injected embryos have all died. The 2ng *rab3c1* ATG MO injected embryos appear normal but have a mildly curved body axis (n = 25/40) (Figure 2.3.7 D). When assayed, most of the 2ng *rab3c1* ATG MO injected embryos responded to the spinning cyclinder of the optokinetic response apparatus (n = 36/40). At 4ng, they present a more severe phenotype, with the head becoming smaller (n = 35/35) but, as with the

2ng ATG MO injected embryos, these embryos were assayed and not considered blind as they responded to the spinning cyclinder of the optokinetic response apparatus (n = 34/35). The embryos injected with 8ng of ATG MO had striking defects: the body axis was greatly reduced; tail structures were reduced; and there was pericardial oedema. In the head, not only was the brain reduced but the eyes were drastically reduced in size or absent (n = 18/18) (Figure 3.2.7 F and G).

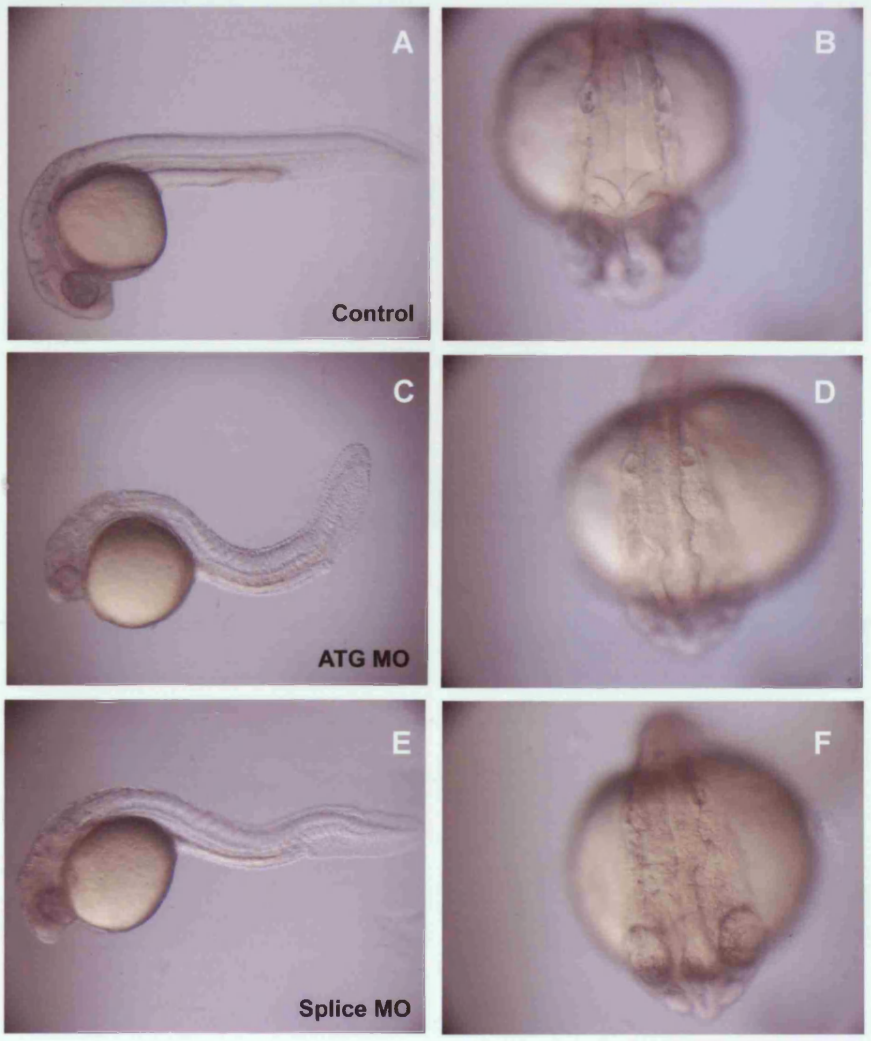

Figure 3.2.6: Lateral view of 24hpf embryos comparing control MO injected embryos (A) with 4ng injected *rab3c1* ATG MO injected embryos (C) and 16ng injected *rab3c1* splice MO injected embryos (E). A close up view comparing the brain structures of control MO injected embryos (B) with 4ng injected *rab3c1* MO injected embryos (D) and 16ng injected *rab3c1* splice MO injected embryos (F).

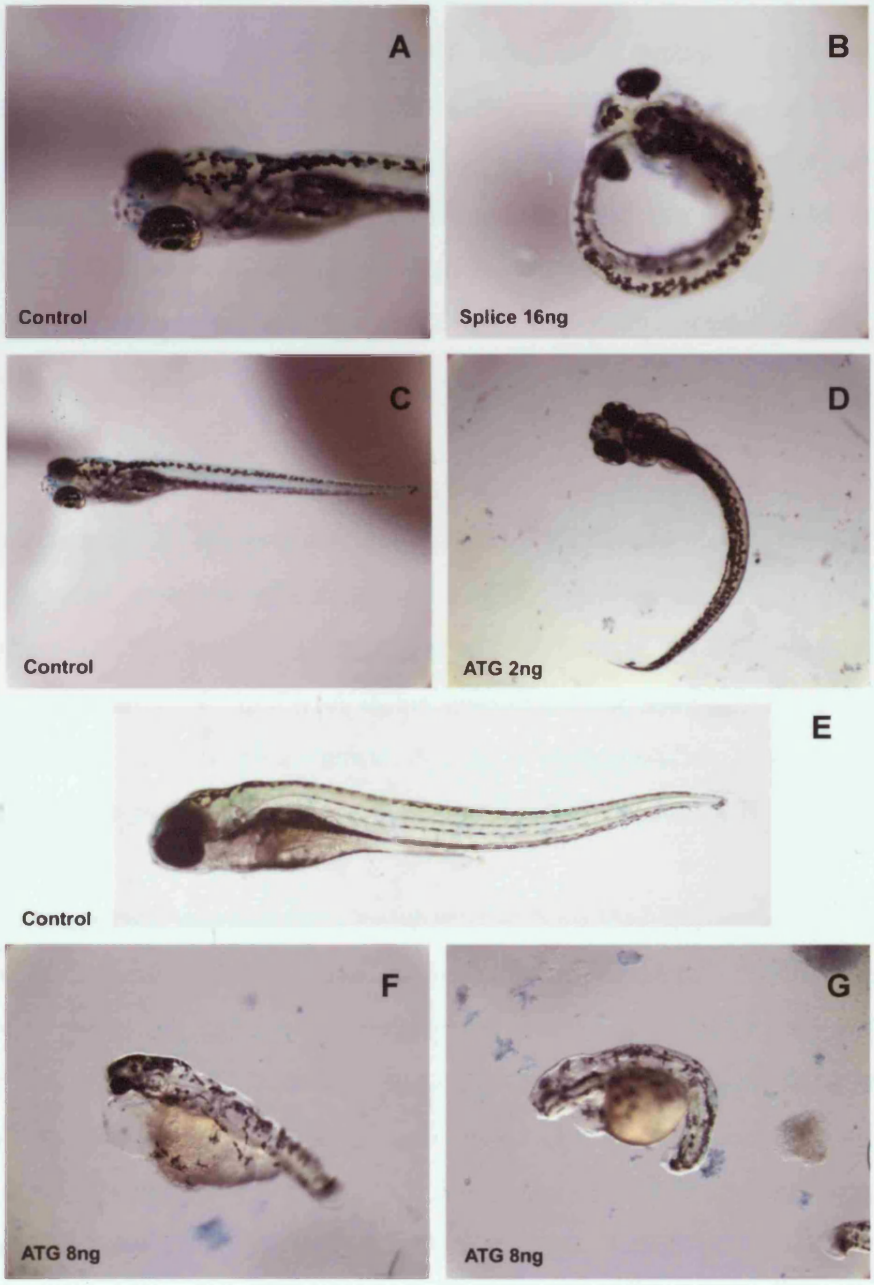

Figure 3.2.7: Dorsal view of five dpf control injected embryos (A) compared to five dpf 16ng splice MO injected embryos (B) and five dpf 2ng ATG MO injected embryos (D) compared to control (C). Lateral view of five dpf control injected embryos (E) compared to 8ng ATG MO injected embryos (F and G).

3.2.2 Rab1a3

The *rab1a3* embryos all gastrulated normally and were similar to the controls. By 24hpf, the 2ng and 4ng MO injected embryos appeared normal (2ng n = 42/42, 4ng n = 40/43). However a small proportion of the 4ng MO injected embryos had slightly reduced head size, compared to control MO injected embryos (n = 3/43). At 8ng, c. 60% of the MO injected embryos had died (n = 28/49), with 25% of the embryos exhibiting a normal phenotype. The last 15% of embryos showed a slightly reduced head size (n = 7/49).

At 48hpf, the 2ng injected embryos still appeared normal, as did the majority of the 4ng injected embryos. The remaining 4ng *rab1a3* MO injected embryos and 15% of the 8ng injected embryos still displayed slightly reduced brain size and reduced melanophore density (4ng n = 3/43 , 8ng n = 7/49) (Figure 3.2.8 D) when compared to controls (Figure 3.2.8 A). Upon closer inspection, the head (Figure 3.2.8 E) and yolk sac (Figure 3.2.8 F) had a reduced density of melanophores, in the 4ng and 8ng MO injected embryos, when compared with controls (Figure 3.2.8 B and C).

Since this phenotype was not fully penetrant the dose was increased to 10ng. Many of the embryos died prior to 24hpf, as would be expected (n = 28/46). Surviving embryos, however, all exhibited a common phenotype (n = 18/18). By 48hpf, the 10ng injected *rab1a3* MO injected embryos displayed a slightly reduced head size and a curved body axis, as well a reduced density of melanophores (Figure 3.2.9 B), compared to controls (Figure 3.2.9 A). Since the curved body axis was a new phenotype, compared with the last pass of injections, further study was warranted. The MO injected embryos possessed U-shaped somites and, interestingly, a shortened body axis, kinks in the notochord (Figure 3.2.9 D and C) and intermittent failure of vacuolation in some of the notochord cells (Figure 3.2.9 F and E).

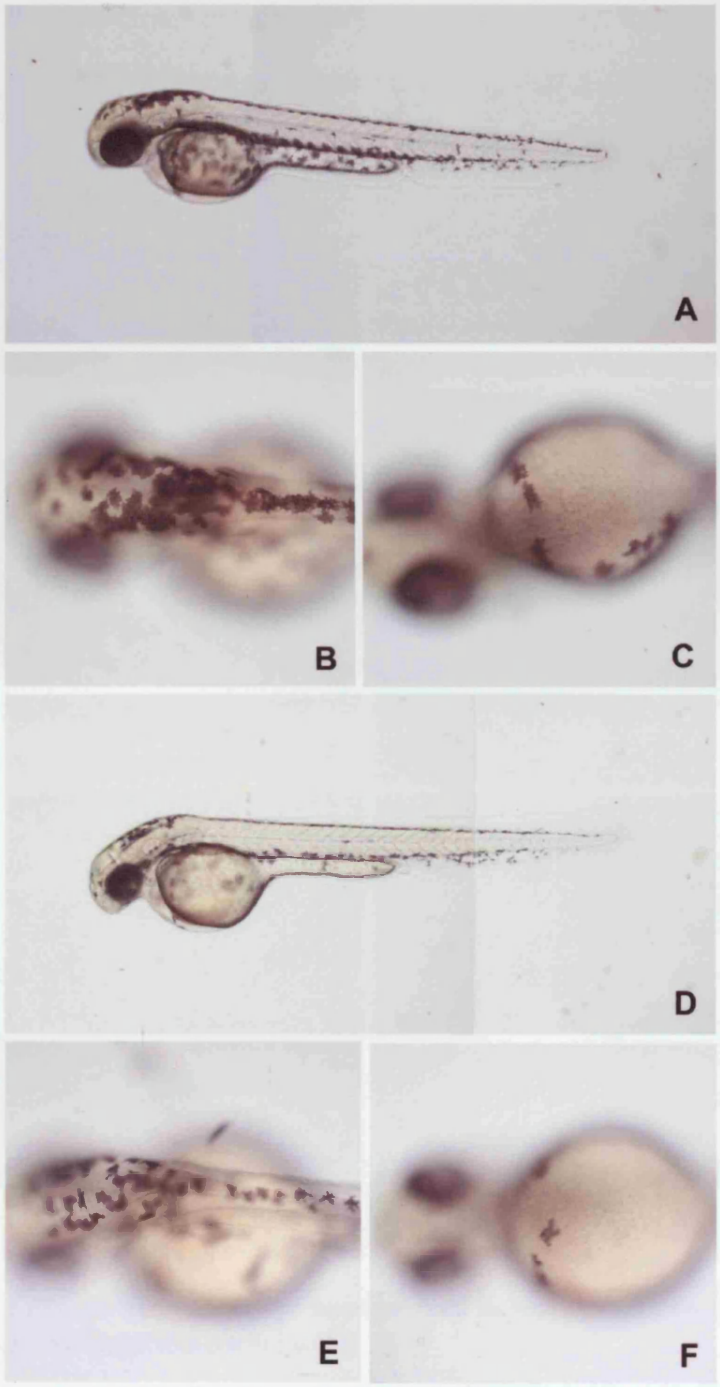

Figure 3.2.8: Lateral view of a 48hpf control MO injected embryo (A) compared to an embryo injected with 8ng *rab1a3* MO (D). Dorsal magnified view of head pigmentation of a control injected embryo (B) compared to an embryo injected with 8ng *rab1a3* MO (E). Ventral magnified view of the yolk pigmentation of a control MO injected embryo (C) compared to an embryo injected with 8ng *rab1a3* MO (F).

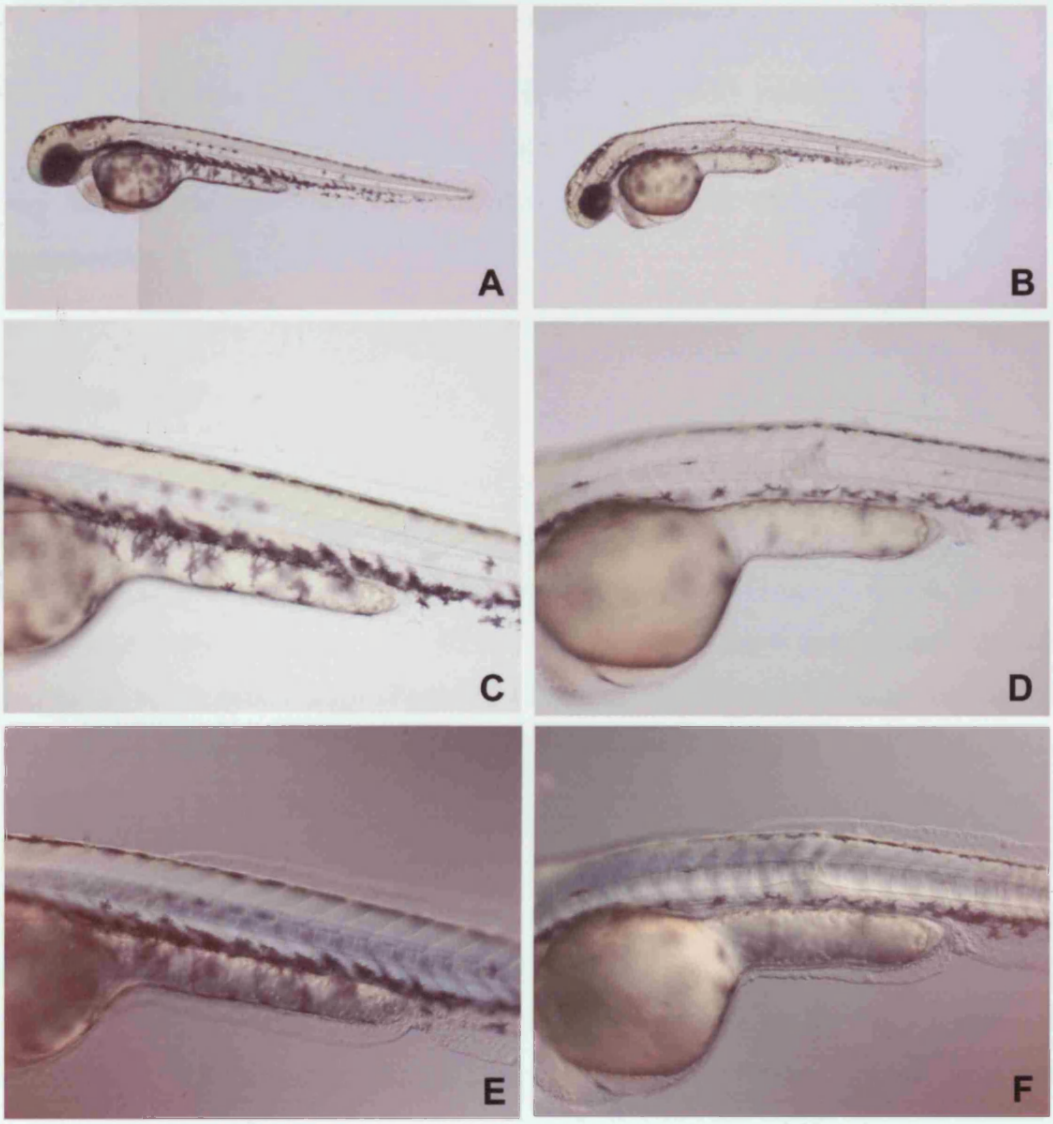

Figure 3.2.9: Lateral view of 48hpf control MO injected embryo (A) compared to 10ng *rab1a3* MO injected embryo (B).

10x magnification of the lateral view of the mid section of control MO injected embryo (C) compared to 10ng *rab1a3* MO injected embryo (D).

10x magnification of the lateral view of the mid section of a control MO injected embryo (E) compared to 10ng *rab1a3* MO injected embryo (F) under reflected light enabling a clearer view of embryo somites and notochord.

3.3 Slowed Development

This section focuses on those Rabs which following MO knockdown resulted in developmental delay. In all cases this delay was seen as early as shield stage with many MO injected embryos reaching shield stage hours after their control MO injected siblings.

3.3.1 Rab 11a1

Injection of 2ng, 4ng or 8ng's of *rab11a1* MO showed an early phenotype. When the control injected embryos had reached shield stage (n = 45) (Figure 3.3.1 A), the *rab11a1* MO injected embryos were still beginning epiboly (2ng n = 46/48, 4ng n = 38/38, 8ng n = 48/50) (Figure 3.3.1 B) and took two hours more than control injected embryos to reach shield stage (Figure 3.3.1 C). At shield stage an accumulation of cells became apparent at the animal pole (2ng n = 43/45, 4ng n = 38/38, 8ng n = 46/50) (Figure 3.3.1 C and A).

By 24hpf, the majority of embryos died, leaving approximately 10% of the 2ng *rab11a1* MO injected embryos (n = 5/48) and approximately 8% of the 4ng MO injected embryos (n = 3/38). All of the embryos injected with the highest dose of *rab11a1* MO died. The surviving *rab11a1* MO injected embryos (2ng and 4ng) had all either arrested at late gastrulation or had shortened tails with U-shaped somites and small heads (2ng = 5/5, 4ng = 3/3) (Figure 3.3.1 E and D).

When the embryos reached 48hpf, the embryos injected with *rab11a1* MO exhibited reduced distance between the eyes and smaller brains (Figure 3.3.1 G and F) and possessed a bent tail, a malformed heart and no evident circulation (Figure 3.3.1 G) (2ng n = 5/5, 4ng n = 3/3)

By 5dpf, the embryos injected with 4ng *rab11a1* MO had died while many of the remaining 2ng injected embryos had failed to hatch. (n = 5). Survivors showed some circulation, however, it was absent from the intersomitic region and blood cells appeared to adhere to the yolk.

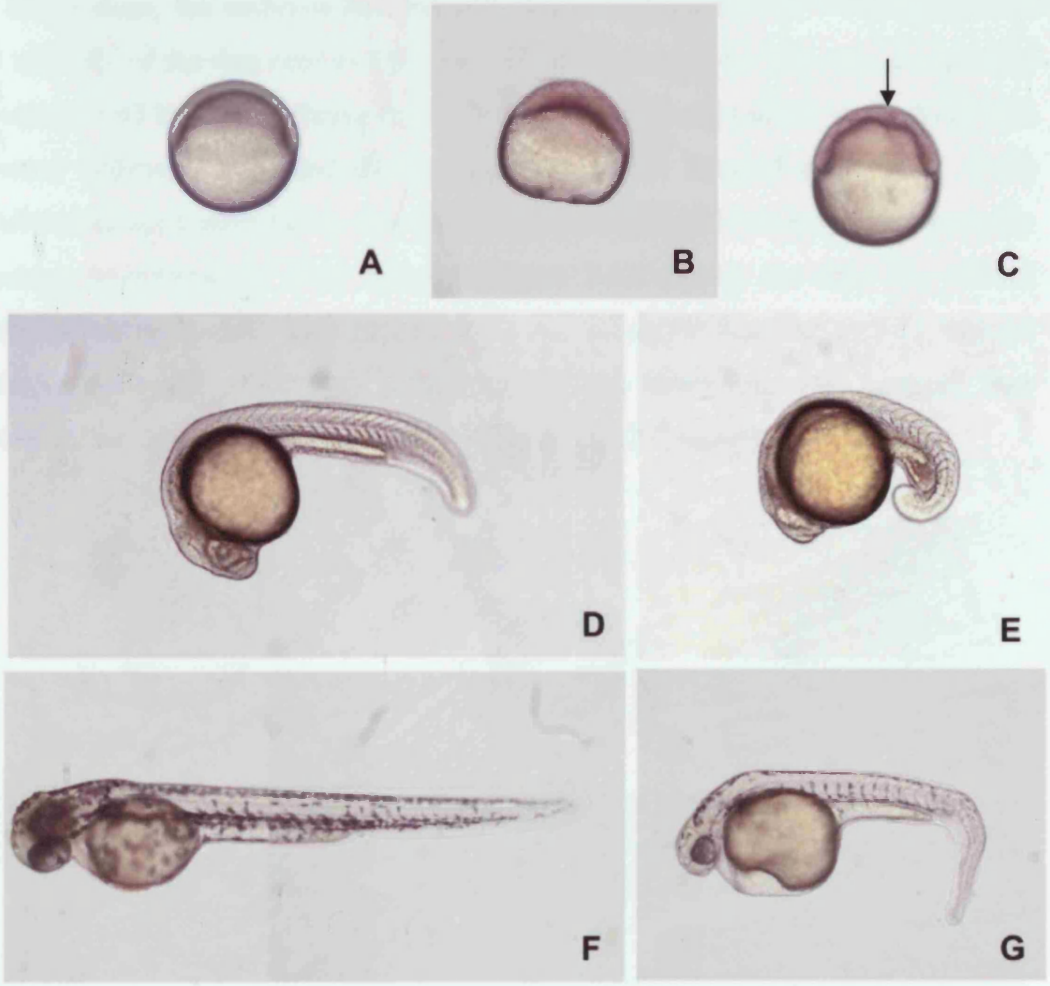

Figure 3.3.1: Shield stage embryos injected with control MO (A) compared to the same time point in embryos injected with *rab11a1* MO (B) and shield stage in embryos injected with *rab11a1* MO, arrow indicates accumulation of cells (C). 24hpf embryos injected with control MO (D) compared to 24hpf embryos injected with *rab11a1* MO (E). 48hpf embryos injected with control MO compared to (F) to 48hpf embryos injected with *rab11a1* MO (G).

3.3.2 Rab1a4

At shield stage, the embryos injected with 2ng of *rab1a4* MO (n = 45), along with the majority of the 4ng *rab1a4* MO injected embryos (n = 40/46), were comparable to control MO injected embryos (n = 47). A small proportion of the 4ng *rab1a4* MO injected embryos (6/46) and all the 8ng *rab1a4* MO injected embryos (n = 41) exhibited delayed gastrulation, this resulted in the *rab1a4* MO injected embryos only reaching approximately 20% epiboly (Figure 3.3.2 B) by the time the control embryos reached shield stage (Figure 3.3.2 A). When the 8ng *rab1a4* MO injected embryos did reach shield stage, approximately two hours later than controls, they possessed an enlarged shield (n = 40/41) (Figure 3.3.2 C and A).

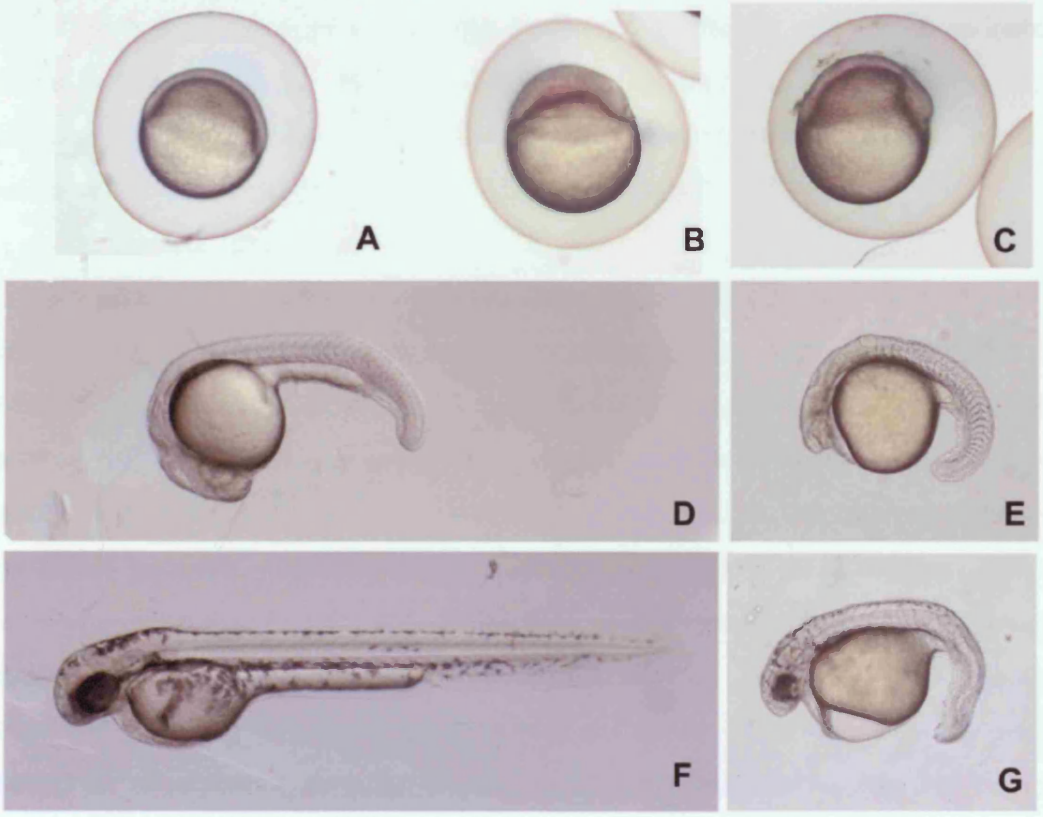

Figure 3.3.2: Shield stage control MO injected embryo (A) compared to the same time point embryo injected with 8ng of *rab1a4* MO (B) and shield stage embryo injected with 8ng of *rab1a4* MO (C). Lateral view of 24hpf control MO injected embryo (D) compared to 24hpf embryo injected with 8ng of *rab1a4* MO (E). Lateral view of 48hpf control MO injected embryo (F) compared to 48hpf embryo injected with 8ng of *rab1a4* MO (G).

By 24hpf, the majority of the 2ng and 4ng *rabl a4* MO injected embryos appeared normal (2ng n = 45, 4ng n = 40/45) although a small proportion displayed smaller brains and kinked tails (2ng n = 0, 4ng n = 6/45). When the 8ng *rabl a4* MO injected embryos reached 24hpf, about. 35% of the embryos were dead (n = 14/41). Those that survived had reduced head structures and a curved tail (n = 27/27) (Figure 3.3.2 E and D).

At 48hpf many of the 2ng and 4ng *rabl a4* MO injected embryos appeared normal; however, a small proportion still possessed small brains and shortened curved tails (2ng n = 0, 4ng n = 6/45). In addition the 4ng *rabl a4* MO injected embryos also showed some pericardial oedema (n = 6/45) and did not hatch (n = 22/45). The 8ng *rabl a4* MO injected embryos did not hatch and displayed pericardial oedema, similar to that seen in the 4ng *rabl a4* MO injected embryos. These embryos also displayed yellowing of the brain, smaller eyes, shortened tails with U-shaped somites and a curving notochord (n = 24/27) (Figure 3.3.2 G and F).

At 3dpf, all the 2ng *rabl a4* MO injected embryos hatched (n = 45) although some had an inward curving body axis and swam in circles (n = 4/45). Although fewer embryos hatched this phenotype was exaggerated in the 4ng *rabl a4* MO injected embryos where the embryos exhibited a curved body axis and swam in a large circular motion on their sides (n = 24/46). Those 4ng *rabl a4* MO injected embryos that failed to hatch exhibited abruptly curved, or 'kinked', tails and pericardial oedema (n = 22/46). At 8ng, only about 10% of embryos hatched (n = 3/27) and these, in common with the 4ng *rabl a4* MO injected embryos, had difficulty swimming normally swimming on their back and sides. Those that did not hatch showed the same phenotype as the 4ng *rabl a4* MO injected embryos (n = 24/47).

3.3.3 Rab18(2)

Injection of 2ngs, 4ngs or 8ng's of *rab18(2)* MO resulted in an early phenotype, with gastrulation in these embryos delayed by approximately two hours (2ng n = 42, 4ng n = 45, 8ng n = 37/39). When the embryos reached shield stage, they showed an elongated and pinched yolk (2ng n = 42, 4ng n = 45, 8ng n = 37/39) (Figure 3.3.3 B and A).

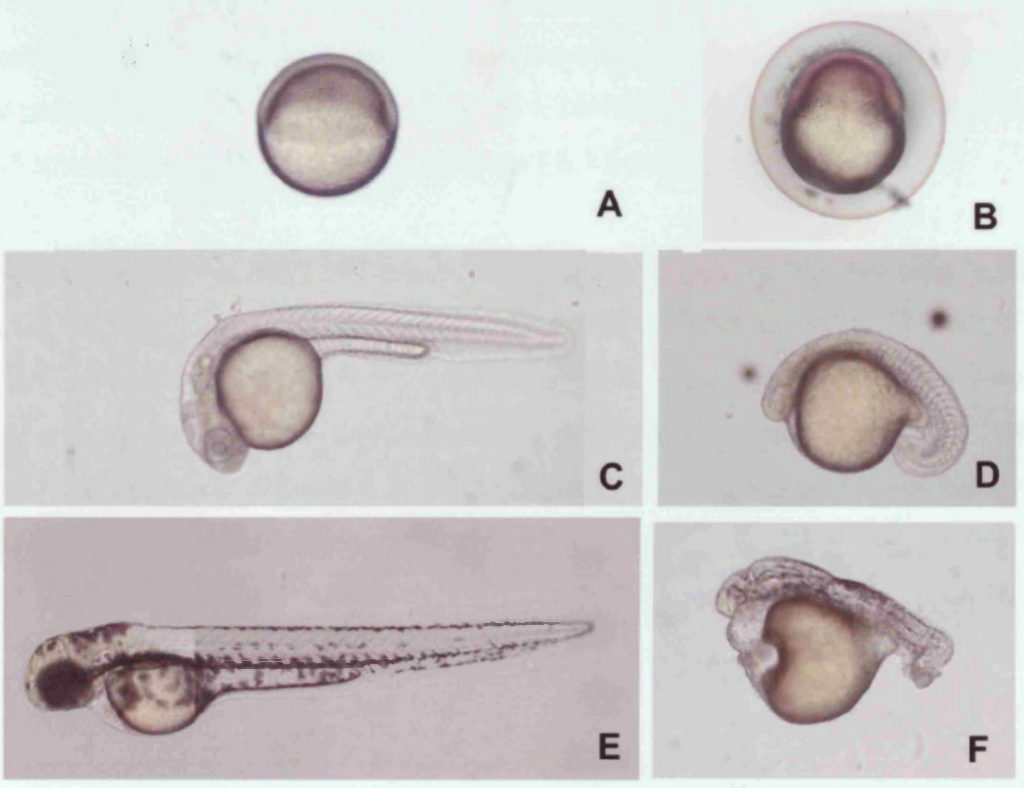

Figure 3.3.3: Shield stage embryos: control MO injected embryo (A) compared to embryo injected with 4ng of *rab18(2)* MO (B). Lateral view of 24hpf embryos: control MO injected embryo (C) compared to embryo injected with 4ng of *rab18* MO (D). Lateral view of 48hpf embryos: control MO injected embryo (E) compared to embryo injected with 4ng of *rab18(2)* MO (F).

By 24hpf, the embryos injected with 2ngs of *rab18(2)* MO possessed a smaller head, while, about. 50% of the 4ng *rab18(2)* MO injected embryos were dead (n = 24/45). The remaining 4ng *rab18(2)* MO injected embryos displayed brain cell death and small eyes (n = 21/21) (Figure 3.3.3 D and C). In addition the 4ng *rab18(2)* MO

injected embryos had tails that were either very short and curved with U-shaped somites, or absent (n = 21/21) (Figure 3.3.3 D). When the dose of the *rab18(2)* MO was increased to 8ng, approximately 87% of the MO injected embryos were dead before 24hpf (n = 34/39). Those that remained were an accumulation of dying cells on the yolk (n = 5/5).

By 48hpf, the 8ng *rab18(2)* MO injected embryos were dead. The 2ng *rab18(2)* MO injected embryos failed to hatched, showed kinked tails and pericardial oedema (n = 37/37). The 4ng *rab18(2)* MO injected embryos showed a similar, if more severe, phenotype, with a small proportion of embryos exhibiting no tail structures and eyes that were substantially reduced, or absent (n = 16/16)(Figure 3.3.3 F). In addition the head structures were greatly reduced (Figure 3.3.3 F and E).

At 3dpf, the 2ng *rab18(2)* MO injected embryos had not hatched and their heads started to develop a yellow/green colour and a thick layer of melanophores (n = 37/37). Consistent with the pericardial oedema the heart was beating slowly and there was no movement of blood. The 4ng *rab18(2)* MO injected embryos did not hatch and exhibited a similar, if slightly more severe, phenotype than the 2ng *rab18(2)* MO injected embryos (n = 16/16).

3.3.4 Rab1a1

Embryos injected with *rab1a1* MO exhibited a developmental delay (2ng = 45, 4ng = 38, 8ng n = 42). When the control embryos had reached shield stage, all of the *rab1a1* MO injected embryos, regardless of the dose of *rab1a1* MO injected, were at least two hours delayed.

By 24hpf, c. 50% of the 2ng *rab1a1* MO injected embryos were dead (n = 23/45). Approximately 10% of the embryos appeared normal (n = 4/45), whereas, the remainder had massive brain cell death and curved tails (n = 18/45) (Figure 3.3.4 B and A). In addition, a small proportion of the phenotypic *rab1a1* MO injected embryos displayed grey cells in the tail indicative of cell death (n = 3/18) (Figure 3.3.4 B). The majority of the 4ng *rab1a1* MO injected embryos had died by 24hpf (n = 35/38). Approximately, 10% survived and these had severe defects, missing head

structure, some tail structure and massive widespread cell death over the whole embryo (n = 3/38). The 8ng *rab1a1* MO injected embryos were all dead.

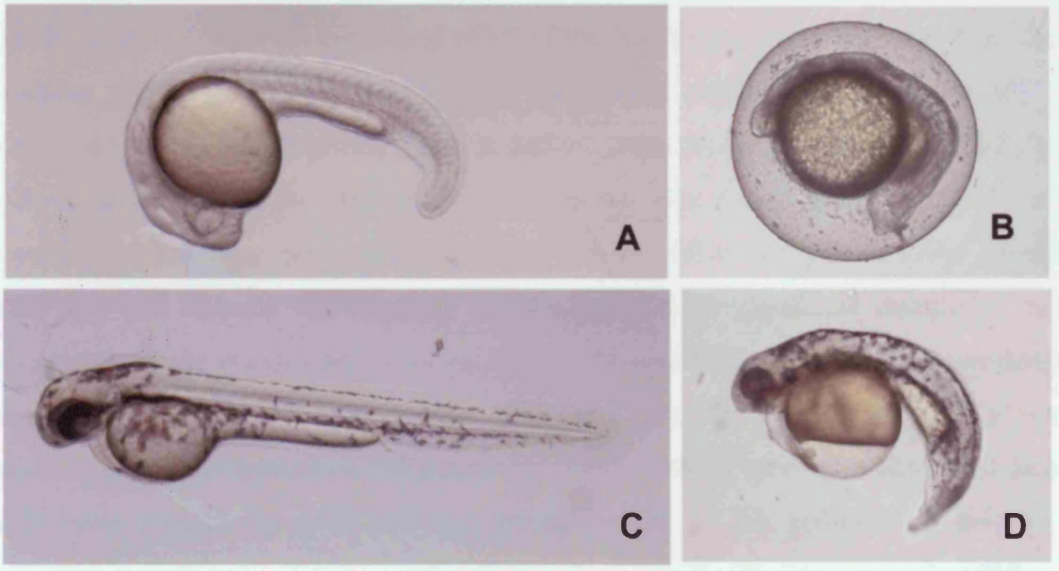

Figure 3.3.4: Lateral view of 24hpf embryos: control MO injected embryos (A) compared to 2ng *rab1a1* MO injected embryos (B) Lateral view of 48hpf embryos: control MO injected embryos (C) compared to 2ng *rab1a1* MO injected embryos (D)

By 48hpf only about 25% of the original clutch of 2ng *rab1a1* MO injected embryos survived (n = 12/45) a third of those remaining appeared normal (n = 4/12). Those *rab1a1* MO injected embryos with a phenotype exhibited reduced head structures with brain cell death, some being so disrupted that they comprised only a pair of eyes on an elongated yolk (n = 3/12). Other *rab1a1* MO injected embryos had pericardial oedema, in addition to short, bent tails with indistinguishable somites (n = 5/12) (Figure 3.3.4 D and C). By this time point, the 4ng *rab1a1* MO injected embryos were all dead.

At 3dpf, remaining *rab1a1* MO injected embryos were either normal (n = 4/9) or displayed a similar phenotype to those at 48hpf, with kinked tails, indistinguishable somites and reduced head structure when compared to controls (n = 5/9).

3.4 Hatching Defects

This section describes those *rabs* that, when knocked-down led to a failure to hatch. Hatching results from the combined effort of the hatching enzyme secreted from the hatching gland, along with osmotic and mechanical mechanisms (Denuce, 1985; Yamagani, 1988). The hatching gland is derived from the prechordal plate which, in turn, is derived from the embryonic shield in the area of the dorsal margin. The prechordal plate cells differentiate to form various different types of cells. Those cells that will become the hatching gland migrate from the dorsal margin of the embryo along the dorsal midline to anterior of the forebrain, where they accumulate to form the polster, upon completion of gastrulation. By 24hpf, the cells of the hatching gland are located on the pericardial membrane. They can be visualised as a semi-circle around the yolk and are prominent due to the presence of brightly refractive cytoplasmic granules within the hatching gland cells (Houart et al., 1998).

3.4.1 Rab11b1

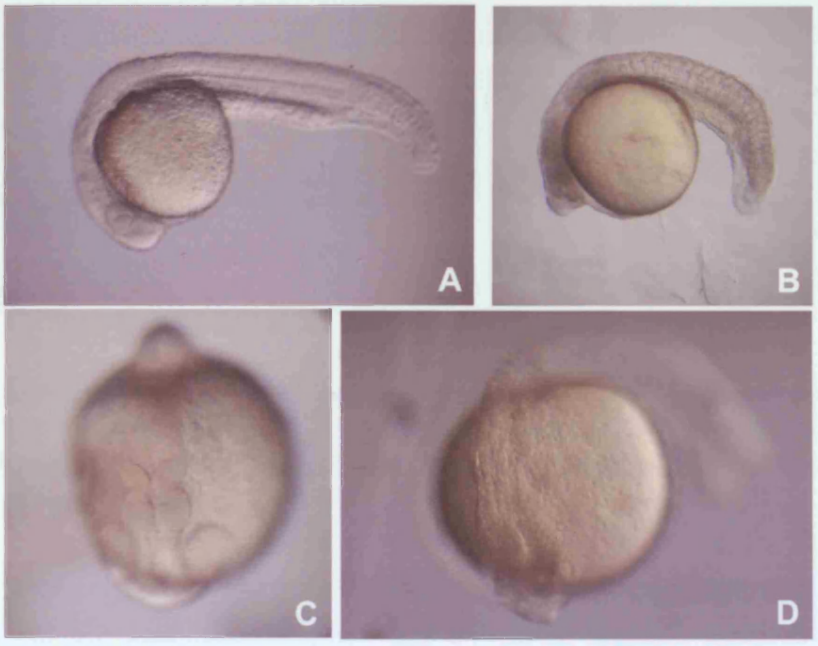

Figure 3.4.1: Lateral view of 24hpf embryos: control MO injected embryo (A) compared to embryo injected with 4ng of *rab11b1* MO (B). Dorsal anterior view of 24hpf embryos: control MO injected embryo (C) compared to embryo injected with 4ng of *rab11b1* MO (D).

All of the embryos gastrulated successfully with the majority of the 2ng *rab11b1* MO injected embryos appearing normal by 24hpf (n = 36/42). However a few 2ng *rab11b1* MO injected embryos exhibited a grey brain, indicative of cell death and a reduction in the size of the eyes (n = 6/42). Increasing the dose of *rab11b1* MO to 4ng resulted in all embryos exhibiting this abnormal phenotype, in addition they exhibited a shortened tail with U-shaped somites (n = 46/46) (Figure 3.4.1 B and A). Injection of 8ng of the *rab11b1* MO resulted in a more severe phenotype with the entire embryo turning grey, indicative of cell death. The 8ng *rab11b1* MO injected embryos exhibited massively reduced brain and head size as well as tail defects (n = 39/39). Closer inspection of 4ng *rab11b1* MO injected embryos revealed small, malformed eyes and badly defined brain structures, resembling an unstructured mass of cells than clearly defined regions (Figure 3.4.1 D and C).

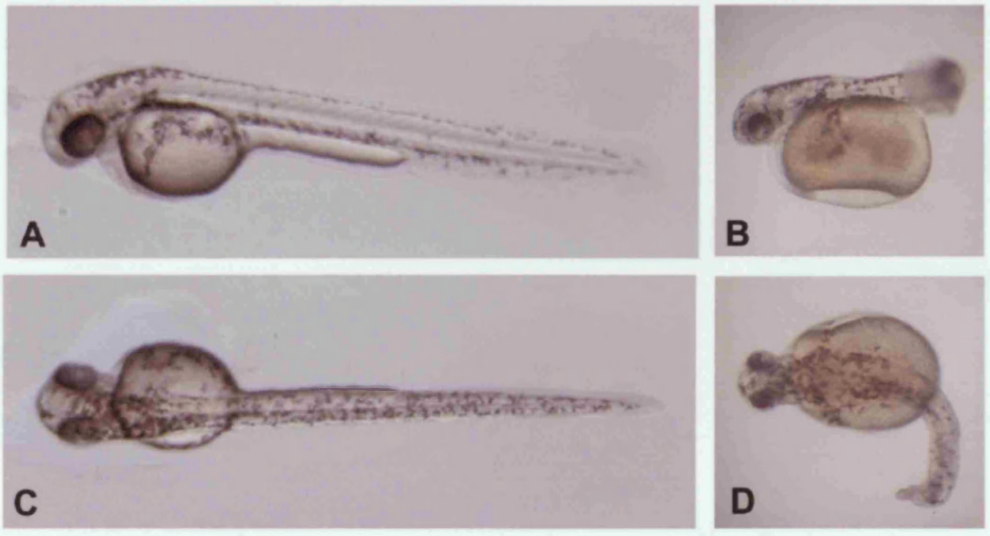

Figure 3.4.2: Lateral view of 48hpf embryos: control MO injected embryo (A) compared to embryos injected with 4ng of *rab11b1* MO (B). Dorsal view of 48hpf embryos: Control MO injected embryo (C) compared to embryos injected with 4ng of *rab11b1* MO (D).

When the phenotypic *rab11b1* MO injected embryos reached 48hpf, they possessed smaller brains and eyes (2ng n = 36/42, 4ng n = 46/46, 8ng n = 39/39) (Figure 3.4.2 B and A) and exhibited bent tails and a curved body axis (Figure 3.4.2 D), compared to controls (Figure 3.4.2 C).

At 4dpf, none of the phenotypic *rab11b1* MO injected embryos had hatched (2ng n = 36/42, 4ng n = 46/46, 8ng n = 39/39) and many displayed pericardial oedema (2ng n = 6/42, 4ng n = 46/46, 8ng n = 39/39).

3.4.2 Rab11b2

The *rab11b2* MO injected embryos all gastrulated comparably with the control embryos (2ng n = 40/40, 4ng n = 42/42, 8ng n = 45/45). At 24hpf, all embryos, regardless of which dose was injected, showed the same phenotype (2ng n = 40/40, 4ng n = 42/42, 8ng n = 45/45). The MO injected embryos all had reduced sized, greying brains, indicative of cell death. Furthermore, they had U-shaped somites, shortened tails and pericardial oedema (Figure 3.4.3 B and A).

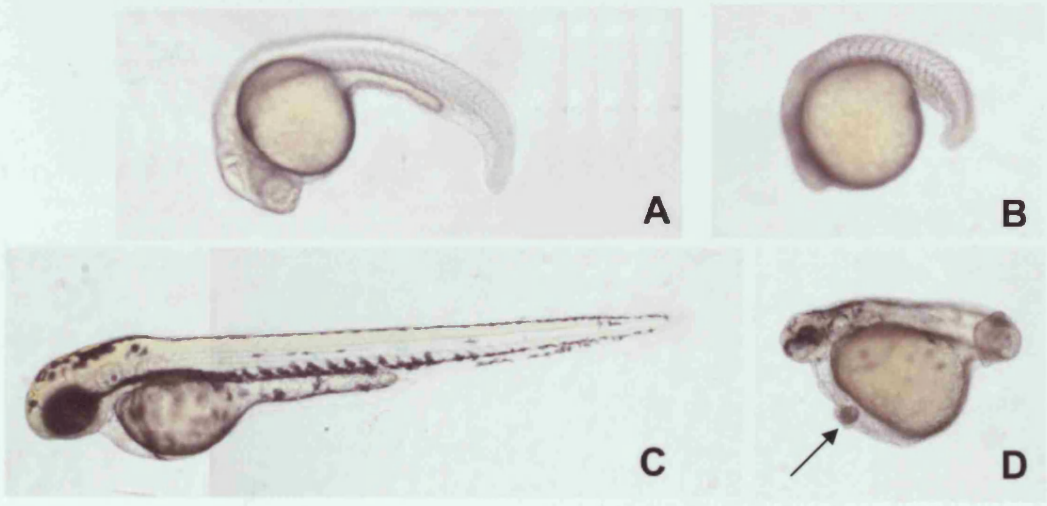

Figure 3.4.3: Lateral view of 24hpf embryos: control MO injected embryo (A) compared to an embryo injected with 4ng of *rab11b2* MO (B). Lateral view of 48hpf embryos: control MO injected embryo (C) compared to an embryo injected with 4ng of *rab11b2* MO (D arrow represents hatching gland cells).

When the embryos reached 48hpf, the *rab11b2* MO injected embryos showed a disjointed 'patchy' hatching gland, with the cells accumulating in peaks in individual areas around the yolk (shown by arrow in Figure 3.4.3 D). The brains of these embryos remained small and had a yellowish tinge (Figure 3.4.3 D), compared to controls (Figure 3.4.3 C). In addition *rab11b2* MO injected embryos had curved and shortened tails, the eyes were small and closer together and they had pericardial oedema (Figure 3.4.3 D) (2ng n = 40/40, 4ng n = 42/42, 8ng n = 45/45).

By 72hpf, none of the *rab11b2* MO injected embryos hatched, the brain remained yellow, the embryos were shortened and pericardial oedema persisted (2ng n = 40/40, 4ng n = 42/42, 8ng n = 45/45). By 5dpf, all the *rab11b2* MO injected embryos were dead.

3.4.3 Rab6a

When the embryos reached shield stage, the *rab6a* MO injected embryos were visually normal. When they reached 24hpf, the 2ng *rab6a* MO injected embryos had small heads, with the distance between the eyes severely reduced, compared to controls. In addition the 2ng *rab6a* MO injected embryos possessed short bent tails with straight somites (n = 43/43) (Figure 3.4.4 B), compared to the V-shaped somites of the controls (n = 45/45) (Figure 3.4.4 A). The majority of the 4ng (n = 42/43), and all the 8ng *rab6a* MO injected embryos (n = 47/47) died. Those of the 4ng *rab6a* MO injected embryos that survived possessed no head structures and greatly reduced tail structures (1/1).

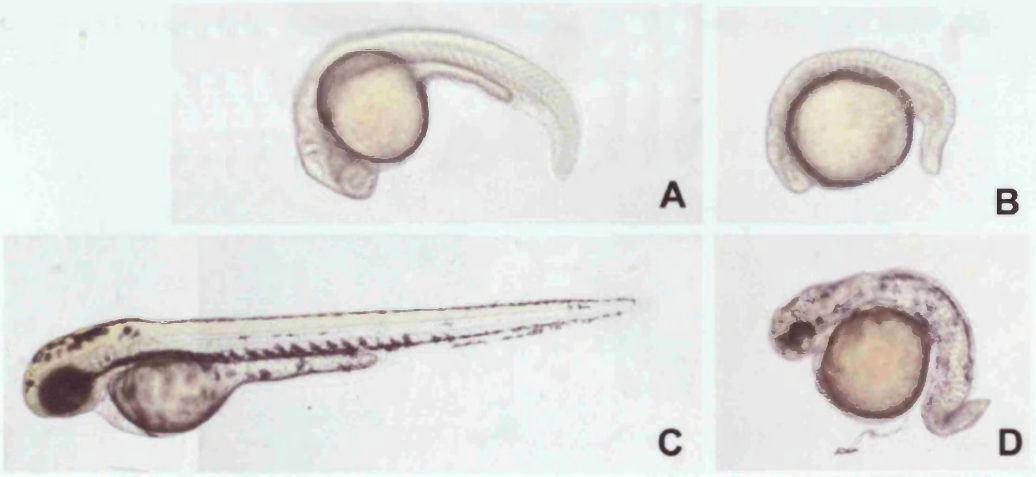

Figure 3.4.4: Lateral view of 24hpf embryos: control MO injected embryo (A) compared to embryo injected with 2ng of *rab6a* MO (Figure B). Lateral view of 48hpf embryos: control MO injected embryo (Figure C) compared embryo injected with 2ng of *rab6a* MO (Figure D).

By 48hpf, all of the 4ng *rab6a* MO injected embryos were dead (n = 1/1), the 2ng *rab6a* MO injected embryos had very small brains and small closely spaced eyes. The tail was shortened and bent posteriorly (n = 43/43) (Figure 3.4.4 D and C).

By 4dpf, most of the *rab6a* MO injected embryos had not hatched and the hatching gland appeared disjointed and patchy with possible pericardial oedema (n = 39/43).

3.4.4 Rab 11a2

All embryos appeared phenotypically normal at gastrulation. At 24hpf, the embryos injected with 2ng of *rab11a2* MO displayed a slightly reduced head size (Figure 3.4.5 B and A) and shortened tails, with U-shaped somites (n = 44). When the dose of *rab11a2* MO was increased to 4ng or 8ng the phenotype remained consistent, but a greater proportion of embryos died before 24hpf (4ng n = 38/41, 8ng n = 43/46 died).

By 48hpf, the 2ng *rab11a2* MO injected embryos had kinked or, in some cases, absent tails, and some pericardial oedema (n = 44). The 4ng *rab11a2* MO injected embryos displayed a yellow tinged head with thick pigment (n = 3/3). At the higher dose of 8ng, the majority of the *rab11a2* MO injected embryos were dead (n = 2/3) while survivors were phenotypically similar to the 4ng *rab11a2* MO injected embryos.

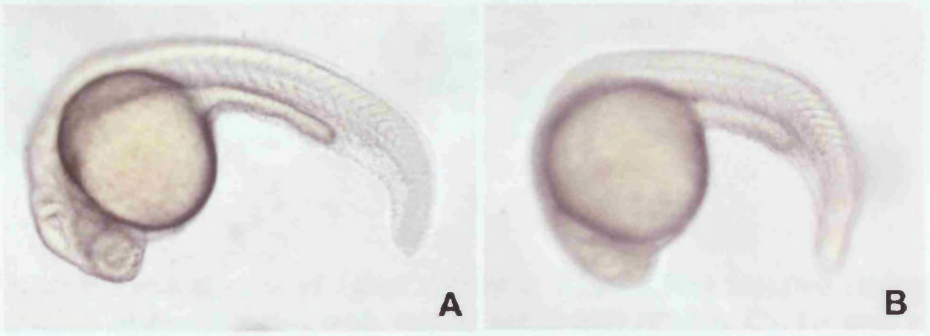

Figure 3.4.5: Lateral view of 24hpf embryos: control injected embryo (A) compared to embryo injected with 2ng of *rab11a2* mopholino (B).

When the embryos reached 4dpf, a large proportion of the 2ng *rab11a2* MO injected embryos remained unhatched and had pericardial oedema (n = 39/44). Most of the 4ng *rab11a2* MO injected embryos were dead and the remainder appeared normal, except for the thick pigment on the dorsal side of the embryo (n =1/1). At 8ngs, all of the *rab11a2* MO injected embryos were dead by 4dpf.

3.5 Swimming Defects

3.5.1 Rab28

During gastrulation the *rab28* MO injected embryos are phenotypically normal. By 24hpf all *rab28* MO injected embryos exhibited a reduced head size (Figure 3.5.1 C and A) regardless of the dose of *rab28* MO injected (2ng n = 43/43, 4ng n = 42/42, 8ng n = 39/39). The 8ng *rab28* MO injected embryos exhibiting greying of the brain, indicative of cell death, and, in a small percentage of cases (n = 5/39) the tail curved upwards.

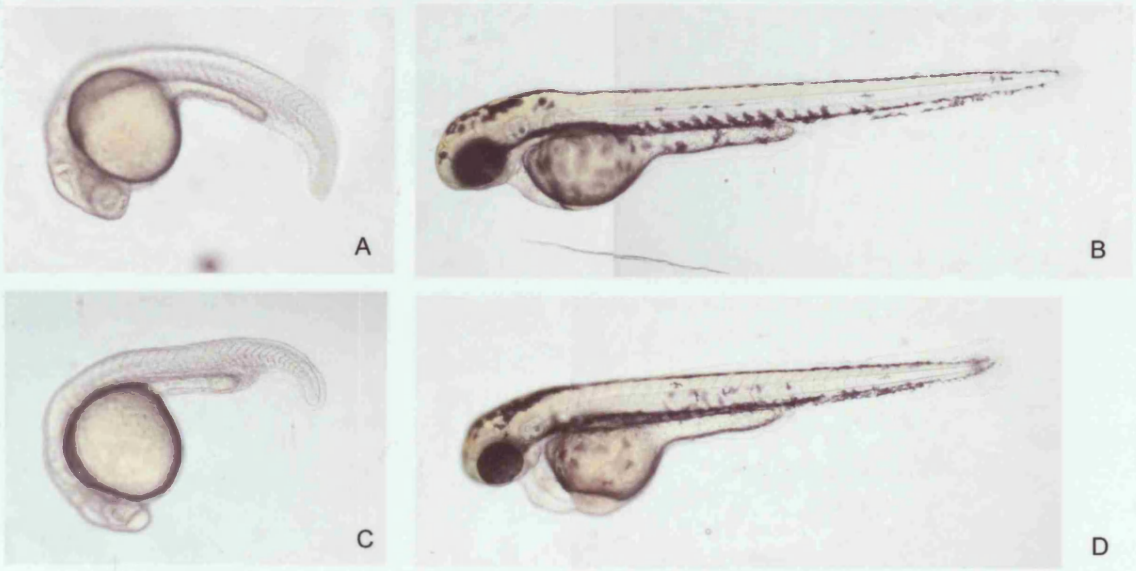

Figure 3.5.1: Lateral view of 24hpf embryos: control MO injected embryo (A) compared to embro injected with 4ng of *rab28* MO (Figure C). Lateral view of 48hpf embryos: control MO injected embryo (Figure B) compared to embryo injected with 4ng of *rab28* MO (Figure D).

By 48hpf, the 2ng *rab28* MO injected embryos appeared normal (n = 43/43), whereas the 4ng *rab28* MO injected embryos had a curved and shortened body axis, in addition to a smaller head and pericardial odeama (n = 42/42) (Figure 3.5.1 D and B). These 4ng *rab28* MO injected embryos showed modified swimming behaviour, with the embryos twitching and swimming in circles. When the dose of *rab28* MO was increased to 8ng embryos showed a similar phenotype to the 4ng *rab28* MO

injected embryos and in addition the 8ng MO injected embryos possessed kinked tails (n = 39/39).

By 4dpf, 2ng *rab28* MO injected embryos appeared phenotypically normal (n = 43/43). The 4ng *rab28* MO injected embryos continued to show pericardial oedema, a shortened body axis and a high proportion of them had bent tails. In addition, the 4ng *rab28* MO injected embryos still displayed abnormal swimming behaviour (n = 42/42). The 8ng *rab28* MO injected embryos again showed a similar phenotype to those injected with 4ng of *rab28* MO (n = 39/39).

3.6 Non-Specific Defects

This section focuses on those Rabs that, when knocked-down, exhibited no specific phenotypes. Each of these Rabs showed brain defects and defects in the tail.

3.6.1 Rab20

The *rab20* MO injected embryos gastrulated normally, regardless of the dose of MO injected. By 24hpf, approximately 20% of the 2ng and 4ng *rab20* MO injected embryos died (2ng n = 9/46, 4ng n= 13/49). The majority of those that survived were phenotypically normal (2ng n = 34/37, 4ng n = 35/36) however, some exhibited reduced head and brain size and slightly shortened tails (2ng n = 3/37, 4ng n = 1/36). When the dose of *rab20* was increased to 8ng a larger percentage of embryos died (n = 34/56) while all the surviving embryos showed reduced head and brain size and slightly shortened tails. In addition, they displayed a slow heart beat and no blood flow (n = 22/22) (Figure 3.6.1 B and A).

By 48hpf, the 8ng *rab20* MO injected embryos exhibited curved tails (Figure 3.6.1 D and C), a sigmoidal body axis (n = 22/22) (Figures 3.6.1 F and E) and reduced head structures.

At 5dpf, the *rab20* MO injected embryos displayed reduced hatching success (n = 15/22) and a shortened curved tail (not shown) when compared to controls. In excess of one third of the *rab20* MO injected embryos failing to hatch exhibited pericardial oedema and had no circulation (n = 5/22).

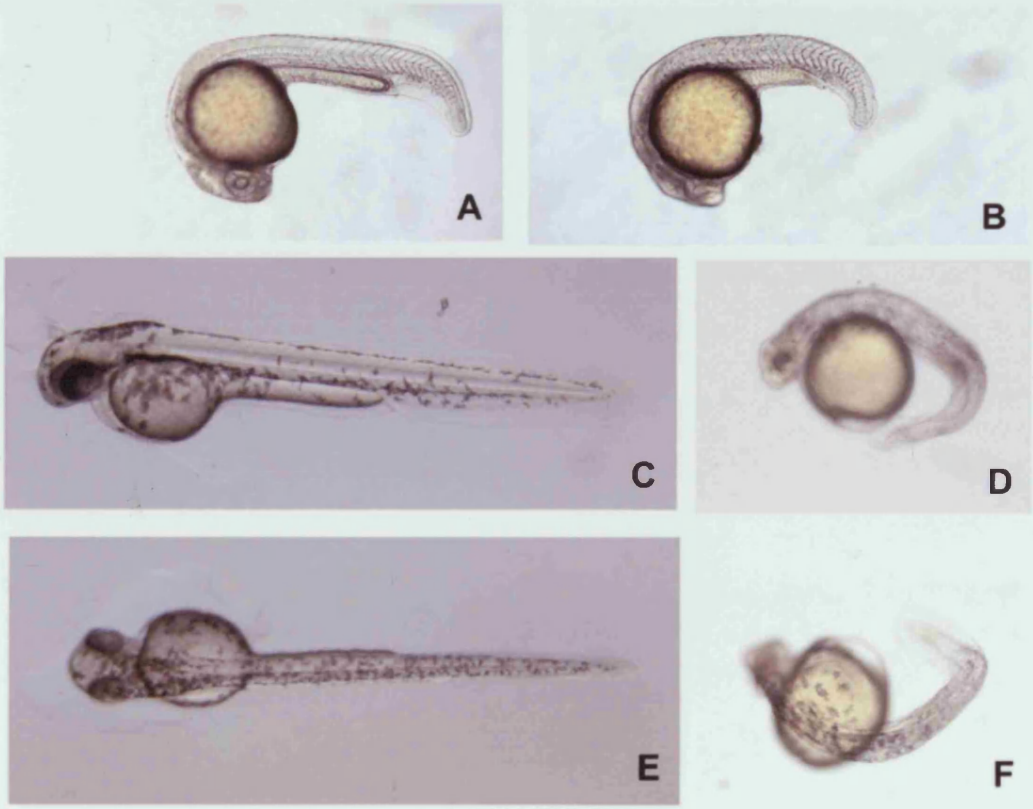

Figure 3.6.1: Lateral view of 24hpf embryos: control MO injected embryo (A) compared to embryo injected with 8ng of *rab20* MO (B). Lateral view of 48hpf embryos: control injected embryo (C) compared to embryo injected with 8ng of *rab20* MO (D). Dorsal aspect of 48hpf embryos: control MO injected embryo (E) compared to embryo injected with 8ng of *rab20* MO (F).

3.6.2 Rab1a2

At shield stage, *rab1a2* MO injected embryos were comparable with the control MO injected embryos, exhibiting no delayed gastrulation and no morphological differences between the organizers, at any of the doses injected. By 24hpf, the majority of the 2ng *rab1a2* injected embryos appeared normal (n = 42/42). The 4ng *rab1a2* MO injected embryos exhibited reduced head size and brain cell death (n = 40/40), when compared to controls (n = 48/48). Increasing the *rab1a2* MO dose to 8ng resulted in the embryos exhibiting a more severe reduction in head size and severe brain cell death (n = 33/33) (Figure 3.6.2 D), when compared with controls (n = 48/48) (Figure 3.6.2 C). In addition to this the 8ng *rab1a2* MO injected embryos

showed severe reduction in tail structures (Figure 3.6.2 B) when compared with controls (Figure 3.6.2 A)

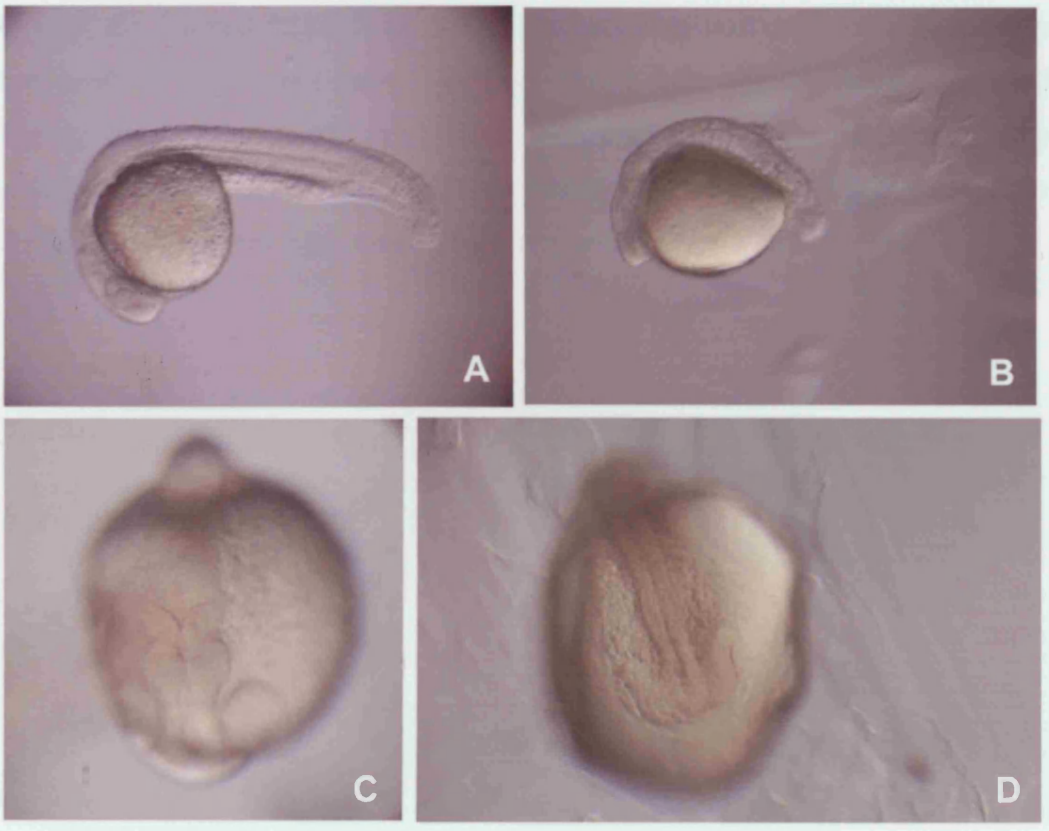

Figure 3.6.2: Lateral view of 24hpf embryos: control MO injected embryo (A) compared to embryo injected with 8ng of *rab1a2* MO (B). 10x magnification of anterior dorsal view of 24hpf embryos: control MO injected embryo (C) compared to embryo injected with 8ng of *rab1a2* MO (D).

At 48hpf, the 2ng *rab1a2* MO injected embryos had smaller heads and smaller eyes (n = 42/42), when compared to controls (n = 48/48). In addition, the 2ng *rab1a2* MO injected embryos had curved tails. The 4ng *rab1a2* MO injected embryos displayed reduced head size, eye size and brain cell death. They also exhibited shortened axis and curved tails (n = 40/40). The 8ng *rab1a2* MO injected embryos had severely reduced head and eye size and brain cell death (Figure 3.6.3 D and C). In addition the 8ng *rab1a2* MO injected embryos showed an oedematous area around the yolk, severely reduced tail structures, with the remainder of the tail being kinked posteriorly (n = 33/33) (Figure 3.6.3 B and A). The notochord in the 8ng *rab1a2* MO

injected embryos was either, curved and misshapen (Figure 3.6.3 F and E) or was not visible (Figure 3.6.3 G and E).

At 4dpf, the 2ng and 4ng *rab1a2* MO injected embryos had smaller heads and eyes than controls and curved tails. The 8ng *rab1a2* MO injected embryos showed severely reduced head and eyes, when compared to controls. In addition they exhibited shortened, kinked tails and an oedematous area round the yolk. Only about 20% of the 8ng *rab1a2* MO injected embryos hatched (n = 7/33).

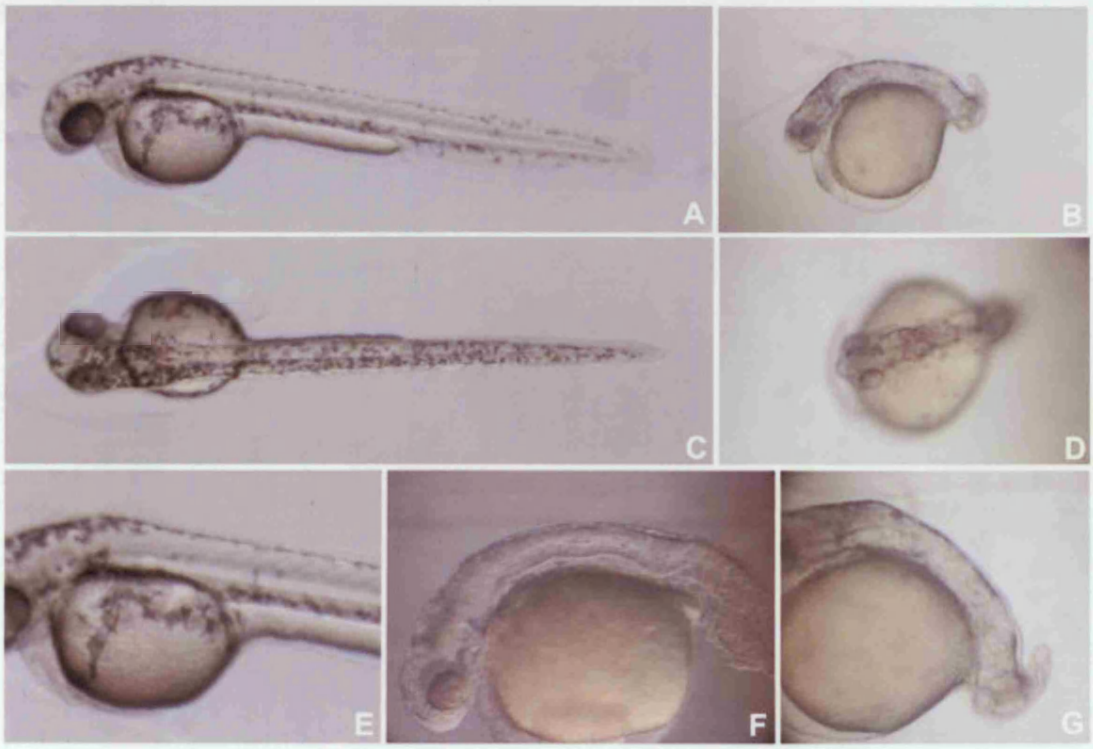

Figure 3.6.3: Lateral view of 48hpf embryos: control MO injected embryo (A) compared to embryo injected with 8ng of *rab1a2* MO (B). Dorsal view of 48npf embryo: control MO injected embryo (C) compared to embryo injected with 8ng of *rab1a2* MO (D). 10x magnified lateral view of rear of head and midtrunk region of 48hpf embryos: control MO injected embryo (E) compared to embryo injected with 8ng of *rab1a2* MO (F). 10x magnified posterior lateral view of 48hpf embryo injected with 8ng of *rab1a2* MO (G).

3.6 Summary of phenotypes.

Gene	Summary of phenotypes in *rab* morpholino injected embryos
Rab1a1	Developmental delay, brain cell death, tail defects, pericardial oedema
Rab1a2	Brain cell death, tail defects inc notochord, pericardial oedema
Rab1a3	Reduced head size, reduced pigment, kinks in notochord
Rab1a4	Developmental delay, enlarged organizer, reduced head size and tail defects, pericardial oedema, reduced hatching success
Rab3c1	Reduced head size, thicker bands of pigment, smaller eyes, protruding lens, swim bladder defect, blind
Rab6a	Reduced head size, tail defects, fail to hatch
Rab11a1	Developmental delay, shield - accumulation of cells on animal pole, tail defects, reduced head size, malformed heart, limited circulation
Rab11a2	Reduced head size, tail defects, pericardial oedema, fail to hatch
Rab11b1	Brain cell death, tail defects, pericardial oedema, fail to hatch
Rab11b2	Brain cell death, tail defects, pericardial oedema, patchy hatching gland, fail to hatch
Rab18(2)	Developmental delay, shield - elongated embryo, reduced head size, tail defects, pericardial oedema, reduced blood flow, fail to hatch
Rab20	Reduced head size, tail defects, pericardial oedema, limited circulation
Rab28	Brain cell death, curved axis, abnormal swimming behaviour, pericardial oedema

Table 3.6.1: Showing the range of phenotypes seen in embryos injected with morpholinos to different rabs.

Chapter 4

Discussion and Further Work

4.1 Screening the Zebrafish Rabs

The *rab* genes have classically been thought of as housekeeping genes because of their ubiquitous expression and vesicle trafficking role (Gurkan et al., 2005; Le Gallic and Fort, 1997). It is easy to assume that, given this ubiquitous expression, loss of a given Rab function would not yield a specific phenotype. However, this is not necessarily the case, a few *rabs* have been implicated in mammalian disorders such as Griscelli's syndrome (Menasche et al., 2000) or Charcot-Marie-Tooth type 2B neuropathy (Verhoeven et al., 2003). The specificity of *rabs*, in addition to some control at the gene expression level, is achieved by post-translational protein modification and the actions of protein regulators i.e. RabGDI. It is, therefore, important to investigate each *rab* to identify any specific role. The continuation of the Rab screen has resulted in the identification of a further 13 Rabs (bringing the total number of *rabs* screened to 37) that, when knocked-down, show defects in normal development. In many of these cases, the defects are very similar and include reduced head size and defects to the tail. However, some *rabs* show more individual phenotypes, including pigmentation defects, slowed development and a failure to hatch.

4.1.1 Pigmentation Defects

The knocking down of the Rab genes *rab3c1* and *rab1a3* resulted in defects in pigmentation. While *rab3c1* MO injected embryos showed a thicker layer of pigment the *rab1a3* MO injected embryos showed the opposite with a reduction in pigmentation.

4.1.1.1 Rab3c1

In mammals Rab3c localizes to synaptic vesicles and cycles on and off the synaptic vesicle membrane with the exocytic release of neurotransmitters. Rab3c dissociates from the synaptic vesicles after the stimulation of exocytosis (Fischer von Mollard et al., 1994) and is thought to perform an important regulatory role in exocytosis rather

than direct involvement (Geppert et al., 1997; Nonet et al., 1997). This synaptic localization may explain the phenotype seen in the *rab3c1* MO injected embryos. At 24hpf, the brain is severely disrupted with forebrain and mid brain structures ill defined, by 5dpf these fish show pigmentation defects and are unable to respond to visual stimulus. When touched, the *rab3c1* MO injected fish were capable of moving their eyes which suggested the fish were blind and unable to see the stimulus, rather than incapacitated and unable to respond. The pigmentation defect in the *rab3c1* MO injected embryos can be explained by their failure to respond to light as control embryos which are capable of subtly altering their chromatophores to blend into their environment (Logan et al., 2006). In bright sunlight or against light backgrounds, zebrafish can aggregate their melanosomes becoming considerably lighter, while in the dark or against a dark background, they can disperse the melanophores and become darker. As the MO injected embryos are unable to see their environment, they are constantly dark adapted so their melanophores are always dispersed, resulting in them appearing darker (Logan et al., 2006). In addition, the *rab3c1* MO injected embryos have no visible swim bladder. This may be due to the swim bladder not developing or not inflating. The abnormal eye morphology in the MO injected fish - small eyes with protruding lenses - may be the cause of the blindness, possibly via a reduced retina, a problem with the lens or other eye components. Malformation or disruption to the optic nerve or visual centres of the brain is also a viable explanation since Rab3c is known to be involved in synaptic transmission (Fischer von Mollard et al., 1994). In the adult rat brain, staining for Rab3a, with which Rab3c has been shown to be localized (Fischer von Mollard et al., 1994), showed no localisation in the optic tract (Xu et al., 1998). However, expression of *rab3c1* in zebrafish shows expression throughout the brain including the post optic areas (Campos, 2004).

A screen in *Drosophila* seeking to identify potential targets for retinal calmodulin proteins found one of the groups of potential targets included proteins with domains similar to the Rab3 GDP/GTP exchange factors (Alvarez et al., 2003). Interestingly although Rab3c itself has never been associated with human disease and disorders its regulators have. Homozygous inactivating mutations in the GTPase activating protein Rab3GAP has been shown to be responsible for Warburg Micro syndrome (WARBM1) (Aligianis et al., 2005). WARBM1 is a severe autosomal recessive

disorder that is characterized by developmental abnormalities of the eye (including microcornea, congenital cataracts and optic atrophy) and the central nervous system (including microcephay). It is thought that defects in Rab3GAP causes a failure of the exocytic pathway to release ocular and neurodevelopmental trophic factors (Aligianis et al., 2005). A more recent paper showed that Martsolf syndrome, which has overlapping characteristics with WARBM1, also has defects in RAB3GAP. RAB3GAP is a heterodimeric protein with one catalytic (RAB3GAP1) and one noncatylitic subunit (RAB3GAP2). Warburg microsyndrome shows defects in RAB3GAP1, while Martsolf syndrome shows defects in the second (Aligianis et al., 2006).

Rab escort protein REP1 is the zebrafish homologue of the human *choroideremia* gene and the first characterized REP. The human disease choroideremia shows X-linked degeneration of the retinal pigment epithelium, resulting in affected males developing night blindness in their teens with progressive loss of peripheral vision and then complete blindness. Loss of function of the gene *choroideremia* found on the X chromosome is responsible (Cremers et al., 1992). Interestingly, a zebrafish mutant for REP1 shows startling similarities to *rab3c1* MO injected embryos. At 5dfp the REP1 mutants had uninflated swim bladders, noticeably smaller eyes and irregular eye pigmentation. The REP1 mutants also showed a patchy, discontinuous distribution of iridophore pigment cells. Electron microscopy showed that the retinal layers were disrupted in the mutants. At 6dpf, oedema was observed around the heart and abdomen. In addition, REP1 mutants had defects in hair cells including the lateral line and the inner ear (Starr et al., 2004).

There is still some concern over the incomplete penetrance of the phenotype observed in *rab3c1* MO injected embryos which could be due to several factors. The first theory is that the phenotype seen in the *rab3c1* MO injected embryos isn't the result of knocking down *rab3c1* alone. It is possible that some of the embryos may have a mutation in other genes only uncovered on knocking down *rab3c1*. A second, more likely possibility is that there is a mutation in the *rab3c1* gene itself. To confirm this it will be necessary to sequence the gene in the *rab3c1* MO injected phenotypic and non-phenotypic siblings and compare.

4.1.1.2 Rab1a3

The *rab1a3* MO injected embryos showed less pigmentation than controls. This phenotype appears to be due to fewer melanophores rather than abnormal distribution of melanosomes within the melanophores. However, the melanosomes in the remaining melanophores of the *rab1a3* mutant embryos appeared to have aggregated. One possibility for this reduction in melanophores is that the cells don't migrate properly from the neural tube, resulting in fewer melanophores reaching their destination. This may result from a defect in neural crest cells. Dr Isabel Campos showed a similar phenotype in the *rab* which she named *rab1b*. Unfortunately, once the zebrafish genome was sequenced, the MO used for this *rab* was shown to partially knock down two additional *rab1* genes. However, the clone which Dr Campos used for the expression pattern of *rab1b* has equally close homology to *rab1a* as it does for *rab1b*, showing 98% identity to the *rab1a3* clone. Therefore, it is probable that these genes are the same. The expression pattern for *rab1b* showed localization in the chordamesoderm, polster, neural crest and blood. The localization in the neural crest is consistent with the phenotype seen in *rab1a3* MO injected embryos. Defects in neural crest cells have been seen in zebrafish to be responsible for the loss of pigment (Kelsh et al., 1996; Parichy et al., 1999; Southard-Smith et al., 1998).

In the zebrafish mutant *colourless* (*cls*) there is extensive loss of pigment cells and enteric nervous system, with large reductions in sensory and sympathetic neurones and putative satellite glia and Schwann cells (Dutton et al., 2001; Kelsh and Eisen, 2000). This phenotype suggests that *cls* functions in specification, proliferation or survival of progenitors for all nonectomesenchymal crest derivatives (Dutton et al., 2001). The *cls* gene encodes a *sox10* homologue, loss of which causes neural crest cells to take ectomesenchymal fates rather than form non-ectomesenchymal fates. If cells do form non-ectomesenchymal fates, they generally fail to migrate and do not overtly differentiate, dying by apoptosis between 35 and 45 hours post fertilisation (Dutton et al., 2001). The melanophore defects in *cls* mutants are thought to be mostly explained by disruption of expression of *microphthalmia (Mitf). Mitf* is a basic helix-loop-helix/leucine zipper transcription factor, known to be required for development of eye and crest pigment cells in the mouse. Interestingly, the human

disorder Waardenburg-Shah syndrome shows reduced enteric nervous system and reduced pigment cell number (Dutton et al., 2001).

An additional explanation for the reduction in melanocytes in *rab1a3* morphant embryos may be a defect in migration. A possible explanation for this defect in migration could be defective cell adhesion, since this has been shown to be required for cell migration (Ulrich et al., 2005). In chick, during delamination in neural crest cells, *N-cadherin* is down-regulated in migrating neural crest (Bronner-Fraser et al., 1992; Nakagawa and Takeichi, 1995; Nakagawa and Takeichi, 1998), whilst *cadherin-6B*, which is expressed in the dorsal neural tube is also down-regulated (Nakagawa and Takeichi, 1995; Nakagawa and Takeichi, 1998). These expression patterns suggest that cadherins mediate strong cell contacts in the neuroepithelium and must be down-regulated for neural crest cells to become migratory (Halloran and Berndt, 2003), suggesting a role for cadherins and cell adhesion in the distribution of melanophores. However, the zebrafish N-cadherin mutant, *parachute*, has no defects in pigmentation (Lele et al., 2002). The zebrafish mutant *sparse* encodes a type III receptor tyrosine kinase, kit, which is expressed in melanocytes and is required, cell autonomously, for melanocyte dispersal and migration from the neural tube (Parichy et al., 1999). The *sparse* mutant exhibits only half the normal complement of melanocytes (Kelsh et al., 1996; Nasevicius and Ekker, 2000; Odenthal et al., 1996).

The *rab1a3* MO injected embryos, in addition to showing reduced melanophore numbers, showed increased aggregation in the remaining melanophores. To ascertain whether the melanophores in theses embryos are unable to diffuse their meloanosomes, it would be interesting to place the *rab1a3* MO injected and control MO injected embryos into either caffine or adrenalin and compare: the aggregation of melanosomes can be achieved by addition of adrenalin, while dispersion can be achieved by addition of caffeine (Rodionov et al., 1998).

4.1.2 Slowed Development

Four of the Rabs in the screen showed slowed development and were deformed as early as shield stage. Such early phenotypes could be down to problems with convergence extension and dorsoventral patterning or epiboly.

In the epiboly mutant *hab*, epiboly begins normally in the blastula and early gastrula stage but, by 70% to 80%, epiboly mutants begin to arrest and dissociate, with their blastoderm peeling off the yolk. When the zygotic and maternal genomes are heterozygous (ZMD) for *hab,* the embryos complete epiboly an hour after their wild type siblings (McFarland et al., 2005). In addition, morphogenesis of the neural tube is abnormal, with gaps forming in the midline during segmentation stages. At later stages, ectopic rows of neurons form in the widened spinal cord and hindbrain (McFarland et al., 2005). The *hab* mutant is caused by a mutation in the zebrafish homolog of the adhesion protein E-cadherin (Shimizu et al., 2005b). E-cadherin is required for the epiblast cells from the interior layer to sequentially move into the exterior layer, where they become restricted to that layer; and participate in subtle cell shape changes that further expand the blastoderm. In *hab* mutants, cells that intercalate into the exterior layer do not change cell shape or become restricted, with many of these cells moving back into the interior layer. *hab*/E-cadherin is necessary for the cell rearrangements that spread the teleost blastoderm over the yolk (Shimizu et al., 2005b). Although the *hab* mutant shows slowed development, the phenotype is quite different from those observed in the slowed development *rabs*. The severest *hab* mutants died before 24hpf, with cells peeling off the yolk – a phenotype not seen in any of the *rab* loss of function experiments in this chapter. The *hab* mutants also show asynchronous movement of cells down the yolk and a large streak of accumulated cells on one side of the embryo. In the *rab* loss of function embryos, this asynchronous movement is not evident and, although there is some cell accumulation in these embryos, it is not as extensive as in the *hab* mutants. This suggests that the phenotypes seen in *rab* loss of function are for the most part unlikely to be due to an effect on epiboly.

The process of convergence and extension occurs during epiboly and it is thought that these movements must be interdependent, as epiboly is slowed in *Xenopus laevis* by treatments that block convergence (Hikasa et al., 2002).The zebrafish *trilobite (tri)* mutant, however, shows reduced convergence and extension movements, while epiboly and involution are not affected (Hammerschmidt et al., 1996a; Sepich et al., 2000; Solnica-Krezel et al., 1996). Since convergence/extension cell movements contribute to lengthening of the embryo (Kimmel et al., 1995), the *tri* mutant embryo is shorter and its somites are wider than in a wild-type embryo. These mutant embryos show normal organizer formation, tissue patterning, and overall development (Sepich et al., 2000; Solnica-Krezel et al., 1996). The convergence movements of lateral cells in *tri* mutants are normal from shield through yolk plug closure, but are reduced, compared with wild-type, by the one somite stage (Sepich et al., 2000). A second convergence/extension mutant *knypek* is required for convergence movements of lateral cells and convergence extension movements of dorsal tissue. The mutants show reduced body length and a shortened malformed tail. The *knypek* gene product regulates cellular movements but not cell fate specification, with the convergent extension movement defects in *knypek* associated with abnormal cell polarity, as mutant cells fail to elongate and align medio-laterally. The *knypek* locus encodes a member of the glypican family of heparan sulfate proteoglycans. Glypican is required during vertebrate gastrulation, as a positive modulator of non-canonical Wnt signalling, to establish polarized cell behaviours, underlying convergent/extension movements (Topczewski et al., 2001). All of the *rab* loss of function experiements that showed slowed development also, showed reduced body length. *rab1a4* and *rab18* showed a more pronounced reduction than *rab11a1*, which is consistent with a defect in convergence and extension. The *tri* mutant showed thicker somites, whereas the somites in these *rabs* appeared normal thickness, although they were U-shaped rather than the chevron shape seen in controls. The *tri* mutant also showed convergence extension defects after the yolk plug closure stage, whereas the *rab* loss of function embryos showed defects in gastrulation at shield stage. Although both *tri* and *knypek* mutants show cyclopia, the head defects seen in the *rab* MO injected embryos are not consistent with this phenotype; they show a more severe phenotype, with smaller head and eye structures. This suggests that altered convergence and extension movement defects are either not responsible for

the defects seen in these *rab* loss of function embryos or that they are accompanied by other defects.

Defects in epiboly and convergence/extension alone don't explain the defects seen in these slow developing *rab* MO injected embryos but a combination of both factors may explain some of the phenotypes seen. The early arrest mutants such as *zombie, spectre* and *speed bump* show head defects similar to those seen in the *rab* MO injected embryos, in addition to a reduction in body axis and defects in the tail (Kane et al., 1996b). However, these arrest mutants do not arrest until 80% epiboly at the earliest, which is inconsistent with the slowed development in the *rab* MO injected embryos apparent at shield stage. Since Rab proteins are responsible for vesicle trafficking, it is possible that these *rabs* might be involved in both epiboly and convergence extension in addition to other as yet unknown process.

4.1.3 Hatching Gland

Zebrafish embryos hatch from their chorions, using a combination of processes. The osmotic pressure of the perivitelline fluid within the chorion increases, while the hatching gland releases enzymes that digest the chorion membrane. The chorion is thus weakened and the embryo can use muscular movements (eg. a flip of the tail), to release itself from the chorion (Buznikov and Ignat'Eva, 1958). Hatching gland cells produce secretory granules that contain the hatching enzyme. These secretory granules increase in number until the hatching gland disappears after hatching (Buznikov and Ignat'Eva, 1958)

In zebrafish, the hatching gland is composed of two cell populations: mesodermally derived hatching gland cells, which express the *hatching gland* gene (*hgg*), and ectodermally derived support cells (Kimmel et al., 1990). The hatching gland is derived from the polster, an accumulation of cells found anterior and below the forebrain of the embryo at tail bud stage. The polster, in turn, is derived from the anterior mesendoderm. Differentiation of the polster and, later, the hatching gland cells, is controlled by specific gene regulation, a process programmed early in embryogenesis (Inohaya et al., 1995; Inohaya et al., 1999). There are many genes

expressed in the pre-polster, the best characterised of these is *Cathepsin L* (*CatL* or *hgg1*), a protease secreted by the hatching gland. Also expressed in the pre-polster, is *cyclase associated protein- 1* (*Cap1*), which is thought to be required for the regulation of actin dynamics within pre-polster cells, influencing cell behaviour during the generation and migration of the polster (Daggett et al., 2004).

An important family of transcription factors in the formation of the polster are the zebrafish Kruppel-like factors (*zKLF4*). *zKLF4* is a zinc finger family of transcription factors, expressed early during polster formation, which are required for further specification of the polster into the hatching gland (Kawahara and Dawid, 2000; Kawahara and Dawid, 2001). KLF4 is one of the earliest markers of the polster and lateral plate mesoderm (LPM), and marks the fate of the hatching gland, blood, and vasculature (Amatruda and Zon, 1999; Oates et al., 2001), with *zKLF4* having a critical role in erythroid cell differentiation in zebrafish (Kawahara and Dawid, 2000; Kawahara and Dawid, 2001). If *zKLF4* is knocked-down, the hatching gland is absent and the embryos do not hatch (Gardiner et al., 2005), although the embryos were normal until this stage, including those cell types derived from the same parent, such as heart and anterior macrophages. If the embryos were manually dechorionated, they developed normally and survived into adulthood.

The four *rab* genes that showed a failure to hatch when knocked-down, also showed a variety of other phenotypes: most notably, pericardial oedema. It is possible thereofore that the hatching defect seen in these *rab* MO injected embryos is due to an effect on the polster or anterior mesoderm. It is, also, possible that these *rabs* affect specification of the hatching gland from the polster. However, due to the multitude of other phenotypes, it is unlikely that these *rabs* affect just the hatching gland cells. The *rab11b2* MO injected showed the hatching gland cells to have accumulated at two points on the yolk, rather than the uniform stripe of cells seen in controls, suggesting a defect in the dispersal of the hatching gland cells. In addition, this accumulation of cells appeared to be dying, which could be due to a number of factors, including apoptosis due to the cells being mis-dispersed or hatching gland cells being poisoned by disrupted secretion. Three out of four of the MO injected *rabs* that showed the hatching defect were from the Rab11 family. It is, therefore, possible that these Rabs may function in the same pathway.

All of the *rab* MO injected embryos with hatching gland defects also showed defects in the tail structures, with *rab11b1, rab11b2 and rab6a* showing the severest defects. These tail defects could be responsible for the inability of MO injected embryos to hatch, since even with a fully functional hatching gland, the embryos would be unable to break their way out of the chorion as their tail movements would be compromised. It is, therefore, possible in such cases that the hatching gland has little to do with the inability to hatch. It is more likely, though, that there is a defect in the hatching gland in some, if not all, of the *rab* genes, especially *rab11b2* MO injected embryos, which show an abnormal hatching gland. This defect in the hatching gland may then be aggravated by the defects in tail structure, resulting in the embryos inability to hatch. To establish if the reduction in hatching success is the result of defects in the hatching gland, expression of genes associated with the gland, such as *hgg1*, could be assayed. While to establish if muscle defects in the tail could be responsible, phalloidan staining could be employed.

4.1.4 Swimming Defects

Many of the MO injected embryos showed some sort of tail defect and, therefore, had abnormal swimming behaviour. The *rab28* MO injected embryos, however, appeared largely normal, compared to many of the other *rab* MO injected embryos in the screen. There was some brain cell death at 24hpf and, by 48hpf, pericardial oedema. However, the most striking defect was the modified swimming behaviour these embryos showed. Some of these MO injected embryos had kinked tails but many of them, other than a slightly shortened body axis, showed normal tail structures. The *rab28* MO injected embryos swam in a circular pattern.

There are many possible explanations for the swimming defect in the *rab28* MO injected fish, including muscle abnormalities, defects in the notochord, basement membrane or neuromuscular junctions and impaired balance.

Embryos with defects in neuromuscular junction usually show short swimming response. *twitch once* mutant embryos, when touched, respond with one or two

swimming strokes, instead of an escape response. This response is called use-dependent fatigue and has been shown to be a consequence of a mutation in the tetratricopeptide domain of muscle rapsyn. This mutation inhibits the formation of subsynaptic acetylcholine receptor clusters. This loss of receptor clusters results in reduced synaptic strength, is augmented by a postsynaptic depression not seen at normal neuromuscular junctions, and results in use-dependent muscle fatigue (Ono et al., 2002). The *shocked* (*sho*) mutant also exhibits an aborted escape response (Granato et al., 1996). *shocked* (*sho*) is a mutation which causes motor deficits attributable to CNS defects. Mutant embryos display reduced spontaneous coiling of the trunk, diminished escape responses when touched, and an absence of swimming. The shocked mutant shows a mutation in the *slc6a9* gene that encodes a glycine transporter (GlyT1). *glyt1* is expressed in the hindbrain and spinal cord, which are regions known to be required for generation of early locomotory behaviours (Cui et al., 2005). A lack of muscle acetylcholinesterase in the mutant *ache* shows slowed synaptic current and so sustained contractions on both sides of the tail (Behra et al., 2002). Embryos with muscle defects, such as dystroglycan MO injected embryos, respond to touch but appear to be less flexible than controls. By 48 hpf, *dystroglycan* MO injected embryos are curved and dystrophic, compared with controls, and move in an uncoordinated fashion (Parsons et al., 2002b). In *lama2* MO injected embryos, there is defective organisation of the muscle tissue and they responded poorly to touch, with uncoordinated movements (Parsons et al., 2002b). None of these defects show comparable swiming behaviour to that seen in the *rab28* MO injected embryos, suggesting the neuromuscular junction, notochord or muscle tissue may not be responsible for the defective swimming behaviour seen in these MO injected embryos. In order to ascertain if this is the case, expression of genes required for notochord, such as *laminins* or *coatomers*, could be assayed, while defects in muscle structure can be investigated by phalloidin. Defects in the neuromuscular junction could be identified by expression analysis of neuronal markers and by pharmaceutical methods, such as addition of acetylcholinesterase inhibitors.

Fish with defects in balance show characteristic swimming behaviour, with the fish swimming in circular motions, resulting in the name "circler" mutants (Nicolson et al., 1998). The causes of balance defects include defects in ear and the lateral line. The inner ear contains two macular organs, the saccule and utricle, which are found

in all vertebrates. The saccule and utricle are pouch-like vestibules which contain a bed of hair cells coupled to calcium carbonate crystals. In fish, the crystals coalesce to form a single large polycrystalline mass called an otolith. Forces that result in the movement of the otolith are transduced to the underlying hair bundles (Nicolson, 2005), with defects in the otoliths or the hair cells causing defects in balance. The gene *starmaker* is needed for otolith formation. Knocking down this gene results in a small fraction of MO injected embryos displayed circling behaviour (Sollner et al., 2003). Defects in hair cells in zebrafish can affect both the ear and the lateral line, since the lateral line is a system of superficial canal hair cells that detects water movements. Glial cells have been implicated in preventing premature development of lateral line hair cells (Grant et al., 2005; Lopez-Schier and Hudspeth, 2005). The swimming defect in these *rab28* MO injected embryos seems quite similar to the defects seen in fish with ear or balance defects. This does not though explain the oedematous region around the heart.

Defects in hair cells could result from defects in all forms of cilia. Monocilia have been proposed to establish the left-right (LR) body axis in vertebrate embryos by creating a directional fluid flow that triggers asymmetric gene expression. Cilia inside Kupffer's vesicle are motile and create a directional fluid flow just prior to the onset of asymmetric gene expression in lateral cells. Ciliated KV cells are required during early somitogenesis for subsequent LR patterning in the brain, heart and gut (Essner et al., 2005). This may explain the brain heart and swimming abnormalities.

4.1.5 Non-Specific Defects

The compex defects seen in the two *rab* MO injected embryos in this group, such as brain cell death, oedema and tail defects, were also seen in many of the other MO injected embryos. The brain and tail structures are under the control of many pathways. Therefore, it is difficult to ascertain which pathways have been disrupted by these *rabs* being knocked-down. It is necessary to look at the data obtained for homologues of these *rabs* in other models

Amoung the first *rab* genes uncovered in rat brain was the homologue of *ytp1*, *rab1*. There have now been two mammalian *rab1* genes identified *rab1a* and *rab1b*. Both mammalian *rab1* genes have been suggested to regulate transport of cargo between the ER and the Golgi apparatus (Palokangas et al., 1998; Plutner et al., 1991; Sannerud et al., 2003; Tisdale et al., 1992). Rab1 in rat brain is seen in neuroblasts and glioblasts (Ayala et al., 1989). This expression may explain the cell death death seen in *rab1a2* MO injected embryos, in addition to that seen in *rab1a4* and *rab1a1*. Interestingly, in yeast, Ypt1p associates with cytoplasmic α-synuclein and elevated expression of Rab1, protected against α-synuclein induced dopaminergic neuron loss in animal models of Parkinsons disease (Cooper et al., 2006).

Rab1a and Rab1b have been found to be highly expressed in human cardiac tissue. In addition, Rab1b has been shown to be highly expressed in murine cardiac tissue. Cardiac specific overexpression of Rab1a in cardiac tissue of mice resulted in a dilated cardiomyopathy that resulted in premature death at six weeks of age. Rab1a overexpression revealed that Golgi stacks and surrounding transitional vesicles were markedly enlarged. This shows a role for *rab1* in heart developmeant and may explain the pericardial oedema in *rab1a1, rab1a2* and *rab1a4*. If the heart is defective in these MO injected embryos, circulation is reduced and oedema may result. However, there was no obvious defect, other than the oedema, in the heart of these *rab1* MO injected embryos but it is possible circulation may have been reduced.

In human cell tissue culture the inactive form of Rab1b has been shown to block forward transport of cargo and induces Golgi disruption (Alvarez et al., 2003). The phenotype is analogous to that induced by brefeldin A (BFA) and causes resident Golgi proteins to relocate to the ER, as well as inducing redistribution of ER-Golgi intermediate compartment proteins. The COPI (Coatomer complex) machinary was shown to be compromised by the release of beta-COP into the cytosol. Inactive Rab1b is reversed by expressing known mediators of COPI recruitment suggesting that Rab1b function influences COPI recruitment. Further evidence is provided by the finding that cells expressing the active form of Rab1b are resistant to BFA. (Lazar et al., 1997). The notochord defect, seen in the *rab1a2* MO injected embryos, may be the the result of the *rab1a* affecting COPI. The zebrafish mutants *sneezy,*

happy, and *dopey* encode the α, β and β' subunits of COPI. These mutants all show defects in their notochord. Coatomer activity is required for normal chordamesoderm differentiation, perinochordal basement membrane formation and pigmentation (Coutinho et al., 2004). Although associations have been seen for Rab1b and COPI all zebrafish *rab1s* share high sequences homology with both *rab1a* and *rab1b*. It is, therefore, possible that any of the zebrafish Rab1s may function in a similar way to mammalian Rab1b.

rab20 has been shown to be expressed in the kidney tubule and intestinal epithelial cells in mice (Curtis and Gluck, 2005). Electron microscopic studies have revealed that Rab20 is located on endocytic structures underlying the plasma membrane, suggesting that they play a role in endocytosis/recycling (Lutcke et al., 1994). However, this is the extent of the current knowlage on *rab20*. It is, therefore, difficult to discuss the mechanisms that could be involved in *rab20* function and those that are defective in the *rab20* MO injected embryos. This problem led Dr Matthew Clark to develop a small inexpensive microarray for the routine analysis of molecular phenotype. In the future, microarray analysis of this and the other *rabs* may provide valuable information on these lesser studied *rabs* as well as new insights into those that are better characterised.

Chapter 5

Characterization of Zebrafish Rab5a2

5.1 Introduction.

5.1.1 An introduction to the Rab5 family.

The *rab5* family is the best characterized of all the *rab* families and has been identified as one of the core *rabs* (Bucci et al., 1992; Chavrier et al., 1990). The Rab5 protein localizes to clathrin coated vesicles, early endosomes and the plasma membrane (Bucci et al., 1992). The protein is essential for *in vitro* homotypic fusion of early endosomes and is able to increase the rate of endocytosis *in vivo* when overexpressed (Gorvel et al., 1991; Gruenberg and Howell, 1989; Li and Stahl, 1993). Original experiments done in mammalian cells assumed only one Rab5 and looked at the function of different parts of the protein (Kinsella and Maltese, 1991). Deletion of the entire C-terminal tetrapeptide motif CCSN abolished *rab5* activity but deletion of only the last three residues showed residual *rab5* activity. A mutant containing a 4-residue deletion from the N-terminus retained full activity while N-terminal deletion of 19 residues partially blocked *rab5* activity (Bucci et al., 1992). An amino acid dominant negative Rab5 (N133L) inhibited endogenous Rab5 activity, while a constitutively activate Rab5 (Q79L) had no effect on Rab5 activity (Bucci et al., 1992; Li and Stahl, 1993). In contrast, subsequent studies have shown that overexpression of constitutively active Rab5 causes dramatic enlargement of early endosomes (Stenmark et al., 1994). Overexpression of the wild-type *rab5* enhanced the rate of transferrin receptor internalisation, with *rab5* mutants deficient for GTP binding inhibiting transferrin receptor uptake (Bucci et al., 1992). Taken together these results suggest that Rab5 activity is rate-limiting in the early endocytic pathway. Rab5 has a role in fusion of clathrin-coated vesicles to early endosomes. A cytosolic component containing Rab5-GDI is essential for the Rab5 clathrin-coated pits to sequester transferrin efficiently. Rab5-GDI has been shown to have a role in the earliest stages of the endocytic pathway and is a direct link between the processes of transport vesicle formation and the recruitment of components required for subsequent fusion reactions (Chavrier et al., 1992).

The original Rab5 has now been renamed Rab5a since the discovery of two separate highly similar genes, Rab5b and Rab5c (Singer-Kruger et al., 1994; Wilson and

Wilson, 1992). Interestingly, in the yeast *Saccharomyces cerevisiae*, three highly related Rab5 proteins had already been isolated and named Ypt51p, Ypt52p, Ypt53p (Bucci et al., 1995). These three Rab5s colocalize at the plasma membrane and early endosomes with Rab5b and Rab5c stimulating early endosome fusion *in vitro* and transferrin endocytosis *in vivo*. The ability of Rab5a to regulate transport in the early endocytic pathway is shared by the Rab5b and Rab5c genes with all three proteins being ubiquitously expressed. It has been suggested that the presence of three Rab5 genes may reflect an evolutionary need to ensure Rab5 function even in the presence of a harmful mutation (Chiariello et al., 1999). Alternatively each gene could fulfill a distinct role and be responsible for fine regulation of the early endocytic pathway (Chiariello et al., 1999). The latter hypothesis is supported by recent work showing that all the Rab5 genes are differentially recognized by different kinases. Rab5a is efficiently phosphorylated by extracellular-regulated kinase 1 while cdc2 kinase preferentially phosphorylates Ser-123 of Rab5b. This differential phosphorylation by these kinases could specifically modulate the function of the different Rab5 genes *in vivo* (Christoforidis et al., 1999b).

Rab5 has a large diverse and complex group of interacting molecules, over 20 polypeptides were isolated from bovine brain cytosol that interact both directly or indirectly with the GTP-bound form of Rab5 (Stenmark et al., 1995). The first Rab5 effector identified was Rabaptin-5 which is essential for early endosome fusion (Lippe et al., 2001a; Lippe et al., 2001b). Rabaptin-5 forms a complex with Rabex-5, which catalyses nucleotide exchange on Rab5. When Rab5 is activated by Rabex-5, the Rabaptin-5–Rabex-5 complex induces its own membrane recruitment through Rabaptin-5 (Rybin et al., 1996). This positive-feedback loop counteracts GTP (Lippe et al., 2001a) which is thought to enrich active Rab5 on the membrane, a region where other Rab5 effectors are recruited (Christoforidis and Zerial, 2000; Lippe et al., 2001a; Lippe et al., 2001b). This localized clustering of activated Rab5 proteins is thought to regulate tethering machinery. GTP-bound Rab5 interacts with several other effectors, such as EEA1, Rabenosin5 (Christoforidis and Zerial, 2000), and hVps34 (Nielsen et al., 2000). EEA1 and Rabenosyn5 possess FYVE domains that bind to phosphatidylinositol3phosphate (PtdIns[3]P) (these have been shown also to be Rab5 effectors) (Bucci et al., 1992; Christoforidis et al., 1999b; Stenmark and Aasland, 1999) (Gonzalez-Gaitan et al., 1994). Binding of the FYVE domain to

PtdIns(3)P, complete with interaction of Rab5, is responsible for specific targeting of these proteins to early endosomes.

5.1.2 Rab5 and its role in cell signalling

An important role for Rab5 has been identified in cell signalling. Strigini and Cohen proposed a role for Rab5 in planar transcytosis mediated spread of Wg in the *drosophila* imaginal disc (Strigini and Cohen, 2000) (section 1.2.6.2). However, more recent data using a temperature-sensitive *dynamin* mutant, *shibire,* in *drosophila* which blocks endocytosis suggests Wg spreads extracellularly (Marois et al., 2006). Wg is expressed in a stripe of cells straddling the dorsal-ventral boundary and forms a symmetrical gradient in dorsal and ventral compartments along the imaginal wing disk. When a dominant negative form of Rab5 was expressed in the dorsal compartment, initially Wg protein levels were elevated in dorsal tissue nearest the Wg-expressing cells but, as time progressed, large amounts of Wg invaded the entire dorsal compartment. The authors theorised that this spatial progression of Wg accumulation resulted from intervening tissue no longer internalizing Wg when endocytosis was disrupted. This suggested that Rab5-dependent endocytosis of Wg normally limits the range over which Wg spreads (Marois et al., 2006). In addition, transcription of both *fz2* (a wingless receptor) and *dlp* (a member of the glypicans which have been implicated in the movement of the morphogens Hh, Dpp and Wg) increases, while that of *arrow* (thought to be a wingless co-receptor) decreases rapidly (Marois et al., 2006).

5.1.3 Rab5 genes in zebrafish

There is very little literature on Rabs in zebrafish, with much of this done by Dr Isabel Campos for her PhD thesis (Campos, 2004) and Dr Mathew Clark (Clark, MD, pers. com.). There are two further publications on the zebrafish Rabs and in particular the Rab5 family, from the laboratories of Brand and Heisenberg at Max Planck Institute for Cell Biology (Scholpp and Brand, 2004; Ulrich et al., 2005). Scholpp and Brand (2004) investigated the control of signalling range of Fgf8 by

endocytosis, while Ulrich, Krieg et al. (2005) investigated Rab5c in cell cohesion during gastrulation and the role of Wnt11 (Ulrich et al., 2005).

5.1.3.1 Rab5 in the spread of Fgf8

Scholpp and Brand (2004) report that Rab5s function in endocytosis as regulators of Fgf8 spread. The data showed that Fgf8 colocalises with Rab5 in 54% of vesicles. Injection of a dominant-negative, form of the Fgf receptor XFD decreased internalization of Fgf8 (Amaya et al., 1993). This resulted in an accumulation of the Fgf8 protein around the receiving cells and detection of the Fgf8 protein at greater distances from the source, when compared to uninjected control embryos. When Rab5 function was disrupted by injecting RN-tre (a GAP), Fgf8 was absent from intracellular vesicles and accumulated extracellularly at a greater distance from the source. However, overexpression of Rab5 reduced the range of Fgf8 spreading and increased the size of the Fgf8-positive intracellular compartments. Transplantation experiments showed that when cells injected with RN-tre were transplanted into control embryos near a source of Fgf8, host cells took up the protein, even if cells inhibited for Rab5 function were located between the source and the receiving cells. In these embryos, little extracellular Fgf8 accumulated, unlike embryos where all cells received RN-tre. In embryos where Rab5-overexpressing cells were transplanted, these cells showed an accumulation of Fgf8, while cells that lay behind them were deficient of Fgf8. In embryos injected with RN-tre, expression of Fgf8 target genes *spry4, pea3* and *erm* showed broadened expression compared to controls, knock down of *rab5a2* also showed a broadened expression of *spry4.* Conversely, embryos injected with *rab5a* RNA showed a severe reduction in the induction of *spry4.* This paper has, therefore, suggested a restrictive clearance model for the spread of Fgf8. Endocytosis serves to *restrict* spreading of Fgf8 protein away from the source, by *clearing* Fgf8 protein from the extracellular space via endocytosis, defining how far the protein is able to spread and determining the width of the target tissue responding to Fgf8 signalling. Given that Fgf8 and Rab5 only localizes in a percentrage of cases Scholpp and Brand suggested that the vesicles, which, didn't co-localise with Rab5 might be destined for degradation (Scholpp and Brand, 2004), as Fgf8 was seen in the intracellular degradative pathway of receiving cells. Therefore, they argue that Fgf8 spreads extracellularly by a diffusion-based

mechanism where target cells can actively influence the gradient through endocytosis and subsequent degradation, with the involvement of Fgf receptors (Scholpp and Brand, 2004).

5.1.3.2 Rab5c and its role in cell cohesion

Ulrich, Kreig *et al* (2005) used Rab5 and in, particular, Rab5c's role in endocytosis, to elucidate the effect of Wnt11 on cell cohesion during gastrulation. In particular, the study is concerned with Wnt11's role in controlling prechordal plate progenitor cell movements. Previous work by the authors had shown that prechordal plate in zebrafish is formed by a highly cohesive group of axial mesendodermal progenitor cells which move in a straight path from the germ ring toward the animal pole of the gastrula (Ulrich et al., 2003) and that E-cadherin-mediated cell cohesion is required for the coordinated movement of prechordal plate progenitor cells during zebrafish gastrulation (Montero et al., 2005). Ulrich *et al.* (2005) showed that in wild-type embryos, prechordal plate progenitors moved both toward the overlying epiblast cell layer and along it toward the animal pole. However, embryos lacking *wnt11* (*silberblick* mutants (*slb)*) showed slower movement toward the animal pole with cells often moving in the opposite direction toward the vegetal pole, although cells moved normally towards the epiblast. The coherence of the prechordal plate progenitor cell movements at the onset of gastrulation were also reduced in *slb/wnt11* mutants. The authors suggest that Wnt11 is required to align the movement of individual prechordal plate progenitors and that this alignment might represent a way by which Wnt11 efficiently coordinates prechordal plate progenitor movement toward the animal pole. In addition, the authors suggested that Wnt11 might control alignment of prechordal plate progenitor movement by regulating the cohesion of these cells. In cell cultures, mutant for *wnt11*, large cell aggregates were reduced while small cell aggregates were increased when compared to wild-type. However, when E-cadherin was knocked-down in cultured *wnt11*$^{-/-}$ mutant cells showed no significant differences in aggregates while wild-type cells displayed an increase in small cell aggregates and a decrease in large cell aggregates, compared to wild-type cells with E-cadherin. Wnt11 expression was, therefore, suggested to lead to changes in the subcellular localization of E-cadherin from the plasma membrane into cytoplasmic dots (Ulrich et al., 2005), these dots localized with injected mRNA YFP-

fusion of the zebrafish Rab5c. Wntl1 overexpression was shown to lead to an increase in the proportion of Rab5c-positive endocytic E-cadherin vesicles as did the overexpression of a constitutively active form of *rab5c-YFP* in *slb/wntl1* mutant embryos. *rab5c* MO injected embryos were shown to frequently have a posteriorly displaced and elongated prechordal plate at the end of gastrulation, phenocopying the *slb/wntl1* mutant phenotype. However, *slb/wntl1* mutant embryos, expressing *da-rab5c-YFP*, formed a prechordal plate that was wild-type in appearance, suggesting a rescue of the mutant phenotype. The de-adhesion forces needed to dissociate wild-type versus *slb/wntl1* mutant cells from E-cadherin substrates were decreased, but could be rescued by expressing low amounts of *wntl1* mRNA. Similarly in *rab5c* MO injected cells there was a decrease in the de-adhesion forces when compared to wild type. The study suggests that Wntl1 modulates E-cadherin dynamics through endocytosis and recycling. E-cadherin being partially, but not exclusively, required for Wntl1 control of mesendodermal cell cohesion, suggests a role for other adhesion molecules such as integrins.

5.1.3.3 The zebrafish *rab5*s

Dr Matthew Clark and Dr Isabel Campos have identified 4 zebrafish Rab5s; two Rab5as, Rab5b and Rab5c. Both Rab5as are in the zebrafish online resource zfin (www.zfin.org) - they are termed 'Rab5a' and 'Rab5a like'. In Dr Campos' thesis these Rabs are re-named Rab5a1 and Rab5a2 respectively (Campos, 2004). Embryos showed no obvious phenotype when *rab5a1* was knocked-down by Dr Campos, however *rab5a2* MO injected embryos showed a very striking gastrulation phenotype, the embryo showed no morphological organizer and died before the completion of epiboly (Figure 5.1.1). In addition, development is drastically slowed when control embryos reach 90% epiboly, compared to *rab5a2* MO injected embryos, which only reach 50% epiboly. In cases where *rab5a2* MO injected embryos reached 80-90% epiboly the blastoderm margin contracted and pinched off the yolk causing its contents to leak and the physiological environment surrounding the blastoderm cells to be disrupted resulting in death (Campos, 2004). *rab5b* MO injected embryos showed thinner and u-shape somites, forebrain defects and cell death in the brain (Campos, 2004). Finally, *rab5c* MO injected embryos showed a similar phenotype to embryos with depleted *rab5b* with u-shape somites, shortened

tail, forebrain defects and cell death in the brain (Campos, 2004). The lack of morphological organizer in the *rab5a2* MO injected embryos led Dr Campos to perform expression analysis for the nodals and their downstream markers. *rab5a2* MO injected embryos displayed a startling lack of expression of the nodals and a majority of their target genes. The MO injected embryos showed no *sqt, cyc, bik, gsc* or *flh* expression and a severe reduction in *ntl* expression compared to control injected embryos (Figure 5.1.2). The dramatic early phenotype seen in *rab5a2* MO injected embryos has, so far, only been seen following the depletion of this Rab, out of all the Rabs screened. Rab5a2's phenotype and the dramatic loss of nodal signalling have led me to further investigate its function and, in particular, its role in nodal signalling.

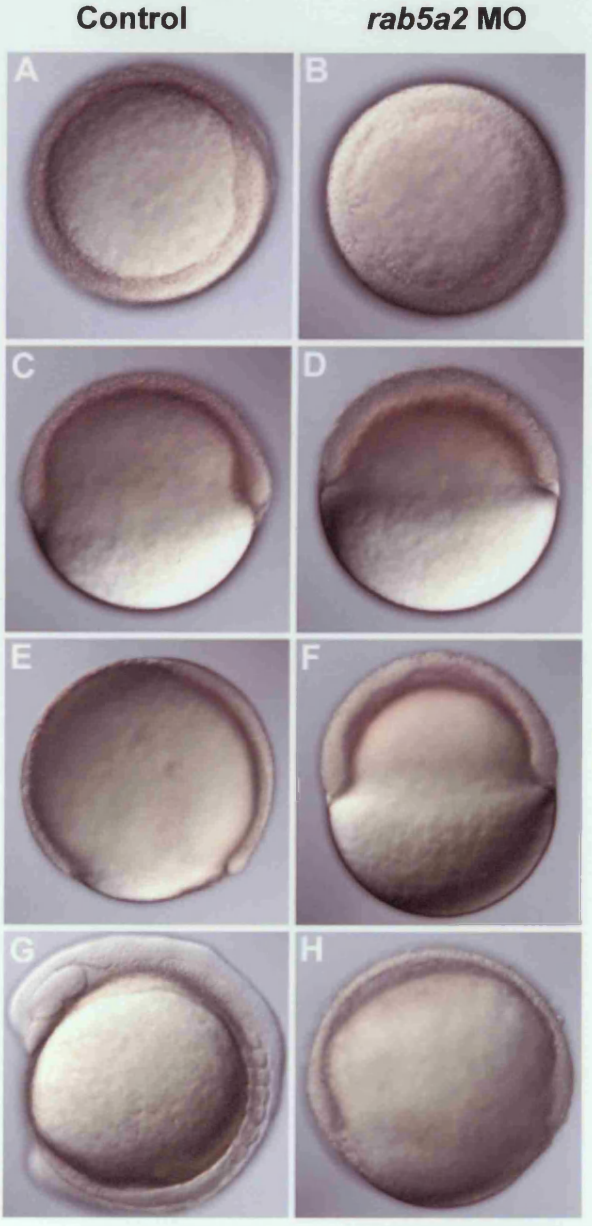

Figure 5.1.1: Time series of 3ng *rab5a2* MO injected embryos (B,D,F,H) compared with control injected embryos (A,C,E,G). Animal view (A) and side view (C) of control injected embryo at shield stage compared to animal view (B) and side view (D) of 3ng *rab5a2* MO injected embryos at the same time point. Control injected embryos at 90% epiboly (E) compared to the same time point in the 3ng *rab5a2* MO injected embryos (F). 8 somite stage control embryo (G) compared to 3ng *rab5a2* MO injected embryo at the same time point (H). (Campos, 2004)

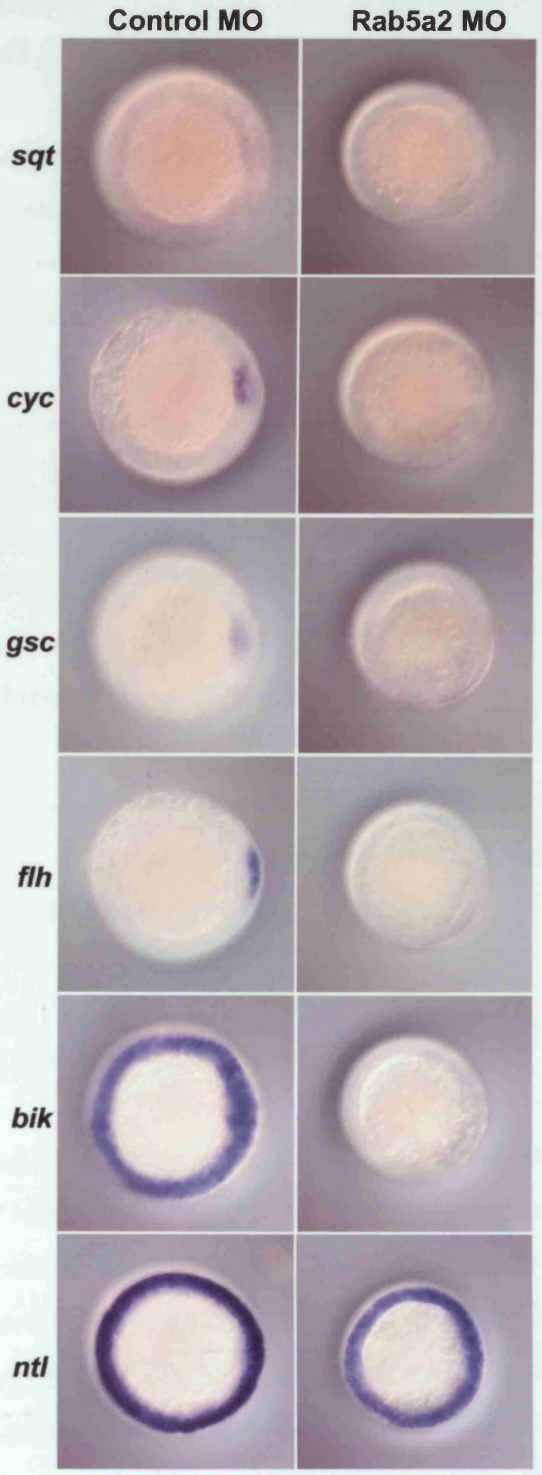

Figure 5.1.2: Comparison of *ish* expression patterns for *sqt*, *cyc*, *gsc flh bik* and *ntl* in shield stage control MO injected (left column) and shield stage 3ng *rab5a2* MO injected embryos (right column)(Campos, 2004).

5.2 Reproducibility and further analysis of the Rab5a2 loss of function phenotype.

To characterize Rab5a2, first, it was necessary to check the reproducibility of the loss of function phenotype and the nodal expression pattern seen in the *rab5a2* MO injected embryos. Following this, it was necessary to look more closely at this expression pattern in order to ascertain if there is a temporal element to the expression pattern seen in the *rab5a2* MO injected embryos. In addition it would be interesting to investigate whether the loss of Nodal signalling was due to maternal or zygotic transcripts. Finally, in all other systems that have been studied Rab5a localized to endosomes and has been shown to be responsible for clatherin-mediated endocytosis (Bucci et al., 1995; Bucci et al., 1992; Gorvel et al., 1991). It was therefore important to investigate Rab5a2s effect on other endocytic pathways, and, for this, the role of endocytosis in epiboly was studied.

The *rab5a2* MO injected embryos (*rab5a2* MO injected embryos) are throughout this study compared to 10ng of control MO injected embryos. This control MO is the *rab5a2* MO containing a five base mismatch.

5.2.1 Reproducing the loss of function phenotype

Using the MO designed by Dr Campos, at the dose used in the original investigations, 3ng of *rab5a2* MO was injected and compared to control MO injected embryos. Since the *rab5a2* MO injected embryos showed no phenotype, the dose was increased until an effect was observed. At 5ng of *rab5a2* MO, all embryos died before completing epiboly (n = 47), while at 4ng of MO they all appeared similar to control MO injected embryos (n = 44). When the dose was increased still further to 6ng, the *rab5a2* MO injected embryos died between 30% and 50% epiboly (n = 41/45). In the 5ng *rab5a2* MO injected embryos, at approximately 30% epiboly, fluid appeared to accumulate between the blastoderm cells and the yolk (Figure 5.2.1) this was not seen in control MO injected embryos. In the 6ng *rab5a2* MO injected embryos, this build-up of fluid up, occurred at the earlier stage of approximately 10% epiboly and was more pronounced. In the control MO injected embryos, the cells

appeared as a smooth blastoderm covering the yolk cell, in the *rab5a2* MO injected embryos, the cells appeared to have a substantially rougher blastoderm with cells appearing as a less cohesive group. Finally the *rab5a2* MO injected embryos, as described by Dr Campos, showed substantial developmental delay, compared to control MO injected embryos (Figure 5.2.1).

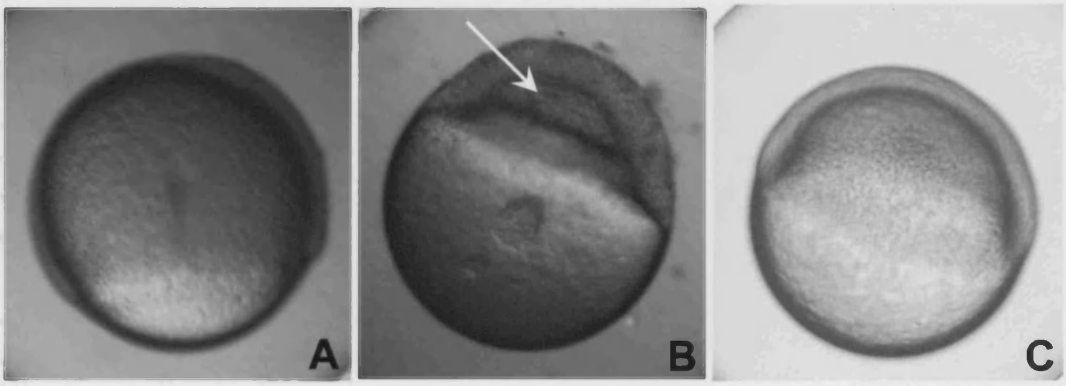

Figure 5.2.1: Control embryo at 70% epiboly (A) compared to 5ng *rab5a2* MO injected embryo at the same time point (B) and control embryo at shield stage (C). Arrow in B indicates the apparent build-up of fluid between the yolk and the cells.

5.2.2 Reproducibility of the expression patterns of nodal and nodal-responsive genes in rab5a2 MO injected embryos.

To reproduce the expression patterns of the nodals and the nodal-responsive genes in the *rab5a2* MO injected embryos, embryos were injected with either 5ng of *rab5a2* MO or 10ng of control MO and fixed at 50% epiboly. The *rab5a2* MO injected embryos showed no expression of the downstream nodal markers *gsc* or *flh* and reduced expression of *ntl* and *bhik.* They also showed no expression of *cyc* (Figure 5.2.2). As with Dr Campos' data, it was difficult to see *sqt* staining in the control embryos, so it is difficult to determine whether *sqt* expression is reduced in the MO injected embryos (Figure 5.2.2). Using a higher dose (6ng) of *rab5a2*, the effect of the MO was to visibly abolish the *bhik* and *ntl* staining in addition to that of *gsc* and *flh.*

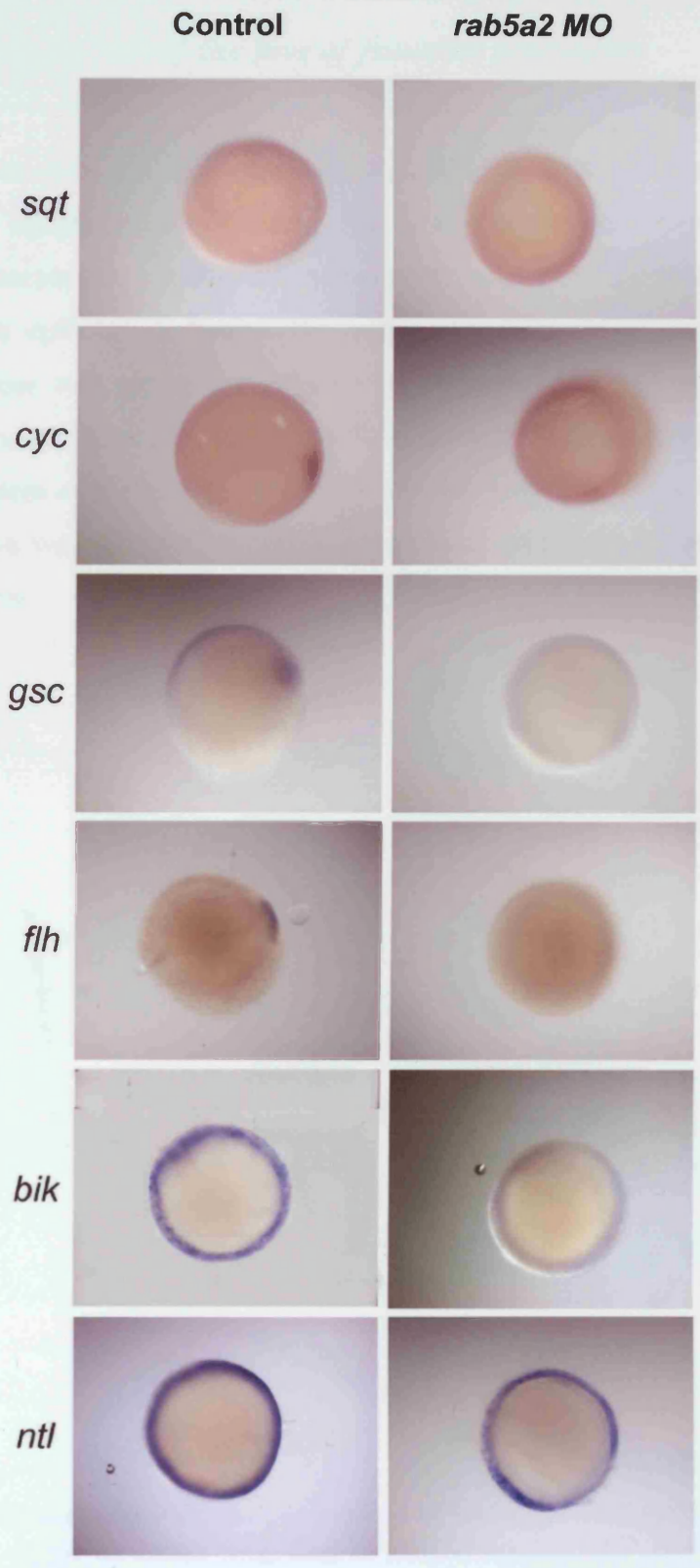

Figure 5.2.2: Animal view of expression patterns of the *nodals* and nodal-responsive genes in shield stage control MO injected and 5ng of *rab5a2* MO injected embryos.

5.2.3 Further analysis of the loss of function phenotype

To establish whether the loss of nodal signalling is time and dose dependent, embryos were injected with either 2ng, 5ng or 8ng of *rab5a2* MO and along with 10ng control morpholino injected embryos were fixed at four time points (30%, 50%, 70% and 90% epiboly). Subsequently, expression patterns of *gsc* and *ntl* were examined. These two genes are induced by differing doses of nodal so should provide an accurate picture of Nodal signalling at these time points. Furthermore, the expression pattern of the dorsal marker *chordin* was recorded, to investigate if nodal signalling alone was affected, or whether the effect relates to the establishment of dorsal in general.

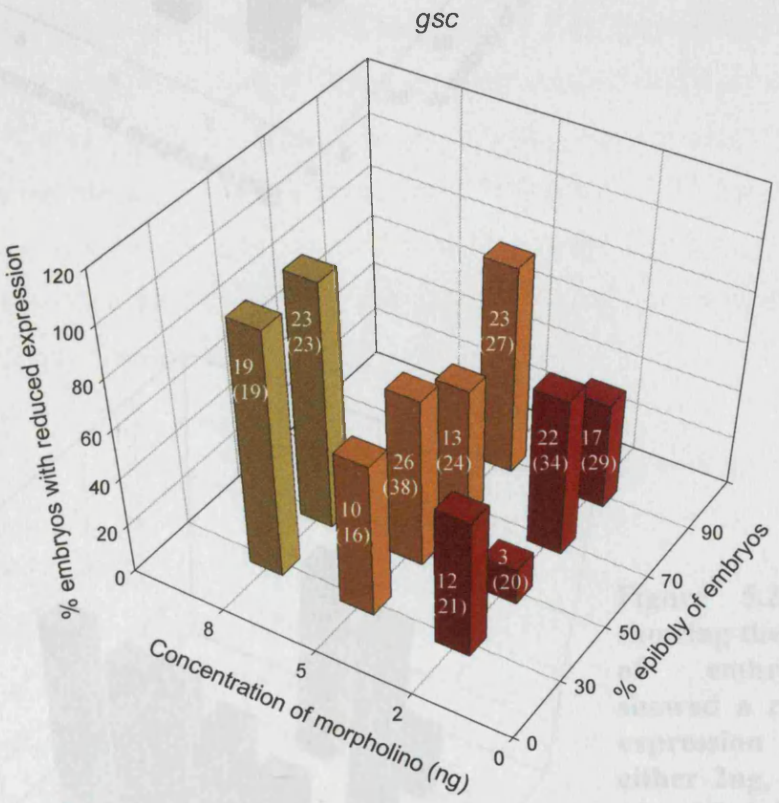

Figure 5.2.3: Graph showing the percentage of embryos that showed a reduction in expression of *gsc* at either 2ng, 5ng or 8ng of *rab5a2* MO and at 30%, 50%, 70% and 90% epiboly stages.

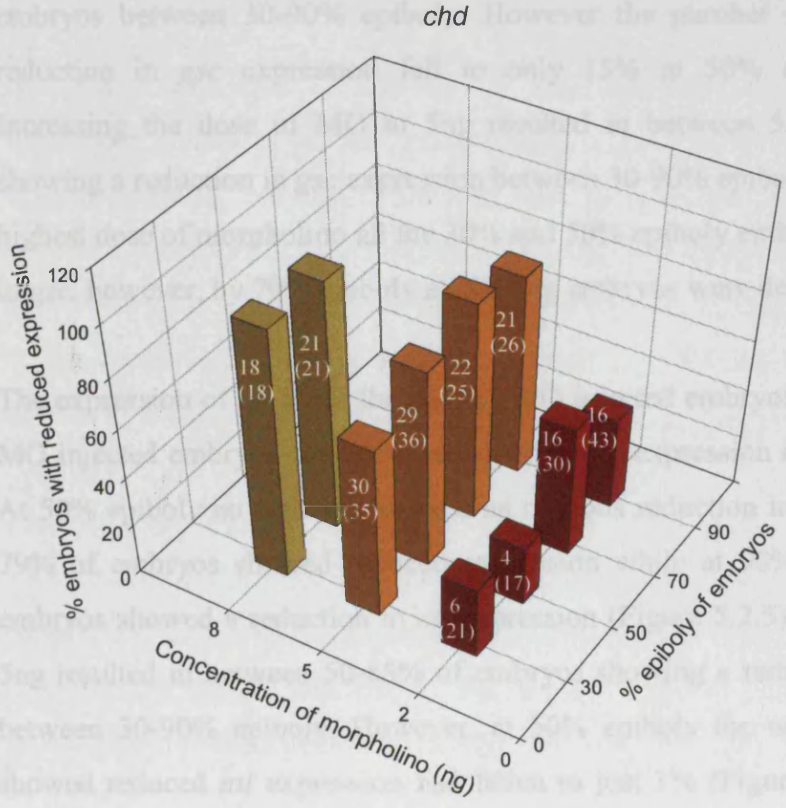

Figure 5.2.4: Graph showing the percentage of embryos that showed a reduction in expression of *chd* at either 2ng, 5ng or 8ng of *rab5a2* MO and at 30%, 50%, 70% and 90% epiboly stages.

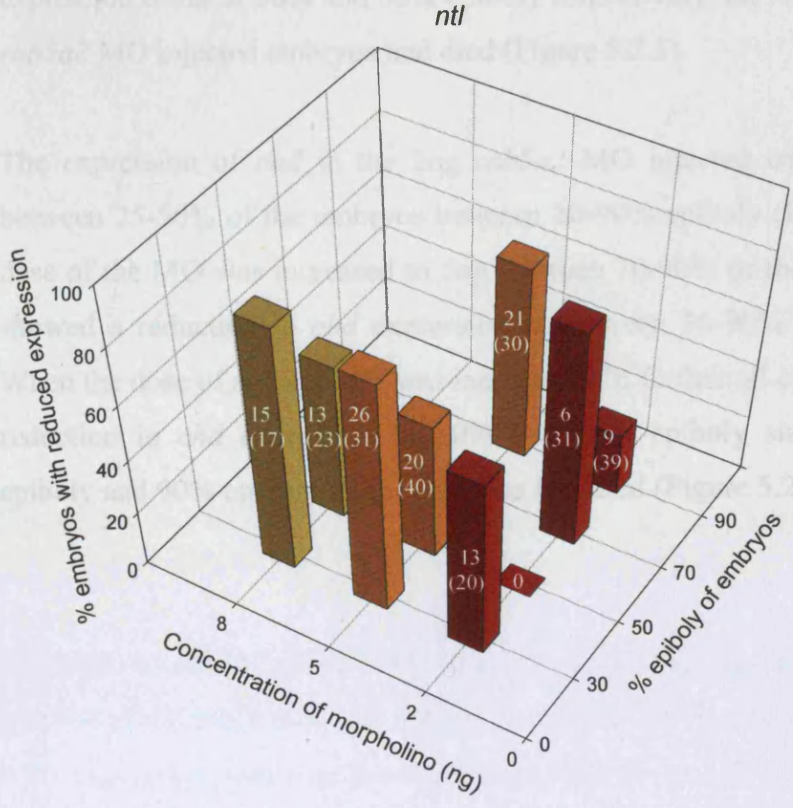

Figure 5.2.5: Graph showing the percentage of embryos that showed a reduction in expression of *ntl* at either 2ng, 5ng or 8ng of *rab5a2* MO and at 30%, 50%, 70% and 90% epiboly stages.

The expression of *gsc* in the 2ng MO injected embryos was reduced in 45-65% of the embryos between 30-90% epiboly. However the number of embryos showing a reduction in *gsc* expression fell to only 15% at 50% epiboly (Figure 5.2.3). Increasing the dose of MO to 5ng resulted in between 55-85% of the embryos showing a reduction in *gsc* expression between 30-90% epiboly (Figure 5.2.3). At the highest dose of morpholino all the 30% and 50% epiboly embryos showed a decrease in *gsc,* however, by 70% epiboly all the 8ng embryos were dead (Figure 5.2.3).

The expression of *ntl* in all the *rab5a2* MO injected embryos was variable. The 2ng MO injected embryos showed a reduction in *ntl* expression of 65% at 30% epiboly. At 50% epiboly no embryos showed an obvious reduction in *ntl* expression, at 70% 79% of embryos showed reduced expression while at 90% epiboly only 23% of embryos showed a reduction in *ntl* expression (Figure 5.2.5). Increasing the dose to 5ng resulted in between 50-85% of embryos showing a reduction in *ntl* expression between 30-90% epiboly. However, at 50% epiboly the number of embryos that showed reduced *ntl* expression had fallen to just 3% (Figure 5.2.5). Increasing the dose still further resulted in 88% and 57% of the embryos showing reduced expression of *ntl* at 30% and 50% epiboly respectively. At 70% and 90% all the 8ng *rab5a2* MO injected embryos had died (Figure 5.2.5).

The expression of *chd* in the 2ng *rab5a2* MO injected embryos was reduced in between 25-50% of the embryos between 30-90% epiboly (Figure 5.2.4). When the dose of the MO was increased to 5ng between 70-90% of the MO injected embryos showed a reduction in *chd* expression at between 30-90% epiboly (Figure 5.2.4). When the dose of *rab5a2* MO was increased still further all of the embryos showed a reduction in *chd* expression at 50% and 30% epiboly stages. However at 70% epiboly and 90% epiboly all the embryos had died (Figure 5.2.4).

5.2.4 Maternal verses zygotic

The early phenotype of the *rab5a2* MO injected embryos and the ubiquitous expression pattern of *rab5a2* seen as early as the one cell stage (zfin) suggests that maternal *rab5a2* plays an important role in zebrafish development. In order to ascertain whether this is the case a splice MO was designed, this straddles a splice site of the gene of interest and so binds, in part, to the intronic and, in part, to the exonic section of the gene. This ensures that the MO only binds to transcripts that have not yet been spliced, such as zygotic transcripts (Draper et al., 2001).

Embryos were injected with either 10ng of *rab5a2* splice MO or 10ng of control MO. At shield stage the *rab5a2* splice MO injected embryos were comparable to controls showing a visible organizer unlike the *rab5a2* morpholino injected embryos. However by 24hpf the *rab5a2* splice MO injected embryos appeared as an accumulation of dead cells on top of the yolk (Figure 5.2.6).

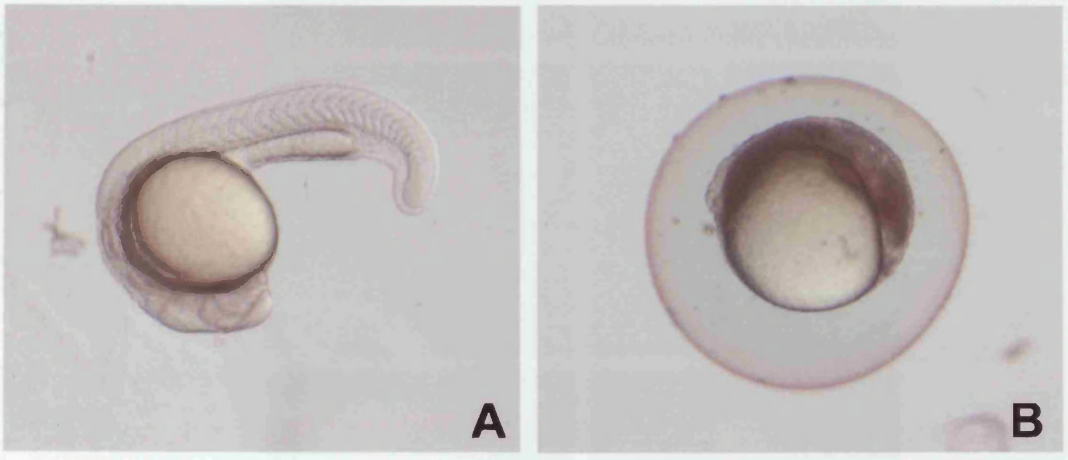

Figure 5.2.6: Lateral view of 24hpf embryos: control MO injected embryo (A) compared to 8ng *rab5a2* splice MO injected embryo (B).

Although the *rab5a2* splice MO injected embryos had showed massive cell death at 24hpf at shield stage they had a visible organizer, it was therefore necessary to look at the expression pattern of the nodal responsive genes *ntl, bik* and *gsc* and the dorsal marker *chd.* The *rab5a2* splice MO injected embryos and control MO injected

embryos were fixed at 50% epiboly. Analysis of the expression patterns for *gsc, ntl* and *chd* in the splice MO injected embryos showed them to be similar to those seen in the controls (Figure 5.2.7). *bik* expression however appeared slightly reduced in the splice MO injected embryos (n = 10/12).

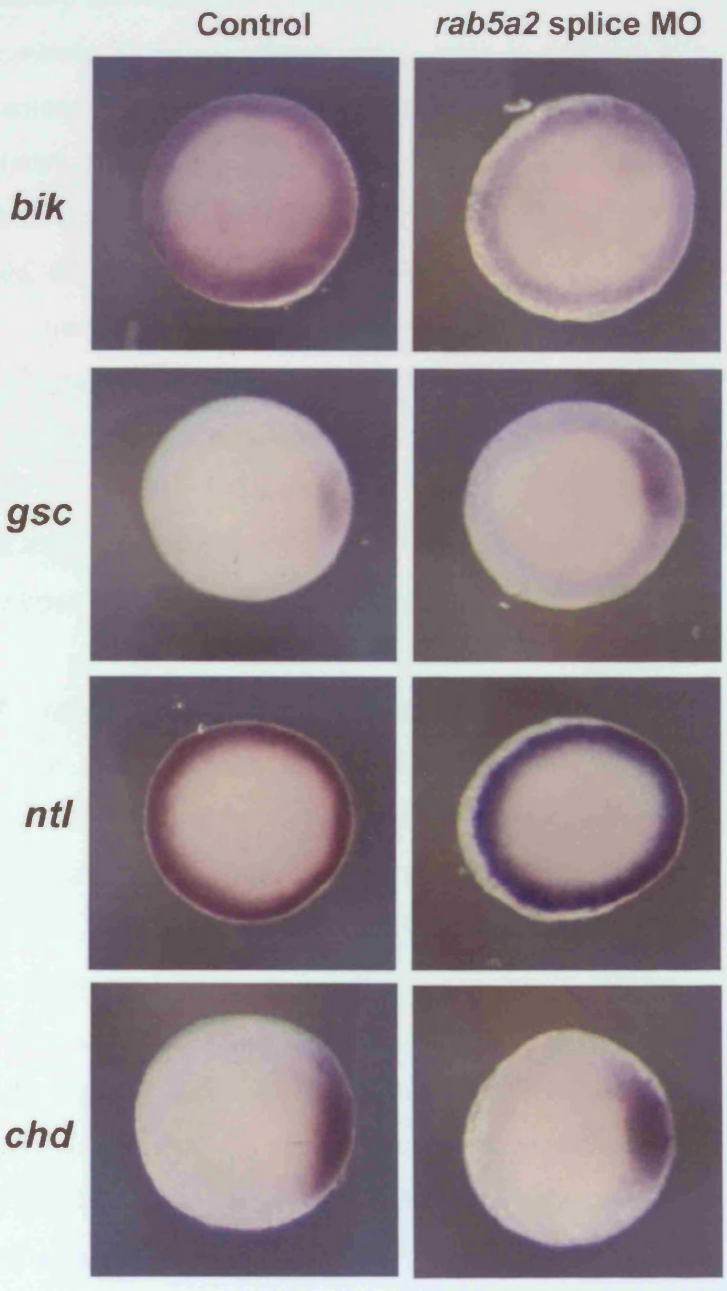

Figure 5.2.7: Animal views of shield stage embryos*: gsc, ntl, chd* and *bik* expression in control MO injected embryos on the left compared to 10ng *rab5a2* splice MO injected embryos on the right

5.2.5 The effect of loss of Rab5a2 function on epiboly movements

Epiboly in zebrafish is considered, in part, an endocytic event (Betchaku and Trinkaus, 1986). Therefore, to ascertain whether the phenotype seen in *rab5a2* MO injected embryos is, in some part, due to its effect on the role of endocytosis during epiboly, the epiboly movements of *rab5a2* MO injected embryos were compared with those of controls, at three different time points of epiboly. The embryos were placed in 1x Danieau solution, containing 5mg/ml biotinylated dextran (10,000mw), at dome stage (start of epiboly), 30% epiboly and shield stage for 15 minutes, they were then washed three times in 1x Danieau solution and immediately fixed in 4% PFA. Once fixed, the embryos were stained for biotin (Solnica-Krezel et al., 1994). The control MO injected embryos, at dome stage and 30% epiboly, all showed a ring of staining around the leading edge of the blastoderm (Figure 5.2.8). At shield stage, this staining formed more of a gradient moving from the dorsal to ventral side of the embryo. The *rab5a2* MO injected embryos showed very little staining at dome stage (n = 13/17) and even less staining at 30% (n = 12/13). There was no staining seen in the *rab5a2* MO injected embryos at shield stage (n = 14/15) (Figure 5.2.8).

The *rab5a2* MO injected embryos showed defects in endocytosis however epiboly did proceed but at a slower pace and did not complete. This suggested that the microtubules in the yolk were unaffected and were responsible for epiboly proceeding as far as it did. Cold shock depolarizes microtubules therefore 5ng *rab5a2* MO injected embryos and control MO injected embryos were placed at 20°C and monitored overnight. The control embryos developed normally (n =16/16) but with some developmental delay whereas the *rab5a2* MO injected embryos arrested and died at sphere stage to very early epiboly (n = 14/14) (Figure 5.2.9, supplemental movie 5.2.9). The *rab5a2* MO injected siblings that were incubated at 28°C died at the later stage of 70% epiboly while the control MO injected siblings incubated at 28°C developed normally.

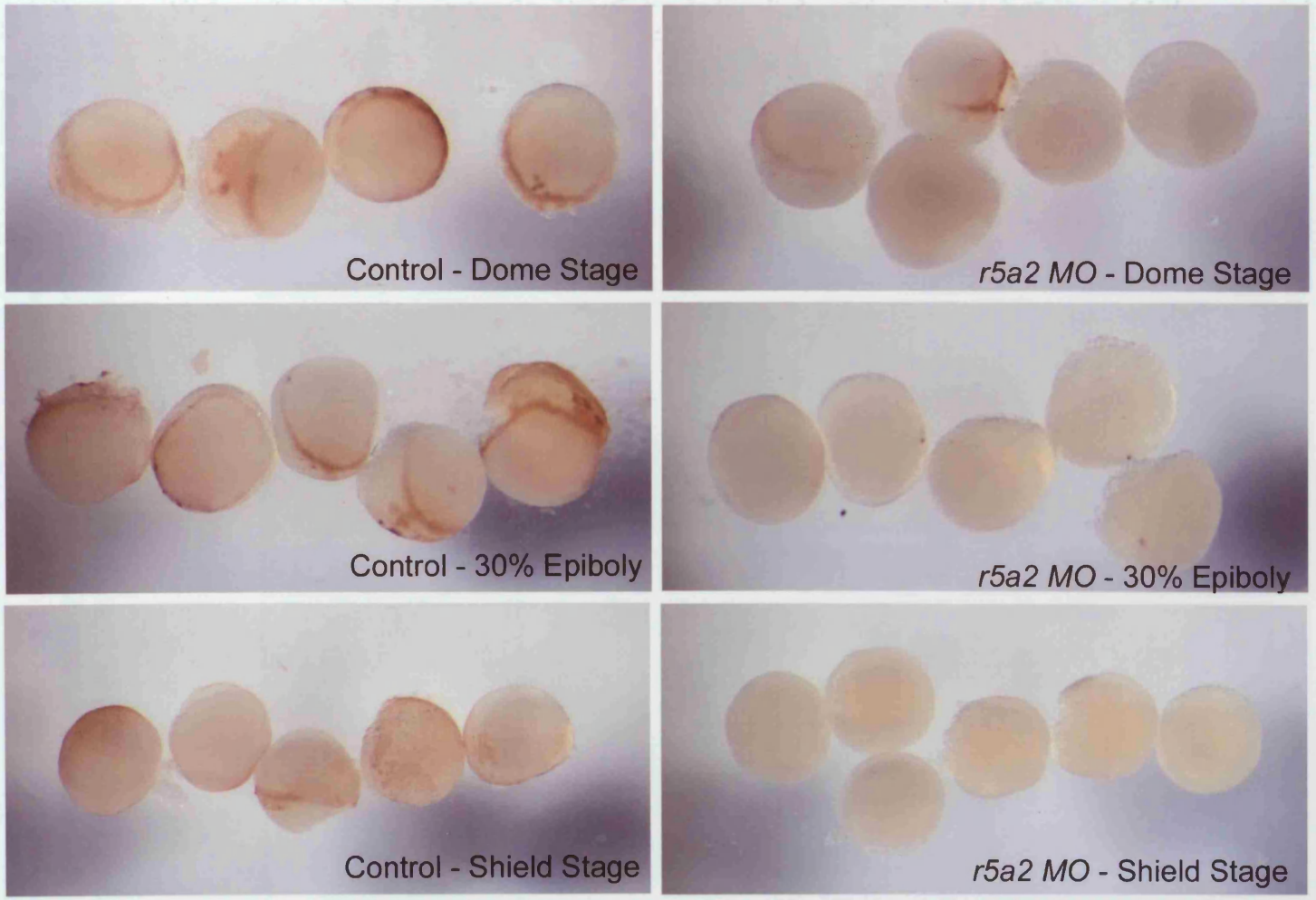

Figure 5.2.8: The right column shows the effect of 5ng of *rab5a2* on different stages of epiboly when compared with control MO injected embryos in the left column.

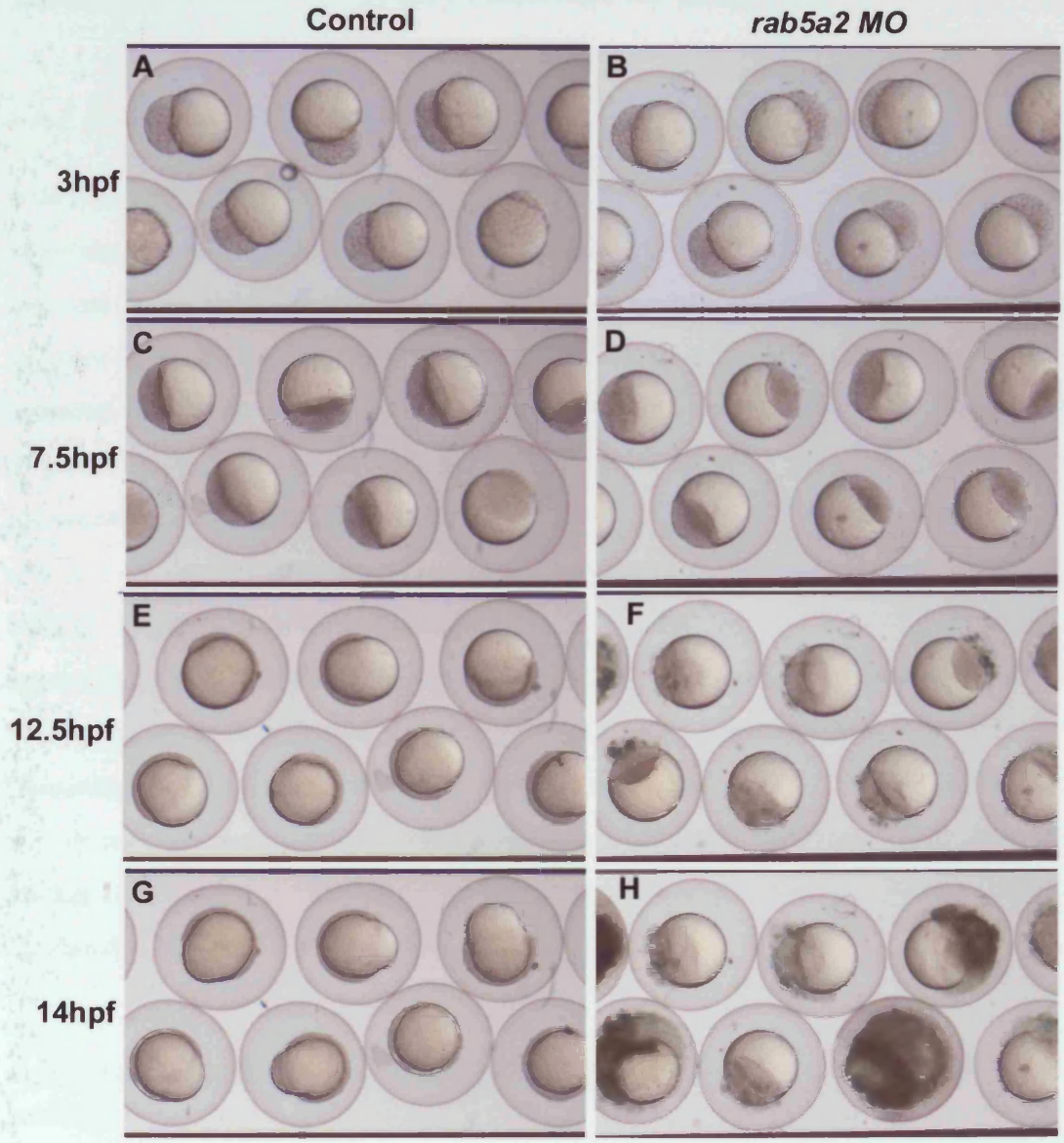

Figure 5.2.9: A time series of embryos cold shocked at 20°C: 3hpf control MO injected embryos (A) compared to *rab5a2* MO injected embryos (B). 7.5hpf control MO injected embryos (C) compared to *rab5a2* MO injected embryos (D). 12.5hpf control MO injected embryos (E) compared to *rab5a2* MO injected embryos (F). 14hpf control MO injected embryos (G) compared to *rab5a2* MO injected embryos (H).

5.3 Analysis of overexpression of Rab5a2

5.3.1 Rab5a2 overexpression

Wild type *rab5a2* mRNA was overexpressed in wild type embryos by injecting 1.5ng of *rab5a2* capped mRNA. At 40-50% epiboly, an accumulation of cells became apparent on the animal pole of approximately one third of the *rab5a2* overexpressing embryos (n = 14/41). In the remaining *rab5a2* overexpressing embryos, the organiser appeared larger (n = 27/41), when compared with MO buffer injected embryos (Figure 5.3.1). The *rab5a2* overexpressing embryos then appeared to arrest for approximately one hour, during which time either the accumulation of cells on the animal pole disappeared, or the enlarged organiser reduced in size and the embryo became what appeared phenotypically wild type (n = 41/41). At 24hpf, approximately two thirds of the *rab5a2* overexpressing embryos appeared similar to MO buffer injected embryos, except for an enlarged yolk extension (n = 27/39). The remaining third had a reduced body axis and reduced head size (n = 12/39). By 5dpf, all the *rab5a2* overexpressing embryos show a severely shortened body axis and thicker, less extended yolks (n = 38/38), compared to MO buffer injected embryos (Figure 5.3.1).

5.3.2 Nodal markers expression pattern in Rab5a2 overexpressing embryos

To establish whether overexpression of *rab5a2* affected the expression pattern of nodal markers, embryos were fixed at shield stage and stained for *bik, ntl, gsc* and *chd* expression by *in situ hybridization*. In both the MO buffer injected embryos and the *rab5a2* overexpressing embryos, the *bik* expression patterns were similar (Figure 5.3.2). A similar expression pattern between MO buffer injected embryos and *rab5a2* overexpressing embryos was also seen for *ntl*. There appeared to be a small difference in the expression pattern of *chd*, with the *rab5a2* overexpressing embryos showing *chd* expression encroaching into the ventral region more than in MO buffer injected embryos (Figure 5.3.2). There was a substantial difference in *gsc* expression pattern between the MO buffer injected embryos and the *rab5a2* overexpressing

embryos. The *rab5a2* overexpressing embryos showed the same *gsc* expression pattern as the MO buffer injected embryos on the dorsal side of the embryo but in addition there was *gsc* expression on the animal pole closest to the ventral side of the embryo (Figure 5.3.2). This expression was not seen in the MO buffer injected embryo (Figure 5.3.2) and was stronger than the dorsal expression seen in these embryos.

To further analyse this result, *rab5a2* overexpressing embryos and MO buffer injected embryos were fixed at 30%, 50%, 70% and 90% epiboly so that the expression pattern of *chd, ntl* and *gsc* could be followed over time. At 30% epiboly, the *rab5a2* overexpressing embryo showed expression of *gsc* in the ventral region, in addition to its usual dorsal expression. This additional expression pattern was seen in 83% of the embryos (n = 10/12). Interestingly, at this stage *ntl* expression in the *rab5a2* overexpressing embryos shows spots of staining in the animal pole, compared to the marginal expression observed in the MO buffer injected embryos. This expression of *ntl* was seen strongly in 50% (n = 6/12) of the *rab5a2* overexpressing embryos, with a further 17% exhibiting weaker staining (n = 2/12) (Figure 5.3.3). At 50% epiboly 73% of the *rab5a2* overexpressing embryos (n = 8/11) show strong additional staining in the animal pole of embryos stained for *gsc* expression, while 18% of the experimental embryos showed fainter (n = 2/11), additional *gsc* staining. At this stage, most of the embryos, stained for *ntl* expression, showed no additional staining (n = 11/12). However 67% of *rab5a2* RNA injected embryos (n = 8/12) showed *ntl* staining which began to encroach on the animal pole from its marginal domain, showing a thicker band of staining round the embryo than is seen in MO buffer injected embryo (Figure 5.3.3).

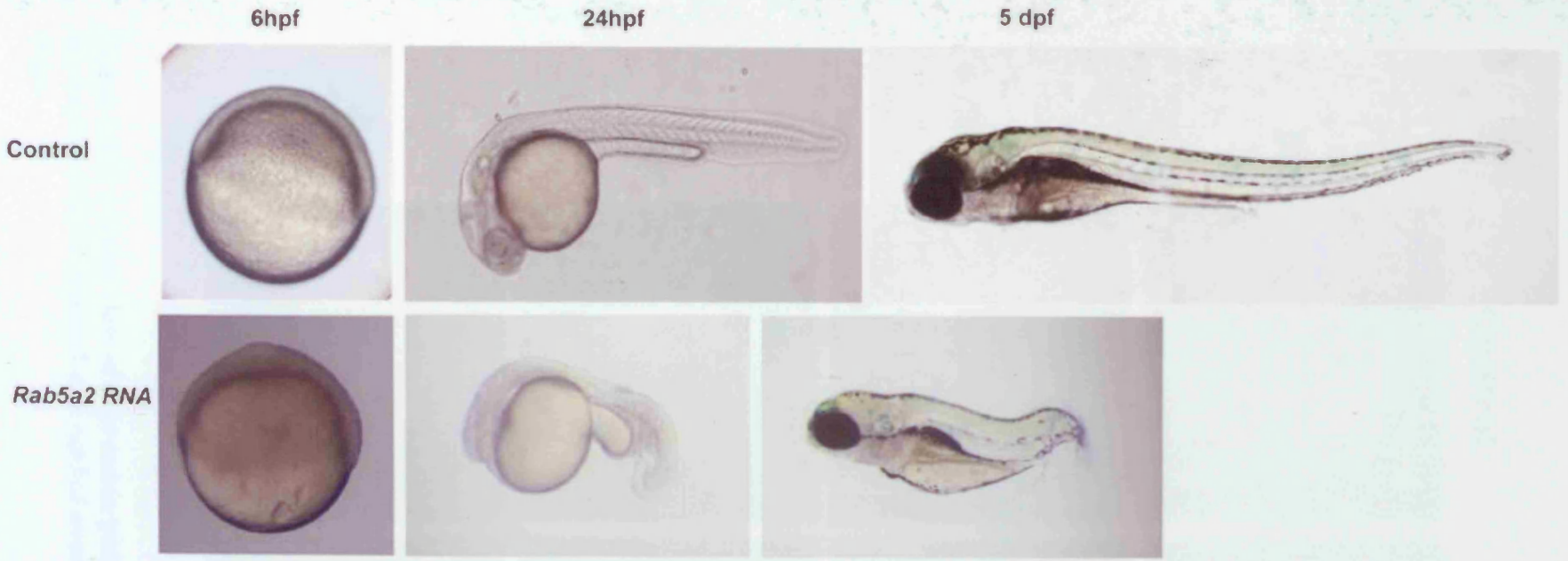

Figure 5.3.1: A shield stage 1.5ng *rab5a2* overexpressing embryo compared to shield stage MO buffer injected embryo. Lateral view of 24hpf 1.5ng *rab5a2* overexpressing embryo compared to 24hpf MO buffer injected embryo. Lateral view of 5dpf 1.5ng *rab5a2* overexpressing embryo compared to 48hpf MO buffer injected embryo

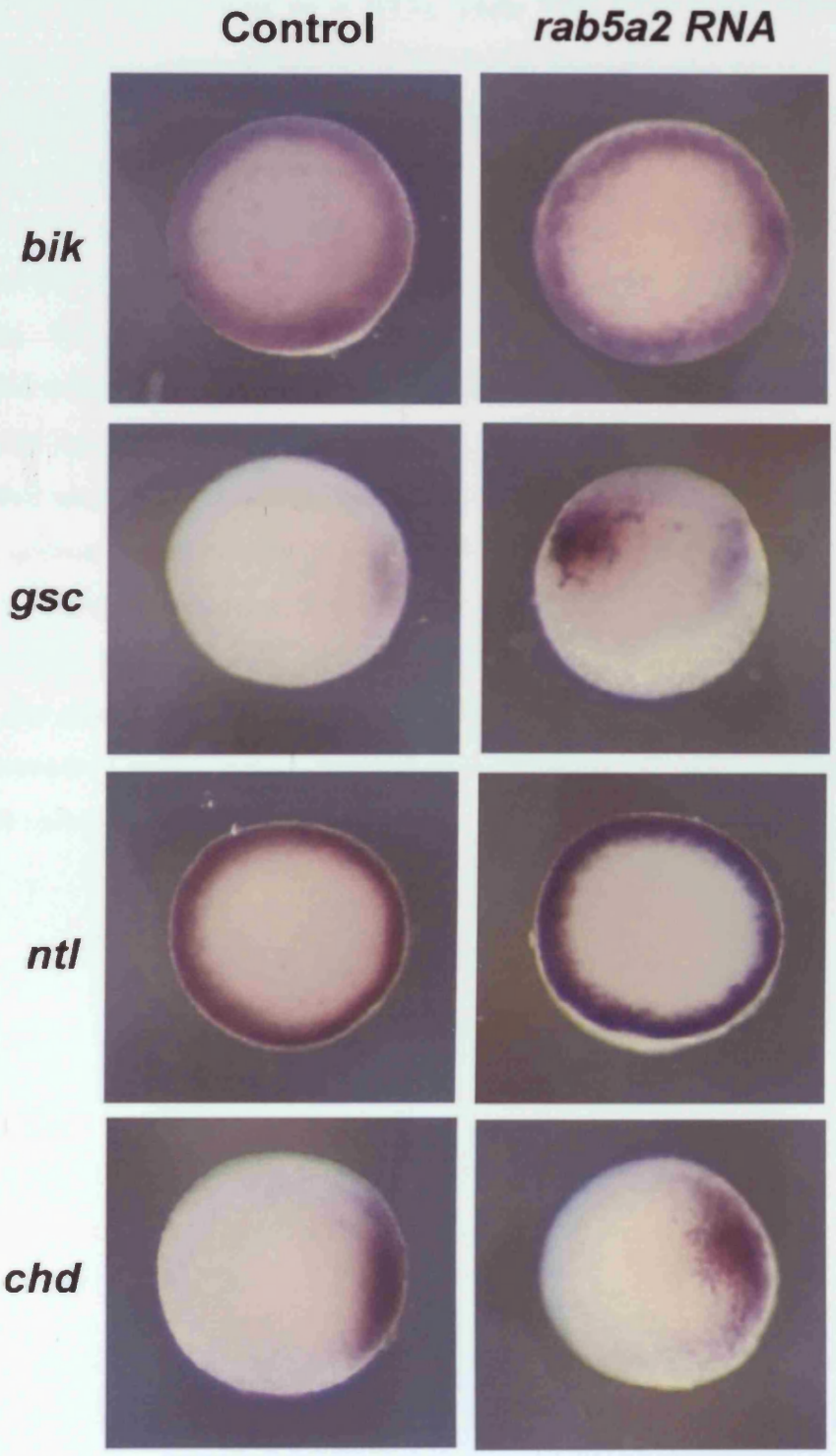

Figure 5.3.2: Animal view of expression patterns of the nodal and dorsal markers in control injected and *rab5a2* overexpression embryos at shield stage.

At 70% epiboly, 39% of *rab5a2* RNA injected embryos show strong additional *gsc* expression in the animal pole (n = 5/13), while 23% show weak additional *gsc* expression (n = 3/13) when compared to MO buffer injected embryos (Figure 5.3.3). *ntl* expression at this stage in *rab5a2* RNA injected embryos is seen in the margin comparable with MO buffer injected embryos. In addition, there is strong staining in the animal pole in 39% of the experimental embryos (n = 5/13), with similar but weaker staining seen in another 31% of experimental embryos (n = 4/13) (Figure 5.3.3). The 90% epiboly *rab5a2* RNA injected embryos continue to show mislocalized expression of both *gsc* and *ntl* with additional staining when compared to MO buffer injected embryos (Figure 5.3.3). At this stage, the number of embryos that have this unusual *gsc* staining has fallen to 50% (n = 5/10) while those that have the strong unusual *ntl* staining remains at around 70% (n = 7/10). The *chd* expression pattern is unchanged in experimental embryos, compared to the MO buffer injected embryos in 30% (n = 12), 50% (n = 11), 70% (n = 10) and 90% (n = 10) epiboly. However, the strength of this expression appears stronger in *rab5a2* RNA injected embryos compared to MO buffer injected embryos at the 70% (n = 10/10) and 90% (n = 10/10) epiboly stages (Figure 5.3.3).

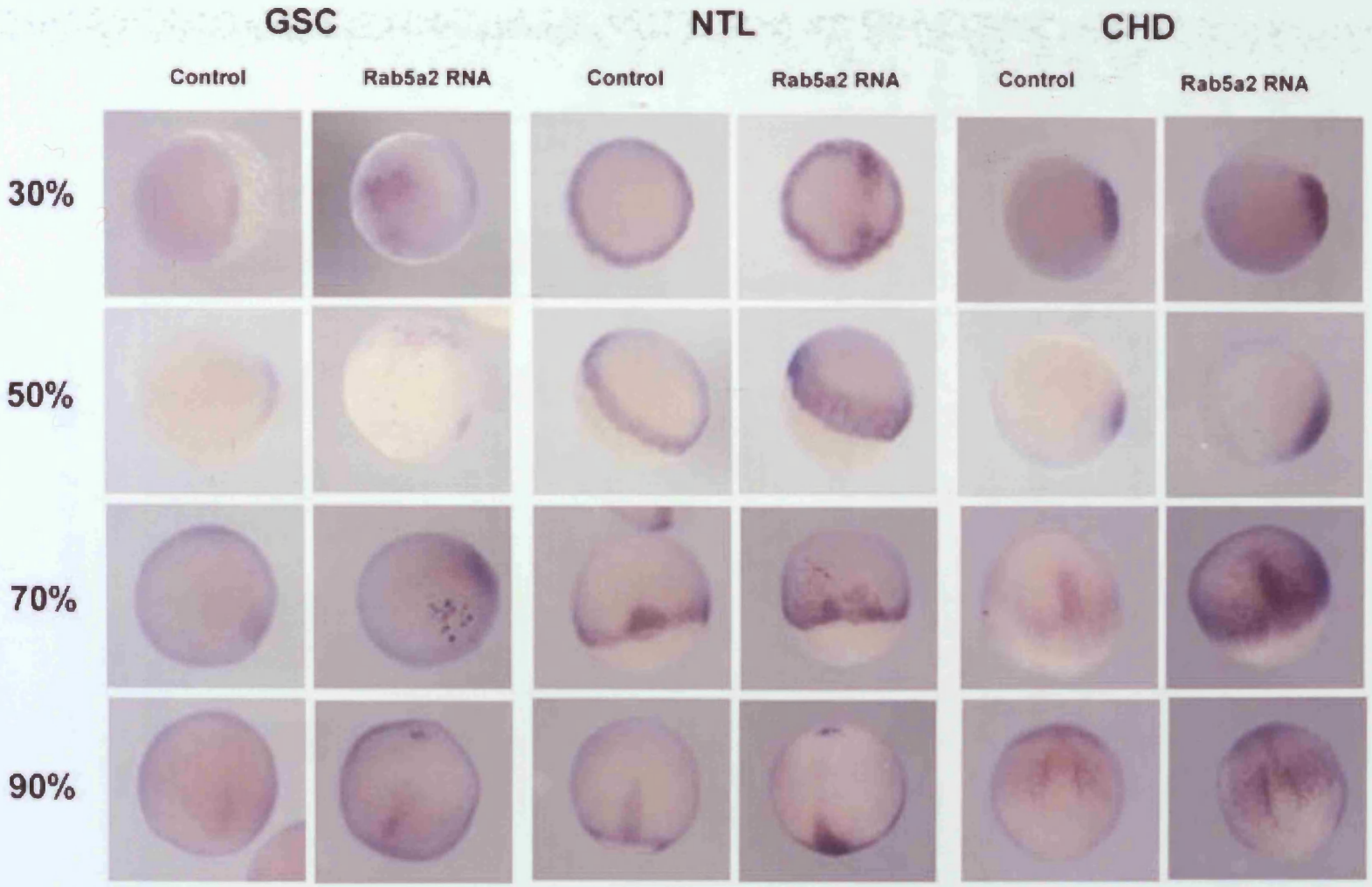

Figure 5.3.3: Showing the expression patterns of *gsc, ntl* and *chd* in control and Rab5a2 overexpressing embryos at 30%, 50%, 70% and 90% epiboly. *gsc* expressing embryos are shown as animal pole views as are 30% epiboly *ntl* expressing embryos and 30% and 50% *chd* expressing embryos. The remainder of the embryos are shown as a side view for improved visualisation of expression patterns

5.3.3 The effect of constitutively active Rab5a2 on the zebrafish embryo

Much of the experimental work described in the literature describes the use of a constitutively active version of Rab5 for overexpression experiments. One base change in the injected RNA ensures that the Rab is locked in its GTP-bound form and so constantly active. The dose of wild-type *rab5a2* RNA, needed to elucidate an overexpression phenotype was high; this is due to the many regulators of Rab function found *in vivo* eg. GAP, GDI etc. In order to overexpress wild type Rab protein, these regulators must be overcome by superior numbers of Rab protein. However, injection of constitutively active *rab5a2* RNA (da-*rab5a2* RNA) would not require such a large dose of RNA as it is locked in the GTP-bound form and, therefore, would be little affected by regulatory factors. Embryos injected with increasing doses of the *da-rab5a2* RNA were examined.

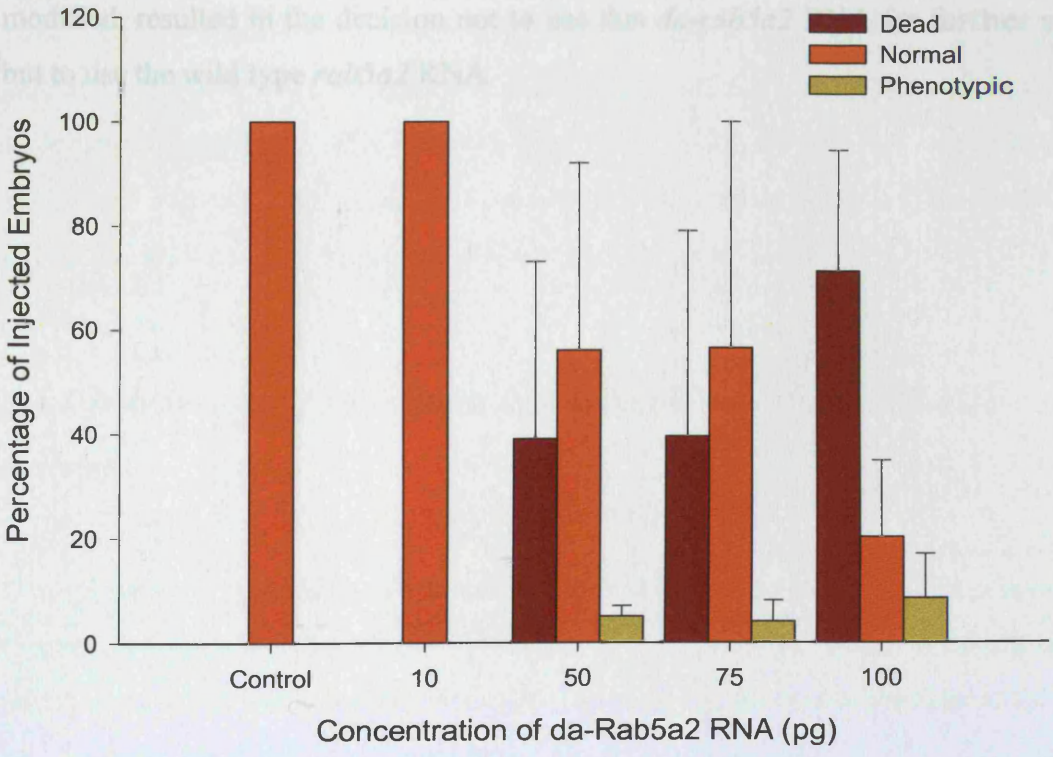

Figure 5.3.4: Comparison of different doses of *da-rab5a2* RNA and the effect it has on 24hpf embryos.

Injection of 10pg of constitutively active *rab5a2* RNA resulted in no phenotype being observed (n = 10/10, n2 = 28/28) and the embryos were comparable with MO buffer injected embryos (n = 51/51) (Figure 5.3.4). Injection of 50pg of *da-rab5a2* RNA showed a small percentage of embryos with a phenotype similar to that seen in wild-type *rab5a2* RNA injected embryos (n1 = 1/39, n2 = 1/15), however, approximately 39% died (n1 = 2/39, n2 = 11/15), while the remainder looked normal (n1 = 36/39, n2 = 3/15). When the dose of *da-rab5a2* RNA was increased to 75pg, again, only a small percentage, approximately 4% (n1 = 7/85, n2 = 0/19), showed a phenotype similar to the wild type *rab5a2* RNA overexpression, while 40% of the *da-rab5a2* overexpressing embryos died (n1 = 67/85, n2 = 0/19). At 100pg over 70% of the da-*rab5a2* RNA injected embryos died (n1 = 86/91, n2 = 11/23), with only 8% showing a wild type *rab5a2* RNA overexpression phenotype (n1 = 0/91, n2 = 4/23) (Figure 5.3.4). Although the percentage of embryos showing a phenotype seemed to increase in relation to the percentage of normal embryos, the actual number that survived became smaller. This reduction in viable embryo numbers, coupled with the fact that constitutively active *rab* RNA has been artificially modified, resulted in the decision not to use this *da-rab5a2* RNA for further studies but to use the wild type *rab5a2* RNA.

5.4 The effect of Rab5a2 on exogenous Nodal signalling

Examining the effect of Rab5a2 on exogenous nodal signalling enables the events that induce nodal signalling in the developing embryo to be separated from those that transport the nodal signal. Squint has been proposed as a morphogen (Chen and Schier 2001) acting directly on target cells over a distance while Cyclops signals in a more localized manner, because of these difference in signalling action it is important to look at both of these nodal proteins. To examine the role of exogenous nodal signalling, RNA encoding either *sqt* or *cyc* was injected, along with the lineage label biotinylated-dextran into a single cell at the centre of the animal pole of embryos at the 128 cell stage. These embryos were allowed to develop for three hours and then fixed for *ntl* and *gsc* expression analysis. The daughter cells of the original injected cell will all produce the nodal signal derived from the RNA with which the original cell was injected. These daughter cells will also stain for biotinylated-dextran allowing accurate visualisation of those cells producing the nodal signal. Injection into the middle of the animal pole avoids the exogenous produced *gsc* or *ntl* expression from encroaching on the area of the embryo where endogenous expression of *gsc* or *ntl* is evident. These single cell injections were performed into embryos injected at the one cell stage with either a control MO, 5ng of *rab5a2* MO or 1.5ng of *rab5a2* RNA.

5.4.1 Injection of 5pg of squint into a single cell of 128 cell stage embryo

Control MO injected embryos showed *gsc* expression close to the cells producing Sqt (Figure 5.4.1) (n = 15/19) with possible faint expression in an additional three embryos (n = 3/19). The *rab5a2* MO injected embryos showed a considerably fainter but broader band of *gsc* expression (n = 8/10) (Figure 5.4.1). In embryos overexpressing *rab5a2 gsc* expression was similar to that seen in control embryos (n = 6/12) with faint expression in an additional four embryos (Figure 5.4.1). Control MO injected embryos showed expression of *ntl* in a broad ring around the Sqt

producing cells (n = 25/25) (Figure 5.4.1). The *rab5a2* MO injected embryos showed reduced intensity of expression of *ntl* (n = 4/14), whilst there was very faint possible expression in an additional seven embryos (Figure 5.4.1). In embryos overexpressing Rab5a2, there was strong *ntl* expression, similar to that seen in control embryos (n=7/8) (Figure 5.4.1).

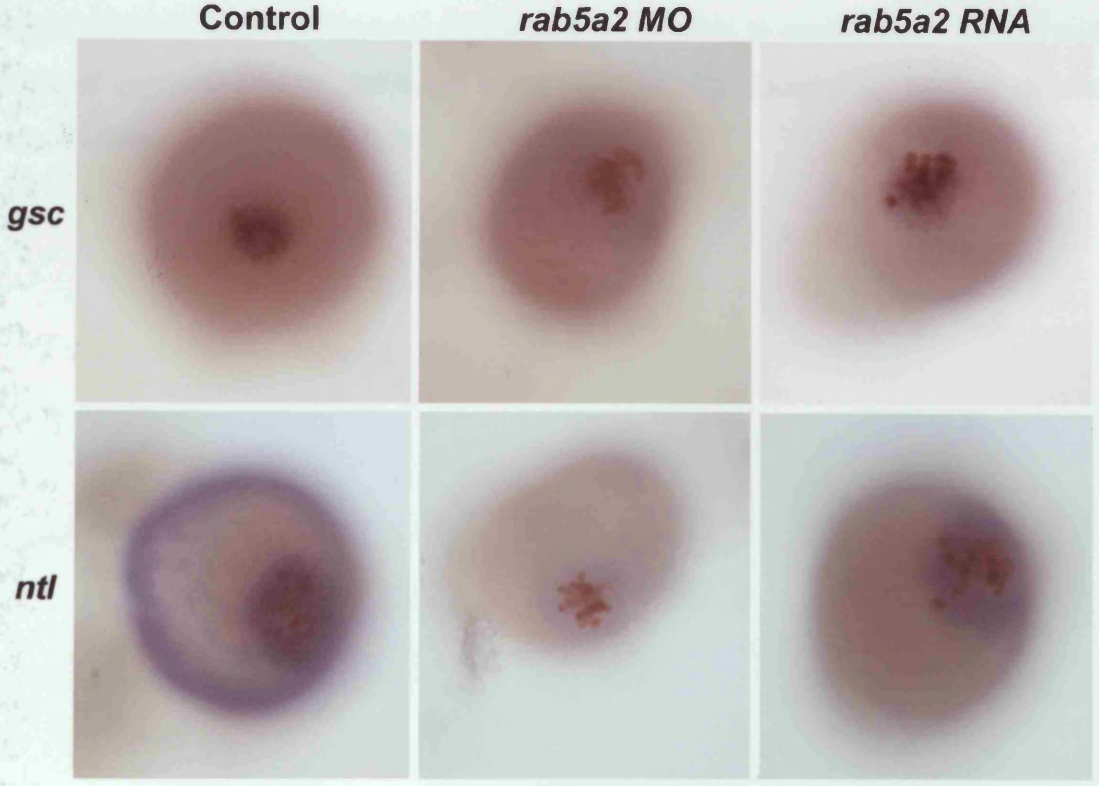

Figure 5.4.1: Showing the expression of *gsc* and *ntl* in control, *rab5a2* MO and *rab5a2* RNA injected embryos when 5pg of *sqt* RNA are injected into the animal pole of 128 cell stage embryos (where blue is *gsc* or *ntl* expression and brown the cells injected with *sqt* RNA).

5.4.2 Injection of 10pg of squint into a single cell of 128 cell stage embryo

Control injected embryos showed exogenous *gsc* expression close to the cells producing the Sqt signal (n = 7/11) (Figure 5.4.2) with reduced expression in the remainder. *ntl* expression in the control embryos was seen as a thick band surrounding the Sqt producing cells (n = 7/8) with reduced expression in the remaining embryo. The *rab5a2* MO injected embryos showed a broad band of faint *gsc* expression (n = 3/12), while some embryos showed very faint staining (n =2/12).

However, over half of the embryos showed no *gsc* expression (n = 7/12). The *rab5a2* MO injected embryos showed faint *ntl* expression (n = 5/21) an additional eight embryos showed very faint to no expression whilst the remaining eight showed no staining (Figure 5.4.2). Exogenous *gsc* expression in *rab5a2* overexpressing cells was comparable to control exogenous expression of *gsc* in (n =10/13). The remaining three embryos showed no *gsc* expression. Exogenous expression of *ntl* in the *rab5a2* overexpressing embryos showed expression comparable to controls (n = 12/21) with reduced expression in an additional seven embryos. The remaining embryos showed no *ntl* expression (Figure 5.4.2).

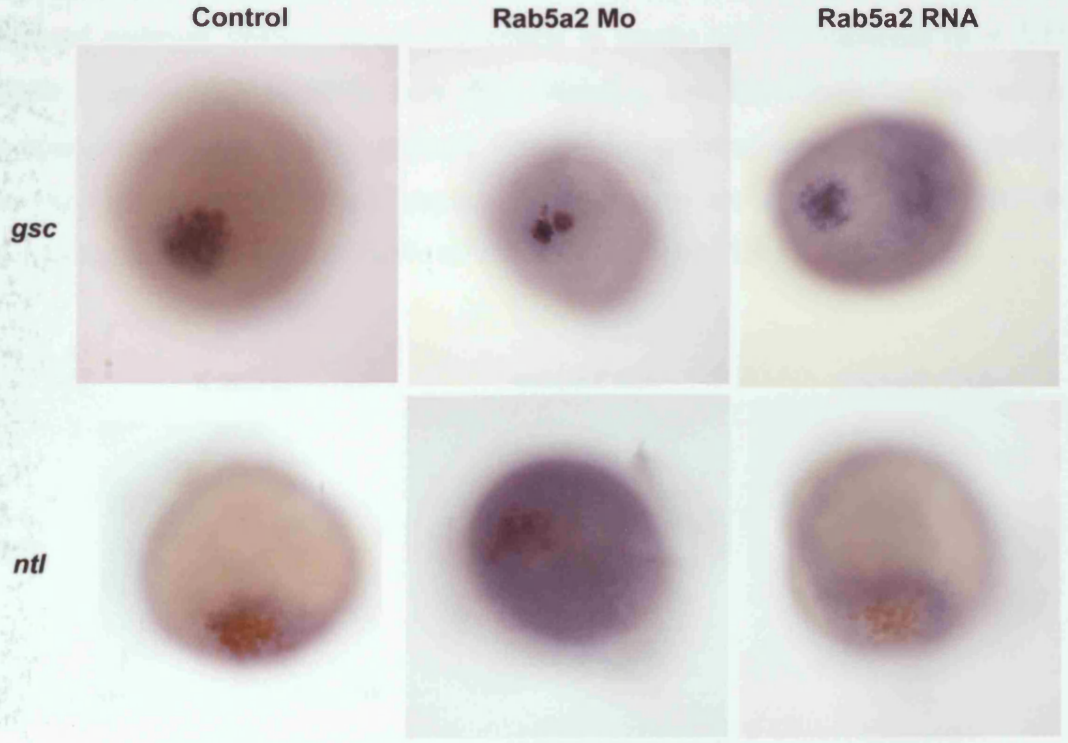

Figure 5.4.2: Showing the expression of *gsc* and *ntl* in control, *rab5a2* MO and *rab5a2* RNA injected embryos when 10pg of *sqt* RNA are injected into the animal pole of 128 cell stage embryos (where blue is *gsc* or *ntl* expression and brown the cells injected with *sqt* RNA).

5.4.3 Injection of 7pg of cyclops into a single cell of 128 cell stage embryo

Control MO injected embryos showed *gsc* expression close to the cells producing Cyclops (n = 7/10) (Figure 5.4.3) with fainter staining in an additional three embryos. The *rab5a2* MO injected embryos showed a fainter expression of *gsc* than in controls (n = 6/19), with the remainder showing no staining (n = 13/19). *rab5a2* overexpressing embryos showed no expression of *gsc* in half of the embryos (n = 6/12), three embryos showed expression comparable to controls while the last three showed faint expression (Figure 5.4.3). Control injected embryos showed a band of *ntl* expression thinly round the Cyclops producing cells (n = 8/9). *rab5a2* MO injected embryos showed no *ntl* expression in nearly half the embryos (n = 7/15) while four showed possible very faint staining and the remainder showed *ntl* expression comparable with controls. The *rab5a2* overexpressing embryos showed *ntl* expression comparable to controls in the majority of embryos (n = 10/14) with the remaining four showing no visible *ntl* expression (Figure 5.4.3).

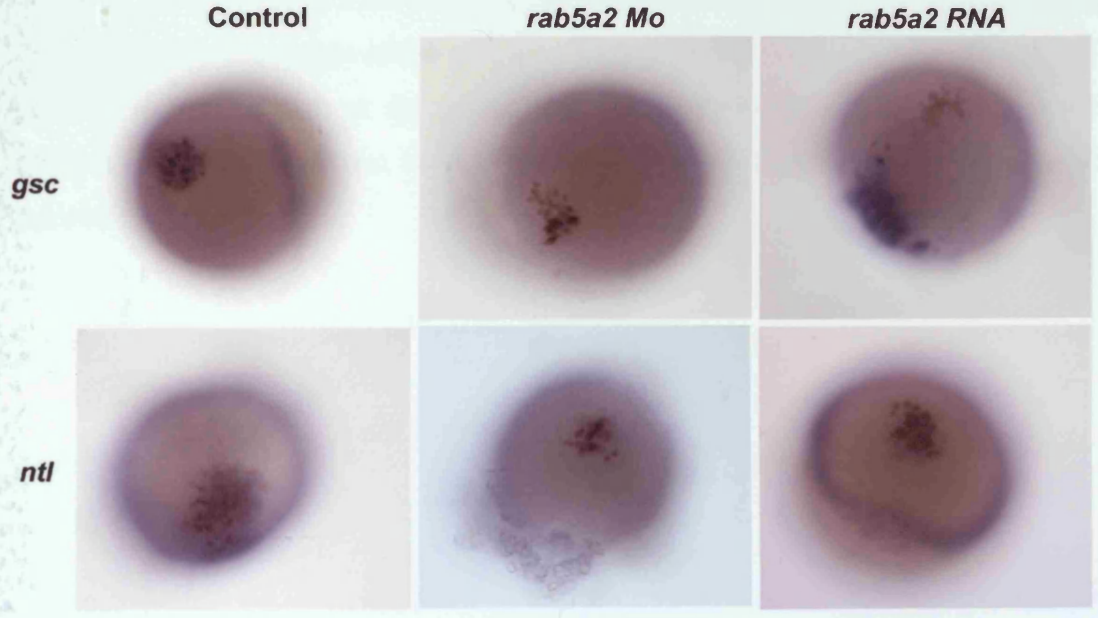

Figure 5.4.3: Showing the expression of *gsc* and *ntl* in control, *rab5a2* MO and *rab5a2* RNA injected embryos when 7pg of *cyc* RNA are injected into the animal pole of 128 cell stage embryos (where blue is *gsc* or *ntl* expression and brown the cells injected with *cyc* RNA).

5.5 Additional functions for Rab5a2 in the developing embryo

5.5.1 The contribution of Rab5a2 in the YSL

A source of many patterning and signalling factors, including Nodal is the YSL; it was, therefore important to ascertain whether Rab5a2 plays a role in the YSL. In order to achieve this, *rab5a2* MO was injected into the yolk cell of 1000 cell stage embryos. Injection into the yolk at this stage is thought to ensures that the MO only has an effect in the yolk as the cells of the embryo after the four cell stage no longer enable free movement of RNA between cells (Hsu et al., 2006).At 24hpf the *rab5a2* MO injected embryos showed slightly curved tails compared to control. By 48hpf, the *rab5a2* MO injected embryos looked dramatically different from controls; retaining the curved tails seen at 24hpf they now showed a thinner axis with reduced pigment (Figure 5.5.1 B) when compared to controls (Figure 5.5.1 A). Most dramatically though, the *rab5a2* MO injected embryos showed an accumulation of what appeared to be dead cells on the part of the yolk attached to the embryo. This section of the embryos in controls is the site of the developing heart with blood being observed on the dorsal part of the yolk (Figure 5.5.1 C). In addition, this section will give rise to organs such as the gut kidney and liver. In the *rab5a2* MO injected embryos there is no apparent heart (Figure 5.5.1 D and E) and the embryos die at approximately 3dpf.

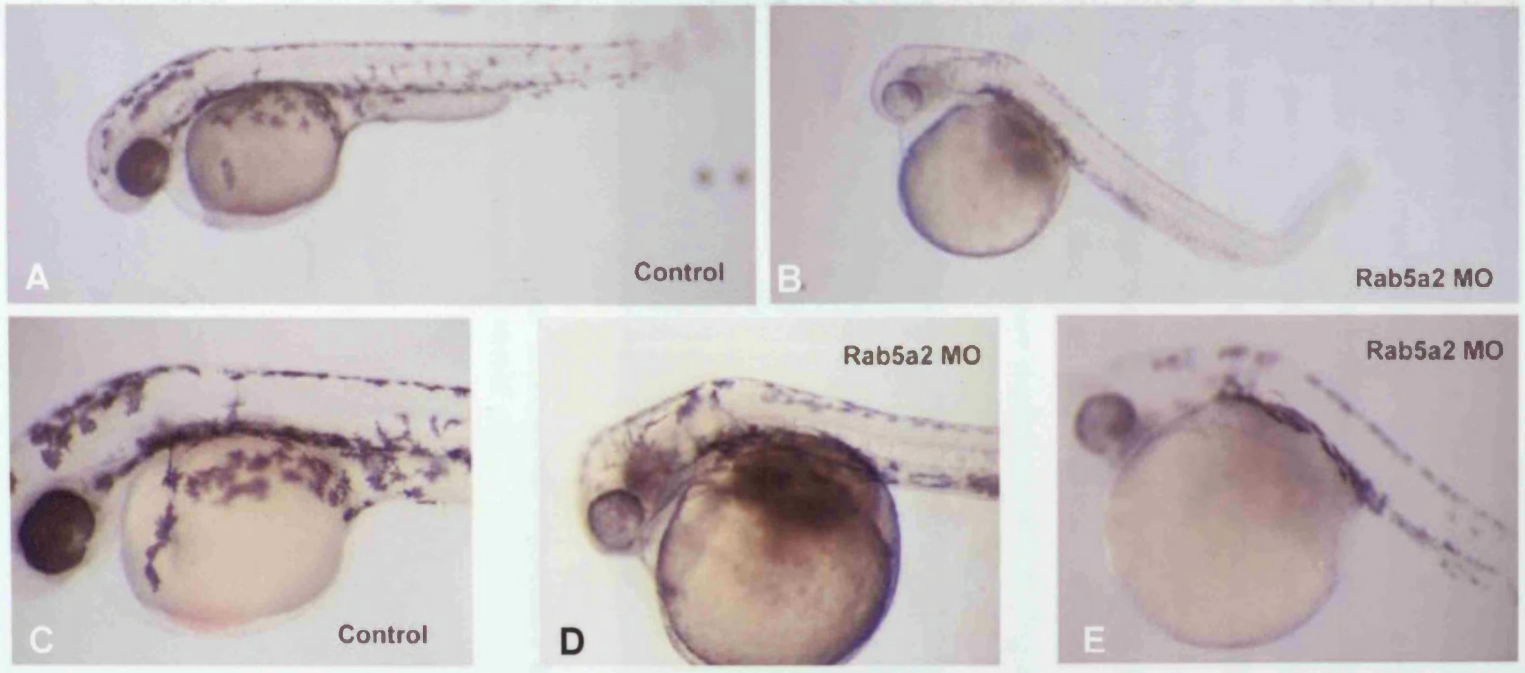

Figure 5.5.1: Lateral view of embryos injected with *rab5a2* MO at 1000 cell stage (B) compared to those injected with a control MO at 1000 cell stage (A). Magnified images of the head and yolk of embryos when injected with *rab5a2* MO at 1000 cell stage under reflected and direct lighting (D and E) compared to those injected with a control MO at 1000 cell stage (C).

5.5.2 Expression of β-catenin in rab5a2 MO injected embryos

β-Catenin localizes to the future dorsal side of the embryo early in development and is one of the earliest DV markers. The *rab5a2* MO injected embryos showed not only a lack of nodal target genes but also a lack of *cyc* expression. This suggested that, *rab5a2* may affect a factor upstream of nodal signalling. It is, therefore, possible that Rab5a2 may be involved in localization of β-Catenin. In order to investigate, this, control and *rab5a2* MO injected embryos were stained, using a β-Catenin antibody conjugated to biotin. The control embryos showed a gradient of staining emanating from the dorsal side of the embryo. Half of the *rab5a2* MO injected embryos showed no staining while three out of 12 of the embryos showed staining all over the embryos, the remainder were similar to controls (Figure 5.5.2).

Figure 5.5.2: Animal view of *β-catenin* expression in control injected and *rab5a2* MO injected embryos at shield stage.

Chapter 6

Microarray analysis of Rab5a2

6.1 Introduction

Microarrays are a powerful tool which can be used to compare, not only the expression of thousands of gene within a sample but, also, between multiple samples. The arrays comprise 'spots' of DNA, RNA or oligonucleotides (probes), which correspond to genes, immobilized on slides or chips made from glass, silicone or plastic. A sample of RNA or cDNA is labelled with a fluorescent dye and hybridized to the microarray. The 'spots' on the slide then bind any complimentary RNA (or cDNA) in the sample in a dose dependent manner. The expression of these genes can then be quantified.

6.1.1 Why Microarray Rabs?

There are currently over 80 zebrafish Rabs, some of these as investigated in this thesis have very specific phenotypes (Chapter 3.). However, many show similar and complex phenotypes which include brain cell death, shortened AP axis and irregular somites. Others have shown no morphological phenotype. The similar and complex phenoypes seen in many of the Rabs makes it very difficult to identify any specific pathway which is affected in MO injected embryos while the presence of MO injected embryos with essentially wild type phenotypes, substantially compounds the problem. In these Rabs which show no phenotype a pathway may be affected, however, it is possible the loss of this Rab in ideal conditions is compensated for. Microarrays provide an efficacious method of screening all these Rabs and elucidating which pathways they affect.

6.1.2 The Microarray

The microarray used in the following experiment was a custom made oligonucleotide array designed specifically to investigate zebrafish developmental genes. Each slide contained 1898 separate oligos which were 65 base pairs in length and were carefully selected so that the 65 bases were unique to the particular gene they were targeting. The genes on the array included XPAT transcripts from ZFIN, approximately 300

handpicked transcripts chosen by the Stemple lab, 213 transcripts thought to be involved in cell – cell signalling chosen by the Wright lab at the Sanger Institute and 109 housekeeping transcripts. These oligos were then immobilized onto a glass slide by an array spotting robot; each oligo was spotted twice to ensure greater reproducibility. This custom oligoarray was probed using two dyes enabling the control RNA samples to be labelled with one dye and hybridized to an array slide whilst the experimental RNA samples were labelled with a second and hybridized to the same array slide (Figure 6.1.1). Placing both control and experimental samples on the same array slide results in reduced experimental variation. To ensure any experimental variations resulting from differences in the dyes is minimised, the dyes were swapped resulting in one slide with Cy5 labeled control and Cy3 labeled experimental RNA and a second slide with Cy3 labeled control and Cy5 labeled experimental RNA.

6.1.3 The Experiment

In order to obtain samples for the array 300, single cell stage embryos were collected from three pairs of parent fish resulting in three groups of 300 embryos. Replicate parent fish came from the same line to reduce variation. Each clutch of 300 embryos is split into two groups with 150 embryos in each dish. One of the groups from each parent is injected with 6ng of control MO. The second is injected with 5ng of *rab5a2* MO. The embryos are left to develop at 28°C until they reached 30% epiboly, at which point 65 embryos are then removed from each of the control embryo injected groups and placed in a 1.5ml Eppendorf tube. The embryos were washed three times with zebrafish egg water. All the water is removed and the embryos are frozen in dry ice for 20minutes before being stored at -80. The same procedure is observed for the *rab5a2* MO injected embryos. At shield stage a further 65 embryos were removed from both the control injected embryo groups and the *rab5a2* MO injected embryos. The method employed for the 30% epiboly stage embryo is repeated for these samples. The remaining embryos are left to develop until 24hpf and their phenotype checked ensuring that there are no anomalies in these embryos and that they show the phenotype expected for these embryos. Embryos were frozen at 30% epiboly and shield stage enabling comparisons to be made between the former stage at which

there is little visual difference between control and MO injected embryos and shield stage when the phenotype becomes apparent in the *rab5a2* MO injected embryos.

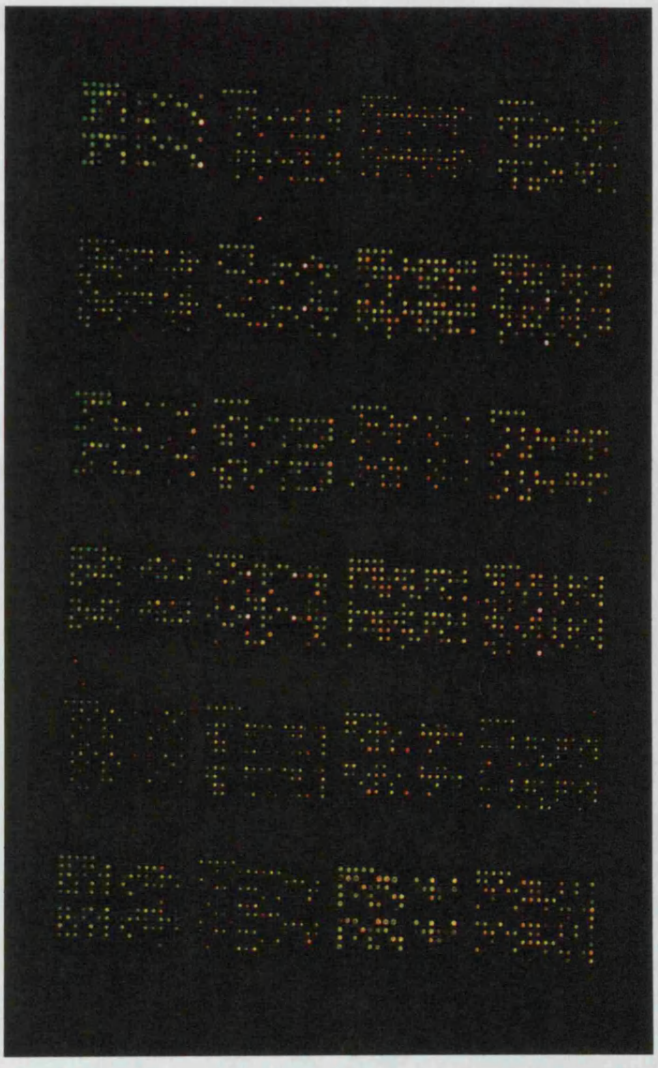

Figure 6.1.1: Image capture of one of the custom made oligonucleotide microarray slides showing hybridization of control and *rab5a2* samples as two colour data. (blue = cy5, red = cyc3 , other colours are a combination of the two samples)

RNA is isolated directly from the frozen samples by homoginising in trizol and the RNA quantified. Given the early stage of these embryos it was necessary to amplify the RNA (see Methods section 2.3.3).

6.2 Results

6.2.1 Establishing an appropriate fold change.

The fold change for each gene that changes in the microarray experiment is plotted by the computer programme Genespring. The programme will then only show genes that change above the fold threshold, in the case of Figure 6.2.1 this is a two fold change. The blank area between the lines represents the majority of the genes while those points outside the lines represent those genes that changed by two fold or more. Due to the large number of genes that changed at the two fold level the fold change threshold was increased to three fold.

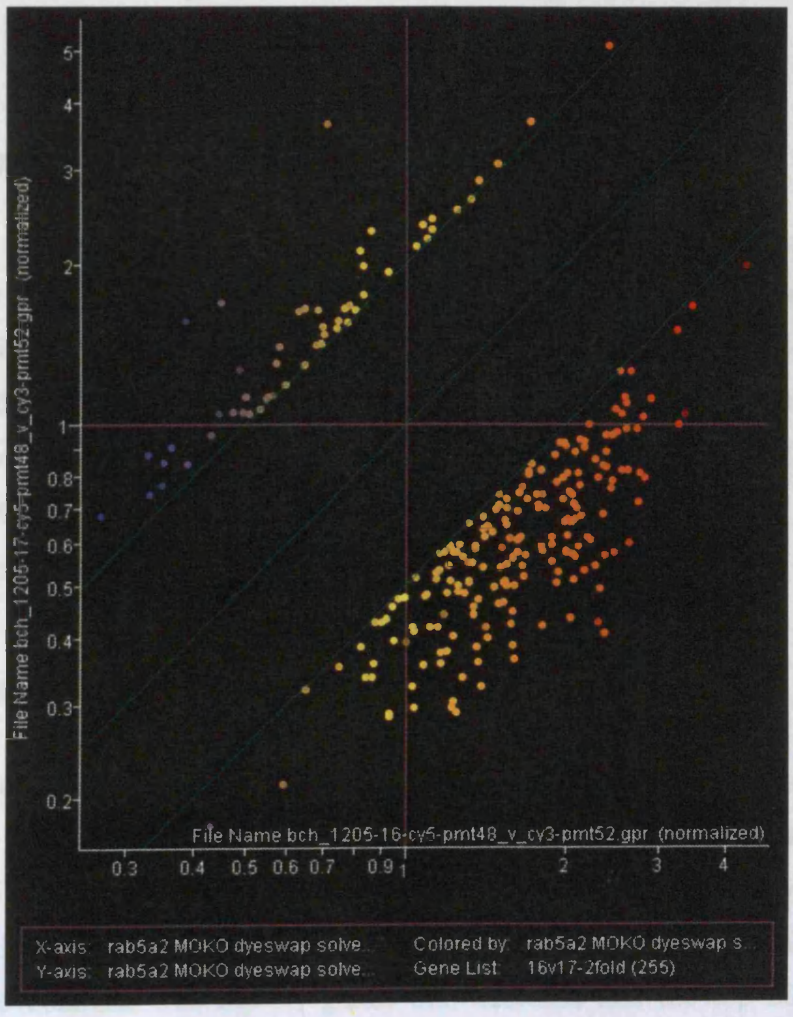

Figure 6.2.1 : Graph plotted in the microarray analysis programme Genespring showing the number of genes that changed more than two fold when *rab5a2* MO injected embryos were compared to control embryos.

6.2.2 The top 50 genes that increased and decreased in rab5a2 MO injected embryos when compared to controls.

After analysis by Genespring the data was tabulated with the accession number from NCBI, the oligo number and the fold change of that oligo. The accession number was then identified and the corresponding gene tabulated. Since most genes have two oligos the list was examined for a second oligo and the fold change for both averaged. Dr Wright's oligos were also checked for duplicates with known genes on the slide, if these matched the fold change was again averaged. Due to the large number of genes that changed more than 3 fold the top 50 genes that increased and the top 50 genes that decreased at each stage were tabulated with their average fold change, the name of the gene and the number if oligos for that gene that changed (Tables 5.2.1-5.2.4).

6.2.2.1 Expression changes at 30% Epiboly Stage

In the 30% epiboly stage embryos at the 3 fold stringency 382 genes changed in the *rab5a2* MO injected embryos when compared to control embryos. 201 genes showed a decrease in activity in *rab5a2* MO injected embryos compared to controls while 181 showed an increase in gene activity in *rab5a2* MO injected embryos when compared to controls. The top 50 genes that decrease and the top 50 genes that increase between *rab5a2* MO injected embryos and control embryos at the 30% epiboly stage are presented in Table 6.2.1 and 6.2.2 respectively.

6.2.2.2 Expression changes at Shield Stage

In the shield stage embryos at the three fold stringency 426 genes changed in the *rab5a2* MO injected embryos when compared to control embryos. 211 genes showed a decrease in activity in *rab5a2* MO injected embryos compared to controls while 215 showed an increase in gene activity in *rab5a2* MO injected embryos when compared to controls. The top 50 genes that decrease and the top 50 genes that increase between *rab5a2* MO injected embryos and control embryos at shield stage are presented in Table 6.2.3 and Table 6.2.4 respectively.

Av. fold change	No oligo's	Description
0.13	1	T-box gene 16
0.17	3	trophoblast glycoprotein-like
0.19	2	bone morphogenetic protein 4
0.22	1	zic family member 3 heterotaxy 1 (odd-paired homolog)
0.22	1	keratin 4
0.23	2	SRY-box containing gene 2
0.25	1	ATPase, Na+/K+ transporting, alpha 1b polypeptide
0.26	2	T-box transcription factor TBX6
0.26	2	zgc:101612
0.27	2	fibroblast growth factor 8
0.28	2	U1 small nuclear ribonucleoprotein polypeptide A
0.29	1	UDP-GlcNAc:betaGal beta-1,3-N-acetylglucosaminyltransferase 5
0.30	1	Unknown
0.30	2	zgc:92414
0.30	2	Type I cytokeratin, enveloping layer
0.32	1	CCAAT/enhancer binding protein alpha
0.32	1	caudal type homeo box transcription factor 4
0.32	1	tyrosine 3-monooxygenase
0.33	2	chordin
0.33	1	fibroblast growth factor 24
0.33	1	methyl-CpG binding domain protein 3b
0.34	2	bonnie and clyde
0.34	2	LIM homeobox 1b
0.35	2	Ved
0.35	1	fibroblast growth factor 19
0.36	1	mannosidase, beta A, lysosomal
0.36	2	protocadherin 8
0.37	1	tyrosyl-tRNA synthetase
0.37	2	gastrulation brain homeobox 1
0.37	1	peroxisomal biogenesis factor 3
0.38	2	mki67 interacting nucleolar phosphoprotein (human) – like
0.38	3	deltaD (dld),
0.39	2	zgc:101000
0.39	2	transgelin 2
0.39	1	AHA1, activator of heat shock ATPase homolog 1, like
0.40	1	hairy and enhancer of split related-7
0.40	2	solute carrier family 3, member 2 like
0.40	2	Vent
0.40	2	lymphocyte cytosolic plastin 1
0.40	2	ubiquitin-activating enzyme E1-domain containing 1
0.40	2	Wnt-11 protein precursor
0.40	2	Rab14
0.40	1	iroquois homeobox protein 1, a isoform 1
0.41	2	CB967 5- similar to Filamin A
0.41	1	glutamate-ammonia ligase
0.42	1	minichromosome maintenance protein 3
0.42	1	tumor protein p73-like isoform alpha 1
0.42	1	SRY-box containing gene 3
0.43	1	cysteine and glycine-rich protein 1
0.43	1	Homeobox protein Hox-B2a (Hox-B2)

Table 6.2.1: The fold change of the top 50 genes that decreased in *rab5a2* MO injected embryos at the 30% epiboly stage compared to control embryos.

Av. fold change	No oligo's	Description
6.70	2	T-box 24
6.04	2	v-fos FBJ murine osteosarcoma viral oncogene homolog
5.99	2	forkhead box I1
4.49	1	unc-45 homolog B (C. elegans) (unc45b),
3.93	1	muscle segment homeobox E
3.91	2	claudin g (cldng),
3.71	2	Insulin gene enhancer protein ISL-2 (Islet-2).
3.69	2	Myoblast determination protein 1 homolog (Myogenic factor 1)
3.55	1	enolase 3, (beta, muscle)
3.53	2	heat shock protein 47
3.50	2	Homeobox protein Dlx6a (DLX-6)
3.43	2	matrix metalloproteinase 13
3.32	1	DIG0228_268
3.26	2	hemoglobin alpha embryonic-1 (hbae1),
3.22	1	septin 9
3.11	2	insulin-like growth factor binding protein 1
3.10	2	Ribosome binding protein 1 homolog (dog)
3.06	2	H1 histone family, member X
3.01	2	Microphthalmia-associated transcription factor a (mitfa),
3.00	1	friend leukemia integration 1
3.00	2	Hypothetical protein
3.00	2	iroquois homeobox protein 7
2.99	2	Eomesodermin homolog
2.89	1	Aminolevulinate, delta-, synthetase 2
2.87	1	endothelium-specific receptor tyrosine kinase 2 (tie2),
2.83	1	hypothetical protein LOC405860
2.67	1	Ras homolog gene family, member E
2.65	1	CB1077 5- similar to Myosin Vb,
2.65	1	hemoglobin beta embryonic-1
2.64	1	SRY-box containing gene 31,
2.63	2	deltaA
2.61	1	myogenic factor 6
2.61	1	Forkhead box B1.1
2.56	2	suppressor of fused homolog (Drosophila) (sufu),
2.55	2	similar to CCCH zinc finger protein C3H-2
2.54	1	HHGP protein
2.53	1	Hypoxia-inducible factor 1 alpha inhibitor
2.52	1	hairy-related 5
2.49	1	bone morphogenetic protein 2b
2.46	2	transforming growth factor, beta receptor II (tgfbr2),
2.45	1	Bcl2-like
2.44	2	ATP synthase, H+ transporting, mitochondrial F0 complex, subunit c
2.43	2	LIM homeobox 8
2.41	2	four and a half LIM domains (fhl),
2.37	1	eyes absent homolog 1 (eya1),
2.34	2	dachshund a (dacha),
2.34	1	Ictacalcin
2.34	1	CUG triplet repeat, RNA-binding protein 1
2.32	1	growth associated protein 43 (gap43),
2.32	2	muscle-specific beta 1 integrin binding protein 2

Table 6.2.2: The fold change of the top 50 genes that increased in rab5a2 MO injected embryos at the 30% epiboly stage compared to control embryos.

Av. fold change	No oligo's	Description
0.07	2	T-box gene 6
0.07	1	zic family member 1 (odd-paired homolog) (zic1),
0.09	2	membrane protein, palmitoylated 1 (mpp1)
0.14	2	Carbonic anhydrase (Carbonate dehydratase)
0.17	3	Trophoblast glycoprotein-like
0.17	2	myeloid ecotropic viral integration site 3
0.20	1	myeloid ecotropic viral integration 1 (meis1),
0.20	1	LTP4
0.21	2	GLI2a
0.21	2	Zgc:92414
0.21	2	myogenic factor 5
0.23	2	Macrophage stimulating 1 (hepatocyte growth factor-like)
0.23	2	type I cytokeratin, enveloping layer
0.23	2	Zgc:101612
0.23	1	midkine-related growth factor b
0.24	2	chordin (chd),
0.24	1	Keratin 4 (krt4),
0.24	2	Mki67 (FHA domain) interacting nucleolar phosphoprotein (human) – like
0.25	1	Caudal type homeo box transcription factor 4 (cdx4),
0.25	2	Beta-2-microglobulin precursor
0.26	2	forkhead box C1b (foxc1b),
0.26	2	protocadherin 8 (pcdh8),
0.27	1	zic family member 3 heterotaxy 1 (odd-paired homolog)
0.27	2	Rab14
0.27	1	tyrosine 3-monooxygenase
0.27	1	mutL homolog 1, colon cancer, nonpolyposis type 2
0.28	2	Clone CB926 5- similar to Gem-associated protein 5
0.28	1	minichromosome maintenance protein 3
0.29	2	Hypothetical protein LOC378998
0.29	2	Bone morphogenetic protein 4
0.29	1	seryl-tRNA synthetase (sars),
0.30	1	Kinesin family member 11(kif11),
0.30	2	Oep
0.31	2	U1 small nuclear ribonucleoprotein polypeptide A
0.31	1	DIG0410_1903
0.31	2	Ved
0.31	2	Lymphocyte cytosolic plastin 1
0.31	2	Roundabout homolog 3 (robo3),
0.32	2	cDNA clone CB473 5
0.32	2	Sine oculis homeobox homolog 3b
0.33	1	Apolipoprotein A-I precursor (Apo-AI) (ApoA-I)
0.33	2	Sp5 transcription factor-like
0.33	3	delta D (dld)
0.34	2	hypothetical protein LOC550434
0.35	1	fibroblast growth factor 19
0.35	2	interleukin 17 receptor D (il17rd),
0.36	2	Sonic hedgehog protein precursor (SHH) (VHH-1)
0.36	1	3-beta-hydroxysteroid dehydrogenase
0.36	2	Hypothetical protein.
0.36	1	retinol dehydrogenase 10

Table 6.2.3: The fold change of the top 50 genes that decreased in rab5a2 MO injected embryos at the shield stage compared to control embryos.

Av. fold change	No oligo's	Description
11.89	1	homeo box B5a
8.90	2	claudin g
7.37	1	MAD homolog 3
7.06	2	neogenin 1
6.46	1	forkhead box B1.1
5.98	1	tyrosyl-tRNA synthetase
5.86	2	protein tyrosine phosphatase, non-receptor type 2, like
5.64	2	v-fos FBJ murine osteosarcoma viral oncogene homolog
5.37	1	sp8 transcription factor
5.14	2	forkhead box I1
4.95	1	dachshund a
4.37	2	ribosome binding protein 1 homolog (dog)
4.22	2	T-box 24
4.08	2	suppressor of fused homolog
3.91	1	Homeobox protein Hox-B5b (Hox-B5-like) (Zf-54)
3.89	1	enolase 3, (beta, muscle)
3.87	2	Insulin gene enhancer protein ISL-2 (Islet-2)
3.64	1	orthodenticle homolog 5
3.52	2	TSC22 domain family 2
3.50	2	zgc:86701 (zgc:86701),
3.50	1	ras homolog gene family, member E
3.43	2	selenoprotein P, plasma, 1b
3.43	1	ATPase, Na+/K+ transporting, alpha 1a.2 polypeptide
3.41	2	musashi homolog 2
3.40	2	Ena-vasodilator stimulated phosphoprotein
3.39	2	linker histone H1M
3.36	2	fused toes homolog
3.36	2	H1 histone family, member X
3.29	3	epithelial V-like antigen 1
3.19	2	Homeobox protein Dlx5a (DLX-4)
3.16	2	Heat shock protein 9B
3.15	2	Epididymal secretory protein E1 precursor
3.15	2	phenylalanine hydroxylase
3.12	2	similar to CCCH zinc finger protein C3H-2
3.10	2	jun B proto-oncogene
3.10	2	unc-45 (C. elegans) related
3.09	1	jagged 1b
3.07	2	zgc:101900 (zgc:101900)
3.07	2	DIX domain containing 1
3.05	1	septin 9
3.04	1	Paired-like homeodomain transcription factor 2a
3.01	2	insulin-like growth factor binding protein 1
2.94	2	dachshund b
2.92	2	translocating chain-associating membrane protein
2.82	3	deltaB
2.79	1	endothelium-specific receptor tyrosine kinase 2
2.77	2	Eomesodermin homolog
2.73	2	Homeobox protein Dlx6a (DLX-6)
2.68	1	T-box 20
2.68	2	Ribonucleoside-diphosphate reductase M2 chain

Table 6.2.4: The fold change of the top 50 genes that increased in rab5a2 MO injected embryos at the shield stage compared to control embryos.

6.2.3 Validation of Results

RT-PCR was used to validate the results of the microarray. The remainder of the uncoupled RNA from the microarray was used in conjuction with fluorescent taqman oligonucleotides for some of the genes that were shown to change and others that were not. The oligos used were for the genes *chordin*, *patched 2.1*, *transferrin receptor(tr)*, *wnt8a*, *fgf8*, *ntl*, *gsc*, *bmp4*, *bmp2*, *lfty1*, *lfty2*, *sqt*, *copa*. The data for these was then plotted in a box and whisker plot showing the fold difference between *rab5a2* MO injected embryos and control embryos. Since not all the genes could be put on a single plate, three different plates and three different dilutions were made. Therefore the housekeeping gene *tr* is plotted three times (blue boxes on Figure 6.2.3 and Figure 6.2.4) on each graph, to evaluate the reproducibility of each dilution plate. The spread of the data seen in *tr* receptor expression (Figure 6.2.3 and Figure 6.2.4) for each plate dilution made it difficult to evaluate the differences between each plate. All the *tr* receptor expression data did fall within the same range but this range was extensive. The 30% epiboly data range for *tr* receptor was less extensive and suggests that at least for the 30% epiboly data each plate dilution was comparable to the other plate dilutions (Figure 6.2.3). *tr* and *copa* are described as housekeeping genes suggesting that their expression does not change (Batista et al., 2004). The microarray data showed that at 30% epiboly the expression of *transferrin a*, a *tr* ligand, was slightly increased (appendix) however there was no change at shield stage. RT-PCR data for *tr* expression both at 30% epiboly and (Figure 6.2.3) at shield stage (Figure 6.2.4) is inconclusive with no obvious fold change. *copa* showed little change in expression, however the median for the 30% data set fell below the one fold change boundary suggesting some weak support for a decrease in gene expression (Figure 6.2.3) although this is inconclusive. The microarray data showed a slight increase in *copa* gene expression in *rab5a2* MO injected embryos at the 30% epiboly stage; however there was no change at shield stage (appendix).

The RT-PCR data set for *bmp2b* spans an extensive range at the 30% epiboly stage, thus proving inconclusive (Figure 6.2.3). The microarray data shows a large increase in *bmp2b* expression in *rab5a2* MO injected with the gene appearing in the top 50 genes that increase at the 30% epiboly stage (Table 6.2.2). At shield stage the

microarray data continues to show an increase in *bmp2b* gene expression but to a lesser extent (appendix). The RT-PCR data for *bmp2b* at shield stage however appears not to change (Figure 6.2.4).

chd and *bmp4* both showed dramatic decreases in gene expression in *rab5a2* MO injected embryos in the RT-PCR data both at 30% epiboly and shield stage (Figure 6.2.3 and Figure 6.2.4). This correlates with the data seen in the microarray where both *chd* and *bmp4* appear in the top 50 genes that decrease at both the 30% epiboly stage and shield stage (Table 6.2.1 and Table 6.2.3). The decrease in *chd* expression also corresponds to the abolition of *chd* expression seen in *ish* analysis reported in chapter 4. *fgf8* also shows a decrease in gene expression of *rab5a2* MO injected embryos in the RT-PCR data at both the 30% epiboly stage and shield stage (Figure 6.2.3 and Figure 6.2.4) corresponding to the substantial decrease in *fgf8* gene expression seen in the microarray data at the 30% epiboly stage (Table 6.2.1). The microarray data did not show any difference for *fgf8* expression at shield, however, this could be a result of the high fold change threshold set.

The nodal target genes *gsc* and *ntl* showed a trend towards decreased expression in *rab5a2* MO injected embryos in the RT-PCR data set at both the 30% epiboly stage (Figure 6.2.3) and shield stage (Figure 6.2.4). *ntl* expression was also reduced in the microarray data at the 30% epiboly stage (appendix), while *gsc* and *ntl* expression have been shown by *ish* analysis to be reduced by *ish* analysis in *rab5a2* MO injected embryos (Chapter 5 Figure 5.2.2). The nodal target gene *flh* was also reduced in *rab5a2* MO injected embryos in chapter 5 (Figure 5.2.2) in addition to being reduced in the 30% epiboly stage microarray data (appendix). Interestingly the expression of nodal *sqt* in *rab5a2* MO injected embryos did not reach the three fold change threshold in the microarray data and the RT-PCR data is inconclusive however there is a weak trend towards decreased expression at the 30% epiboly stage (Figure 6.2.3).

Finally *wnt8* and *wnt11* both showed decreased expression in *rab5a2* MO injected embryos in the microarray data. *wnt11* showed a significant decrease at the 30% epiboly stage (Table 6.2.1) but did not reach the fold change threshold at shield stage, however expression of *wnt11* at shield stage in the *rab5a2* MO injected

embryos was shown by *ish* analysis to be decreased (Figure 6.2.2). *wnt8a* expression was decreased in both 30% and shield stage MO injected embryos in the microarray data (appendix) and the RT-PCR data (Figure 6.2.3 and Figure 6.2.4).

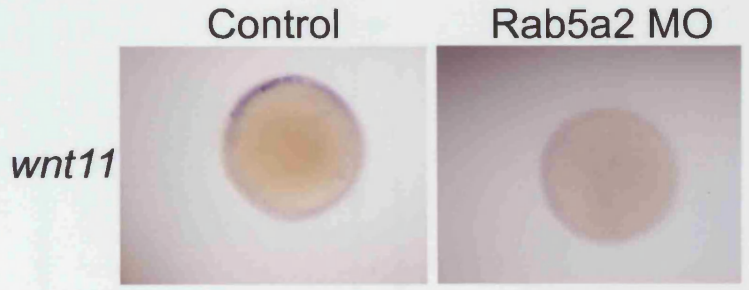

Figure 6.2.2: *ish* analysis of *wnt11* expression in *rab5a2* MO injected embryos compared to control embryos at shield stage.

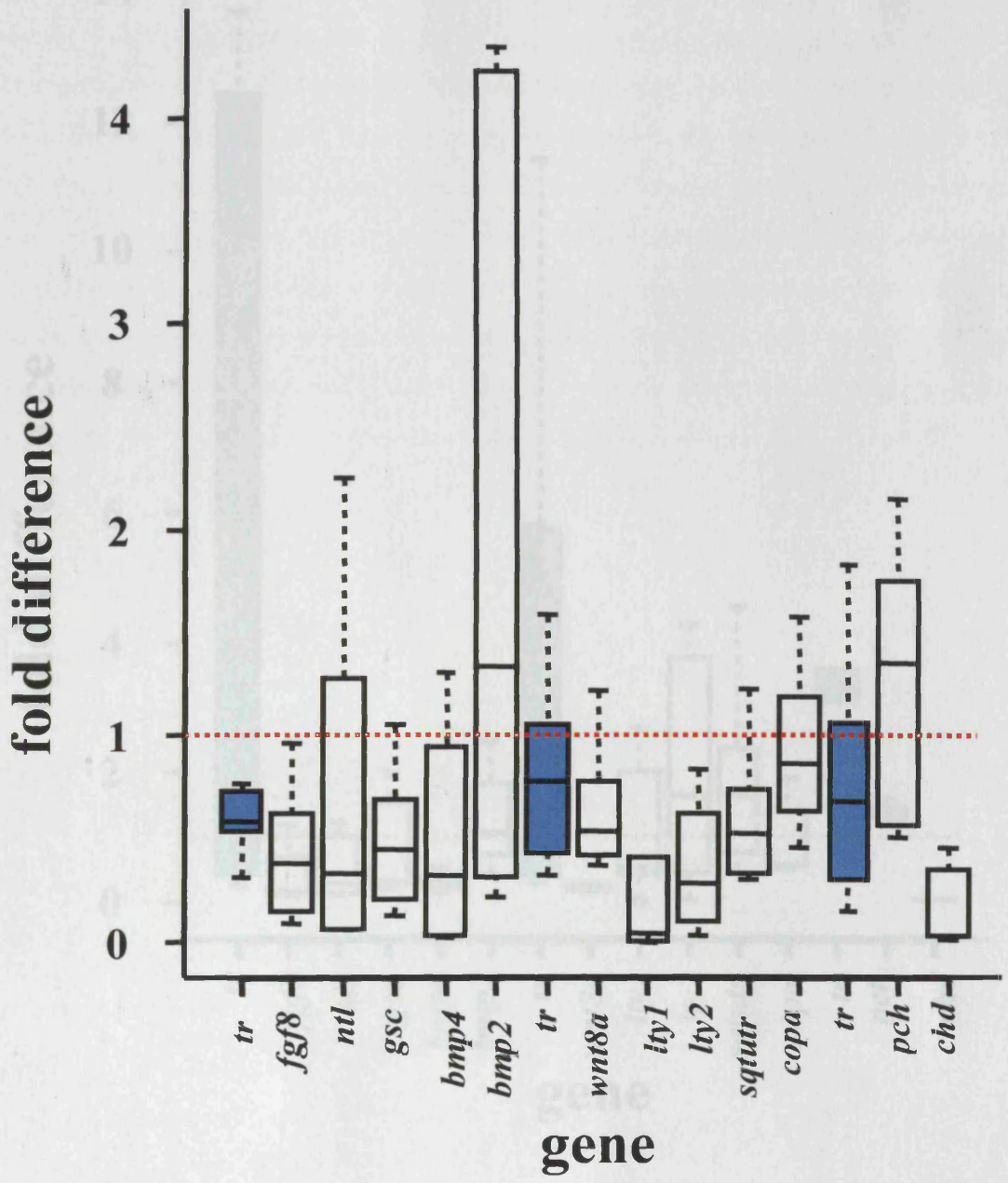

Figure 6.2.3.: Box and whisker plot showing the fold change of gene expression in *rab5a2* MO injected embryos when compared to control embryos at the 30% epiboly stage. Where the upper and lower bounds of the box represent the upper and lower quartiles respectively, the line that bisects the box represents the median and the whiskers extend 1.5 times the inter-quartile range beyond the 25% and 75% quartiles (boxes). The red dotted line represents the point at which there was no change in expression and the blue boxes show *tr*.

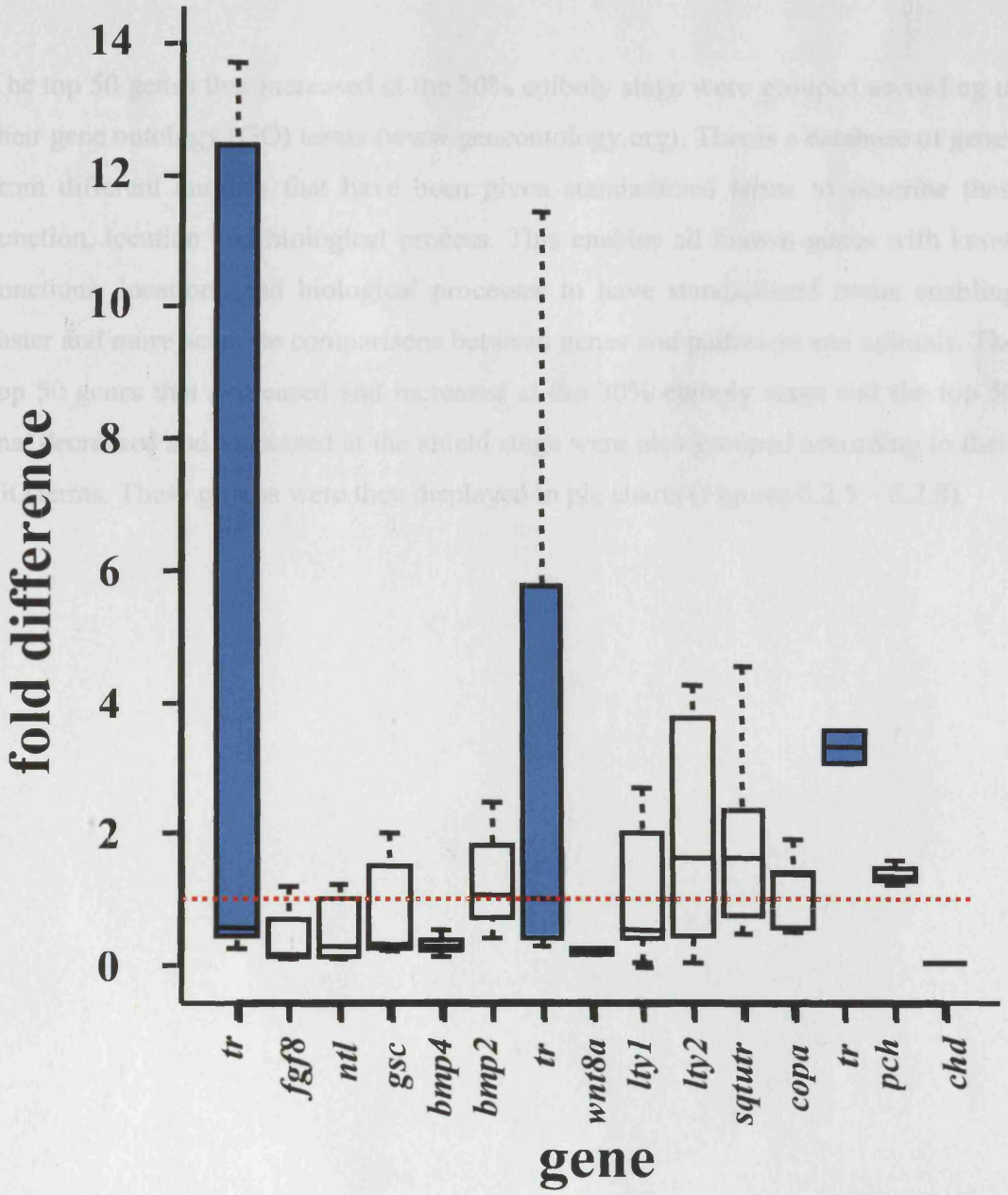

Figure 6.2.4: Box and whisker plot showing the fold change of gene expression in *rab5a2* MO injected embryos when compared to control embryos at shield stage. Where the upper and lower bounds of the box represent the upper and lower quartiles respectively, the line that bisects the box represents the median and the whiskers extend 1.5times the inter-quartile range beyond the 25% and 75% quartiles (boxes). The red dotted line represents the point at which there was no change in expression and the blue boxes show *tr*.

6.2.4 Identifiction of groups of genes with similar function whoose expression changed with knock down of rab5a2.

The top 50 genes that increased at the 30% epiboly stage were grouped according to their gene ontology (GO) terms (www.geneontology.org). This is a database of genes from different animals that have been given standardized terms to describe their function, location and biological process. This enables all known genes with know functions, locations and biological processes to have standardized terms enabling faster and more accurate comparisons between genes and pathways and animals. The top 50 genes that decreased and increased at the 30% epiboly stage and the top 50 that decreased and increased at the shield stage were also grouped according to their GO terms. These groups were then displayed in pie charts (Figures 6.2.5 – 6.2.8).

6.2.4.1 Groups of genes that decreased at 30% epiboly stage

The majority of the genes that decreased at the 30% epiboly stage had either no gene ontology or the gene function was unknown. The majority of genes with known function are involved in transcription whilst genes involved in DV patterning are also significantly represented (Figure 6.2.5).

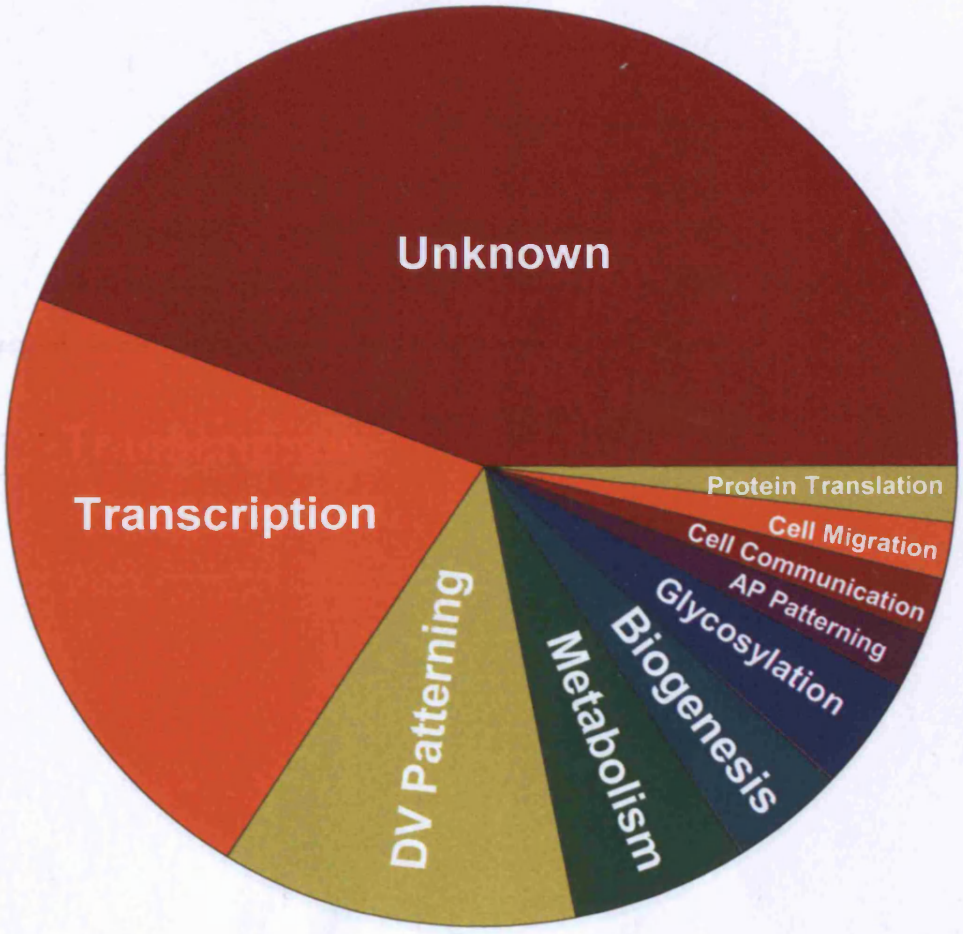

Figure 6.2.5: Pie chart showing the gene ontology biological processes of the top 50 genes that decreased in *rab5a2* MO injected embryos at the 30% epiboly stage.

6.2.4.2 Groups of genes that increased at 30% epiboly stage

The majority of genes that increased were either unknown or had unknown function in the gene ontology database. As with the genes that decreased the majority of genes with known gene ontology function are involved in transcription. Interestingly ranked joint forth are genes involved in DV patterning (Figure 6.2.6).

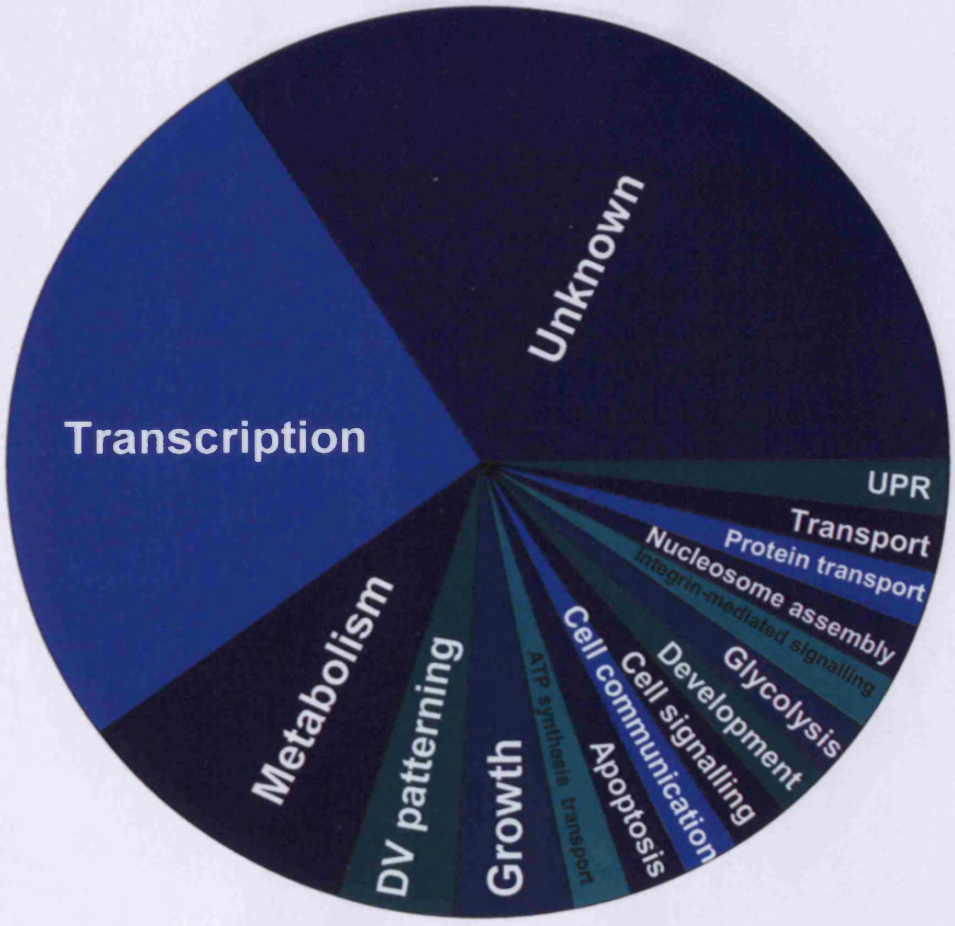

Figure 6.2.6: Pie chart showing the gene ontology biological processes of the top 50 genes that increased in *rab5a2* MO injected embryos at the 30% epiboly stage.

6.2.4.3 Groups of genes that decreased at shield stage

In the top 50 genes that decreased at shield stage the majority had unknown function in the gene ontology data base or were unknown genes. Interestingly the majority of known genes that decreased at shield stage were implicated in DV patterning while those genes involved in transcription were ranked third (Figure 6.2.7).

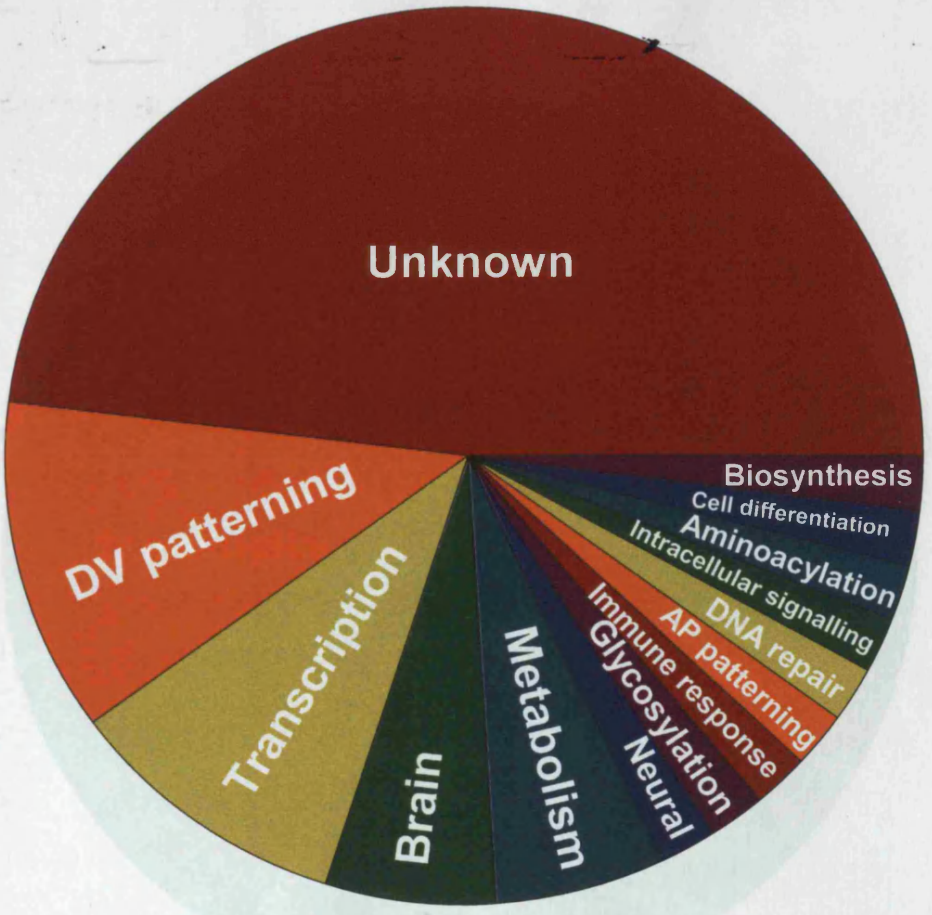

Figure 6.2.7: Pie chart showing the gene ontology biological processes of the top 50 genes that decreased in *rab5a2* MO injected embryos at shield stage.

6.2.4.4 Groups of genes that increased at shield stage

In the top 50 genes that increased at shield stage the majority again had unknown function in the gene ontology data base or were unknown genes. The majority of known genes that increased appear to be implicated in transcription, with those involved in protein processing ranking third. Interestingly the number of genes involved in DV patterning at shield stage, compared to 30% epiboly stage, appeared to have fallen resulting in the DV patterning genes being ranked at the bottom (Figure 6.2.7).

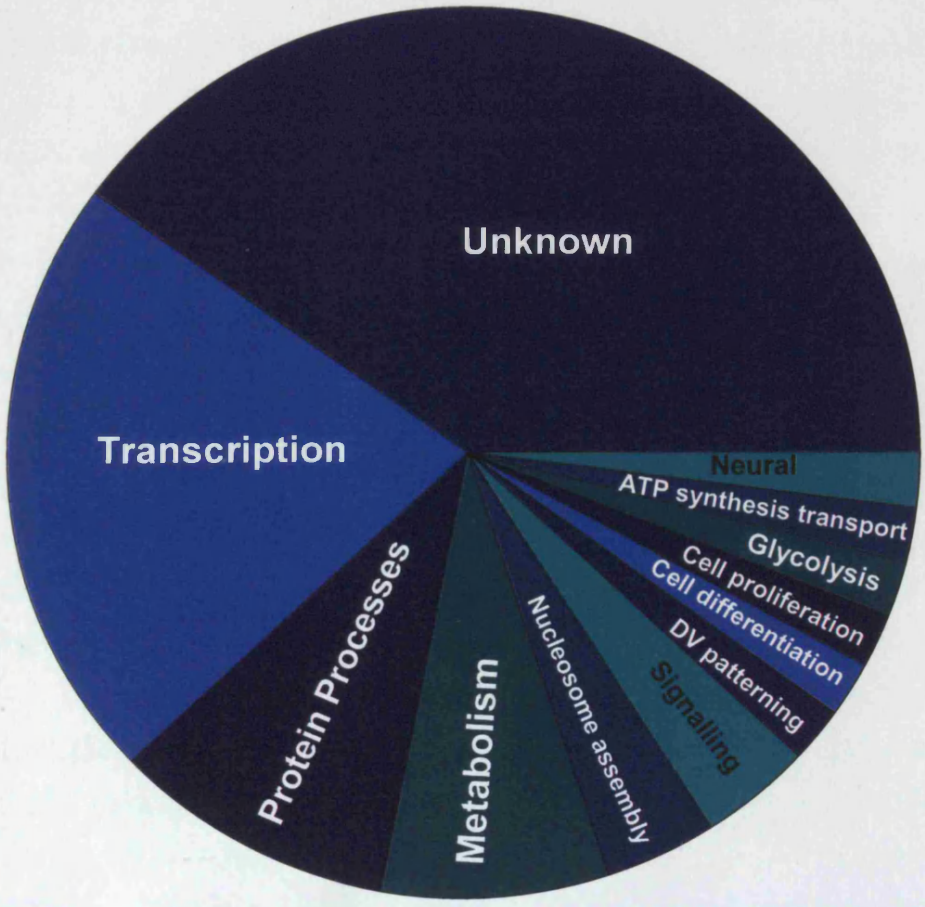

Figure 6.2.8: Pie chart showing the gene ontology biological processes of the top 50 genes that increased in *rab5a2* MO injected embryos at shield stage.

Chapter 7

Discussion and Further Work

7.1 Characterization of Rab5a2

In total, 37 *rab* genes have been screened by knocking down the *rabs* using oligonucleotide MOs. Those *rabs* screened include members of the *rab1*, *rab6*, *rab7*, *rab8*, *rab11* and all the members of the *rab5* family, genes whose homologues in yeast are considered essential because of their lethality when knocked-down. *rab5a2* is the only *rab* gene in zebrafish which, when knocked-down, causes death before 24hpf.

In 1996, the Tubingen screen for new zebrafish mutants uncovered four zygotic mutants that affect epiboly. The most severe of these, *hab*, resulted in death before 24hpf (Kane et al., 1996; McFarland et al., 2005). Subsequently, it was shown that all these mutants resulted from mutations in E-cadherin (Kane et al., 2005). E-cadherin has been shown, in conjunction with Rab5c, to be responsible for Wnt11's function in cell cohesion during zebrafish gastrulation. The *hab* mutant is presently the only known zebrafish epiboly mutant. Although there is no evidence for E-cadherin involvement in the *rab5a2* MO injected phenotype, *wnt11* was seen to be decreased in the microarray data (Figure 6.2.1) for the *rab5a2* MO injected embryos. Disrupted cell adhesion may be responsible for the rougher appearance of the blasdoderm in *rab5a2* MO injected embryos. A loss of adhesion between the blastoderm cells and the yolk may also be responsible for the liquid observed building up between the yolk and the blastoderm in the *rab5a2* MO injected embryos (Figure 5.2.1). Interestingly, the homophilic cell adhesion gene *protocadherin8* was shown by the microarray data to be decreased in *rab5a2* MO injected embryos (Figure 6.2.1 and 6.2.3).

The reduction of Nodal signalling seen in the *rab5a2* MO injected embryos (Figure 5.1.2 and 5.2.2) implies a role for Rab5a2 in nodal signalling. This involvement of *rab5a2* with zebrafish signalling factors is not without precedent, as zebrafish *rab5* has been shown to play a role in the effective signalling range of Fgf8 (Scholpp and Brand, 2004). A reduction of Rab5, using the reportedly Rab5 specific GAP RN-tre, showed an increase in the range of Fgf8 signalling. In contrast to these results, the

microarray data suggests that *rab5a2* reduces Fgf8 signalling (Figure 6.2.1). The microarray shows that, at 30% epiboly, *fgf8* gene expression is severely reduced in *rab5a2* MO injected embryos.

The contrast between Scholpp's data and that reported by the microarray, may be due to the use of RN-tre, a Rab5 GTPase activation factor (GAP). Although it is reported to be a Rab5 specific GAP (Lanzetti et al., 2004), further research has shown that its Rab5 activity is weak and that RN-tre has a greater specific catalytic activity towards Rab41 (Haas et al., 2005). In addition, RN-tre is reported to act as a Rab5 effector, although this is also disputed in the later report. It is, therefore, unclear whether the increased Fgf8 signalling range is the result of a reduction in *rab5*. Scholpp (2004), however, addressed this issue by using antisense oligonucleotides to knock down *rab5a* function and showed that the result is the same as that seen for RN-tre.

The conflict beween those results seen in the microarray and Scholpp's data may, therefore, lie in the dose of MO used. The dose of MO used for the microarray was chosen to ensure the embryos showed a phenotype (Section 5.2.1). This is higher than that used for Scholpp's data, where the dose used would possibly have only been enough to reduce *rab5a* signalling by a small amount. Also, there is an additional *rab5a* gene and, although the clone used for overexpression analysis corresponds to *rab5a2*, the identity of the MO used is not stated. Scholpp implies that *rab5c* RNA is used in some of these experiments and on occasion refers to the mRNA as *rab5*. Therefore, it becomes unclear as to which RNA is being used, which could explain the conflict seen between the microarry data and Scholpp's data, since, although both *rab5a* and *rab5c* share high sequence homology, their functional homology in zebrafish has not been fully explored. However, overexpression of *rab5a* mRNA from the clone that corresponds to *rab5a2* does show reduction of Fgf8 signalling, allegedly corroborating the effect seen in the *rab5a* MO. The reduced range of Fgf8, seen in the *rab5a* overexpressing embryos, does not directly measure Fgf8 signalling range but uses expression of the Fgf8 target gene *spry4*. In addition, it measures this effect using exogenously supplied Fgf8. The *rab5a* MO used also looks at the target gene *spry4* but uses endogenous Fgf8. This thesis suggests that the conflict might be reconciled if a potential dual role is performed by *rab5a2* in early zebrafish development.

Overexpression of *rab5a2* results in expression of *gsc* and *ntl* in the animal pole of the embryo (Figure 5.3.2) in addition to the normal expression pattern of these genes seen at the margin. The *rab5a2* overexpression embryos also show either accumulation of cells in the animal pole or an enlarged organiser (Figure 5.3.1). These results, coupled with the lack of visible organizer and the reduction of *cyc, chd* and nodal responsive genes in *rab5a2* MO injected embryos, suggest a role for Rab5a2 in DV patterning and the establishment of the organizer. Interestingly, many of the genes that decreased in *rab5a2* MO injected embryos, when compared to controls, have been implicated in DV patterning (Fainsod et al., 1997; Fekany et al., 1999; Furthauer et al., 2004). At shield stage, this became more pronounced. In addition, some of the genes that increased in *rab5a2* MO injected embryos have also been implicated in DV patterning (Hild et al., 1999; Melby et al., 2000; Ramel et al., 2005). This is unsurprising, since DV patterning is a balancing act between genes which promote or antagonise ventral and dorsal signals. Those which promote ventral domains and inhibit dorsal include *bmp4, ved* and *vox*. While those which promote dorsal and inhibit ventral include *chd, fgf8* and *fgf24*.

In the *rab5a2* MO injected embryos *chd, fgf8 and fgf24* are all decreased. This would suggest that an increase in expression of ventralizing genes should be seen in the *rab5a2* MO injected embryos due to a reduction of pro-dorsal genes inhibiting them. However, this is not the case. The microarray data shows that genes which decrease in *rab5a2* MO injected embryos both promote and antagonise ventral and dorsal domains. Expression of *bmp4,* which is known to induce ventral fates within the embryo, was shown to be decreased (Figure 6.2.1 and 6.2.3) as was *wnt8a* another ventralizing gene. *wnt8a* has been shown to act through the transcriptional repressors *ved* and *vent* also shown to decrease in the microarray (Figure 6.2.1 and 6.2.3). *ved* and *vent* act to repress dorsalizing genes, their main target is *chd* but in addition, they repress *gsc* and *flh*. Therefore, a decrease in *vent* and *ved* expression should result in an increase in *gsc, chd* and *flh* expression. However, the expression of these genes is also decreased (Figure 5.1.2 and 5.2.2). In addition if *rab5a2* were responsible for the establishment of the organizer, the accumulation of cells in the animal pole of *rab5a2* overexpressing embryos might be a second organizer, while the enlarged organizer would show an expansion of the dorsal domain However,

there is no additional or expanded expression of *chd* in these embryos and a second axis is not apparent, which is what would be expected if the accumulation of cells in the animal pole were a second organizer. Instead, the embryos show mostly normal development, except for a severely reduced body axis (Figure 5.3.1). Interestingly, the microarray data shows that expression of the ventralizing gene *bmp2b* is increased in 30% epiboly stage *rab5a2* MO injected embryos. It was also increased in shield stage MO injected, but not to the extent seen at the 30% stage. While, the RT-PCR was inconclusive. This increase in *bmp2b* is unsurprising, as those factors which inhibit *bmp2b* are down regulated in *rab5a2* MO injected embryos. However, *bmp4*, which is also inhibited by these factors, is decresed (Table 6.2.1 and 6.2.3).

The transcriptional repressor genes *vent*, *ved* and *vox* prevent the transcription of *boz* and other dorsal genes, particularly *chd* but also *gsc* and *flh* (Imai et al., 2001) (Kawahara et al., 2000a; Kawahara et al., 2000b; Melby et al., 2000; Shimizu et al., 2002). All three genes *vox, ved* and *vent* are activated by *wnt8* (Ramel and Lekven, 2004), which has been suggested to regulate these genes in conjunction with *bmp2b*, since loss of function of *vox, vent* and *ved* phenocopies the *wnt8/swr (bmp2b)* double mutant phenotype (Ramel et al., 2005). Both *vent* and *ved* are decreased in *rab5a2* MO injected embryos, as is *wnt8* but to a lesser extent (Appendix 1 and 2). Interestingly, analysis of *vox* expression in control and *rab5a2* MO injected embryos, showed an increase in *vox* expression in the *rab5a2* MO injected embryos (Figure 7.1.1). The possible increase in *vox* expression may be due to the increase in *bmp2*, whilst the decrease in *ved* and *vox* may be the result of decreased *wnt8* expression. Therefore, it is possible that the reduction in *chd, flh* and *gsc* expression is the result of an increase in Bmp2b repression acting through *vox*. It has been suggested that *chd* is not needed if *bmps* are inactivated (Schulte-Merker et al., 1997), since *chordin* mutants have a ventralized phenotype (Chen and Schier, 2001), whereas *bmp2b;chordin* double mutants are dorsalized. This implies it is more likely that the increase in Bmp2b may be repressing *chd*, rather than decreased Chd effecting *bmp2b*.

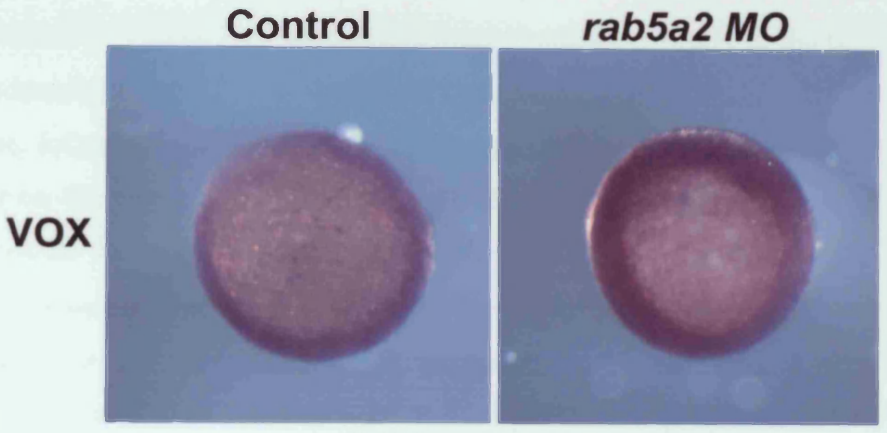

Figure 7.1.1 : Difference in expression pattern of the homeobox gene *vox* in *rab5a2* MO injected embryos when compared to controls.

bmp4 acts to specify the formation of ventral mesoderm and suppress neural fates, whilst *bmp2b* is described as necessary for mesoderm cell fate commitment (Graff et al., 1994; Hawley et al., 1995; Schneider et al., 1996; Suzuki et al., 1994). Both *bmp2b* and *bmp4* act to specify ventral identity and are negative regulators of endodermal cell fate specification. Therefore, it may be the difference between mesoderm cell fate commitment and mesoderm formation that results in the different expression profiles in the *rab5a2* MO injected embryos. Other genes down regulated in the *rab5a2* MO injected embryos also have roles in the mesoderm. *fgf8* and *fgf24* are coexpressed in mesoderm precursors during gastrulation (Draper et al., 2003). A defect in the gene *tbx16* is responsible for the mutant *spadetail*. *tbx6* and *ntl* are expressed in mesoderm and are known to regulate region-specific gene expression and developmental fate (Goering et al., 2003).

An additional interesting twist is that *bonnie and clyde*, which is involved in endoderm formation, is down regulated in *rab5a2* MO injected embryos at 30% (Table 6.2.1) but increased slightly at shield (Appendix 2). Endodermal determination, initiated by the Nodal signalling pathway, has been shown to require a multitude of genes. Included in these are, as mentioned, *bonnie and clyde* (Trinh et al., 2003), as well as *eomesodermin* (*eomes*) (Bjornson et al., 2005), which is up regulated in the *rab5a2* MO injected embryos. *eomes*, a maternal T-box gene and transcriptional activator, has also been shown to determine dorsal identity. Initially

after fertilization *eomes* is expressed in a vegetal animal gradient in the embryo, with Eomesodermin protein (Eom) distributed cytoplasmically throughout the blastoderm. However, following midblastula transition, nuclear-localized Eomesodermin is only detected on the dorsal side of the embryo (Bruce et al., 2003). Overexpression of *eomes* results in Nodal-dependent and *nieuwkoid/dharma* (*nwk/dhm*) independent ectopic expression of the organizer markers *gsc*, *chd* and *flh*, and in the formation of a secondary axis (Bruce et al., 2003). Interestingly, the knocking down of *rab5a2* results in the increase of *eomes* (Figure 6.2.2 and 6.2.4) with the decrease of *gsc*, *chd* and *flh* (Figure 5.1.2 and 5.2.2) and pre-24hpf embryonic lethality (Figure 5.1.1).

Overexpression of *eomes* has been shown not to have any effect on *cyc*, *sqt, bmp2b, vega1/vox* or *nwk/dhm*, although *eomes'* effect on *gsc*, *chd* and *flh* is nodal dependent and it has been speculated that *eomes* possibly regulates *sqt* (Bruce et al., 2003). Therefore, this raises the possibility that *rab5a2* may affect nodal signalling by interfering with the pathway between *eomes* and *sqt*. *eomes* is suggested to activate, and possibly maintain, its own transcription (Bruce et al., 2003). If knock down of *rab5a2* does disrupt the pathway between *eomes* and *sqt* the *eomes* expression might be increased to compensate. However, *eomes* autoregulation is suggested to be Nodal-independent, since injection of *eomes* into MZoep embryos resulted in induction of *eomes* expression (Bjornson et al., 2005). This increased expression of *eomesodermin* in *rab5a2* MO injected embryos may be linked to the conflicting expression seen for *bmp2b* and *bmp4* although there is no direct evidence linking the *bmps* to *eomesodermin*

Another possibility is that *rab5a2* knock down results in mislocalization, or inhibition, of the early localization to individual cells of *sqt*, seen in the four cell embryo (Gore et al., 2005). Preliminarily data looking at the effect of *rab5a2* on early *sqt* expression shows no *sqt* localization to individual cells in the 8-16 cells stage of control or *rab5a2* MO injected embryos but does show localization in *rab5a2* overexpresing embryos (Figure 7.1.2). Since there is no localized expression of *sqt* in the controls, as reported by Gore *et al* (2005), the signal was increased by injecting 15pg in 1.4nl of *alexa-sqt* into the yolk of control MO injected, *rab5a2* MO injected and *rab5a2* overexpressing embryos. Gore reports that this localizes in the same manner as endogenous *sqt*. Localization to individual cells of the 8-16 cell

stage embryos was seen in control MO injected embryos, *rab5a2* MO injected embryos and *rab5a2* overexpressing embryos (Figure 7.1.2). However, the expression of *sqt* in the *rab5a2* overexpressing embryos developed before that of the control and *rab5a2* MO injected embryos. These data suggest that *rab5a2* may effect zebrafish development at a very early stage. This would be consistent with the misexpression of *β-catenin* expression seen in the *rab5a2* MOs, when compared to the gradient of *β-catenin* expression emanating from the dorsal side of control embryos (Figure 5.5.2). Such results imply a role for *rab5a2* early in development, although it is unclear how and what role the early maternal transcripts of *sqt* or *β-catenin* may play in this.

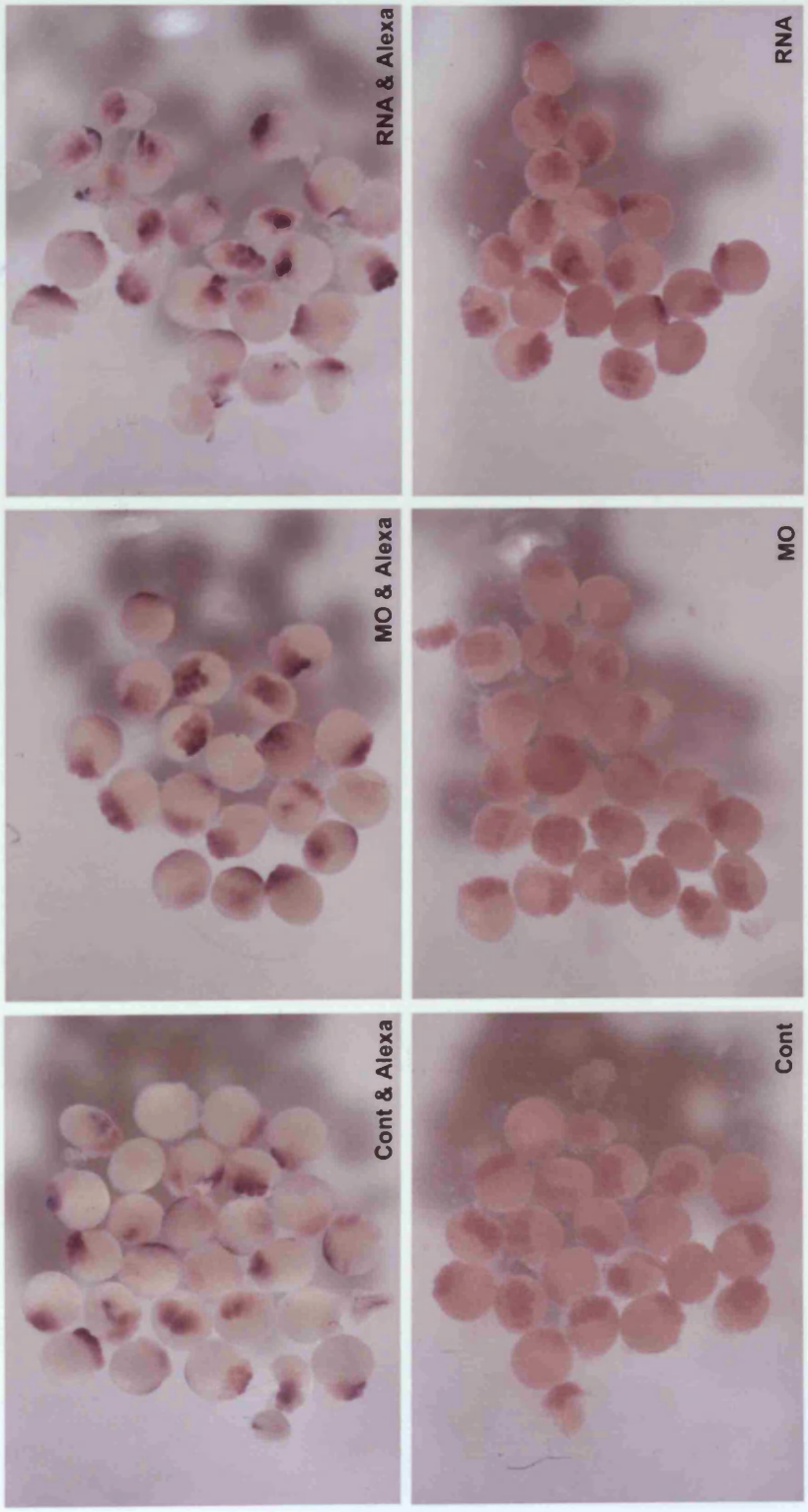

Figure 7.2.1: Identifying localized *sqt* expression in 8-16 cell embryos injected with control MO, 5ng *rab5a2* MO or *rab5a2* 1.5ng RNA. In addition to identifying localized *sqt* expression in 8-16 cell embryos injected with 15pg *alexa-sqt* and either control MO, 5ng *rab5a2* MO or 1.5ng of *rab5a2* RNA

The early phenotypes seen in *rab5a2* MO injected embryos, including the reduction of nodal target gene expression and *chd* expression, are possibly the result of the maternal *rab5a2* transcripts on early developmental factors. Knocking down only the

zygotic transcripts of *rab5a2* resulted in embryos with a visible organizer and normal speed of development, as well as expression of *bik, ntl, gsc* and *chd* being unaffected. However, the *rab5a2* MO injected embryos, deficient in only zygotic transcripts, died before 24hpf, suggesting an equally important role for zygotic *rab5a2* in later development.

To examine how Rab5a2 might directly affect nodal signalling, *sqt* or *cyc* was injected into one cell of a 128 stage embryo. Sqt has been proposed as a morphogen acting directly on target cells over a distance while Cyclops signals in a more localized manner (Chen and Schier, 2001).

In embryos overexpressing *rab5a2*, injection of either 5pg or 10pg of *sqt* resulted in similar *gsc* and *ntl* expression to that seen in controls (Figure 5.4.1 and 5.4.2). This conflicts with evidence from the signalling factor *fgf8*, where overexpression of *rab5a* resulted in the *fgf8* target gene *spty4* showing a reduction in range of expression. This reduction in range was suggested to result from increased clearance, by *rab5a,* of the Fgf8 ligand present in the extracellular space – a process termed "restrictive clearance". Injection of 5pg of *sqt* into *rab5a2* MO injected embryos resulted in a large proportion of embryos showing severe reduction of intensity of both *gsc* and *ntl* expression, with *gsc* showing a broader range of expression. However, many of the *rab5a2* MO injected embryos showed no expression of either *gsc* or *ntl.* When the dose of *sqt* was increased to 10pg, a greater proportion of the embryos showed no expression of *gsc* or *ntl.*

This data is contradictory: the broader range of *gsc* expression would be consistent with the Scholpp's theory of "restrictive clearance", however, many embryos showed no expression, which is at odds with this (Scholpp and Brand, 2004). In addition, since *gsc* is induced at high doses of nodal and *ntl* induced at lower doses, the *ntl* expression would also be expected to be expanded. This contradictory data might be the result of the high background staining seen in *rab5a2* MO injected embryos, masking the already weak *gsc* and *ntl* expression. The weak signal, seen in the *rab5a2* MO injected embryos may result from the broader expression pattern. Therefore, if the embryo produced an even broader expression pattern this might be masked by the background staining. One theory is that extracelluar Sqt binds to its

receptor but the receptor cannot be internalized and, therefore, it cannot activate target genes. If the receptors cannot be internalized, then Sqt cannot be restrictively cleared form the extracellular space and extracellular Sqt can travel further. If there is not complete knock down of *rab5a2*, then some of the receptors will be internalized and will activate target genes. Since Sqt has not been cleared, the extracellular dose would be high, so *gsc* is induced. This theory assumes that percentage of receptor occupancy is responsible for the type of target gene expression, i.e. if greater than a certain percentage of receptors are occupied, one target gene is induced, whereas, if less than this percentage are occupied, a different target gene is induced.

The effect of Rab5a2 on Cyc signalling differed to that of Sqt. Injection of *cyc* into *rab5a2* MO injected embryos resulted in the majority of embryos showing a lack of *gsc* and *ntl* expression (Figure 5.4.3). Those which did show *gsc* expression failed to show the expanded expression pattern observed for the *sqt* injected embryos, while those that showed *ntl* derived from the exogenous *cyc* also showed endogenous *ntl* expression, suggesting that there was not complete knock down of *rab5a2*. Injection of *cyc* into *rab5a2* overexpressing embryos showed either absence or reduction of intensity of *gsc* expression in the majority of embryos, while *ntl* signalling was unaffected (Figure 5.4.3). These data seem contradictory but suggest a role for *rab5a2* in Cyc signalling. It is possible that *rab5a2* may have role in the secretion of the Cyc protein and with its internalization, once bound to a target cell receptor. If *rab5a2* had a role in secretion, reduction of this gene would cause impaired secretion of Cyc and no target gene expression. Overexpression, on the other hand, might result in normal secretion, since the production of Cyc would be unaffected, but would result in increased internalization. This increased internalization would result in Cyc being removed from the extracellular space, lowering its extracellular dose and resulting in *ntl* expression rather than *gsc.* Since the *rab5* genes have been well characterized as regulators of endocytosis (Bucci et al., 1992; Chavrier et al., 1990; Gorvel et al., 1991), it is probable that *rab5a2* wouldn't be directly responsible for secretion. The microarray data showed a reduction in the expression of *rab14* in *rab5a2* MO injected embryos (Figure 6.2.1 and 6.2.3). Rab14 has been shown to be involved in membrane trafficking between the golgi complex and endosomes. It is

possible that these two *rabs* work in co-operation to ensure normal Cyc signalling, however, the data is inconclusive.

The RT-PCR data, used to validate the microarray, is also inconclusive. Much of this is due to the large degree of variation seen in these samples. This variation is controlled in the microarray data by the increased number of replicates, as well as by normalization of the data. Although the RT-PCR data is inconclusive for some of the genes, particularly the supposed non-changing housekeeping genes, the trend observed does suggest that the microarray data is accurate. Stronger evidence corroborating this is found in the expression patterns of *chd, flh,* and *ntl* in chapter 4. The down regulation of *chd* seen in the microarray data for *rab5a2* MO injected embryos is validated by *ish* with the abolishment of *chd* expression seen in *rab5a2* MO injected embryos.

The microarray data showed hundreds of genes whose expression was changed when *rab5a2* was knocked down even when the base line for change was set as high as three fold. This data suggests an early effect for *rab5a2* and correspond with the early phenotype seen in these embryos. Even at the 30% stage, where there is no visual difference between the *rab5a2* embryos and the control embryos, hundreds of genes changed their expression. The shield stage data showed an increase in the genes which changed, when compared to 30% epiboly embryos. This is expected given the suggestion that *raba5a2* acts early in development and has an effect on signalling factors (Campos, 2004; Scholpp and Brand, 2004; Ulrich et al., 2005). The earlier in development *rab5a2* acts, the further up the signalling cascade it is likely to act and, in disrupting an upstream signalling factor, Rab5a2 affects all the downstream factors acted upon by that initial factor. Therefore, analysis of gene expression at later stages of development should be predicted to show an increased number of genes that change.

7.2 Further Work

7.2.1 Further analysis of Rab5a2

Due to the complex nature of *rab5a2* and the high degree of regulation of the protein it has been very difficult to fully explore its effect on Nodal signalling. It is possible that *rab5a2* knock down or overexpression could be indirectly interfering with the secretion or synthesis of the Sqt and Cyc proteins. Transplantation of *sqt* and *cyc* overexpression cells into *rab5a2* MO injected or overexpressing embryos would enable the role of *rab5a2* in cells producing or receiving the *sqt* or *cyc* to be separated. This results from the cells transcribing and secreting the Nodal related proteins having wild type *rab5a2* expression.

So far, much of the analysis has involved looking at Nodal responsive genes as an indicator of Nodal, rather than Nodal itself. To this end, *sqt-gfp* and *cyc-gfp* fusion proteins have been made by inserting a GFP region after the cleavage site, between the pro and mature domains of *sqt* and *cyc* (see Methods section 2.2.11). This ensures that when the proteins are cleaved, the GFP attaches to the mature domain.

To ascertain whether the *sqt-gfp* construct was producing the same effect as wild type *sqt*, 10pg of *sqt-gfp* RNA was injected into single cells of 128 cell stage embryos. These were then compared to embryos injected in the same manner with 10pg of wild type *sqt* RNA and those injected with 10pg of control RNA. Subsequently, each group of embryos was fixed at shield stage and examined for *ntl* expression. A similar procedure was completed for *cyc-gfp*, where it was compared against wild type *cyc* and control RNA. Expression of *ntl* was seen in the animal pole in both wild type *sqt* and *sqt-gfp* injected embryos, while the controls showed normal expression round the margin (Figure 7.2.1). Embryos injected with either *cyc* or *cyc-gfp* also showed expression of *ntl* in the animal pole (Figure 7.2.1). This suggested that the *sqt-gfp* and *cyc-gfp* was producing a similar affect to the wild type *sqt* and *cyc* RNA.

To further compare wild type *sqt* and *cyc* with *sqt-gfp* and *cyc-gfp,* 5pg or 10 pg of either *sqt, cyc, sqt-gfp* or *cyc-gfp* were injected into single cell embryos. These were left to develop until shield stage, when they were snap frozen and prepared for RT-PCR analysis (see Methods section 2.2.10), using taqman oligos for Nodal responsive markers. g*sc, flh, chd* and *lfy2* expression was increased compared to controls in embryos injected with either 5 or 10pg of *sqt,* 5 or 10pg of *cyc,* 5 or 10 pg of *sqt-gfp* or 10 pg of *cyc-gfp* (Figure 7.2.2). *ntl* and *lty1* expression was increased in embryos injected with either 5pg or 10pg of *sqt*, 5pg of *sqt-gfp* 5pg of 10pg of *cyc-gfp. lfy1* was also increase in embryos injected with 5 or 10pg of *cyc* (Figure 7.2.2)

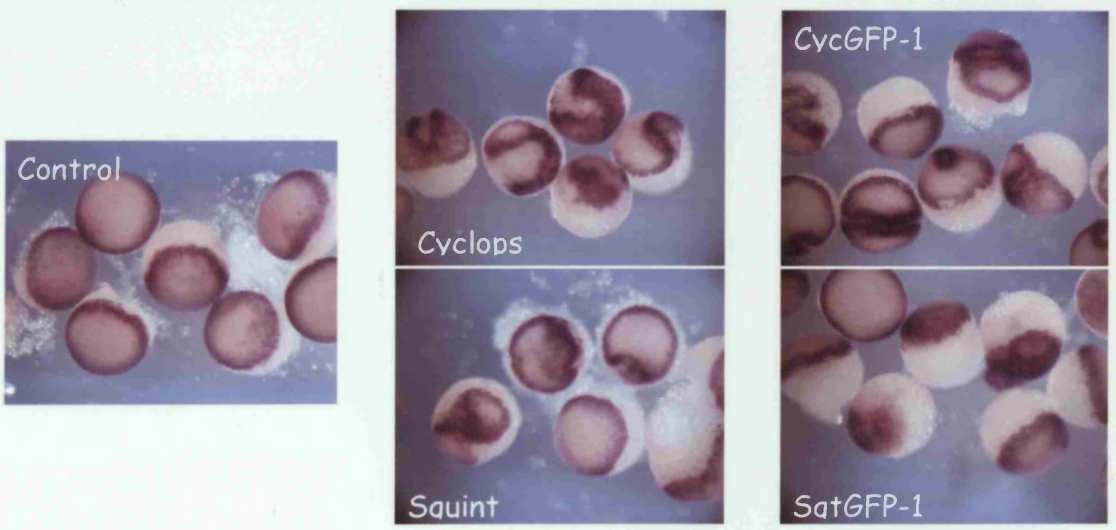

Figure 7.2.1: Comparison of *sqt* and *cyc* RNA to *sqt-GFP* and *cyc*-GFP fusion constructs.

Comparison of *ntl* expression in embryos injected with 10pg of *sqt* RNA compared to embryos injected with 10pg of *sqt-GFP* RNA and embryos injected with 10pg of *cyc* RNA compared to embryos injected with 10pg of *cyc –GFP* RNA. *ntl* expression in control injected embryos are also shown.

Finally, the *sqt-gfp* construct was checked for GFP activity. This was achieved by injecting a single cell in a 128 cell stage embryos with the lineage label rhodamine and 10pg of *sgt-gfp*. The embryos were then observed under a confocal microscope for GFP activity. GFP was seen accumulating round cells containing rhodamine, which suggested that the *sqt-gfp* was functional (Figure 7.2.3 supl mov 7.2.3).

Injection of these GFP-nodal fusion constucts would enable the Nodal ligand to be followed in the developing embryo. Therefore, it would be possible to observe the

range of the ligand directly, instead of using target gene expression. Injecting these constructs into one cell of 128 cell embryo, either overexpressing *rab5a2* or with *rab5a2* knocked-down, would potentially enable visualization of the ligand being secreted or produced, and enable investigation into whether *rab5a2* effects the secretion of the ligand. In addition, it would be interesting to transplant cells from embryos overexpressing these constructs into embryos, overexpressing *rab5a2* or knocked-down for *rab5a2*. This would enable the visualization of these Nodals through the developing embryo without the secretion, or production, of the Nodal-GFP ligands being altered by alterations in *rab5a2*.

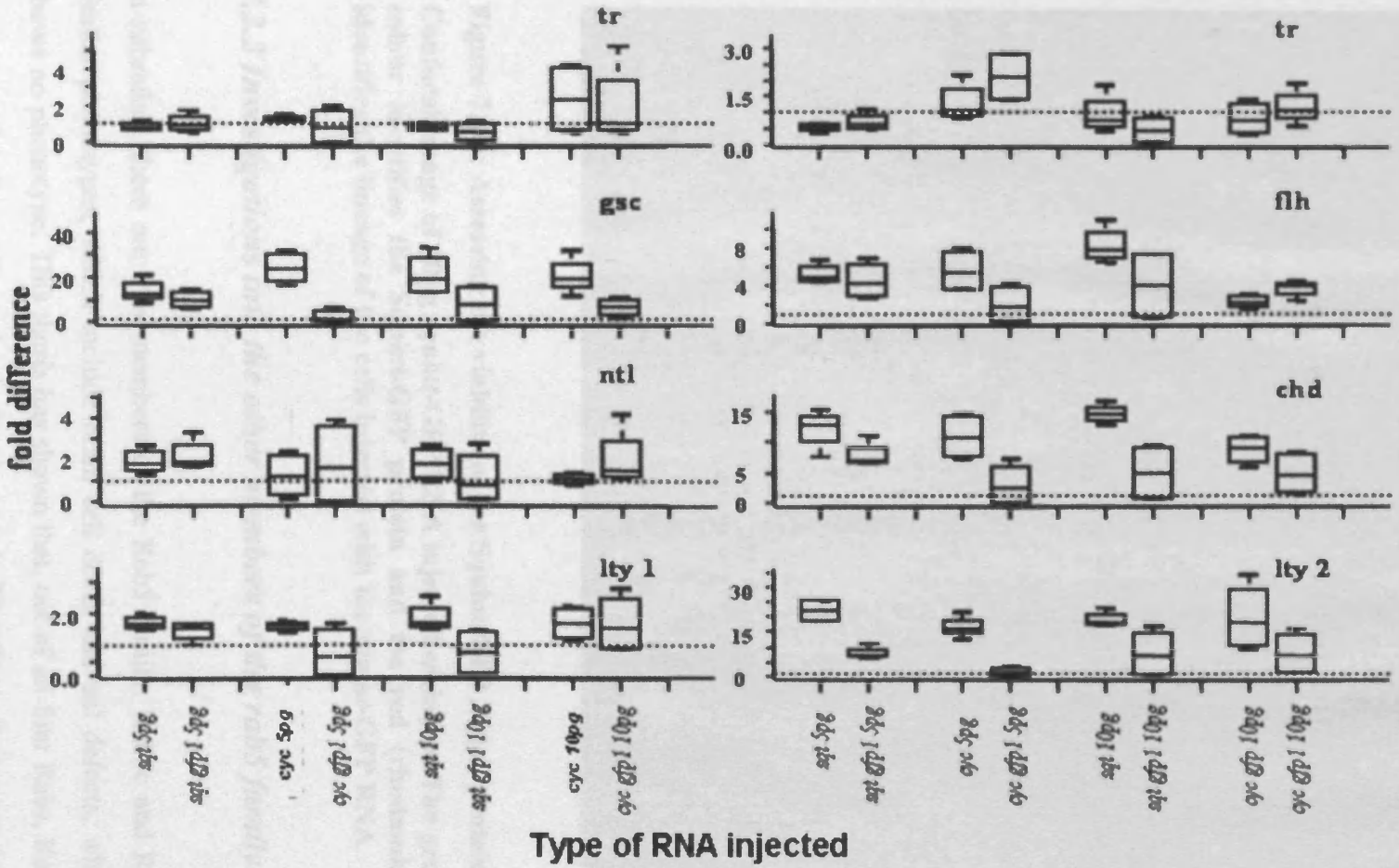

Figure 7.2.2: Box and whisker plots showing the fold change (compared to wild type embryos) of *gsc*, *ntl*, *flh*, *tr*, *lty1*, *lty2* and *chd* expression in embryos injected with 5pg of *sqt*, 5pg of *sqt-gfp*, 10pg of *sqt*, 10pg of *sqt-gfp*, 5pg of *cyc*, 5pg of *cyc-gfp*, 10pg of *cyc* or 10pg of *cyc-gfp*.

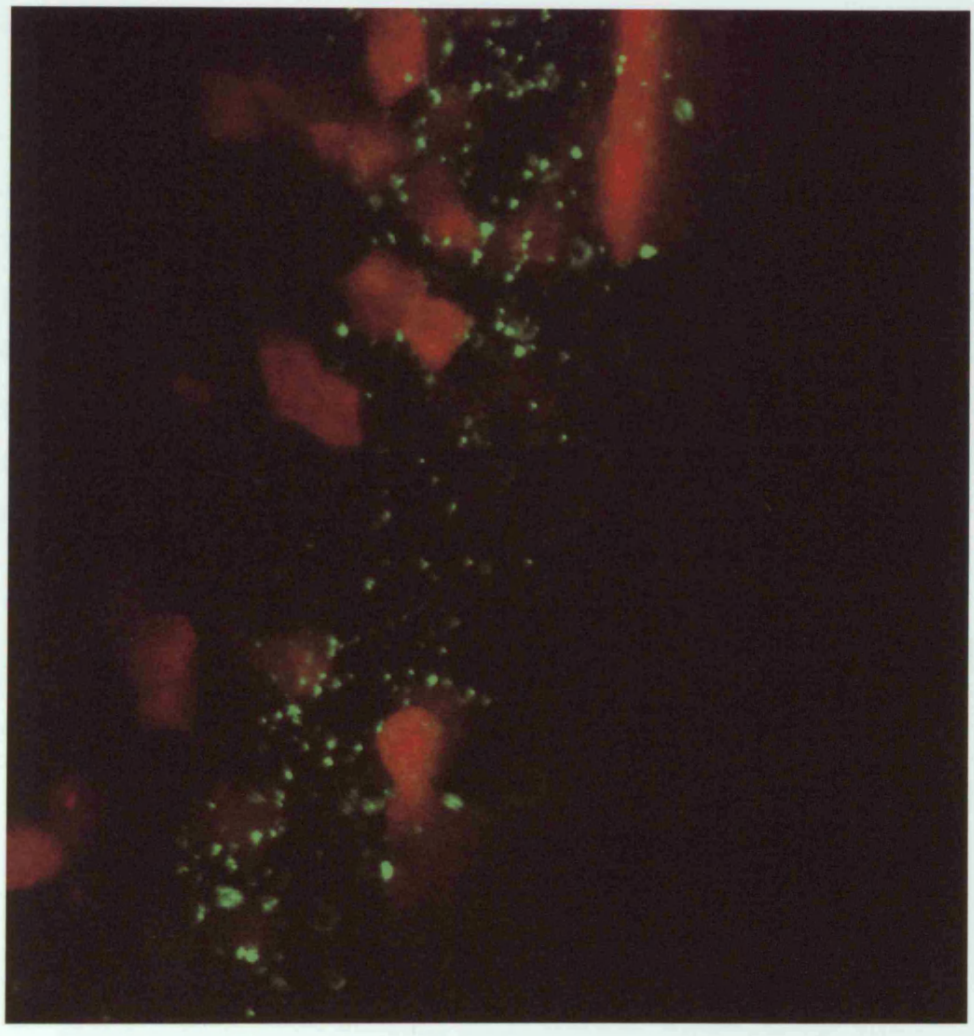

Figure 7.2.3: Assessing the viability of the Squint-GFP fusion protein.

Confocal image of 10pg *squint*-GFP RNA injected embryos. The green colour identifies the Squint-GFP protein and the red (rhodamine) identifies the lineage of the cells injected with the *squint*-GFP RNA.

7.2.2 Investigations into the other members of the rab5 family.

In zebrafish, there are four members of the Rab5 family. Rab5c and Rab5b show similar phenotypes, which include brain cell death and tail defects, while Rab5a1 shows no phenotype. This thesis has shown that, out of all four Rabs, Rab5a2 is the most essential for early embryo development. Therefore, it is now important to

establish whether these remaining Rab5s are even partially redundant and whether they have a role in cell signalling, in particular Nodal signalling.

Initial studies looking at the expression of dorsal and Nodal responsive gene have shown that *rab5a1* appears to be redundant in regard to Nodal signalling (Figure 7.2.4). However, *rab5c* and *rab5b* show a degree of down regulation. Rab5b particularly showed downregulation of all the genes investigated, while Rab5c showed down regulation of *bhik*. Therefore, it would be interesting to conduct microarray analysis on each of these genes to further quantifly to what extent these *rabs* effect cell signalling and which of these pathways, if any, overlap with other members of the Rab5 family.

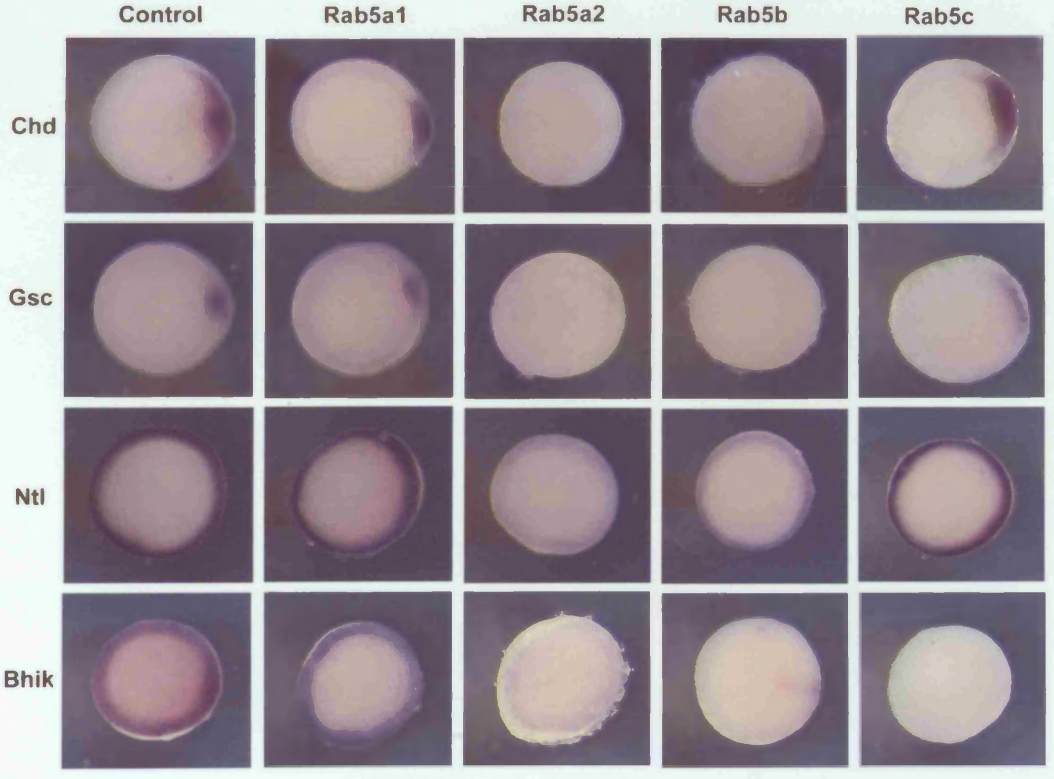

Figure 7.2.4: Animal views of shield stage embryos: *gsc, ntl, chd* and *bik* expression in control MO injected embryos on the left compared to embryos injected with 12ng of *rab5a1* MO, 8ng of *rab5a2* MO and 8ng *rab5c* MO.

Chapter 8

Conclusions

Conclusions

This thesis presents the results of extensive experiments into the functions of members of the *rab* family of GTPases in the zebrafish. Results for more than a third (13) of the 37 *rab* genes that have been investigated to date are presented in this thesis. The results demonstrate the essential nature of many of these genes for early embryonic development, with a loss-of function screen using antisense MO oligonucleotides leading to severe, and in some cases, highly specific, developmental defects.

Of the 13 *rabs* investigated in detail and described in this thesis, *rab3c1, rab28* and *rab1a3* show very specific defects when knocked down. *rab3c1* MO injected embryos display pigment defects, investigations into which demonstrate that these MO injected embryos are blind. *rab28* MO injected embryos show circular swimming behaviour, which may result from defects in balance, while knocking down *rab1a3* shows a reduction in pigmentation. These defects show that, far from being purely housekeeping genes, *rabs* can exhibit tissue specificity. This corresponds to the effect seen in mammals, where five *rabs* have shown very specific phenotypes, with two of these responsible for human disorders (Menasche et al., 2000; Verhoeven et al., 2003).

To date, members of the *rab1*, *rab6*, *rab7, rab8* and *rab11* families, as well as all the members of the *rab5* family – genes whose homologues in yeast are considered essential due to the ensuing lethality when absent – have been studied. Of these, only *rab5a2*, when knocked-down, causes death before 24hpf. Given the proposed housekeeping function of many of the *rab* genes, in particular those considered essential, it seems counter-intuitive that only *rab5a2* should show such a dramatic early lethality. This thesis elucidates a novel, essential and complex role for the maternal transcripts of *rab5a2* in Nodal signalling. The knocking down of *rab5a2* results in a severe reduction of *cyc*, Nodal-responsive genes and the dorsal marker *chd*. Overexpression of *rab5a2* results in locally up-regulated expression of *gsc* and *ntl* in the animal pole, in addition to endogenous expression in the margin, but had

little effect on *chd* expression. These results suggest that *rab5a2* is a vital component of the Nodal signalling pathway. The results of this study show no evidence for the restrictive clearance model, suggested by Scholpp (Scholpp and Brand, 2004), for the movement of Fgf8, in Nodal signalling. However, this cannot be ruled out as experiments using exogenous *sqt* and *cyc* to investigate the effect of overexpression or knock-down of *rab5a2* on Nodal signalling proved inconclusive. To address this, further studies using GFP tagged Nodals are necessary.

This thesis suggests a complex role for *rab5a2* in DV patterning, since knocking down *rab5a2* affects many DV patterning signals. Intriguingly, both dorsal promoting genes and some dorsal antagonists are affected by knocking down *rab5a2*, while other dorsal antagonists, such as *bmp2b*, are not affected. An important role is also established for *rab5a2* in epiboly, and so early zebrafish development. Evidence for this is provided by the large number of genes whose expression changed when *rab5a* was knocked down

In conclusion, the *rab* genes are an interesting group of genes whose function can specifically impact on many important developmental processes. Although many of these genes show similar phenotypes, some show interesting and unique phenotypes that deserve further study. The unique phenotype of *rab5a2* has shown this gene to be essential for early development and Nodal signalling with an interesting role in DV patterning, one again worthy of further study.

Appendices and References

Appendix 1

Genes in *rab5a2* morpholino injected embryos that changed more than 3 fold compared to controls at the 30% epiboly stage

Gene Name	Fold Change			Av.	Description
NM_131058.1_3prime500bases378		0.13		0.13	ENSDARG00000007329:T-box gene 16 [Source:RefSeq_peptide;Acc:NP_571133];
NM_194392.1_3prime500bases194	0.20	0.17	0.12	0.16	ENSDARG00000040216:trophoblast glycoprotein-like [Source:RefSeq_peptide;Acc:NP_919373];
NM_131342.2_3prime500bases296		0.18	0.19	0.19	ENSDARG00000019995:bone morphogenetic protein 4 [Source:RefSeq_peptide;Acc:NP_571417];
NM_001001950.1_3prime500bases137		0.22		0.22	ENSDARG00000009849:zic family member 3 heterotaxy 1 (odd-paired homolog, Drosophila) [Source:RefSeq_peptide;Acc:NP_001001950];
NM_131509.1_3prime500bases430		0.22		0.22	keratin 4
NM_213118.1_3prime500bases147		0.19	0.28	0.23	ENSDARG00000014243:SRY-box containing gene 2 [Source:RefSeq_peptide;Acc:NP_998283];
NM_131690.1_3prime500bases388		0.25		0.25	ENSDARG00000019856:ATPase, Na+/K+ transporting, alpha 1b polypeptide [Source:RefSeq_peptide;Acc:NP_571765];
NM_131052.1_3prime500bases417		0.27	0.24	0.26	ENSDARG00000006939:T-box transcription factor TBX6 (T-box protein 6). [Source:Uniprot/SWISSPROT;Acc:P79742];
NM_001007454.1_3prime500bases299		0.25	0.28	0.26	ENSDARG00000027699:zgc:101612 [Source:RefSeq_peptide;Acc:NP_001007455];
NM_131281.2_3prime500bases201		0.26	0.28	0.27	ENSDARG00000003399:fibroblast growth factor 8 [Source:RefSeq_peptide;Acc:NP_571356];
NM_001003875.1_3prime500bases285		0.29	0.27	0.28	ENSDARG00000037931:U1 small nuclear ribonucleoprotein polypeptide A [Source:RefSeq_peptide;Acc:NP_001003875];
NM_198876.1_3prime500bases405		0.29		0.29	ENSDARG00000018971:UDP-GlcNAc:betaGal beta-1,3-N-acetylglucosaminyltransferase 5 [Source:RefSeq_peptide;Acc:NP_942577];
DIG0410_1903		0.30		0.30	
NM_001002332.1_3prime500bases404		0.26	0.34	0.30	ENSDARG00000007024:zgc:92414 [Source:RefSeq_peptide;Acc:NP_001002332];
NM_131108.1_3prime500bases390		0.31	0.30	0.30	ENSDARG00000036830:type I cytokeratin, enveloping layer [Source:RefSeq_peptide;Acc:NP_571182];
NM_131885.2_3prime500bases167		0.32		0.32	ENSDARG00000036074:CCAAT/enhancer binding protein alpha [Source:RefSeq_peptide;Acc:NP_571960];
NM_131109.1_3prime500bases25		0.32		0.32	ENSDARG00000036292:caudal type homeo box transcription factor 4 [Source:RefSeq_peptide;Acc:NP_571184];
NM_201513.1_3prime500bases433		0.32		0.32	ENSDARG00000042539:tyrosine 3-monooxygenase/tryptophan 5-monooxygenase activation protein, theta polypeptide
NM_130973.1_3prime500bases361		0.30	0.36	0.33	ENSDARESTG00000005532 chordin
NM_182871.1_3prime500bases170		0.33		0.33	ENSDARG00000037677:fibroblast growth factor 24 [Source:RefSeq_peptide;Acc:NP_878291];
NM_212580.1_3prime500bases426		0.33		0.33	ENSDARESTG00000023644 methyl-CpG binding domain protein 3b
NM_130940.1_3prime500bases425		0.32	0.37	0.34	ENSDARG00000009737:bonnie and clyde [Source:RefSeq_peptide;Acc:NP_571015];
NM_131207.1_3prime500bases102		0.33	0.35	0.34	ENSDARG00000007944:LIM homeobox 1b [Source:RefSeq_peptide;Acc:NP_571282];
NM_183074.1_3prime500bases334		0.37	0.32	0.35	ENSDARG00000042503:ventrally expressed dharma/bozozok antagonist [Source:RefSeq_peptide;Acc:NP_898897];
NM_001012246.1_3prime500bases23		0.35		0.35	ENSDARG00000035748:fibroblast growth factor 19 [Source:RefSeq_peptide;Acc:NP_001012246];
NM_200159.1_3prime500bases291		0.36		0.36	ENSDARG00000008238:mannosidase, beta A, lysosomal [Source:RefSeq_peptide;Acc:NP_956453];
NM_131209.1_3prime500bases394		0.41	0.32	0.36	protocadherin 8
NM_201316.1_3prime500bases415		0.37		0.37	ENSDARG00000035913:tyrosyl-tRNA synthetase [Source:RefSeq_peptide;Acc:NP_958473];
NM_174861.2_3prime500bases259		0.41	0.34	0.37	ENSDARG00000019268:gastrulation brain homeobox 1 [Source:RefSeq_peptide;Acc:NP_777286];

NM_200228.1_3prime500bases99		0.37		0.37	ENSDARG00000013973:peroxisomal biogenesis factor 3 [Source:RefSeq_peptide;Acc:NP_956522];
NM_173288.1_3prime500bases371		0.38	0.38	0.38	ENSDARG00000040666:mki67 (FHA domain) interacting nucleolar phosphoprotein (human) - like [Source:RefSeq_peptide;Acc:NP_775395];
NM_001003774.1_3prime500bases342		0.32	0.45	0.39	ENSDARG00000015123:zgc:101000 [Source:RefSeq_peptide;Acc:NP_001003774];
NM_201576.1_3prime500bases131		0.43	0.36	0.39	ENSDARG00000034351:transgelin 2 [Source:RefSeq_peptide;Acc:NP_963870];
NM_212602.1_3prime500bases425		0.39		0.39	ENSDARG00000011127:AHA1, activator of heat shock 90kDa protein ATPase homolog 1, like [Source:RefSeq_peptide;Acc:NP_997767];
NM_131609.1_3prime500bases422		0.40		0.40	ENSDARG00000017917:hairy and enhancer of split related-7 [Source:RefSeq_peptide;Acc:NP_571684];
NM_201514.1_3prime500bases375		0.38	0.41	0.40	ENSDARG00000037012:solute carrier family 3, member 2 like [Source:RefSeq_peptide;Acc:NP_958922];
NM_131700.1_3prime500bases289		0.38	0.41	0.40	ENSDARG00000017164:ventral expressed homeobox [Source:RefSeq_peptide;Acc:NP_571775];
NM_130955.1_3prime500bases324 DIG0402_1561	0.35	0.39	0.45	0.40	ENSDARESTG00000012353 deltaD (dld),
NM_131320.1_3prime500bases353		0.39	0.41	0.40	ENSDARG00000023188:lymphocyte cytosolic plastin 1 [Source:RefSeq_peptide;Acc:NP_571395];
BC046031.1_3prime500bases262		0.43	0.38	0.40	ENSDARG00000029074 ubiquitin-activating enzyme E1-domain containing 1, mRNA , containing frame-shift errors
NM_130956.1_3prime500bases123		0.42	0.39	0.40	ENSDARG00000004256:Wnt-11 protein precursor. [Source:Uniprot/SWISSPROT;Acc:O73864];
NM_201495.1_3prime500bases221		0.32	0.48	0.40	RAB14
NM_207184.1_3prime500bases429		0.40		0.40	ENSDARG00000009510:iroquois homeobox protein 1, a isoform 1 [Source:RefSeq_peptide;Acc:NP_997067];
CF673281.1_3prime500bases425		0.43	0.39	0.41	ENSDARESTG00000018874 CB967 5- similar to Filamin A
NM_205732.1_3prime500bases414		0.41		0.41	glutamate-ammonia ligase
NM_212567.1_3prime500bases8		0.42		0.42	ENSDARG00000024204:minichromosome maintenance protein 3 [Source:RefSeq_peptide;Acc:NP_997732];
NM_152986.1_3prime500bases147		0.42		0.42	ENSDARG00000044356:tumor protein p73-like isoform alpha 1 [Source:RefSeq_peptide;Acc:NP_694518];
NM_001001811.1_3prime500bases418		0.42		0.42	ENSDARG00000036440:SRY-box containing gene 3 [Source:RefSeq_peptide;Acc:NP_001001811];
NM_205567.1_3prime500bases270		0.43		0.43	ENSDARG00000006603:cysteine and glycine-rich protein 1 [Source:RefSeq_peptide;Acc:NP_991130];
NM_131116.2_3prime500bases13		0.43		0.43	ENSDARG00000000175:Homeobox protein Hox-B2a (Hox-B2). [Source:Uniprot/SWISSPROT;Acc:O42367];
DIG0203_403		0.43		0.43	
DIG0395_973		0.43		0.43	
NM_198817.1_3prime500bases426		0.53	0.34	0.43	ENSDARESTG00000016981 starmaker (stm),
NM_214722.1_3prime500bases256		0.45	0.41	0.43	ENSDARG00000018806:cathepsin C [Source:RefSeq_peptide;Acc:NP_999887];
NM_130908.1_3prime500bases107		0.43	0.44	0.43	OTTDARG00000002166:zgc:55628:Novel_CDS
BU670752.1_34		0.44		0.44	ENSDARG00000039072 Similar to ectoplacental cone, invasive trophoblast giant cells, extraembryonic ectoderm and chorion sequence 3,
NM_001003501.1_3prime500bases284		0.43	0.44	0.44	ENSDARG00000012341:zgc:92451 [Source:RefSeq_peptide;Acc:NP_001003501];
NM_131882.2_3prime500bases379		0.40	0.48	0.44	ENSDARG00000022476 chemokine (C-X-C motif) receptor 4a (cxcr4a)
NM_131163.1_3prime500bases430		0.44		0.44	ENSDARG00000039694:Beta-2-microglobulin precursor. [Source:Uniprot/SWISSPROT;Acc:Q04475];
NM_131884.2_3prime500bases139		0.46	0.42	0.44	ENSDARG00000045369:CCAAT/enhancer binding protein beta [Source:RefSeq_peptide;Acc:NP_571959];
NM_201493.1_3prime500bases125		0.44		0.44	ENSDARG00000036291:nucleobindin 2a [Source:RefSeq_peptide;Acc:NP_958901];
DIG0109_1354		0.45		0.45	ENSDARG00000054161:fibroblast growth factor receptor 4 [Source:RefSeq_peptide;Acc:NP_571505];

NM_131110.1_3prime500bases292	0.41	0.49	0.45	ENSDARG00000011166:Carbonic anhydrase (EC 4.2.1.1) (Carbonate dehydratase). [Source:Uniprot/SWISSPROT;Acc:Q92051];
NM_200659.1_3prime500bases358	0.45		0.45	ENSDARG00000025948:mutL homolog 1, colon cancer, nonpolyposis type 2 [Source:RefSeq_peptide;Acc:NP_956953];
NM_131861.1_3prime500bases69	0.50	0.41	0.45	ENSDARG00000030289:Jagged-1a precursor (Jagged1a) (Jagged1). [Source:Uniprot/SWISSPROT;Acc:Q90Y57];
NM_001002717.1_3prime500bases329	0.51	0.41	0.46	ENSDARG00000010206:p21-activated kinase 2 [Source:RefSeq_peptide;Acc:NP_001002717];
NM_131162.1_3prime500bases301	0.48	0.45	0.46	ENSDARG00000009905:Brachyury protein homolog (T protein homolog) (T-box protein ZFT) (ZF- T) (No tail protein).
CF673253.1_3prime500bases193	0.46		0.46	ENSDARESTG00000008362 CB894 5- similar to Nogo-66 receptor homolog-1, mRNA sequence
NM_152980.1_3prime500bases185	0.46		0.46	ENSDARG00000031855:macrophage stimulating 1 (hepatocyte growth factor-like) [Source:RefSeq_peptide;Acc:NP_694512];
NM_173244.1_3prime500bases425	0.47		0.47	ENSDARG00000024904:TAL1 (SCL) interrupting locus like [Source:RefSeq_peptide;Acc:NP_775351];
CF569085.1_3prime500bases370	0.47		0.47	ENSDARG00000020386 CB939 5- similar to ATP-binding cassette transporter 1
NM_131287.2_3prime500bases377	0.40	0.55	0.47	ENSDARG00000041345:SRY-box 17 [Source:RefSeq_peptide;Acc:NP_571362];
NM_130946.1_3prime500bases316	0.48	0.47	0.47	ENSDARG00000010355:wnt8-like protein 2 [Source:RefSeq_peptide;Acc:NP_001018637];
NM_131668.3_3prime500bases390	0.48		0.48	ENSDARG00000013144:ATPase, Na+/K+ transporting, beta 1a polypeptide [Source:RefSeq_peptide;Acc:NP_571743];
NM_212612.1_3prime500bases264	0.47	0.48	0.48	DEAD (Asp-Glu-Ala-Asp) box polypeptide 5 (ddx5),
NM_214808.1_3prime500bases249	0.49	0.47	0.48	ENSDARG00000023520:Fibroblast growth factor-17b precursor (FGF-17b). [Source:Uniprot/SWISSPROT;Acc:Q6SJP8];
NM_173261.1_3prime500bases339	0.49	0.48	0.48	ENSDARG00000010948:kinesin family member 11 [Source:RefSeq_peptide;Acc:NP_775368];
CB333812.1_3prime500bases133	0.45	0.52	0.48	cDNA clone CB159 5- similar to Epiplakin
DIG0345_1024	0.48		0.48	ENSDARG00000040815:hypothetical protein LOC325958 [Source:RefSeq_peptide;Acc:NP_956027];
NM_131557.1_3prime500bases429	0.49		0.49	ENSDARG00000035831:GATA-binding protein 6 [Source:RefSeq_peptide;Acc:NP_571632];
NM_194371.2_3prime500bases155	0.51	0.46	0.49	ENSDARG00000010124:Sp5 transcription factor-like [Source:RefSeq_peptide;Acc:NP_919352];
CD808440.1_3prime500bases377	0.49		0.49	gastrula stage cDNA library Danio rerio cDNA clone CB473 5
NM_173221.2_3prime500bases432	0.49		0.49	ENSDARG00000013839:aldehyde dehydrogenase 3 family, member D1 [Source:RefSeq_peptide;Acc:NP_775328];
NM_001005390.1_3prime500bases12	0.41	0.57	0.49	ENSDARG00000035329:calpain, small subunit 1 [Source:RefSeq_peptide;Acc:NP_001005390];
NM_131025.2_3prime500bases229	0.42	0.56	0.49	ENSDARG00000035750:G1/S-specific cyclin D1. [Source:Uniprot/SWISSPROT;Acc:Q90459];
NM_201124.1_3prime500bases423	0.49		0.49	ENSDARG00000011545:arrestin, beta 2 [Source:RefSeq_peptide;Acc:NP_957418];
NM_131414.1_3prime500bases435	0.50		0.50	ENSDARG00000040346 eph receptor B4a (ephb4a),
NM_212770.1_3prime500bases190	0.50	0.49	0.50	ENSDARG00000005185:carboxypeptidase N, polypeptide 1 [Source:RefSeq_peptide;Acc:NP_997935];
NM_131027.1_3prime500bases413	0.50		0.50	ENSDARG00000002952:smoothened homolog [Source:RefSeq_peptide;Acc:NP_571102];
NM_131092.1_3prime500bases291	0.43	0.57	0.50	ENSDARG00000035095:one-eyed pinhead [Source:RefSeq_peptide;Acc:NP_571167];
DIG0366_880	0.50		0.50	ENSDARG00000056950:hypothetical protein LOC550602 [Source:RefSeq_peptide;Acc:NP_001017903];
AB097826.1_3prime500bases19	0.51		0.51	ENSDARG00000002403:Hypothetical protein YF-9 (Fragment). [Source:Uniprot/SPTREMBL;Acc:Q7T2W2];
NM_201475.1_3prime500bases382	0.47	0.55	0.51	ENSDARG00000031495:SET translocation (myeloid leukemia-associated) A [Source:RefSeq_peptide;Acc:NP_958883];
NM_131245.1_3prime500bases275	0.48	0.53	0.51	inhibitor of DNA binding 6
NM_001004578.1_3prime500bases336	0.55	0.47	0.51	ENSDARG00000014793:zgc:92331 [Source:RefSeq_peptide;Acc:NP_001004578];

NM_199211.1_3prime500bases380		0.54	0.48	0.51	ENSDARG00000030700:CTP synthase [Source:RefSeq_peptide;Acc:NP_954681];
NM_199429.1_3prime500bases154		0.51		0.51	ENSDARG00000038097:phosphatidylinositol glycan, class Q [Source:RefSeq_peptide;Acc:NP_955461];
NM_201586.1_3prime500bases423		0.47	0.56	0.51	dapper homolog 2, antagonist of beta-catenin
NM_131300.1_3prime500bases423		0.51		0.51	ENSDARG00000011956:Homeobox protein Dlx4a (DLX-8). [Source:Uniprot/SWISSPROT;Acc:Q98879];
NM_131221.1_3prime500bases428		0.51		0.51	ENSDARG00000015790:ATPase, Na+/K+ transporting, beta 3a polypeptide [Source:RefSeq_peptide;Acc:NP_571296];
NM_131114.1_3prime500bases186		0.53	0.50	0.52	ENSDARG00000036141 even-skipped-like1 (eve1)
CF673239.1_3prime500bases30		0.49	0.54	0.52	ENSDARESTG00000011746 CB996 5- similar to Poly [ADP-ribose] polymerase-2 (
NM_131560.1_3prime500bases60		0.47	0.56	0.52	ENSDARG00000027205:mix-type homeobox gene 1 [Source:RefSeq_peptide;Acc:NP_571635];
NM_201331.1_3prime500bases423		0.52		0.52	ENSDARG00000012369:retinol dehydrogenase 10 [Source:RefSeq_peptide;Acc:NP_958488];
NM_194369.1_3prime500bases417		0.52		0.52	ENSDARG00000037563:CD99 antigen-like 2 [Source:RefSeq_peptide;Acc:NP_919350];
NM_212777.1_3prime500bases392		0.53		0.53	ENSDARESTG00000022602 bromodomain containing 8 (brd8),
NM_131415.1_3prime500bases4		0.52	0.54	0.53	ENSDARG00000017354:eph-like receptor tyrosine kinase 6 [Source:RefSeq_peptide;Acc:NP_571490];
NM_213047.1_3prime500bases244		0.49	0.57	0.53	ENSDARG00000037109:PWP2 periodic tryptophan protein homolog [Source:RefSeq_peptide;Acc:NP_998212];
NM_131205.1_3prime500bases434		0.53		0.53	ENSDARG00000029079 ets related protein erm (erm),
nomo_3prime500bases177		0.53		0.53	ENSDARG00000034683
NM_131637.1_3prime500bases240		0.56	0.51	0.54	ENSDARG00000014047:Claudin-like protein ZF4A22 (Claudin-7). [Source:Uniprot/SWISSPROT;Acc:Q9YH92];
NM_131146.2_3prime500bases230		0.54		0.54	ENSDARG00000033999:Cytochrome P450 26A1 (EC 1.14.-.-) (Retinoic acid-metabolizing cytochrome) (P450RAI) (Retinoic acid 4-hydroxylase).
NM_205585.1_3prime500bases175		0.54		0.54	ENSDARG00000035521:secreted frizzled-related protein 1 [Source:RefSeq_peptide;Acc:NP_991148];
NM_199558.1_3prime500bases365		0.54		0.54	ENSDARG00000027109:zinc finger RNA binding protein [Source:RefSeq_peptide;Acc:NP_955852];
NM_130960.1_3prime500bases226		0.56	0.52	0.54	ENSDARG00000019920:lefty1 [Source:RefSeq_peptide;Acc:NP_571035];
NM_131851.1_3prime500bases133		0.51	0.57	0.54	ENSDARG00000041341:SRY-box containing gene 32 [Source:RefSeq_peptide;Acc:NP_571926];
NM_214692.1_3prime500bases406		0.53	0.56	0.54	membrane protein, palmitoylated 1 (mpp1),
DIG0389_910		0.54		0.54	
NM_131482.1_3prime500bases380		0.60	0.49	0.55	ENSDARG00000005645:roundabout homolog 3 [Source:RefSeq_peptide;Acc:NP_571557];
NM_200099.1_3prime500bases116		0.60	0.49	0.55	ENSDARG00000012000:dynein light chain (10.3 kD) (dlc-1) [Source:RefSeq_peptide;Acc:NP_956393];
NM_200104.1_3prime500bases385		0.55		0.55	ENSDARG00000036675:heterogeneous nuclear ribonucleoprotein A1 [Source:RefSeq_peptide;Acc:NP_956398];
AY648733.1_3prime500bases414		0.51	0.59	0.55	ENSDARG00000045321:DNA polymerase alpha (Fragment). [Source:Uniprot/SPTREMBL;Acc:Q6DRM6];
NM_001002312.1_3prime500bases360		0.55		0.55	ENSDARG00000041870:intraflagellar transport 172 [Source:RefSeq_peptide;Acc:NP_001002312];
AY216588.1_3prime500bases143		0.56		0.56	ENSDARG00000023220:Selenoprotein T2 (Fragment). [Source:Uniprot/SPTREMBL;Acc:Q802G4];
CB923492.1_3prime500bases387		0.57	0.54	0.56	ENSDARG00000004713:hypothetical protein LOC550434 [Source:RefSeq_peptide;Acc:NP_001017739];
NM_131227.1_3prime500bases133		0.56		0.56	ENSDARG00000043071:Retinal homeobox protein Rx3. [Source:Uniprot/SWISSPROT;Acc:O42358];
NM_201452.1_3prime500bases308		0.56		0.56	ENSDARG00000009484:ADP-ribosylation factor 1 [Source:RefSeq_peptide;Acc:NP_958860];
NM_131450.2_3prime500bases260		0.58	0.54	0.56	ENSDARG00000020711:Ribonucleoside-diphosphate reductase M2 chain (EC 1.17.4.1) (Ribonucleotide reductase protein R2 class I).

DIG0121_607	0.56		0.56	ENSDARG00000017320:F11 receptor [Source:RefSeq_peptide;Acc:NP_001004667];
NM_131455.1_3prime500bases385	0.56		0.56	ENSDARG00000014017:Ribonucleoside-diphosphate reductase large subunit (Ribonucleoside-diphosphate reductase M1 subunit)
BQ826572.1_3prime500bases187	0.57		0.57	cDNA clone CB349 5- similar to Complement component C7
DIG0349_1819	0.57		0.57	
NM_201463.1_3prime500bases130	0.57		0.57	ENSDARG00000022232:peter pan homolog [Source:RefSeq_peptide;Acc:NP_958871];
DIG0099_2026	0.57		0.57	
DIG0346_877	0.57		0.57	ENSDARG00000021607:Iglon1 [Source:RefSeq_peptide;Acc:NP_001003851];
DIG0131_1438	0.57		0.57	ENSDARG00000058538:hypothetical protein LOC323048 [Source:RefSeq_peptide;Acc:NP_997799];
CF673237.1_3prime500bases83	0.57		0.57	ENSDARG00000007781 CB994 5- similar to P70193 Membrane glycoprotein
NM_131291.1_3prime500bases223	0.57		0.57	fibroblast growth factor 3 (fgf3
NM_131098.1_3prime500bases249	0.59	0.57	0.58	ENSDARG00000040295:Apolipoprotein Eb precursor (Apo-Eb). [Source:Uniprot/SWISSPROT;Acc:O42364];
AJ494837.1_3prime500bases199	0.50	0.66	0.58	ENSDARG00000036558:Collagen XVIII (Fragment). [Source:Uniprot/SPTREMBL;Acc:Q8AWC6];
NM_212609.1_3prime500bases159	0.58		0.58	ENSDARESTG00000014051 guanine nucleotide binding protein (G protein), beta polypeptide 1 (gnb1),
NM_199547.1_3prime500bases139	0.62	0.55	0.58	ENSDARG00000029252:Sjogren syndrome antigen B (autoantigen La) [Source:RefSeq_peptide;Acc:NP_955841];
NM_198871.1_3prime500bases153	0.60	0.57	0.59	zgc:63569 (zgc:63569),
BC075970.1_3prime500bases424	0.59		0.59	ENSDARG00000006427:Intestinal fatty acid-binding protein. [Source:Uniprot/SPTREMBL;Acc:Q8AX65];
NM_207048.1_3prime500bases204	0.60	0.57	0.59	ENSDARESTG00000012052 cyclin F (ccnf),
NM_131066.1_3prime500bases239	0.59		0.59	ENSDARG00000044163:snail homolog 1a [Source:RefSeq_peptide;Acc:NP_571141];
NM_200111.1_3prime500bases156	0.59		0.59	ENSDARG00000017748:hypothetical protein LOC378998 [Source:RefSeq_peptide;Acc:NP_956405];
DIG0401_1450	0.59		0.59	ENSDARG00000002336:Delta-like protein C precursor (DeltaC protein) (delC). [Source:Uniprot/SWISSPROT;Acc:Q9IAT6];
NM_200080.2_3prime500bases345	0.56	0.63	0.59	ENSDARG00000029086:keratin 8 [Source:RefSeq_peptide;Acc:NP_956374];
NM_173219.1_3prime500bases266	0.60		0.60	LIM domain only 1 (lmo1),
NM_200084.1_3prime500bases329	0.60		0.60	ENSDARG00000040464 phosphomannomutase 2 (pmm2),
CK445313.1_3prime500bases394	0.62	0.58	0.60	ENSDARG00000004017 CB1089 5- similar to sperm associated antigen 1,
BQ169366.1_3prime500bases3	0.60		0.60	ENSDARG00000013841 CB272 5- similar to TYROSINE-PROTEIN KINASE ABL2
NM_130964.1_3prime500bases414	0.61		0.61	ENSDARG00000007204 islet3 (isl3),
NM_181559.1_3prime500bases359	0.61		0.61	ENSDARG00000039128:glutamine synthetase 1 [Source:RefSeq_peptide;Acc:NP_853537];
NM_201459.1_3prime500bases430	0.61		0.61	ENSDARG00000002792:archain 1 [Source:RefSeq_peptide;Acc:NP_958867];
NM_001008615.1_3prime500bases182	0.59	0.63	0.61	ENSDARG00000041065:heat shock protein 1 [Source:RefSeq_peptide;Acc:NP_001008615];
NM_001003882.2_3prime500bases425	0.61		0.61	ENSDARG00000008237:seryl-tRNA synthetase [Source:RefSeq_peptide;Acc:NP_001003882];
NM_130937.1_3prime500bases293	0.61	0.61	0.61	ENSDARG00000034894:Wnt-5 protein precursor. [Source:Uniprot/SWISSPROT;Acc:Q92050];
NM_205702.1_3prime500bases229	0.61		0.61	zgc:76868 (zgc:76868),
NM_131874.1_3prime500bases111	0.58	0.65	0.62	ENSDARG00000035622:X-box binding protein 1 [Source:RefSeq_peptide;Acc:NP_571949];

NM_001002869.1_3prime500bases19	0.59	0.64	0.62	ENSDARG00000024593:DEAD (Asp-Glu-Ala-Asp) box polypeptide 27 [Source:RefSeq_peptide;Acc:NP_001002869];
NM_131834.1_3prime500bases233	0.62		0.62	ENSDARG00000041959:chemokine (C-X-C motif), receptor 4b [Source:RefSeq_peptide;Acc:NP_571909];
NM_198922.1_3prime500bases281	0.62		0.62	ENSDARG00000029305:BAI1-associated protein 2-like 1 [Source:RefSeq_peptide;Acc:NP_944604];
CF417054.1_3prime500bases17	0.63	0.62	0.62	cDNA clone CB850 5- similar to Methylmalonate-semialdehyde dehydrogenase
NM_212603.1_3prime500bases166	0.63		0.63	ENSDARG00000023330:acidic (leucine-rich) nuclear phosphoprotein 32 family, member B [Source:RefSeq_peptide;Acc:NP_997768];
NM_198908.1_3prime500bases138	0.62	0.64	0.63	ENSDARG00000007294:aconitase 2, mitochondrial [Source:RefSeq_peptide;Acc:NP_944590];
CF417014.1_3prime500bases203	0.63		0.63	ENSDARESTG00000002702 clone CB810 5- similar to Beta-1 integrin
CK445305.1_3prime500bases82	0.63		0.63	cDNA clone CB896 5- similar to Spalt transcription factor Sall1
NM_131055.1_3prime500bases433	0.63		0.63	ENSDARG00000021201:floating head [Source:RefSeq_peptide;Acc:NP_571130];
NM_181757.2_3prime500bases66	0.64	0.62	0.63	ENSDARG00000016470:annexin A5 [Source:RefSeq_peptide;Acc:NP_861422];
NM_131511.1_3prime500bases250	0.62	0.65	0.63	ENSDARG00000014673:frizzled 9 [Source:RefSeq_peptide;Acc:NP_571586];
NM_131516.1_3prime500bases368	0.64		0.64	ENSDARG00000002768:Parvalbumin beta. [Source:Uniprot/SWISSPROT;Acc:Q9I8V0];
NM_199274.1_3prime500bases294	0.64		0.64	ENSDARG00000040175:regulator of G-protein signalling 4 [Source:RefSeq_peptide;Acc:NP_954968];
DIG0408_1690	0.64		0.64	
NM_131363.1_3prime500bases153	0.64		0.64	ENSDARG00000045102:sine oculis homeobox homolog 3b [Source:RefSeq_peptide;Acc:NP_571438];
DIG0557_1492	0.64		0.64	
CF269292.1_3prime500bases211	0.64		0.64	CB751 5- similar to Vitamin K-dependent gamma-glutamyl carboxylase
NM_131235.2_3prime500bases8	0.64		0.64	GATA-binding protein 5 (gata5),
BI326806.1_3prime500bases170	0.65		0.65	ENSDARESTG00000000352 CB63 5- similar to SW:PGCV_CHICK Q90953 VERSICAN CORE PROTEIN PRECURSOR,
NM_183410.1_3prime500bases289	0.65		0.65	ENSDARG00000039645:annexin 11a isoform 1 [Source:RefSeq_peptide;Acc:NP_861430];
NM_131784.1_3prime500bases435	0.65		0.65	BMP and activin membrane-bound inhibitor (Xenopus laevis) homolog (bambi),
BU670702.1_3prime500bases280	0.65		0.65	ENSDARG00000003509 CB407 5- similar to SPT:Q8UVV4 ATP-binding cassette transporter 1,
NM_130988.1_3prime500bases427	0.65		0.65	ENSDARG00000038798:Patched protein homolog 1 (Patched 1) (PTC1). [Source:Uniprot/SWISSPROT;Acc:Q98864];
NM_131115.1_3prime500bases327	0.65		0.65	ENSDARG00000008174:Homeobox protein Hox-B1a (Hox-B1). [Source:Uniprot/SWISSPROT;Acc:O42366];
CF269323.1_3prime500bases12	0.65		0.65	cDNA library Danio rerio cDNA clone CB732 5- similar to Centrin
NM_198870.1_3prime500bases332	0.65		0.65	ENSDARG00000009336:hypothetical protein LOC321033 [Source:RefSeq_peptide;Acc:NP_942571];
NM_131290.1_3prime500bases274	0.65	0.66	0.65	ENSDARG00000021032:forkhead box D3 [Source:RefSeq_peptide;Acc:NP_571365];
NM_131632.1_3prime500bases37	0.65		0.65	ENSDARG00000022606:atonal homolog 7 [Source:RefSeq_peptide;Acc:NP_571707];
NM_201292.1_3prime500bases426	0.65		0.65	ENSDARG00000029928:adaptor-related protein complex 3, mu 1 subunit [Source:RefSeq_peptide;Acc:NP_958449];
NM_001002686.1_3prime500bases394	0.66		0.66	ENSDARG00000021003:zgc:91854 [Source:RefSeq_peptide;Acc:NP_001002686];
NM_201176.1_3prime500bases372	0.66		0.66	ENSDARG00000017775:similar to ATP synthase, H+ transporting, mitochondrial F0 complex, subunit c (subunit 9) isoform 3
CF673299.1_3prime500bases379	0.66		0.66	ENSDARESTG00000014248 CB926 5- similar to Gem-associated protein 5
DIG0123_592	0.66		0.66	

NM_131860.1_3prime500bases339	0.66		0.66	ENSDARG00000015472:knypek [Source:RefSeq_peptide;Acc:NP_571935];
NM_200075.1_3prime500bases316	0.66		0.66	ENSDARG00000007665:Similar to RIKEN cDNA 1500019G21 gene [Source:RefSeq_peptide;Acc:NP_956369];
BC055500.1_3prime500bases312	0.66		0.66	ENSDARG00000029172:Polr1a protein (Fragment). [Source:Uniprot/SPTREMBL;Acc:Q7SXQ2];
DIG0163_640	0.66		0.66	ENSDARG00000003061:PREDICTED: similar to CD276 antigen isoform b [Source:RefSeq_peptide_predicted;Acc:XP_700973];
NM_201491.1_3prime500bases432	0.66		0.66	ENSDARG00000042853:isovaleryl Coenzyme A dehydrogenase [Source:RefSeq_peptide;Acc:NP_958899];
NM_213103.1_3prime500bases427	0.67		0.67	ENSDARG00000045902:hypothetical protein LOC406376 [Source:RefSeq_peptide;Acc:NP_998268];
CB333792.1_3prime500bases355	1.50		1.50	cDNA library Danio rerio cDNA clone CB116 3
NM_130948.1_3prime500bases53	1.50		1.50	ENSDARG00000037995:DVR-1 protein precursor. [Source:Uniprot/SWISSPROT;Acc:P35621];
NM_131305.1_3prime500bases228	1.51		1.51	ENSDARG00000013125:Homeobox protein Dlx1a (DLX-1). [Source:Uniprot/SWISSPROT;Acc:Q98875];
NM_131734.2_3prime500bases396	1.51		1.51	ENSDARG00000005039:glutathione S-transferase pi [Source:RefSeq_peptide;Acc:NP_571809];
NM_201329.1_3prime500bases38	1.51		1.51	ENSDARG00000034771:RAB13, member RAS oncogene family [Source:RefSeq_peptide;Acc:NP_958486];
DIG0188_1237	1.52		1.52	ENSDARG00000056084:PREDICTED: similar to CG33141-PA [Source:RefSeq_peptide_predicted;Acc:XP_696105];
NM_201178.1_3prime500bases414	1.52		1.52	ENSDARG00000014577:Rhophilin 2 (GTP-Rho binding protein 2). [Source:Uniprot/SWISSPROT;Acc:Q6TNR1];
NM_213387.1_3prime500bases47	1.53		1.53	ENSDARG00000044399:phosphoglycerate kinase 1 [Source:RefSeq_peptide;Acc:NP_998552];
NM_131878.1_3prime500bases369	1.53		1.53	ENSDARG00000025516:nanos homolog [Source:RefSeq_peptide;Acc:NP_571953];
NM_001004122.1_3prime500bases414	1.53		1.53	ENSDARG00000042947:myostatin-2 [Source:RefSeq_peptide;Acc:NP_001004122];
DIG0311_361	1.54		1.54	
NM_198912.1_3prime500bases424	1.54		1.54	ENSDARESTG00000005713 peptidase D (pepd),
NM_131047.1_3prime500bases235	1.54		1.54	ENSDARG00000043276:calreticulin [Source:RefSeq_peptide;Acc:NP_571122];
NM_212823.1_3prime500bases272	1.55		1.55	ENSDARG00000040602 ?
NM_131664.1_3prime500bases338	1.55		1.55	ENSDARESTG00000014726 epithelial protein lost in neoplasm (eplin),
NM_173255.1_3prime500bases278	1.55		1.55	ENSDARESTG00000018904 ATPase, H+ transporting, lysosomal, V0 subunit c (atp6v0c),
NM_201577.1_3prime500bases427	1.55		1.55	ENSDARG00000005675 SEC61, beta subunit (sec61b),
NM_153662.1_3prime500bases434	1.56		1.56	ENSDARG00000018788:sialyltransferase 8 [Source:RefSeq_peptide;Acc:NP_705948];
NM_213058.1_3prime500bases432	1.56		1.56	ENSDARG00000004665:heat shock 70kDa protein 5 [Source:RefSeq_peptide;Acc:NP_998223];
NM_200074.3_3prime500bases186	1.57		1.57	ENSDARESTG00000025067 calcium homeostasis endoplasmic reticulum protein (cherp)
CF269307.1_3prime500bases359	1.62	1.51	1.57	ENSDARG00000017906:hypothetical protein LOC554101 [Source:RefSeq_peptide;Acc:NP_001019574];
CD808453.1_3prime500bases353	1.55	1.58	1.57	ENSDARESTG00000024342 clone CB654 5- similar to Histone protein Hist2h3c1,
BU808703.1_3prime500bases5	1.57		1.57	cDNA clone CB516 5- similar to C-ets-1 protein
NM_199333.1_3prime500bases147	1.57		1.57	ENSDARG00000003933:pyruvate kinase, muscle [Source:RefSeq_peptide;Acc:NP_955365];
NM_201213.1_3prime500bases388	1.57		1.57	ENSDARG00000010316:glutaminyl-tRNA synthetase [Source:RefSeq_peptide;Acc:NP_957507];
NM_001007282.1_3prime500bases238	1.65	1.50	1.58	glutathione peroxidase 4a
NM_200088.1_3prime500bases361	1.58		1.58	ENSDARG00000035332:hypothetical protein LOC368366 [Source:RefSeq_peptide;Acc:NP_956382];

NM_212835.1_3prime500bases46	1.58		1.58	ENSDARG00000041954:chymotrypsin C (caldecrin) [Source:RefSeq_peptide;Acc:NP_956180];
NM_001007371.1_3prime500bases41	1.58		1.58	ENSDARG00000032640:zgc:101900 (zgc:101900), mRNA [Source:RefSeq_dna;Acc:NM_001007371];
NM_201470.1_3prime500bases432	1.58		1.58	ENSDARG00000008310:inositol hexaphosphate kinase 2 [Source:RefSeq_peptide;Acc:NP_958878];
NM_201587.1_3prime500bases206	1.58		1.58	islet cell autoantigen (ica),
NM_200108.1_3prime500bases408	1.58		1.58	ENSDARESTG00000009408 zgc:55309 (zgc:55309),
NM_200025.1_365	1.59		1.59	ENSDARG00000037071:ribosomal protein S26 [Source:RefSeq_peptide;Acc:NP_956319];
NM_001007774.1_3prime500bases319	1.60		1.60	ENSDARESTG00000005461 zgc:101730 (zgc:101730), mRNA
NM_194401.1_3prime500bases291	1.60		1.60	ENSDARG00000002131:CUG triplet repeat, RNA binding protein 2 [Source:RefSeq_peptide;Acc:NP_919382];
NM_201457.1_3prime500bases430	1.60		1.60	ENSDARG00000008175:replication factor C (activator 1) 3 [Source:RefSeq_peptide;Acc:NP_958865];
NM_131555.1_3prime500bases397	1.61		1.61	ENSDARESTG00000011910 dopachrome tautomerase (dct), mRNA
NM_131528.1_3prime500bases298	1.61		1.61	ENSDARG00000036693:Homeobox protein Hox-C9a (Hox-C9). [Source:Uniprot/SWISSPROT;Acc:Q9YGS6];
NM_131757.1_3prime500bases427	1.63		1.63	ENSDARG00000015707:dishevelled, dsh homolog 3 [Source:RefSeq_peptide;Acc:NP_571832];
CB891031.1_3prime500bases308	1.63		1.63	CB628 5- similar to Protein-tyrosine phosphatase X precursor
NM_131513.1_3prime500bases430	1.63		1.63	ENSDARG00000038528 cyclin B1 (ccnb1),
CF673298.1_3prime500bases136	1.63		1.63	ENSDARESTG00000024736 clone CB984 5- similar to Receptor-type protein-tyrosine phosphatase mu precursor
NM_213208.1_3prime500bases114	1.53	1.74	1.64	ENSDARG00000013307:60S ribosomal protein L19. [Source:Uniprot/SWISSPROT;Acc:Q6P5L3];
NM_212707.1_3prime500bases162	1.67	1.61	1.64	ENSDARG00000000068:solute carrier family 9 (sodium/hydrogen exchanger), isoform 3 regulator 1
NM_199216.1_3prime500bases16	1.64		1.64	ENSDARG00000004964:cytochrome P450, family 4 [Source:RefSeq_peptide;Acc:NP_954686];
NM_130939.1_3prime500bases418	1.65		1.65	cth1 (cth1)
BU670753.1_3prime500bases358	1.65		1.65	OTTDARG00000011035:si:ch211-76m11.4:Novel_CDS;OTTDARG00000011034:si:ch211-76m11.3:Novel_CDS;
NM_131826.1_3prime500bases50	1.58	1.73	1.66	ENSDARG00000009182:sprouty (Drosophila) homolog 4 [Source:RefSeq_peptide;Acc:NP_571901];
NM_212795.1_3prime500bases117	1.74	1.57	1.66	ENSDARG00000022813:Dead end protein 1. [Source:Uniprot/SWISSPROT;Acc:Q7T1H5];
NM_131105.2_3prime500bases297	1.66		1.66	alpha-tropomyosin (tpma),
DIG0187_604	1.66		1.66	
NM_173257.1_3prime500bases146	1.66		1.66	ENSDARG00000015911:MCM2 minichromosome maintenance deficient 2, mitotin [Source:RefSeq_peptide;Acc:NP_775364];
NM_131142.1_3prime500bases105	1.71	1.61	1.66	ENSDARG00000001353:Homeobox protein Hox-B1b (Hox-A1). [Source:Uniprot/SWISSPROT;Acc:Q90423];
NM_001008581.1_3prime500bases327	1.67		1.67	ENSDARG00000040046:hypothetical protein LOC494038 [Source:RefSeq_peptide;Acc:NP_001008581];
NM_131322.2_3prime500bases422	1.67		1.67	ENSDARG00000014626:Homeobox protein Dlx3b (DLX-3). [Source:Uniprot/SWISSPROT;Acc:Q01702];
NM_001002486.1_247	1.67		1.67	ENSDARG00000043977 zgc:92860 (zgc:92860),
NM_199538.1_3prime500bases295	1.64	1.70	1.67	ENSDARG00000033768:hypothetical protein LOC321203 [Source:RefSeq_peptide;Acc:NP_955832];
NM_131506.1_3prime500bases351	1.68		1.68	ENSDARG00000005150:T-box 20 [Source:RefSeq_peptide;Acc:NP_571581];
NM_201487.1_3prime500bases385	1.59	1.78	1.68	ENSDARG00000014230:dihydrolipoamide S-succinyltransferase [Source:RefSeq_peptide;Acc:NP_958895];
NM_152956.1_3prime500bases377	1.68		1.68	ENSDARG00000034785:dachshund b [Source:RefSeq_peptide;Acc:NP_694488];

NM_181766.1_3prime500bases179		1.77	1.62	1.69	annexin A11b (anxa11b),
NM_152948.1_3prime500bases351		1.69		1.69	ENSDARG00000043658:coxsackie virus and adenovirus receptor [Source:RefSeq_peptide;Acc:NP_694480];
NM_173241.1_3prime500bases267		1.72	1.70	1.71	ENSDARG00000023002:denticleless homolog [Source:RefSeq_peptide;Acc:NP_775348];
NM_001003509.1_3prime500bases419		1.72		1.72	ENSDARG00000004806:zgc:92443 [Source:RefSeq_peptide;Acc:NP_001003509];
NM_178222.2_3prime500bases356		1.72		1.72	ENSDARG00000023316:single-minded homolog 1 [Source:RefSeq_peptide;Acc:NP_835740];
CF416980.1_3prime500bases316		1.81	1.64	1.72	ENSDARG00000042428 cDNA clone CB870 5- similar to Glutathione S-transferase 1
NM_198980.1_3prime500bases177		1.51	1.96	1.73	ENSDARG00000004311:low density lipoprotein receptor adaptor protein 1 [Source:RefSeq_peptide;Acc:NP_945331];
DIG0406_2221		1.74		1.74	
NM_153651.1_3prime500bases435		1.74		1.74	ENSDARG00000011273:homeo box 11-like [Source:RefSeq_peptide;Acc:NP_705937];
NM_178286.2_3prime500bases402		1.72	1.78	1.75	ENSDARESTG00000006588 selenoprotein M (sepm),
NM_131644.1_3prime500bases279		1.75		1.75	ENSDARG00000043923:SRY-box containing gene 9b [Source:RefSeq_peptide;Acc:NP_571719];
CF943689.1_3prime500bases114		1.76		1.76	ENSDARG00000045305 CB1053 5- similar to High-affinity cAMP-specific 3-,5--cyclic phosphodiesterase 7A
CB923498.1_3prime500bases313		1.79		1.79	ENSDARG00000018678 clone CB453 5- similar to Ras-related protein Rab-40C (SOCS box containing protein RAR3),
NM_131294.1_3prime500bases435		1.80		1.80	ENSDARG00000043848:Superoxide dismutase [Cu-Zn] (EC 1.15.1.1). [Source:Uniprot/SWISSPROT;Acc:O73872];
NM_212574.1_3prime500bases193		1.65	1.95	1.80	ENSDARESTG00000014835 solute carrier family 11 (proton-coupled divalent metal ion transporters), member 2 (slc11a2)
NM_200090.1_3prime500bases311		1.97	1.63	1.80	ENSDARG00000040730:hypothetical protein LOC368478 [Source:RefSeq_peptide;Acc:NP_956384];
NM_198807.1_3prime500bases67		1.81		1.81	ENSDARG00000020289:PIF1 homolog [Source:RefSeq_peptide;Acc:NP_942102];
NM_201206.1_3prime500bases257		1.81		1.81	ENSDARG00000011626:COX15 homolog, cytochrome c oxidase assembly protein [Source:RefSeq_peptide;Acc:NP_957500];
NM_200105.1_3prime500bases210		1.64	1.99	1.81	ENSDARG00000026862:fused toes homolog [Source:RefSeq_peptide;Acc:NP_956399];
NM_131267.1_3prime500bases432		1.82		1.82	ENSDARG00000036097:iroquois homeobox protein 3a [Source:RefSeq_peptide;Acc:NP_571342];
NM_001001941.1_3prime500bases82		1.84		1.84	ENSDARG00000004173:coatomer protein complex, subunit alpha [Source:RefSeq_peptide;Acc:NP_001001941];
NM_131875.1_3prime500bases0		2.16	1.54	1.85	SRY-box containing gene 10 (sox10),
NM_200960.1_3prime500bases153		1.63	2.07	1.85	ENSDARG00000011175:ATPase, H+ transporting, V1 subunit D [Source:RefSeq_peptide;Acc:NP_957254];
NM_001007038.1_3prime500bases269		2.06	1.64	1.85	ENSDARG00000044593:ATP-binding cassette, sub-family C (CFTR/MRP), member 4 (abcc4), mRNA
NM_130945.1_3prime500bases213		1.86		1.86	ENSDARG00000015717:fms-related tyrosine kinase 4 [Source:RefSeq_peptide;Acc:NP_571020];
NM_130947.1_3prime500bases404		1.87		1.87	ENSDARG00000040836:Wnt-4a protein precursor. [Source:Uniprot/SWISSPROT;Acc:P47793];
NM_178297.2_3prime500bases120		1.73	2.02	1.87	ENSDARESTG00000020068 selenoprotein P, plasma, 1a (sepp1a),
NM_201299.1_3prime500bases275		1.73	2.05	1.89	ENSDARG00000025904:glycoprotein, synaptic 2 [Source:RefSeq_peptide;Acc:NP_958456];
NM_183071.1_3prime500bases384		2.20	1.58	1.89	ENSDARG00000040344:linker histone H1M [Source:RefSeq_peptide;Acc:NP_898894];
NM_001004602.1_3prime500bases143		1.76	2.03	1.89	zgc:86701
NM_173223.2_3prime500bases346		1.82	1.97	1.90	ENSDARG00000002731:syndecan 2 [Source:RefSeq_peptide;Acc:NP_775330];
NM_131665.1_3prime500bases403	1.54	2.28		1.91	ENSDARG00000021389:jagged 2 isoform 1 [Source:RefSeq_peptide;Acc:NP_571937];
NM_194374.1_3prime500bases181		1.83	2.01	1.92	ENSDARG00000041217:exportin 6 [Source:RefSeq_peptide;Acc:NP_919355];

NM_212817.1_3prime500bases313	1.89	2.01	1.95	ENSDARG00000038964:tnf receptor-associated factor 4b [Source:RefSeq_peptide;Acc:NP_997982];
NM_212817.1_3prime500bases337	2.01	1.89	1.95	ENSDARG00000038964:tnf receptor-associated factor 4b [Source:RefSeq_peptide;Acc:NP_997982];
NM_001001399.1_3prime500bases370	1.93	1.96	1.95	ENSDARG00000005230:signal sequence receptor, beta [Source:RefSeq_peptide;Acc:NP_001001399];
NM_201499.1_3prime500bases421	1.96		1.96	ENSDARG00000025375:isocitrate dehydrogenase 1 (NADP+), soluble [Source:RefSeq_peptide;Acc:NP_958907];
NM_200107.1_3prime500bases149	1.97	2.01	1.99	ENSDARG00000037618:hypothetical protein LOC378866 [Source:RefSeq_peptide;Acc:NP_956401];
DIG0379_421	1.99		1.99	
CF417020.1_3prime500bases393	2.01		2.01	ENSDARG00000034829 CB816 5- similar to Procollagen-lysine,2-oxoglutarate 5-dioxygenase 3 precursor
NM_001002468.1_3prime500bases415	2.01		2.01	ENSDARG00000025350:hypothetical protein LOC436741 [Source:RefSeq_peptide;Acc:NP_001002468];
NM_199532.1_3prime500bases125	1.68	2.36	2.02	ENSDARG00000004402:ELOVL family member 6, elongation of long chain fatty acids [Source:RefSeq_peptide;Acc:NP_955826];
NM_130922.1_3prime500bases109	2.24	1.81	2.02	ENSDARG00000020298:B-cell translocation gene 2 [Source:RefSeq_peptide;Acc:NP_570997];
NM_001007124.1_3prime500bases325	2.03		2.03	ENSDARG00000028415 met proto-oncogene (hepatocyte growth factor receptor) (met),
NM_199212.1_3prime500bases100	1.93	2.15	2.04	ENSDARG00000025522:serum/glucocorticoid regulated kinase [Source:RefSeq_peptide;Acc:NP_954682];
BC081600.1_3prime500bases407	2.05		2.05	ENSDARG00000016771:transferrin-a [Source:RefSeq_peptide;Acc:NP_001015057];
NM_131247.1_3prime500bases435	2.05		2.05	lactate dehydrogenase B4 (ldhb),
Cab	2.05		2.05	
NM_131041.1_3prime500bases430	2.06		2.06	ENSDARG00000037231:Neurogenin 1 (Neurogenic differentiation factor 3) (NeuroD3) (Neurogenin related protein-1).
NM_131500.1_3prime500bases388	2.06		2.06	ENSDARG00000040159:wingless-type MMTV integration site family, member 4b [Source:RefSeq_peptide;Acc:NP_571575];
NM_131503.1_3prime500bases104	2.04	2.12	2.08	ENSDARG00000026534:Axin-1 (Axis inhibition protein 1). [Source:Uniprot/SWISSPROT;Acc:P57094];
BM402118.1_3prime500bases243	2.15	2.02	2.09	ENSDARG00000014499:hypothetical protein LOC445204 [Source:RefSeq_peptide;Acc:NP_001003598];
NM_200109.1_3prime500bases196	1.72	2.47	2.09	ENSDARG00000039527 TSC22 domain family 2 (tsc22d2)
NM_131848.1_3prime500bases415	1.91	2.30	2.11	ENSDARG00000004729:transcription factor binding to IGHM enhancer 3a [Source:RefSeq_peptide;Acc:NP_571923];
CF924885.1_3prime500bases240	2.09	2.13	2.11	ENSDARESTG00000025399 cDNA clone CB1014 5- similar to Q8wux2 Similar to RIKEN cDNA 2510006C20 gene
NM_198978.1_3prime500bases380	2.12		2.12	ENSDARESTG00000016872 programmed cell death 4b (pdcd4b),
NM_198072.1_3prime500bases142	2.03	2.22	2.13	ENSDARESTG00000006053 5-methyltetrahydrofolate-homocysteine methyltransferase (mtr),
NM_131247.1_3prime500bases423	2.13		2.13	ENSDARG00000035139 lactate dehydrogenase B4 (ldhb),
NM_198978.1_3prime500bases371	2.15		2.15	ENSDARG00000041022:programmed cell death 4 [Source:RefSeq_peptide;Acc:NP_945329];
NM_178298.2_3prime500bases266	1.72	2.59	2.16	ENSDARESTG00000011008 selenoprotein P, plasma, 1b (sepp1b)
DIG0565_1528	2.16		2.16	ENSDARG00000037493:hypothetical protein LOC553785 [Source:RefSeq_peptide;Acc:NP_001018583];
NM_199519.2_3prime500bases22	1.93	2.45	2.19	Enah/Vasp-like a (evla),
NM_199273.1_3prime500bases79	2.32	2.07	2.19	ENSDARESTG00000011553 zgc:66433 (zgc:66433),
NM_131729.2_3prime500bases151	2.21		2.21	OTTDARG00000006320:si:dkey-197d18.1:Novel_CDS
NM_131184.2_3prime500bases100	1.99	2.44	2.22	ENSDARG00000028148 paired box gene 2a (pax2a),
NM_001003512.1_3prime500bases320	2.24		2.24	ENSDARG00000031616:zgc:92368 [Source:RefSeq_peptide;Acc:NP_001003512];

NM_182878.1_3prime500bases422		2.24		2.24	ENSDARG00000013443:ATPase, H+ transporting, lysosomal, V1 subunit B, member a [Source:RefSeq_peptide;Acc:NP_878298];
NM_212815.1_3prime500bases352		2.27		2.27	ENSDARG00000026797:v-akt murine thymoma viral oncogene homolog 2, like [Source:RefSeq_peptide;Acc:NP_997980];
NM_212994.1_3prime500bases261		2.41	2.14	2.27	ENSDARESTG00000019878 heterogeneous nuclear ribonucleoprotein K (hnrpk),
NM_130954.1_3prime500bases250	1.61	2.35	2.90	2.29	ENSDARG00000010791:deltaA [Source:RefSeq_peptide;Acc:NP_571029];
NM_173222.1_3prime500bases325		1.89	2.72	2.30	ENSDARG00000043257:creatine kinase, brain [Source:RefSeq_peptide;Acc:NP_775329];
NM_198208.1_3prime500bases109		1.98	2.66	2.32	ENSDARESTG00000005100 transcription factor Dp-2 (tfdp2),
NM_131893.1_3prime500bases348		2.32		2.32	ENSDARESTG00000004657 myeloid ecotropic viral integration 1 (meis1),
NM_198877.1_3prime500bases272		2.30	2.34	2.32	ENSDARG00000042931:muscle-specific beta 1 integrin binding protein 2 [Source:RefSeq_peptide;Acc:NP_942578];
NM_131341.1_3prime500bases304		2.32		2.32	ENSDARESTG00000000876 growth associated protein 43 (gap43),
NM_131613.1_3prime500bases337		2.34		2.34	ENSDARG00000005315:CUG triplet repeat, RNA-binding protein 1 [Source:RefSeq_peptide;Acc:NP_571688];
NM_212761.1_2		2.34		2.34	ENSDARG00000009978:ictacalcin [Source:RefSeq_peptide;Acc:NP_997926];
NM_152955.1_3prime500bases117		1.85	2.84	2.34	ENSDARESTG00000012272 dachshund a (dacha),
NM_131193.1_3prime500bases146		2.37		2.37	eyes absent homolog 1 (eya1),
NM_199217.1_3prime500bases187		2.60	2.21	2.41	four and a half LIM domains (fhl),
NM_001003980.1_3prime500bases380		2.29	2.56	2.43	ENSDARG00000002330:LIM homeobox 8 [Source:RefSeq_peptide;Acc:NP_001003980];
NM_131761.1_3prime500bases338		2.40	2.48	2.44	ENSDARG00000009447:ATP synthase, H+ transporting, mitochondrial F0 complex, subunit c (subunit 9)
NM_131807.1_3prime500bases404		2.45		2.45	ENSDARG00000008434:bcl2-like [Source:RefSeq_peptide;Acc:NP_571882];
NM_182855.1_3prime500bases382		2.57	2.36	2.46	ENSDARG00000040030 transforming growth factor, beta receptor II (tgfbr2),
NM_131360.1_3prime500bases428		2.49		2.49	ENSDARG00000041430:bone morphogenetic protein 2b [Source:RefSeq_peptide;Acc:NP_571435];
NM_131077.1_3prime500bases386		2.52		2.52	ENSDARG00000008796:hairy-related 5 [Source:RefSeq_peptide;Acc:NP_571152];
NM_201496.1_3prime500bases413		2.53		2.53	ENSDARG00000031915:Hypoxia-inducible factor 1 alpha inhibitor (EC 1.14.11.16) (Hypoxia- inducible factor asparagine hydroxylase).
NM_131802.1_3prime500bases421		2.54		2.54	ENSDARG00000011683:HHGP protein [Source:RefSeq_peptide;Acc:NP_955812];
zfp36l1_3prime500bases67		2.83	2.28	2.55	ENSDARG00000016154
NM_201309.1_3prime500bases192		2.31	2.82	2.56	suppressor of fused homolog (Drosophila) (sufu),
NM_131283.1_3prime500bases432		2.61		2.61	ENSDARG00000039228:forkhead box B1.1 [Source:RefSeq_peptide;Acc:NP_571358];
NM_001003982.1_3prime500bases262		2.61		2.61	ENSDARG00000029830:myogenic factor 6 [Source:RefSeq_peptide;Acc:NP_001003982];
BC056835.1_3prime500bases399		2.64		2.64	ENSDARG00000040266 SRY-box containing gene 31,
NM_131759.1_3prime500bases434		2.65		2.65	ENSDARG00000036516:hemoglobin beta embryonic-1 [Source:RefSeq_peptide;Acc:NP_571834];
CF943713.1_3prime500bases61		2.65		2.65	ENSDARG00000003001 CB1077 5- similar to Myosin Vb,
NM_199522.1_3prime500bases430		2.67		2.67	ENSDARG00000034539:ras homolog gene family, member E [Source:RefSeq_peptide;Acc:NP_955816];
DIG0161_670		2.83		2.83	ENSDARG00000017389:hypothetical protein LOC405860 [Source:RefSeq_peptide;Acc:NP_998089];
NM_131461.1_3prime500bases418		2.87		2.87	endothelium-specific receptor tyrosine kinase 2 (tie2),
NM_131682.2_3prime500bases18		2.89		2.89	ENSDARG00000041945:Aminolevulinate, delta-, synthetase 2 (Fragment). [Source:Uniprot/SPTREMBL;Acc:Q5RIZ3];

NM_131679.3_3prime500bases168		2.72	3.25	2.99	ENSDARG00000006640:eomesodermin homolog [Source:RefSeq_peptide;Acc:NP_571754];
NM_131881.1_3prime500bases266		2.83	3.16	3.00	ENSDARG00000002601:iroquois homeobox protein 7 [Source:RefSeq_peptide;Acc:NP_571956];
CA854263.1_3prime500bases122		2.88	3.11	3.00	ENSDARG00000043457:Hypothetical protein (Fragment). [Source:Uniprot/SPTREMBL;Acc:Q5XJ10];
NM_131348.2_3prime500bases39		3.00		3.00	ENSDARG00000014125:friend leukemia integration 1 [Source:RefSeq_peptide;Acc:NP_571423];
NM_130923.1_3prime500bases410		2.44	3.59	3.01	microphthalmia-associated transcription factor a (mitfa),
NM_199276.1_3prime500bases122		2.91	3.21	3.06	ENSDARG00000028462:H1 histone family, member X [Source:RefSeq_peptide;Acc:NP_954970];
NM_199431.1_3prime500bases312		3.01	3.19	3.10	ENSDARG00000041703:ribosome binding protein 1 homolog (dog) [Source:RefSeq_peptide;Acc:NP_955463];
NM_173283.3_3prime500bases165		3.32	2.90	3.11	ENSDARG00000014947:insulin-like growth factor binding protein 1 [Source:RefSeq_peptide;Acc:NP_775390];
NM_198911.1_3prime500bases435		3.22		3.22	ENSDARG00000020235:septin 9 [Source:RefSeq_peptide;Acc:NP_944593];
NM_182940.2_3prime500bases403		2.40	4.13	3.26	ENSDARG00000036515 hemoglobin alpha embryonic-1 (hbae1),
DIG0228_268		3.32		3.32	
NM_201503.1_3prime500bases263		3.92	2.95	3.43	ENSDARG00000012395:matrix metalloproteinase 13 [Source:RefSeq_peptide;Acc:NP_958911];
NM_131323.1_3prime500bases422		3.70	3.31	3.50	ENSDARG00000042291:Homeobox protein Dlx6a (DLX-6). [Source:Uniprot/SWISSPROT;Acc:Q98877];
NM_131204.1_3prime500bases136		3.07	3.99	3.53	ENSDARG00000019949:heat shock protein 47 [Source:RefSeq_peptide;Acc:NP_571279];
NM_214723.1_3prime500bases352		3.55		3.55	ENSDARG00000039007:enolase 3, (beta, muscle) [Source:RefSeq_peptide;Acc:NP_999888];
NM_131262.1_3prime500bases166		4.00	3.38	3.69	ENSDARG00000030110:Myoblast determination protein 1 homolog (Myogenic factor 1). [Source:Uniprot/SWISSPROT;Acc:Q90477];
NM_130970.1_3prime500bases144		4.63	2.79	3.71	ENSDARG00000003971:Insulin gene enhancer protein ISL-2 (Islet-2). [Source:Uniprot/SWISSPROT;Acc:P53406];
NM_180965.3_3prime500bases316		3.63	4.20	3.91	ENSDARESTG00000019581 claudin g (cldng),
NM_131273.1_3prime500bases426		3.93		3.93	ENSDARG00000007641:muscle segment homeobox E [Source:RefSeq_peptide;Acc:NP_571348];
NM_153673.1_3prime500bases417		4.49		4.49	ENSDARG00000008433 unc-45 homolog B (C. elegans) (unc45b),
NM_181735.1_3prime500bases304		5.37	6.62	5.99	ENSDARG00000019659:forkhead box I1 [Source:RefSeq_peptide;Acc:NP_859424];
NM_205569.1_3prime500bases115		4.50	7.58	6.04	ENSDARG00000031683:v-fos FBJ murine osteosarcoma viral oncogene homolog [Source:RefSeq_peptide;Acc:NP_991132];
NM_153666.1_3prime500bases311		6.82	6.58	6.70	ENSDARG00000011785:T-box 24 [Source:RefSeq_peptide;Acc:NP_705952];

Appendix 2

Genes in *rab5a2* morpholino injected embryos that changed more than 3 fold compared to controls at shield stage

Gene Name	Fold Change			Av	Description
NM_131052.1_3prime500bases417		0.07	0.07	0.07	ENSDARG00000006939:T-box transcription factor TBX6 (T-box protein 6).
NM_130933.1_3prime500bases429		0.07		0.07	zic family member 1 (odd-paired homolog, Drosophila) (zic1),
NM_214692.1_3prime500bases406		0.10	0.09	0.09	membrane protein, palmitoylated 1 (mpp1
NM_131110.1_3prime500bases292		0.14	0.15	0.14	ENSDARG00000011166:Carbonic anhydrase (EC 4.2.1.1) (Carbonate dehydratase).
NM_194392.1_3prime500bases194	0.16	0.18	0.15	0.17	ENSDARG00000040216:trophoblast glycoprotein-like [Source:RefSeq_peptide;Acc:NP_919373];
NM_131778.1_3prime500bases132		0.21	0.14	0.17	ENSDARG00000002795:myeloid ecotropic viral integration site 3 [Source:RefSeq_peptide;Acc:NP_571853];
NM_131893.1_3prime500bases348		0.20		0.20	ENSDARESTG00000004657
LTP4		0.20		0.20	
NM_130967.1_3prime500bases278		0.27	0.15	0.21	ENSDARG00000025641:GLI-Kruppel family member GLI2a [Source:RefSeq_peptide;Acc:NP_571042];
NM_001002332.1_3prime500bases404		0.20	0.22	0.21	ENSDARG00000007024:zgc:92414 [Source:RefSeq_peptide;Acc:NP_001002332];
NM_131576.1_3prime500bases2		0.23	0.20	0.21	ENSDARG00000007277:myogenic factor 5 [Source:RefSeq_peptide;Acc:NP_571651];
NM_152980.1_3prime500bases185		0.19	0.26	0.23	ENSDARG00000031855:macrophage stimulating 1 (hepatocyte growth factor-like) [Source:RefSeq_peptide;Acc:NP_694512];
NM_131108.1_3prime500bases390		0.23	0.23	0.23	ENSDARG00000036830:type I cytokeratin, enveloping layer [Source:RefSeq_peptide;Acc:NP_571182];
NM_001007454.1_3prime500bases299		0.23	0.24	0.23	ENSDARG00000027699:zgc:101612 [Source:RefSeq_peptide;Acc:NP_001007455];
NM_131716.1_3prime500bases434		0.23		0.23	ENSDARG00000020708:midkine-related growth factor b [Source:RefSeq_peptide;Acc:NP_571791];
NM_130973.1_3prime500bases361		0.23	0.24	0.24	ENSDARESTG00000005532
NM_131509.1_3prime500bases430		0.24		0.24	keratin 4 (krt4),
NM_173288.1_3prime500bases371		0.16	0.32	0.24	ENSDARG00000040666:mki67 (FHA domain) interacting nucleolar phosphoprotein (human) - like [Source:RefSeq_peptide;Acc:NP_775395];
NM_131109.1_3prime500bases25		0.25		0.25	ENSDARG00000036292:caudal type homeo box transcription factor 4 [Source:RefSeq_peptide;Acc:NP_571184];
NM_131163.1_3prime500bases115		0.30	0.20	0.25	ENSDARG00000039694:Beta-2-microglobulin precursor. [Source:Uniprot/SWISSPROT;Acc:Q04475];
NM_131729.2_3prime500bases151		0.17	0.35	0.26	OTTDARG00000006320:si:dkey-197d18.1:Novel_CDS
NM_131209.1_3prime500bases394		0.24	0.29	0.26	protocadherin 8 (pcdh8),
NM_001001950.1_3prime500bases137		0.27		0.27	ENSDARG00000009849:zic family member 3 heterotaxy 1 (odd-paired homolog, Drosophila) [Source:RefSeq_peptide;Acc:NP_001001950];
NM_201495.1_3prime500bases221		0.24	0.30	0.27	Rab14
NM_201513.1_3prime500bases433		0.27		0.27	ENSDARG00000042539:tyrosine 3-monooxygenase/tryptophan 5-monooxygenase activation protein, theta polypeptide
NM_200659.1_3prime500bases358		0.27		0.27	ENSDARG00000025948:mutL homolog 1, colon cancer, nonpolyposis type 2 [Source:RefSeq_peptide;Acc:NP_956953];
CF673299.1_3prime500bases366		0.30	0.25	0.28	ENSDARESTG00000014248 clone CB926 5- similar to Gem-associated protein 5
NM_212567.1_3prime500bases8		0.28		0.28	ENSDARG00000024204:minichromosome maintenance protein 3 [Source:RefSeq_peptide;Acc:NP_997732];
NM_200111.1_3prime500bases156		0.34	0.23	0.29	ENSDARG00000017748:hypothetical protein LOC378998 [Source:RefSeq_peptide;Acc:NP_956405];
NM_131342.2_3prime500bases296		0.27	0.31	0.29	ENSDARG00000019995:bone morphogenetic protein 4 [Source:RefSeq_peptide;Acc:NP_571417];
NM_001003882.2_3prime500bases425		0.29		0.29	ENSDARG00000008237:seryl-tRNA synthetase [Source:RefSeq_peptide;Acc:NP_001003882];

NM_173261.1_3prime500bases339		0.28	0.32	0.30	ENSDARG00000010948:kinesin family member 11 [Source:RefSeq_peptide;Acc:NP_775368];
NM_131092.1_3prime500bases291		0.29	0.31	0.30	ENSDARG00000035095:one-eyed pinhead [Source:RefSeq_peptide;Acc:NP_571167];
NM_001003875.1_3prime500bases285		0.31	0.30	0.31	ENSDARG00000037931:U1 small nuclear ribonucleoprotein polypeptide A [Source:RefSeq_peptide;Acc:NP_001003875];
DIG0410_1903		0.31		0.31	
NM_183074.1_3prime500bases334		0.31	0.30	0.31	ENSDARG00000042503:ventrally expressed dharma/bozozok antagonist [Source:RefSeq_peptide;Acc:NP_898897];
NM_131320.1_3prime500bases353		0.34	0.28	0.31	ENSDARG00000023188:lymphocyte cytosolic plastin 1 [Source:RefSeq_peptide;Acc:NP_571395];
NM_131482.1_3prime500bases380		0.35	0.28	0.31	ENSDARG00000005645:roundabout homolog 3 [Source:RefSeq_peptide;Acc:NP_571557];
CD808440.1_3prime500bases215		0.31	0.32	0.32	cDNA clone CB473 5
NM_131363.1_3prime500bases153		0.32	0.32	0.32	ENSDARG00000045102:sine oculis homeobox homolog 3b [Source:RefSeq_peptide;Acc:NP_571438];
NM_131128.1_3prime500bases396		0.33		0.33	ENSDARG00000012076:Apolipoprotein A-I precursor (Apo-AI) (ApoA-I). [Source:Uniprot/SWISSPROT;Acc:O42363];
NM_194371.2_3prime500bases155		0.34	0.33	0.33	ENSDARG00000010124:Sp5 transcription factor-like [Source:RefSeq_peptide;Acc:NP_919352];
NM_130955.1_3prime500bases324	0.35	0.35	0.31	0.33	ENSDARESTG00000012353 Delta D
CB923492.1_3prime500bases387		0.36	0.33	0.34	ENSDARG00000004713:hypothetical protein LOC550434 [Source:RefSeq_peptide;Acc:NP_001017739];
NM_001012246.1_3prime500bases23		0.35		0.35	ENSDARG00000035748:fibroblast growth factor 19 [Source:RefSeq_peptide;Acc:NP_001012246];
NM_153660.1_3prime500bases190		0.36	0.34	0.35	ENSDARESTG00000012343
NM_131063.1_3prime500bases24		0.43	0.29	0.36	ENSDARG00000035998:Sonic hedgehog protein precursor (SHH) (VHH-1). [Source:Uniprot/SWISSPROT;Acc:Q92008];
NM_212797.1_3prime500bases426		0.36		0.36	ENSDARG00000019747:3-beta-hydroxysteroid dehydrogenase [Source:RefSeq_peptide;Acc:NP_997962];
AF339031.1_3prime500bases363		0.36	0.36	0.36	ENSDARG00000008487:Hypothetical protein. [Source:Uniprot/SPTREMBL;Acc:Q503T6];
NM_201331.1_3prime500bases423		0.36		0.36	ENSDARG00000012369:retinol dehydrogenase 10 [Source:RefSeq_peptide;Acc:NP_958488];
CF417004.1_3prime500bases377		0.36		0.36	ENSDARG00000036999 clone CB800 5- similar to Zygotic DNA replication factor MCM6b
NM_198876.1_3prime500bases405		0.37		0.37	ENSDARG00000018971:UDP-GlcNAc:betaGal beta-1,3-N-acetylglucosaminyltransferase 5 [Source:RefSeq_peptide;Acc:NP_942577];
CB333812.1_3prime500bases133		0.33	0.42	0.37	CB159 5- similar to Epiplakin
NM_177984.1_3prime500bases24		0.35	0.40	0.37	ENSDARG00000013853:LIM domain only 4 [Source:RefSeq_peptide;Acc:NP_817093];
NM_131690.1_3prime500bases388		0.29	0.48	0.38	ENSDARG00000019856:ATPase, Na+/K+ transporting, alpha 1b polypeptide [Source:RefSeq_peptide;Acc:NP_571765];
NM_194369.1_3prime500bases417		0.38		0.38	ENSDARG00000037563:CD99 antigen-like 2 [Source:RefSeq_peptide;Acc:NP_919350];
NM_131455.1_3prime500bases385		0.43	0.34	0.39	ENSDARG00000014017:Ribonucleoside-diphosphate reductase large subunit ((Ribonucleotide reductase protein R1 class I).
NM_173221.2_3prime500bases432		0.39		0.39	ENSDARG00000013839:aldehyde dehydrogenase 3 family, member D1 [Source:RefSeq_peptide;Acc:NP_775328];
DIG0123_592		0.39		0.39	
NM_131139.1_3prime500bases322		0.36	0.42	0.39	ENSDARG00000041755
NM_131876.2_3prime500bases270		0.45	0.33	0.39	ENSDARG00000025372:anti-dorsalizing morphogenic protein [Source:RefSeq_peptide;Acc:NP_571951];
NM_213103.1_3prime500bases427		0.39		0.39	ENSDARG00000045902:hypothetical protein LOC406376 [Source:RefSeq_peptide;Acc:NP_998268];
CK445313.1_3prime500bases394		0.32	0.47	0.39	ENSDARG00000004017 clone CB1089 5- similar to sperm associated antigen 1
NM_131027.1_3prime500bases413		0.41	0.37	0.39	ENSDARG00000002952:smoothened homolog [Source:RefSeq_peptide;Acc:NP_571102];
NM_131882.2_3prime500bases379		0.43	0.37	0.40	ENSDARG00000022476

BU492951.1_3prime500bases183	0.40		0.40	ENSDARG00000035835:hypothetical protein LOC437013 [Source:RefSeq_peptide;Acc:NP_001002740];
NM_131285.1_3prime500bases429	0.40		0.40	ENSDARG00000045569:forkhead box B1.2 [Source:RefSeq_peptide;Acc:NP_571360];
NM_001001811.1_3prime500bases418	0.40		0.40	ENSDARG00000036440:SRY-box containing gene 3 [Source:RefSeq_peptide;Acc:NP_001001811];
NM_201176.1_3prime500bases372	0.40		0.40	ENSDARG00000017775:similar to ATP synthase, H+ transporting, mitochondrial F0 complex, subunit c (subunit 9) isoform 3
NM_130932.1_3prime500bases430	0.41		0.41	ENSDARG00000006355 creatine kinase, muscle (ckm),
NM_200228.1_3prime500bases99	0.41		0.41	ENSDARG00000013973:peroxisomal biogenesis factor 3 [Source:RefSeq_peptide;Acc:NP_956522];
NM_131557.1_3prime500bases429	0.41		0.41	ENSDARG00000035831:GATA-binding protein 6 [Source:RefSeq_peptide;Acc:NP_571632];
NM_199211.1_3prime500bases380	0.45	0.38	0.41	ENSDARG00000030700:CTP synthase [Source:RefSeq_peptide;Acc:NP_954681];
NM_001007768.1_3prime500bases425	0.42		0.42	ENSDARG00000016864:hypothetical protein LOC493608 [Source:RefSeq_peptide;Acc:NP_001007769];
NM_131414.1_3prime500bases435	0.42		0.42	ENSDARG00000040346
NM_001005390.1_3prime500bases12	0.42	0.44	0.43	ENSDARG00000035329:calpain, small subunit 1 [Source:RefSeq_peptide;Acc:NP_001005390];
NM_131250.2_3prime500bases406	0.43		0.43	ENSDARG00000043643:Homeobox protein OTX1 (ZOTX1). [Source:Uniprot/SWISSPROT;Acc:Q91994];
NM_130946.1_3prime500bases316	0.48	0.39	0.43	ENSDARG00000010355:wnt8-like protein 2 [Source:RefSeq_peptide;Acc:NP_001018637];
NM_174861.2_3prime500bases259	0.42	0.44	0.43	ENSDARG00000019268:gastrulation brain homeobox 1 [Source:RefSeq_peptide;Acc:NP_777286];
NM_131511.1_3prime500bases250	0.42	0.44	0.43	ENSDARG00000014673:frizzled 9 [Source:RefSeq_peptide;Acc:NP_571586];
NM_130918.1_3prime500bases156	0.41	0.45	0.43	ENSDARG00000015116:frizzled homolog 8a [Source:RefSeq_peptide;Acc:NP_571629];
NM_131822.1_3prime500bases414	0.44		0.44	ENSDARG00000035563:nocA related zinc finger 1 [Source:RefSeq_peptide;Acc:NP_571897];
NM_212770.1_3prime500bases190	0.44	0.44	0.44	ENSDARG00000005185:carboxypeptidase N, polypeptide 1 [Source:RefSeq_peptide;Acc:NP_997935];
NM_199545.3_3prime500bases397	0.44		0.44	ENSDARESTG00000009422 glutamate dehydrogenase 1b (glud1b),
NM_131066.1_3prime500bases239	0.39	0.50	0.44	ENSDARG00000044163:snail homolog 1a [Source:RefSeq_peptide;Acc:NP_571141];
NM_001003501.1_3prime500bases284	0.43	0.46	0.44	ENSDARG00000012341:zgc:92451 [Source:RefSeq_peptide;Acc:NP_001003501];
DIG0166_2731	0.44		0.44	ENSDARG00000014323:hypothetical protein LOC436960 [Source:RefSeq_peptide;Acc:NP_001002687];
NM_183072.1_3prime500bases189	0.40	0.49	0.45	ENSDARESTG00000016845 thioredoxin reductase 1 (txnrd1),
NM_213118.1_3prime500bases147	0.49	0.41	0.45	ENSDARG00000014243:SRY-box containing gene 2 [Source:RefSeq_peptide;Acc:NP_998283];
NM_199949.2_3prime500bases413	0.45		0.45	ENSDARG00000044521:eukaryotic translation elongation factor 1 beta 2 [Source:RefSeq_peptide;Acc:NP_956243];
NM_131884.2_3prime500bases139	0.43	0.47	0.45	ENSDARG00000045369:CCAAT/enhancer binding protein beta [Source:RefSeq_peptide;Acc:NP_571959];
NM_130960.1_3prime500bases226	0.43	0.47	0.45	ENSDARG00000019920:lefty1 [Source:RefSeq_peptide;Acc:NP_571035];
NM_198817.1_3prime500bases426	0.42	0.48	0.45	ENSDARESTG00000016981 starmaker (stm)
CF416995.1_3prime500bases416	0.42	0.49	0.46	CB791 5- similar to Cytochrome P450
NM_212612.1_3prime500bases264	0.41	0.51	0.46	DEAD (Asp-Glu-Ala-Asp) box polypeptide 5 (ddx5),
NM_183343.1_3prime500bases271	0.36	0.56	0.46	ENSDARG00000037593:prickle-like 2 [Source:RefSeq_peptide;Acc:NP_899186];
NM_200080.2_3prime500bases345	0.42	0.50	0.46	ENSDARG00000029086:keratin 8 [Source:RefSeq_peptide;Acc:NP_956374];
DIG0408_1690	0.47		0.47	
NM_200297.1_3prime500bases253	0.47		0.47	ENSDARG00000036820:monoglyceride lipase [Source:RefSeq_peptide;Acc:NP_956591];

NM_200703.2_3prime500bases423	0.47		0.47	ENSDARG00000013627 golgi reassembly stacking protein 2 (gorasp2),
NM_131251.1_3prime500bases235	0.46	0.50	0.48	ENSDARG00000011235:Homeobox protein OTX2 (ZOTX2). [Source:Uniprot/SWISSPROT;Acc:Q91981];
NM_199543.1_3prime500bases70	0.51	0.45	0.48	ENSDARG00000025147:Cd63 antigen [Source:RefSeq_peptide;Acc:NP_955837];
NM_205567.1_3prime500bases270	0.48		0.48	ENSDARG00000006603:cysteine and glycine-rich protein 1 [Source:RefSeq_peptide;Acc:NP_991130];
NM_131851.1_3prime500bases133	0.45	0.51	0.48	ENSDARG00000041341:SRY-box containing gene 32 [Source:RefSeq_peptide;Acc:NP_571926];
NM_131637.1_3prime500bases240	0.50	0.47	0.49	ENSDARG00000014047:Claudin-like protein ZF4A22 (Claudin-7). [Source:Uniprot/SWISSPROT;Acc:Q9YH92];
CF416991.1_3prime500bases421	0.49		0.49	OTTDARG00000002123:add1:Novel_CDS
NM_130908.1_3prime500bases107	0.48	0.50	0.49	OTTDARG00000002166:zgc:55628:Novel_CDS
NM_212636.1_3prime500bases290	0.46	0.53	0.49	ENSDARG00000035720
CF673281.1_3prime500bases425	0.47	0.52	0.50	ENSDARESTG00000018874 clone CB967 5- similar to Filamin A,
NM_130934.1_3prime500bases362	0.48	0.52	0.50	ENSDARESTG00000012572 hematopoietically expressed homeobox (hhex),
NM_207048.1_3prime500bases204	0.55	0.46	0.50	ENSDARESTG00000012052
NM_200042.1_3prime500bases0	0.62	0.39	0.50	ENSDARG00000034443:hypothetical protein LOC336959 [Source:RefSeq_peptide;Acc:NP_956336];
CF673300.1_3prime500bases47	0.54	0.47	0.51	ENSDARG00000009569 clone CB882 5- similar to Transcriptional enhancer factor TEF-5
NM_205702.1_3prime500bases229	0.51		0.51	
NM_131146.2_3prime500bases230	0.48	0.53	0.51	ENSDARG00000033999:Cytochrome P450 26A1 (EC 1.14.-.-) (Retinoic acid-metabolizing cytochrome) (P450RAI) (Retinoic acid 4-hydroxylase).
DIG0131_1438	0.51		0.51	ENSDARG00000058538:hypothetical protein LOC323048 [Source:RefSeq_peptide;Acc:NP_997799];
golgb1_3prime500bases306	0.51		0.51	ENSDARESTG00000025521
NM_212602.1_3prime500bases425	0.52		0.52	ENSDARG00000011127:AHA1, activator of heat shock 90kDa protein ATPase homolog 1, like [Source:RefSeq_peptide;Acc:NP_997767];
map3k4_3prime500bases366	0.54	0.51	0.52	ENSDARG00000039153:Hypothetical protein (Fragment). [Source:Uniprot/SPTREMBL;Acc:Q5BJ15];
NM_182855.1_3prime500bases391	0.52		0.52	ENSDARG00000040030
CF673278.1_148	0.52		0.52	ENSDARG00000013040 clone CB964 5- similar to adaptor-related protein complex AP-3, beta 1 subunit,
NM_131207.1_3prime500bases102	0.53	0.51	0.52	ENSDARG00000007944:LIM homeobox 1b [Source:RefSeq_peptide;Acc:NP_571282];
NM_173244.1_3prime500bases425	0.52		0.52	ENSDARG00000024904:TAL1 (SCL) interrupting locus like [Source:RefSeq_peptide;Acc:NP_775351];
NM_131205.1_3prime500bases434	0.52		0.52	ENSDARG00000029079
DIG0144_634	0.53		0.53	ENSDARG00000040543:LOC407680 protein (Fragment). [Source:Uniprot/SPTREMBL;Acc:Q6NW88];
NM_131221.1_3prime500bases428	0.53		0.53	ENSDARG00000015790:ATPase, Na+/K+ transporting, beta 3a polypeptide [Source:RefSeq_peptide;Acc:NP_571296];
NM_173219.1_3prime500bases185	0.47	0.60	0.53	
NM_199433.1_3prime500bases434	0.54		0.54	ENSDARG00000045679:meiosis-specific nuclear structural protein 1 [Source:RefSeq_peptide;Acc:NP_955465];
NM_198824.1_3prime500bases417	0.57	0.51	0.54	ENSDARESTG00000013713
NM_131404.1_3prime500bases5	0.54		0.54	ENSDARG00000042750:Proliferating cell nuclear antigen (PCNA). [Source:Uniprot/SWISSPROT;Acc:Q9PTP1];
NM_131300.1_3prime500bases373	0.55		0.55	ENSDARG00000011956:Homeobox protein Dlx4a (DLX-8). [Source:Uniprot/SWISSPROT;Acc:Q98879];
NM_131079.1_3prime500bases285	0.55	0.55	0.55	ENSDARESTG00000005674
NM_001003774.1_3prime500bases342	0.54	0.56	0.55	ENSDARG00000015123:zgc:101000 [Source:RefSeq_peptide;Acc:NP_001003774];

NM_130943.1_3prime500bases110		0.47	0.63	0.55	ENSDARG00000018383:frizzled-related protein [Source:RefSeq_peptide;Acc:NP_571018];
NM_131112.1_3prime500bases408		0.55		0.55	ENSDARG00000044774:POU domain, class 5, transcription factor 1 (POU domain protein 2). [Source:Uniprot/SWISSPROT;Acc:Q90270];
NM_001007282.1_3prime500bases238		0.55		0.55	glutathione peroxidase 4a (gpx4a),
NM_001012263.1_3prime500bases63		0.55		0.55	ENSDARG00000036126:fibroblast growth factor receptor-like 1b [Source:RefSeq_peptide;Acc:NP_001012263];
BU808676.1_3prime500bases100		0.58	0.53	0.55	ENSDARESTG00000018543 clone CB477 5- similar to Cysteine proteinase
NM_131290.1_3prime500bases274		0.56	0.55	0.55	ENSDARG00000021032:forkhead box D3 [Source:RefSeq_peptide;Acc:NP_571365];
NM_131516.1_3prime500bases368		0.56		0.56	ENSDARG00000002768:Parvalbumin beta. [Source:Uniprot/SWISSPROT;Acc:Q9I8V0];
NM_214731.1_3prime500bases116		0.51	0.60	0.56	ENSDARG00000039675:dapper homolog 1, antagonist of beta-catenin (xenopus) [Source:RefSeq_peptide;Acc:NP_999896];
DIG0345_1024		0.56		0.56	ENSDARG00000040815:hypothetical protein LOC325958 [Source:RefSeq_peptide;Acc:NP_956027];
NM_152953.2_3prime500bases421		0.56		0.56	ENSDARESTG00000017250
NM_201586.1_3prime500bases434		0.56		0.56	
NM_212690.1_3prime500bases326		0.47	0.65	0.56	ENSDARG00000042728:phospholipase A2-activating protein [Source:RefSeq_peptide;Acc:NP_997855];
NM_200059.1_3prime500bases52		0.56		0.56	ENSDARG00000017514:ribosomal protein S3A [Source:RefSeq_peptide;Acc:NP_956353];
NM_001008615.1_3prime500bases182		0.55	0.57	0.56	ENSDARG00000041065:heat shock protein 1 [Source:RefSeq_peptide;Acc:NP_001008615];
NM_131668.3_3prime500bases390		0.56		0.56	ENSDARG00000013144:ATPase, Na+/K+ transporting, beta 1a polypeptide [Source:RefSeq_peptide;Acc:NP_571743];
NM_130937.1_3prime500bases293		0.51	0.63	0.57	ENSDARG00000034894:Wnt-5 protein precursor. [Source:Uniprot/SWISSPROT;Acc:Q92050];
NM_199521.2_3prime500bases181		0.62	0.52	0.57	ENSDARG00000030871:Ubiquitin ligase Siah1 (EC 6.3.2.-) (Seven in absentia homolog 1) (Siah-1). [Source:Uniprot/SWISSPROT;Acc:Q7ZVG6];
NM_131874.1_3prime500bases111		0.54	0.61	0.57	ENSDARG00000035622:X-box binding protein 1 [Source:RefSeq_peptide;Acc:NP_571949];
NM_212777.1_3prime500bases148		0.58		0.58	ENSDARG00000025071:bromodomain containing 8 [Source:RefSeq_peptide;Acc:NP_997942];
NM_131685.1_3prime500bases48		0.58	0.58	0.58	ENSDARG00000018259:ATPase, Na+/K+ transporting, alpha 3b polypeptide [Source:RefSeq_peptide;Acc:NP_571760];
NM_181559.1_3prime500bases48		0.58		0.58	ENSDARG00000039128:glutamine synthetase 1 [Source:RefSeq_peptide;Acc:NP_853537];
NM_200025.1_365		0.58		0.58	ENSDARG00000037071:ribosomal protein S26 [Source:RefSeq_peptide;Acc:NP_956319];
NM_182871.1_3prime500bases170		0.55	0.62	0.58	ENSDARG00000037677:fibroblast growth factor 24 [Source:RefSeq_peptide;Acc:NP_878291];
NM_200583.1_3prime500bases141		0.61	0.56	0.58	ENSDARG00000013475:chaperonin containing TCP1, subunit 4 (delta) [Source:RefSeq_peptide;Acc:NP_956877];
NM_200099.1_3prime500bases116		0.58	0.59	0.59	ENSDARG00000012000:dynein light chain (10.3 kD) (dlc-1) [Source:RefSeq_peptide;Acc:NP_956393];
NM_205585.1_3prime500bases190		0.59		0.59	ENSDARG00000035521:secreted frizzled-related protein 1 [Source:RefSeq_peptide;Acc:NP_991148];
NM_201099.1_3prime500bases418		0.59		0.59	ENSDARG00000035320:similar to heterogeneous nuclear ribonucleoprotein L [Source:RefSeq_peptide;Acc:NP_957393];
NM_131114.1_3prime500bases186		0.59		0.59	ENSDARG00000036141
BU670726.1_3prime500bases263		0.64	0.55	0.59	ENSDARG00000010946:cystathionine-beta-synthase [Source:RefSeq_peptide;Acc:NP_001014367];
NM_131058.1_3prime500bases378		0.59		0.59	ENSDARG00000007329:T-box gene 16 [Source:RefSeq_peptide;Acc:NP_571133];
NM_131417.1_3prime500bases247		0.53	0.65	0.59	OTTDARG00000007314:si:ch211-132p20.4:Novel_CDS
CF673276.1_3prime500bases105		0.56	0.63	0.60	ENSDARESTG00000010586 clone CB960 5- similar to Nucleolar RNA helicase II,
NM_201206.1_3prime500bases257		0.60		0.60	ENSDARG00000011626:COX15 homolog, cytochrome c oxidase assembly protein [Source:RefSeq_peptide;Acc:NP_957500];
BU670702.1_3prime500bases280		0.66	0.54	0.60	ENSDARG00000003509 CB407 5- similar to SPT:Q8UVV4 ATP-binding cassette transporter 1

NM_194388.1_3prime500bases354		0.59	0.61	0.60	ENSDARG00000036700:tubulin, alpha 1 [Source:RefSeq_peptide;Acc:NP_919369];
NM_131287.2_3prime500bases377		0.56	0.64	0.60	ENSDARG00000041345:SRY-box 17 [Source:RefSeq_peptide;Acc:NP_571362];
NM_199536.2_3prime500bases255		0.59	0.61	0.60	ENSDARESTG00000007995
NM_173236.1_3prime500bases247		0.60		0.60	ENSDARG00000015427:histone deacetylase 1 [Source:RefSeq_peptide;Acc:NP_775343];
NM_131415.1_3prime500bases4		0.59	0.61	0.60	ENSDARG00000017354:eph-like receptor tyrosine kinase 6 [Source:RefSeq_peptide;Acc:NP_571490];
NM_201514.1_3prime500bases375		0.56	0.64	0.60	ENSDARG00000037012:solute carrier family 3, member 2 like [Source:RefSeq_peptide;Acc:NP_958922];
NM_131140.1_3prime500bases144		0.61		0.61	
NM_205732.1_3prime500bases414		0.61		0.61	
NM_001007761.1_3prime500bases0		0.61		0.61	ENSDARG00000026759:adaptor-related protein complex 1 mu 1 subunit [Source:RefSeq_peptide;Acc:NP_991277];
NM_199995.1_157		0.61		0.61	
NM_201576.1_3prime500bases131		0.61		0.61	ENSDARG00000034351:transgelin 2 [Source:RefSeq_peptide;Acc:NP_963870];
NM_131245.1_3prime500bases275		0.61	0.61	0.61	
NM_201325.1_3prime500bases341		0.61		0.61	ENSDARG00000021242:major vault protein [Source:RefSeq_peptide;Acc:NP_958482];
NM_130971.1_3prime500bases0		0.62	0.61	0.62	ENSDARG00000037879:Beta-1,3-N-acetylglucosaminyltransferase lunatic fringe (EC 2.4.1.222) (O-fucosylpeptide 3-beta-N-acetylglucosaminyltransferase).
NM_131069.2_3prime500bases167		0.62		0.62	
NM_131860.1_3prime500bases339		0.62		0.62	ENSDARG00000015472:knypek [Source:RefSeq_peptide;Acc:NP_571935];
BC090314.1_3prime500bases19		0.62	0.63	0.62	ENSDARG00000013575:hypothetical protein LOC503590 [Source:RefSeq_peptide;Acc:NP_001013296];
NM_001003890.2_3prime500bases158		0.59	0.66	0.62	ENSDARG00000020869:polo-like kinase 1 [Source:RefSeq_peptide;Acc:NP_001003890];
NM_131116.2_3prime500bases13		0.63		0.63	ENSDARG00000000175:Homeobox protein Hox-B2a (Hox-B2). [Source:Uniprot/SWISSPROT;Acc:O42367];
NM_201475.1_3prime500bases382		0.63		0.63	ENSDARG00000031495:SET translocation (myeloid leukemia-associated) A [Source:RefSeq_peptide;Acc:NP_958883];
NM_131355.1_3prime500bases253		0.63		0.63	ENSDARG00000014943:kinesin family member 23 [Source:RefSeq_peptide;Acc:NP_571430];
NM_001005919.1_3prime500bases364		0.64	0.63	0.64	ENSDARG00000019848:Ephrin type-A receptor 4a (EC 2.7.1.112) (Tyrosine-protein kinase receptor ZEK2) (EPH-like kinase 2) (Fragment).
NM_199430.1_3prime500bases422		0.64		0.64	ENSDARG00000036180:cyclin B2 [Source:RefSeq_peptide;Acc:NP_955462];
NM_201488.1_3prime500bases105		0.64		0.64	ENSDARG00000020468:protein phosphatase 1G (formerly 2C), magnesium-dependent, gamma isoform [Source:RefSeq_peptide;Acc:NP_958896];
NM_194377.2_3prime500bases431		0.64		0.64	ENSDARG00000011665:aldolase a, fructose-bisphosphate [Source:RefSeq_peptide;Acc:NP_919358];
DIG0407_1918		0.64		0.64	ENSDARG00000038547:Semaphorin-4E precursor (Semaphorin-7) (Semaphorin Z7) (Sema-Z7). [Source:Uniprot/SWISSPROT;Acc:Q9YHX4];
NM_152949.1_3prime500bases275		0.62	0.66	0.64	ENSDARESTG00000006863
AY216588.1_3prime500bases143		0.64		0.64	ENSDARG00000023220:Selenoprotein T2 (Fragment). [Source:Uniprot/SPTREMBL;Acc:Q802G4];
BC075970.1_3prime500bases424		0.64		0.64	ENSDARG00000006427:Intestinal fatty acid-binding protein. [Source:Uniprot/SPTREMBL;Acc:Q8AX65];
NM_200076.1_3prime500bases137		0.65		0.65	ENSDARG00000034396:methionine-tRNA synthetase [Source:RefSeq_peptide;Acc:NP_956370];
NM_201491.1_3prime500bases432		0.65		0.65	ENSDARG00000042853:isovaleryl Coenzyme A dehydrogenase [Source:RefSeq_peptide;Acc:NP_958899];
NM_212603.1_3prime500bases94		0.65		0.65	ENSDARG00000023330:acidic (leucine-rich) nuclear phosphoprotein 32 family, member B [Source:RefSeq_peptide;Acc:NP_997768];
AB097826.1_3prime500bases19		0.65		0.65	ENSDARG00000002403:Hypothetical protein YF-9 (Fragment). [Source:Uniprot/SPTREMBL;Acc:Q7T2W2];
BM402093.1_3		0.65		0.65	ENSDARG00000037980:Hypothetical protein (Fragment). [Source:Uniprot/SPTREMBL;Acc:Q7SYJ8];

NM_001002312.1_3prime500bases360	0.66	0.64	0.65	ENSDARG00000041870:intraflagellar transport 172 [Source:RefSeq_peptide;Acc:NP_001002312];
NM_200458.2_3prime500bases36	0.65		0.65	ENSDARG00000003016:eukaryotic translation elongation factor 2, like [Source:RefSeq_peptide;Acc:NP_956752];
NM_201153.1_3prime500bases426	0.65		0.65	ENSDARG00000046119:ribosomal protein S3 [Source:RefSeq_peptide;Acc:NP_957447];
DIG0366_880	0.66		0.66	
CF569085.1_3prime500bases370	0.66		0.66	ENSDARG00000020386 CB939 5- similar to ATP-binding cassette transporter 1,
NM_001009884.1_3prime500bases206	0.66		0.66	ENSDARG00000041895:carbamoyl-phosphate synthetase 2, aspartate transcarbamylase, and dihydroorotase [Source:RefSeq_peptide;Acc:NP_001009884];
NM_200772.1_3prime500bases421	0.66		0.66	ENSDARG00000007880
NM_194423.1_3prime500bases225	0.66		0.66	ENSDARG00000029370:ankyrin repeat domain 6 [Source:RefSeq_peptide;Acc:NP_919404];
NM_198914.2_3prime500bases225	0.24	1.74	0.99	ENSDARG00000033170:sulfotransferase family, cytosolic sulfotransferase 2 [Source:RefSeq_peptide;Acc:NP_944596];
NM_130945.1_3prime500bases213	1.50		1.50	ENSDARG00000015717:fms-related tyrosine kinase 4 [Source:RefSeq_peptide;Acc:NP_571020];
NM_200103.1_3prime500bases358	1.50		1.50	ENSDARG00000005254:KDEL (Lys-Asp-Glu-Leu) endoplasmic reticulum protein retention receptor 2 [Source:RefSeq_peptide;Acc:NP_956397];
NM_201499.1_3prime500bases421	1.51		1.51	ENSDARG00000025375:isocitrate dehydrogenase 1 (NADP+), soluble [Source:RefSeq_peptide;Acc:NP_958907];
NM_001004494.1_3prime500bases331	1.52		1.52	ENSDARG00000010511:protein regulator of cytokinesis 1 (prc1), mRNA [Source:RefSeq_dna;Acc:NM_001004494];
NM_131684.2_3prime500bases122	1.52		1.52	ENSDARG00000036815:ATPase, Na+/K+ transporting, alpha 3a polypeptide [Source:RefSeq_peptide;Acc:NP_571759];
NM_205716.1_3prime500bases20	1.53		1.53	ENSDARG00000029911:cancer susceptibility candidate 3 [Source:RefSeq_peptide;Acc:NP_991279];
DIG0311_361	1.53		1.53	
NM_001007774.1_3prime500bases195	1.51	1.57	1.54	ENSDARG00000043631:BCAS2 protein homolog. [Source:Uniprot/SWISSPROT;Acc:Q5RKQ0];
NM_201292.1_3prime500bases426	1.54		1.54	ENSDARG00000029928:adaptor-related protein complex 3, mu 1 subunit [Source:RefSeq_peptide;Acc:NP_958449];
NM_194418.1_3prime500bases329	1.54		1.54	ENSDARG00000038227:selenoprotein W, 2b (sepw2b), mRNA [Source:RefSeq_dna;Acc:NM_194418];
NM_131105.2_3prime500bases297	1.56		1.56	
NM_201178.1_3prime500bases401	1.56		1.56	ENSDARG00000014577:Rhophilin 2 (GTP-Rho binding protein 2). [Source:Uniprot/SWISSPROT;Acc:Q6TNR1];
NM_199218.1_3prime500bases428	1.56		1.56	ENSDARESTG00000008073
NM_200318.2_3prime500bases431	1.56		1.56	ENSDARG00000035948:ADP-ribosylation factor-like 4 [Source:RefSeq_peptide;Acc:NP_956612];
NM_200078.1_3prime500bases197	1.56	1.57	1.56	ENSDARG00000028514:Cbp/p300-interacting transactivator, with Glu/Asp-rich carboxy-terminal domain, 2 [Source:RefSeq_peptide;Acc:NP_956372];
NM_198811.1_3prime500bases372	1.57		1.57	
cos2.fas_3prime500bases156	1.58	1.56	1.57	ENSDARG00000033099:kinesin family member 7 [Source:RefSeq_peptide;Acc:NP_001014816];
NM_131047.1_3prime500bases235	1.57		1.57	ENSDARG00000043276:calreticulin [Source:RefSeq_peptide;Acc:NP_571122];
NM_212676.1_3prime500bases153	1.58		1.58	ENSDARG00000042533
NM_131100.1_3prime500bases400	1.58		1.58	ENSDARG00000042769:orthopedia protein [Source:RefSeq_peptide;Acc:NP_571175];
BU670740.1_3prime500bases139	1.59		1.59	ENSDARG00000035052 CB457 5- similar to SPT:Q96S59 Q96s59 RanBPM
NM_214759.1_3prime500bases129	1.59		1.59	ENSDARG00000039150:hypothetical protein LOC406625 [Source:RefSeq_peptide;Acc:NP_999924];
NM_198978.1_3prime500bases380	1.59		1.59	ENSDARESTG00000016872
NM_199432.1_3prime500bases65	1.57	1.62	1.59	ENSDARG00000039168:hypothetical protein LOC368331 [Source:RefSeq_peptide;Acc:NP_955464];
NM_181663.1_3prime500bases94	1.60		1.60	ENSDARG00000022987:sizzled [Source:RefSeq_peptide;Acc:NP_858049];

NM_131233.1_3prime500bases410		1.60		1.60	
NM_199533.1_3prime500bases407		1.60		1.60	ENSDARG00000008867:RAS related protein 1b [Source:RefSeq_peptide;Acc:NP_955827];
CF569098.1_3prime500bases382		1.60		1.60	ENSDARG00000004169 clone CB959 5- similar to Stathmin
BU808703.1_3prime500bases5		1.60		1.60	CB516 5- similar to C-ets-1 protein, mRNA sequence
NM_212801.1_3prime500bases323		1.60		1.60	ENSDARG00000039211:hypothetical protein LOC378987 [Source:RefSeq_peptide;Acc:NP_997966];
NM_200081.1_3prime500bases230		1.71	1.51	1.61	ENSDARG00000032802:kinectin 1 [Source:RefSeq_peptide;Acc:NP_956375];
NM_212648.1_3prime500bases409		1.61		1.61	ENSDARG00000012936:dishevelled 2, dsh homolog [Source:RefSeq_peptide;Acc:NP_997813];
NM_131613.1_3prime500bases161		1.57	1.66	1.62	ENSDARG00000005315:CUG triplet repeat, RNA-binding protein 1 [Source:RefSeq_peptide;Acc:NP_571688];
NM_198871.1_3prime500bases153		1.62		1.62	
BM402137.1_3prime500bases375		1.63		1.63	ENSDARESTG00000017103 CB193 5- similar to PROSTAGLANDINE D SYNTHASE,
NM_131759.1_3prime500bases434		1.63		1.63	ENSDARG00000036516:hemoglobin beta embryonic-1 [Source:RefSeq_peptide;Acc:NP_571834];
NM_212795.1_3prime500bases117		1.51	1.75	1.63	ENSDARG00000022813:Dead end protein 1. [Source:Uniprot/SWISSPROT;Acc:Q7T1H5];
NM_212572.1_3prime500bases190		1.63		1.63	ENSDARG00000037846:histocompatibility 13 [Source:RefSeq_peptide;Acc:NP_997737];
NM_131282.1_3prime500bases360		1.59	1.69	1.64	ENSDARG00000036385:forkhead box A sequence [Source:RefSeq_peptide;Acc:NP_571357];
NM_130923.1_3prime500bases410		1.51	1.77	1.64	microphthalmia-associated transcription factor a (mitfa),
NM_131227.1_3prime500bases133		1.58	1.70	1.64	ENSDARG00000043071:Retinal homeobox protein Rx3. [Source:Uniprot/SWISSPROT;Acc:O42358];
NM_212608.1_3prime500bases359		1.76	1.53	1.65	ENSDARG00000017422:bscv (C20orf3) homolog [Source:RefSeq_peptide;Acc:NP_997773];
NM_199212.1_3prime500bases100		1.63	1.67	1.65	ENSDARG00000025522:serum/glucocorticoid regulated kinase [Source:RefSeq_peptide;Acc:NP_954682];
NM_200110.1_3prime500bases107		1.65	1.65	1.65	ENSDARG00000042152:nudix-type motif 4 [Source:RefSeq_peptide;Acc:NP_956404];
NM_213348.2_3prime500bases384		1.65		1.65	
NM_212748.1_3prime500bases192		1.81	1.53	1.67	
NM_194401.1_3prime500bases291		1.55	1.79	1.67	ENSDARG00000002131:CUG triplet repeat, RNA binding protein 2 [Source:RefSeq_peptide;Acc:NP_919382];
NM_212664.1_3prime500bases341		1.67		1.67	ENSDARG00000040004
NM_131246.1_3prime500bases227		1.78	1.56	1.67	ENSDARG00000040856:L-lactate dehydrogenase A chain (EC 1.1.1.27) (LDH-A). [Source:Uniprot/SWISSPROT;Acc:Q9PVK5];
NM_131775.1_3prime500bases4		1.67		1.67	ENSDARG00000004251:dihydrofolate reductase [Source:RefSeq_peptide;Acc:NP_571850];
NM_131247.1_3prime500bases423		1.68		1.68	ENSDARG00000035139
NM_198805.1_3prime500bases186		1.58	1.79	1.68	ENSDARG00000018174:guanine nucleotide binding protein (G protein), alpha inhibiting activity polypeptide a [Source:RefSeq_peptide;Acc:NP_942100];
CF924899.2_42		1.69		1.69	ENSDARG00000040469:hypothetical protein LOC541400 [Source:RefSeq_peptide;Acc:NP_001013545];
NM_001007351.1_3prime500bases48		1.69		1.69	ENSDARG00000043495:hypothetical protein LOC492479 [Source:RefSeq_peptide;Acc:NP_001007352];
NM_201465.2_3prime500bases195		1.69		1.69	ENSDARG00000020103:calreticulin like [Source:RefSeq_peptide;Acc:NP_958873];
NM_201454.1_3prime500bases258		1.60	1.79	1.69	ENSDARG00000020261:RAB2, member RAS oncogene family [Source:RefSeq_peptide;Acc:NP_958862];
NM_131664.1_3prime500bases224		1.57	1.82	1.70	ENSDARESTG00000014726
NM_130954.1_3prime500bases259		1.70		1.70	ENSDARG00000010791:deltaA [Source:RefSeq_peptide;Acc:NP_571029];
NM_130922.1_3prime500bases109		1.76	1.65	1.70	ENSDARG00000020298:B-cell translocation gene 2 [Source:RefSeq_peptide;Acc:NP_570997];

NM_131802.1_3prime500bases421	1.71		1.71	ENSDARG00000011683:HHGP protein [Source:RefSeq_peptide;Acc:NP_955812];
NM_198980.1_3prime500bases80	1.73		1.73	ENSDARG00000004311:low density lipoprotein receptor adaptor protein 1 [Source:RefSeq_peptide;Acc:NP_945331];
NM_200075.1_3prime500bases326	1.73		1.73	ENSDARG00000007665:Similar to RIKEN cDNA 1500019G21 gene [Source:RefSeq_peptide;Acc:NP_956369];
NM_130939.1_3prime500bases418	1.74		1.74	cth1 (cth1),
NM_205728.1_3prime500bases429	1.74		1.74	ENSDARG00000040316:GLI-Kruppel family member GLI3 [Source:RefSeq_peptide;Acc:NP_991291];
AJ245493.1_3prime500bases233	1.79	1.71	1.75	hypothetical protein clone sd70
ZfKif3a_3prime500bases159	1.90	1.61	1.76	
DIG0206_970 DIG0124_1096	1.68	1.84	1.76	ENSDARG00000006604:Poliovirus receptor-related protein 3 precursor. [Source:Uniprot/SWISSPROT;Acc:Q58EG3];
NM_199683.1_3prime500bases383	1.77		1.77	ENSDARG00000041607:Eukaryotic translation initiation factor 4E-1A binding protein (eIF4E- 1A binding protein) (4E-BP).
NM_198810.1_3prime500bases236	1.80	1.74	1.77	
DIG0351_1132	1.77		1.77	
NM_201299.1_3prime500bases275	1.82	1.72	1.77	ENSDARG00000025904:glycoprotein, synaptic 2 [Source:RefSeq_peptide;Acc:NP_958456];
NM_001007120.1_3prime500bases305	1.87	1.67	1.77	ENSDARG00000034731:homeodomain leucine zipper [Source:RefSeq_peptide;Acc:NP_001007121];
BQ826572.1_3prime500bases187	1.79		1.79	cDNA clone CB349 5- similar to Complement component C7, mRNA sequence
NM_212790.1_3prime500bases415	1.79		1.79	ENSDARG00000016424:yippee-like 3 [Source:RefSeq_peptide;Acc:NP_997955];
NM_001001725.1_3prime500bases42	1.79		1.79	ENSDAREST G00000002678 intraflagellar transport 88 homolog (ift88),
NM_173222.1_3prime500bases325	1.72	1.86	1.79	ENSDARG00000043257:creatine kinase, brain [Source:RefSeq_peptide;Acc:NP_775329];
CF417021.1_3prime500bases292	1.54	2.06	1.80	ENSDAREST G00000021028 CB817 5- similar to ZO-1 MDCK
NM_201577.1_3prime500bases427	1.80		1.80	ENSDARG00000005675
NM_131184.2_3prime500bases100	1.51	2.09	1.80	ENSDARG00000028148
NM_153674.1_3prime500bases325	1.81		1.81	ENSDARG00000027397:vang-like 2 (van gogh, Drosophila) (vangl2), mRNA [Source:RefSeq_dna;Acc:NM_153674];
NM_214808.1_3prime500bases249	2.00	1.61	1.81	ENSDARG00000023520:Fibroblast growth factor-17b precursor (FGF-17b). [Source:Uniprot/SWISSPROT;Acc:Q6SJP8];
NM_199481.1_3prime500bases292	1.83	1.80	1.82	ENSDARG00000037742:cyclin G1 (ccng1), mRNA [Source:RefSeq_dna;Acc:NM_199481];
NM_131848.1_3prime500bases424	1.82		1.82	ENSDARG00000004729:transcription factor binding to IGHM enhancer 3a [Source:RefSeq_peptide;Acc:NP_571923];
NM_001003980.1_3prime500bases380	1.83		1.83	ENSDARG00000002330:LIM homeobox 8 [Source:RefSeq_peptide;Acc:NP_001003980];
BM402118.1_3prime500bases243	1.79	1.87	1.83	ENSDARG00000014499:hypothetical protein LOC445204 [Source:RefSeq_peptide;Acc:NP_001003598];
CF416980.1_3prime500bases316	1.92	1.74	1.83	ENSDARG00000042428 5- similar to Glutathione S-transferase 1
CF417024.1_1	1.83		1.83	ENSDARG00000024746:Novel protein similar to heat shock protein 90-alpha (Hsp90a).ENSDARG00000010478:Heat shock protein HSP 90-alpha.
NM_130948.1_3prime500bases351	1.83		1.83	ENSDARG00000037995:DVR-1 protein precursor. [Source:Uniprot/SWISSPROT;Acc:P35621];
NM_131271.1_3prime500bases267	1.84		1.84	ENSDARG00000043147:forkhead box D1 [Source:RefSeq_peptide;Acc:NP_571346];
NM_131360.1_3prime500bases428	1.84		1.84	ENSDARG00000041430:bone morphogenetic protein 2b [Source:RefSeq_peptide;Acc:NP_571435];
NM_201461.1_3prime500bases414	1.77	1.92	1.84	ENSDARG00000029072:Kruppel-like factor 6 [Source:RefSeq_peptide;Acc:NP_958869];
NM_181766.1_3prime500bases400	1.85		1.85	ENSDARG00000002632
DIG0203_403	1.85		1.85	

NM_131348.2_3prime500bases108		1.65	2.10	1.87	ENSDARG00000014125:friend leukemia integration 1 [Source:RefSeq_peptide;Acc:NP_571423];
NM_199976.1_3prime500bases342		1.85	1.90	1.87	ENSDARG00000042644:manganese-containing superoxide dismutase precursor [Source:RefSeq_peptide;Acc:NP_956270];
Rab23_3prime500bases355		1.71	2.04	1.87	ENSDARG00000004151:hypothetical protein LOC553778 [Source:RefSeq_peptide;Acc:NP_001018579];
NM_200086.1_3prime500bases368		1.88		1.88	ENSDARG00000014351;ENSDARG00000035957:geminin, DNA replication inhibitor [Source:RefSeq_peptide;Acc:NP_956380];
NM_131219.1_3prime500bases62		1.88		1.88	ENSDARG00000038386:achaete-scute complex-like 1a [Source:RefSeq_peptide;Acc:NP_571294];
NM_198877.1_3prime500bases272		1.87	1.90	1.88	ENSDARG00000042931:muscle-specific beta 1 integrin binding protein 2 [Source:RefSeq_peptide;Acc:NP_942578];
NM_131765.1_3prime500bases258		1.98	1.81	1.89	ENSDARG00000043128:claudin e [Source:RefSeq_peptide;Acc:NP_571840];
DIG0118_859		1.90		1.90	ENSDARG00000018065:Iglon2 [Source:RefSeq_peptide;Acc:NP_001003852];
NM_130940.1_3prime500bases425		1.89	1.93	1.91	ENSDARG00000009737:bonnie and clyde [Source:RefSeq_peptide;Acc:NP_571015];
DIG0557_1492		1.91		1.91	
NM_201213.1_3prime500bases388		1.74	2.10	1.92	ENSDARG00000010316:glutaminyl-tRNA synthetase [Source:RefSeq_peptide;Acc:NP_957507];
AY576808.1_3prime500bases157		2.10	1.74	1.92	ENSDARG00000023532:pin2/trf1-interacting protein 1 [Source:RefSeq_peptide;Acc:NP_001013283];
NM_131641.1_3prime500bases408		1.93		1.93	ENSDARESTG00000016274
CF924885.1_3prime500bases240		2.03	1.84	1.93	ENSDARESTG00000025399 clone CB1014 5- similar to Q8wux2 Similar to RIKEN cDNA 2510006C20 gene
NM_152948.1_3prime500bases351		1.88	1.99	1.93	ENSDARG00000043658:coxsackie virus and adenovirus receptor [Source:RefSeq_peptide;Acc:NP_694480];
NM_199278.1_3prime500bases252		1.80	2.10	1.95	ENSDARESTG00000024671
DIG0046_445		1.95		1.95	ENSDARG00000010025:hypothetical protein LOC553218 [Source:RefSeq_peptide;Acc:NP_001020643];
NM_182940.2_3prime500bases403		2.12	1.80	1.96	ENSDARG00000036515
NM_212994.1_3prime500bases261		1.81	2.14	1.97	ENSDARESTG00000019878
NM_131362.1_3prime500bases419		2.00		2.00	ENSDARG00000039772:sine oculis homeobox homolog 3a [Source:RefSeq_peptide;Acc:NP_571437];
NM_212791.1_3prime500bases423		2.01		2.01	ENSDARG00000039429:adenosine kinase a (adka), mRNA [Source:RefSeq_dna;Acc:NM_212791];
NM_212761.1_2		2.01		2.01	ENSDARG00000009978:ictacalcin [Source:RefSeq_peptide;Acc:NP_997926];
NM_201468.1_3prime500bases429		2.04		2.04	ENSDARG00000003920:SET translocation (myeloid leukemia-associated) B [Source:RefSeq_peptide;Acc:NP_958876];
NM_001008581.1_3prime500bases149		1.83	2.26	2.05	ENSDARG00000040046:hypothetical protein LOC494038 [Source:RefSeq_peptide;Acc:NP_001008581];
NM_153668.3_3prime500bases276		2.25	1.84	2.05	ENSDARESTG00000010313
NM_201317.1_3prime500bases349		2.11	1.99	2.05	ENSDARG00000037773:RING1 and YY1 binding protein [Source:RefSeq_peptide;Acc:NP_958474];
NM_131229.1_3prime500bases431		2.06		2.06	ENSDARG00000005541:Wnt inhibitory factor 1 precursor (WIF-1). [Source:Uniprot/SWISSPROT;Acc:Q9W6F9];
NC_002333.2_3prime500bases20		1.84	2.28	2.06	Danio rerio mitochondrion, complete genome
NM_131267.1_3prime500bases432		2.07		2.07	ENSDARG00000036097:iroquois homeobox protein 3a [Source:RefSeq_peptide;Acc:NP_571342];
NM_131117.2_3prime500bases3		2.18	1.97	2.07	ENSDARG00000029263:Homeobox protein Hox-B3a (Hox-B3). [Source:Uniprot/SWISSPROT;Acc:O42368];
NM_200295.1_3prime500bases100		2.15	2.05	2.10	ENSDARG00000007279:golgi membrane protein SB140 [Source:RefSeq_peptide;Acc:NP_956589];
NM_194374.1_3prime500bases181		1.66	2.53	2.10	ENSDARG00000041217:exportin 6 [Source:RefSeq_peptide;Acc:NP_919355];
NM_001007364.1_3prime500bases393		2.21	2.02	2.12	ENSDARESTG00000011774 zgc:103652 (zgc:103652),
NM_131262.1_3prime500bases166		1.78	2.45	2.12	ENSDARG00000030110:Myoblast determination protein 1 homolog (Myogenic factor 1). [Source:Uniprot/SWISSPROT;Acc:Q90477];

NM_131875.1_3prime500bases0	2.14		2.14	
NM_131503.1_3prime500bases104	1.80	2.48	2.14	ENSDARG00000026534:Axin-1 (Axis inhibition protein 1). [Source:Uniprot/SWISSPROT;Acc:P57094];
NM_131311.1_3prime500bases274	2.16	2.16	2.16	ENSDARG00000014446:Homeobox protein Dlx2a (DLX-2). [Source:Uniprot/SWISSPROT;Acc:P50574];
NM_200159.1_3prime500bases279	2.17		2.17	ENSDARG00000008238:mannosidase, beta A, lysosomal [Source:RefSeq_peptide;Acc:NP_956453];
NM_201493.1_3prime500bases125	2.23		2.23	ENSDARG00000036291:nucleobindin 2a [Source:RefSeq_peptide;Acc:NP_958901];
NM_201329.1_3prime500bases116	1.65	2.83	2.24	ENSDARG00000034771:RAB13, member RAS oncogene family [Source:RefSeq_peptide;Acc:NP_958486];
NM_201496.1_3prime500bases203	2.19	2.34	2.26	ENSDARG00000031915:Hypoxia-inducible factor 1 alpha inhibitor (EC 1.14.11.16) (Hypoxia- inducible factor asparagine hydroxylase).
NM_200882.1_3prime500bases377	2.13	2.40	2.27	ENSDARG00000021140:poly A binding protein, cytoplasmic 1 a [Source:RefSeq_peptide;Acc:NP_957176];
NM_212815.1_3prime500bases352	2.27		2.27	ENSDARG00000026797:v-akt murine thymoma viral oncogene homolog 2, like [Source:RefSeq_peptide;Acc:NP_997980];
NM_214734.1_3prime500bases256	2.28		2.28	ENSDARG00000033971:paired mesoderm homeobox 1a [Source:RefSeq_peptide;Acc:NP_999899];
NM_001001402.1_3prime500bases397	2.57	2.01	2.29	ENSDARG00000043042:ectodermal-neural cortex (with BTB-like domain) [Source:RefSeq_peptide;Acc:NP_001001402];
NM_178297.2_3prime500bases120	1.56	3.02	2.29	ENSDARESTG00000020068
NM_001001399.1_3prime500bases370	2.30	2.29	2.29	ENSDARG00000005230:signal sequence receptor, beta [Source:RefSeq_peptide;Acc:NP_001001399];
NM_182878.1_3prime500bases422	2.32		2.32	ENSDARG00000013443:ATPase, H+ transporting, lysosomal, V1 subunit B, member a [Source:RefSeq_peptide;Acc:NP_878298];
CA854263.1_3prime500bases122	2.32	2.34	2.33	ENSDARG00000043457:Hypothetical protein (Fragment). [Source:Uniprot/SPTREMBL;Acc:Q5XJ10];
NM_001007038.1_3prime500bases269	2.42	2.29	2.35	ENSDARG00000044593:ATP-binding cassette, sub-family C (CFTR/MRP), member 4 (abcc4), mRNA [Source:RefSeq_dna;Acc:NM_001007038];
NM_213172.1_3prime500bases365	2.40	2.31	2.35	ENSDARG00000017602:cyclin G2 [Source:RefSeq_peptide;Acc:NP_998337];
NM_130947.1_3prime500bases310	2.36		2.36	ENSDARG00000040836:Wnt-4a protein precursor. [Source:Uniprot/SWISSPROT;Acc:P47793];
NM_199217.1_3prime500bases187	2.32	2.40	2.36	
DIG0565_1528	2.38		2.38	ENSDARG00000037493:hypothetical protein LOC553785 [Source:RefSeq_peptide;Acc:NP_001018583];
NM_001004578.1_3prime500bases336	2.38	2.37	2.38	ENSDARG00000014793:zgc:92331 [Source:RefSeq_peptide;Acc:NP_001004578];
NM_205750.1_3prime500bases420	2.41		2.41	ENSDARG00000004305:vang-like 1 (van gogh, Drosophila) [Source:RefSeq_peptide;Acc:NP_991313];
NM_131807.1_3prime500bases404	2.42		2.42	ENSDARG00000008434:bcl2-like [Source:RefSeq_peptide;Acc:NP_571882];
NM_213153.1_3prime500bases424	2.42		2.42	ENSDARG00000005464:deoxyribonuclease I-like 3 [Source:RefSeq_peptide;Acc:NP_998318];
NM_131077.1_3prime500bases386	2.42		2.42	ENSDARG00000008796:hairy-related 5 [Source:RefSeq_peptide;Acc:NP_571152];
NM_131120.1_3prime500bases395	2.44		2.44	ENSDARG00000014115:Homeobox protein Hox-B8a (Hox-B8). [Source:Uniprot/SWISSPROT;Acc:Q8AWZ0];
NM_131305.1_3prime500bases415	2.44		2.44	ENSDARG00000013125:Homeobox protein Dlx1a (DLX-1). [Source:Uniprot/SWISSPROT;Acc:Q98875];
NM_131881.1_3prime500bases266	2.46	2.43	2.44	ENSDARG00000002601:iroquois homeobox protein 7 [Source:RefSeq_peptide;Acc:NP_571956];
NM_201332.1_3prime500bases424	2.45		2.45	OTTDARG00000005626:si:ch211-150c22.4:Novel_CDS
NM_201587.1_3prime500bases206	2.14	2.78	2.46	
NM_199538.1_3prime500bases295	2.32	2.64	2.48	ENSDARG00000033768:hypothetical protein LOC321203 [Source:RefSeq_peptide;Acc:NP_955832];
NM_001002720.1_3prime500bases146	2.58	2.42	2.50	ENSDARG00000014013:lamin B receptor [Source:RefSeq_peptide;Acc:NP_001002720];
NM_199532.1_3prime500bases125	2.35	2.69	2.52	ENSDARG00000004402:ELOVL family member 6, elongation of long chain fatty acids [Source:RefSeq_peptide;Acc:NP_955826];
NM_213151.1_3prime500bases351	2.75	2.33	2.54	ENSDARG00000027860:glyoxalase 1 [Source:RefSeq_peptide;Acc:NP_998316];

DIG0387_631		2.54		2.54	
NM_199277.2_3prime500bases279		2.54		2.54	ENSDARESTG00000024128
NM_200106.1_3prime500bases20		2.58		2.58	ENSDARG00000012135:F-box and leucine-rich repeat protein 2 [Source:RefSeq_peptide;Acc:NP_956400];
NM_131682.2_3prime500bases18		2.73	2.54	2.63	ENSDARG00000041945:Aminolevulinate, delta-, synthetase 2 (Fragment). [Source:Uniprot/SPTREMBL;Acc:Q5RIZ3];
NM_131670.1_3prime500bases344		2.64		2.64	ENSDARG00000042837:ATPase, Na+/K+ transporting, beta 3b polypeptide [Source:RefSeq_peptide;Acc:NP_571745];
NM_131450.2_3prime500bases260		2.83	2.52	2.68	ENSDARG00000020711:Ribonucleoside-diphosphate reductase M2 chain (EC 1.17.4.1) (Ribonucleotide reductase protein R2 class I).
NM_131506.1_3prime500bases351		2.68		2.68	ENSDARG00000005150:T-box 20 [Source:RefSeq_peptide;Acc:NP_571581];
NM_131323.1_3prime500bases422		2.05	3.41	2.73	ENSDARG00000042291:Homeobox protein Dlx6a (DLX-6). [Source:Uniprot/SWISSPROT;Acc:Q98877];
NM_131679.3_3prime500bases168		2.07	3.47	2.77	ENSDARG00000006640:eomesodermin homolog [Source:RefSeq_peptide;Acc:NP_571754];
NM_131461.1_3prime500bases418		2.79		2.79	
NM_130958.1_3prime500bases293	1.64	3.44	3.38	2.82	ENSDARG00000004232:deltaB [Source:RefSeq_peptide;Acc:NP_571033];
NM_153669.2_3prime500bases139		2.39	3.46	2.92	ENSDARG00000019137:translocating chain-associating membrane protein [Source:RefSeq_peptide;Acc:NP_705955];
NM_152956.1_3prime500bases377		3.26	2.62	2.94	ENSDARG00000034785:dachshund b [Source:RefSeq_peptide;Acc:NP_694488];
NM_173283.3_3prime500bases165		2.25	3.76	3.01	ENSDARG00000014947:insulin-like growth factor binding protein 1 [Source:RefSeq_peptide;Acc:NP_775390];
NM_130975.1_3prime500bases429		3.04		3.04	ENSDARG00000036192:Paired-like homeodomain transcription factor 2a. [Source:Uniprot/SPTREMBL;Acc:Q568C4];
NM_198911.1_3prime500bases435		3.05		3.05	ENSDARG00000020235:septin 9 [Source:RefSeq_peptide;Acc:NP_944593];
NM_182884.1_3prime500bases422		3.16	2.98	3.07	ENSDARG00000025302:DIX domain containing 1 [Source:RefSeq_peptide;Acc:NP_878304];
NM_001007371.1_3prime500bases41		3.21	2.93	3.07	ENSDARG00000032640:zgc:101900 (zgc:101900), mRNA [Source:RefSeq_dna;Acc:NM_001007371];
NM_131863.1_3prime500bases281		3.09		3.09	
NM_153673.1_3prime500bases417		3.26	2.94	3.10	ENSDARG00000008433
NM_213556.3_3prime500bases194		3.01	3.19	3.10	ENSDARG00000036470:jun B proto-oncogene [Source:RefSeq_peptide;Acc:NP_998721];
zfp36l1_3prime500bases67		3.30	2.95	3.12	ENSDARG00000016154
NM_200551.1_3prime500bases42		3.68	2.61	3.15	ENSDARG00000020143:phenylalanine hydroxylase [Source:RefSeq_peptide;Acc:NP_956845];
NM_173224.1_3prime500bases147		2.96	3.34	3.15	ENSDARG00000033412:Epididymal secretory protein E1 precursor (Niemann Pick type C2 protein homolog) (16.5 kDa secretory protein).
NM_201326.2_3prime500bases287		2.71	3.61	3.16	ENSDARG00000037516
NM_131306.1_3prime500bases355		3.31	3.07	3.19	ENSDARG00000042296:Homeobox protein Dlx5a (DLX-4). [Source:Uniprot/SWISSPROT;Acc:P50576];
NM_212763.1_3prime500bases351 DIG0174_373	1.92	4.13	3.79	3.28	ENSDARG00000027345:epithelial V-like antigen 1 [Source:RefSeq_peptide;Acc:NP_997928];
NM_199276.1_3prime500bases122		3.81	2.90	3.36	ENSDARG00000028462:H1 histone family, member X [Source:RefSeq_peptide;Acc:NP_954970];
NM_200105.1_3prime500bases210		3.13	3.59	3.36	ENSDARG00000026862:fused toes homolog [Source:RefSeq_peptide;Acc:NP_956399];
NM_183071.1_3prime500bases384		3.55	3.24	3.39	ENSDARG00000040344:linker histone H1M [Source:RefSeq_peptide;Acc:NP_898894];
NM_199519.2_3prime500bases22		2.76	4.04	3.40	
NM_212796.1_3prime500bases231		3.60	3.23	3.41	ENSDARESTG00000020670
NM_131687.1_3prime500bases424		3.43		3.43	ENSDARG00000007739:ATPase, Na+/K+ transporting, alpha 1a.2 polypeptide [Source:RefSeq_peptide;Acc:NP_571762];
NM_178298.2_3prime500bases266		3.78	3.08	3.43	ENSDARESTG00000011008

NM_199522.1_3prime500bases430		3.50		3.50	ENSDARG00000034539:ras homolog gene family, member E [Source:RefSeq_peptide;Acc:NP_955816];
NM_001004602.1_3prime500bases143		3.28	3.73	3.50	zgc:86701 (zgc:86701),
NM_200109.1_3prime500bases196		3.42	3.61	3.52	ENSDARG00000039527
NM_181331.3_3prime500bases55		3.64		3.64	ENSDARG00000043483:orthodenticle homolog 5 [Source:RefSeq_peptide;Acc:NP_851848];
NM_130970.1_3prime500bases144		4.44	3.30	3.87	ENSDARG00000003971:Insulin gene enhancer protein ISL-2 (Islet-2). [Source:Uniprot/SWISSPROT;Acc:P53406];
NM_214723.1_3prime500bases352		3.89		3.89	ENSDARG00000039007:enolase 3, (beta, muscle) [Source:RefSeq_peptide;Acc:NP_999888];
NM_131537.2_3prime500bases375		3.91		3.91	ENSDARG00000005395:Homeobox protein Hox-B5b (Hox-B5-like) (Zf-54). [Source:Uniprot/SWISSPROT;Acc:P09013];
NM_201309.1_3prime500bases192		4.17	3.98	4.08	
NM_153666.1_3prime500bases311		4.07	4.36	4.22	ENSDARG00000011785:T-box 24 [Source:RefSeq_peptide;Acc:NP_705952];
NM_199431.1_3prime500bases312		4.87	3.88	4.37	ENSDARG00000041703:ribosome binding protein 1 homolog (dog) [Source:RefSeq_peptide;Acc:NP_955463];
NM_152955.1_3prime500bases423		4.95		4.95	ENSDARESTG00000012272
NM_181735.1_3prime500bases304		3.84	6.44	5.14	ENSDARG00000019659:forkhead box I1 [Source:RefSeq_peptide;Acc:NP_859424];
NM_213241.1_3prime500bases265		5.37		5.37	ENSDARG00000011870:sp8 transcription factor [Source:RefSeq_peptide;Acc:NP_998406];
NM_205569.1_3prime500bases115		5.08	6.20	5.64	ENSDARG00000031683:v-fos FBJ murine osteosarcoma viral oncogene homolog [Source:RefSeq_peptide;Acc:NP_991132];
NM_212654.1_3prime500bases404		5.96	5.77	5.86	ENSDARG00000035986:protein tyrosine phosphatase, non-receptor type 2, like [Source:RefSeq_peptide;Acc:NP_997819];
NM_201316.1_3prime500bases415		5.98		5.98	ENSDARG00000035913:tyrosyl-tRNA synthetase [Source:RefSeq_peptide;Acc:NP_958473];
NM_131283.1_3prime500bases432		6.46		6.46	ENSDARG00000039228:forkhead box B1.1 [Source:RefSeq_peptide;Acc:NP_571358];
NM_173218.1_3prime500bases208		3.26	10.85	7.06	ENSDARG00000008937:neogenin 1 [Source:RefSeq_peptide;Acc:NP_775325];
NM_131571.1_3prime500bases149		7.37		7.37	ENSDARG00000036096:MAD homolog 3 [Source:RefSeq_peptide;Acc:NP_571646];
NM_180965.3_3prime500bases316		8.37	9.43	8.90	ENSDARESTG00000019581
NM_131101.2_3prime500bases423		11.89		11.89	

References

Aanstad, P. and Whitaker, M. (1999). Predictability of dorso-ventral asymmetry in the cleavage stage zebrafish embryo: an analysis using lithium sensitivity as a dorso-ventral marker. *Mech Dev* **88**, 33-41.

Aligianis, I. A., Johnson, C. A., Gissen, P., Chen, D., Hampshire, D., Hoffmann, K., Maina, E. N., Morgan, N. V., Tee, L., Morton, J. et al. (2005). Mutations of the catalytic subunit of RAB3GAP cause Warburg Micro syndrome. *Nat Genet* **37**, 221-3.

Aligianis, I. A., Morgan, N. V., Mione, M., Johnson, C. A., Rosser, E., Hennekam, R. C., Adams, G., Trembath, R. C., Pilz, D. T., Stoodley, N. et al. (2006). Mutation in Rab3 GTPase-activating protein (RAB3GAP) noncatalytic subunit in a kindred with Martsolf syndrome. *Am J Hum Genet* **78**, 702-7.

Allan, B. B., Moyer, B. D. and Balch, W. E. (2000). Rab1 recruitment of p115 into a cis-SNARE complex: programming budding COPII vesicles for fusion. *Science* **289**, 444-8.

Alvarez, C., Garcia-Mata, R., Brandon, E. and Sztul, E. (2003). COPI recruitment is modulated by a Rab1b-dependent mechanism. *Mol Biol Cell* **14**, 2116-27.

Amatruda, J. F. and Zon, L. I. (1999). Dissecting hematopoiesis and disease using the zebrafish. *Dev Biol* **216**, 1-15.

Amaya, E., Stein, P. A., Musci, T. J. and Kirschner, M. W. (1993). FGF signalling in the early specification of mesoderm in Xenopus. *Development* **118**, 477-87.

Anant, J. S., Desnoyers, L., Machius, M., Demeler, B., Hansen, J. C., Westover, K. D., Deisenhofer, J. and Seabra, M. C. (1998). Mechanism of Rab geranylgeranylation: formation of the catalytic ternary complex. *Biochemistry* **37**, 12559-68.

Anders, R. A., Dore, J. J., Jr., Arline, S. L., Garamszegi, N. and Leof, E. B. (1998). Differential requirement for type I and type II transforming growth factor beta receptor kinase activity in ligand-mediated receptor endocytosis. *J Biol Chem* **273**, 23118-25.

Armstrong, J. (2000). How do Rab proteins function in membrane traffic? *The International Journal of Biochemistry and Cell Biology.* **32**, 303-307.

Ayala, J., Olofsson, B., Touchot, N., Zahraoui, A., Tavitian, A. and Prochiantz, A. (1989). Developmental and regional expression of three new members of the ras-gene family in the mouse brain. *J Neurosci Res* **22**, 384-9.

Babb, S. G. and Marrs, J. A. (2004). E-cadherin regulates cell movements and tissue formation in early zebrafish embryos. *Dev Dyn* **230**, 263-77.

Bafico, A., Liu, G., Yaniv, A., Gazit, A. and Aaronson, S. A. (2001). Novel mechanism of Wnt signalling inhibition mediated by Dickkopf-1 interaction with LRP6/Arrow. *Nat Cell Biol* **3**, 683-6.

Bahadoran, P., Aberdam, E., Mantoux, F., Busca, R., Bille, K., Yalman, N., de Saint-Basile, G., Casaroli-Marano, R., Ortonne, J. P. and Ballotti, R. (2001). Rab27a: A key to melanosome transport in human melanocytes. *J Cell Biol* **152**, 843-50.

Batista, A., Millan, J., Mittelbrunn, M., Sanchez-Madrid, F. and Alonso, M. A. (2004). Recruitment of transferrin receptor to immunological synapse in response to TCR engagement. *J Immunol* **172**, 6709-14.

Bauer, H., Lele, Z., Rauch, G. J., Geisler, R. and Hammerschmidt, M. (2001). The type I serine/threonine kinase receptor Alk8/Lost-a-fin is required for Bmp2b/7 signal transduction during dorsoventral patterning of the zebrafish embryo. *Development* **128**, 849-58.

Beard, M., Satoh, A., Shorter, J., and Warren, G. (2005). A Cryptic Rab1-binding Site in the p115 Tethering Protein. *J. Biol. Chem.* **280**: 25840-25848.

Behra, M., Cousin, X., Bertrand, C., Vonesch, J. L., Biellmann, D., Chatonnet, A. and Strahle, U. (2002). Acetylcholinesterase is required for neuronal and muscular development in the zebrafish embryo. *Nat Neurosci* **5**, 111-8.

Bejsovec, A. and Wieschaus, E. (1995). Signaling activities of the Drosophila wingless gene are separately mutable and appear to be transduced at the cell surface. *Genetics* **139**, 309-20.

Belenkaya, T. Y., Han, C., Yan, D., Opoka, R. J., Khodoun, M., Liu, H. and Lin, X. (2004). Drosophila Dpp morphogen movement is independent of dynamin-mediated endocytosis but regulated by the glypican members of heparan sulfate proteoglycans. *Cell* **119**, 231-44.

Bellipanni, G., Varga, M., Maegawa, S., Imai, Y., Kelly, C., Myers, A. P., Chu, F., Talbot, W. S. and Weinberg, E. S. (2006). Essential and opposing roles of zebrafish beta-catenins in the formation of dorsal axial structures and neurectoderm. *Development* **133**, 1299-309.

Bellot, F., Crumley, G., Kaplow, J. M., Schlessinger, J., Jaye, M. and Dionne, C. A. (1991). Ligand-induced transphosphorylation between different FGF receptors. *Embo J* **10**, 2849-54.

Benli, M., Doring, F., Robinson, D. G., Yang, X. and Gallwitz, D. (1996). Two GTPase isoforms, Ypt31p and Ypt32p, are essential for Golgi function in yeast. *Embo J* **15**, 6460-75.

Bennett, M. K., Calakos, N. and Scheller, R. H. (1992). Syntaxin: a synaptic protein implicated in docking of synaptic vesicles at presynaptic active zones. *Science* **257**, 255-9.

Bernards, A. and Settleman, J. (2004). GAP control: regulating the regulators of small GTPases. *Trends Cell Biol* **14**, 377-85.

Betchaku, T. and Trinkaus, J. P. (1986). Programmed endocytosis during epiboly of Fundulus heteroclitus. *Am. Zool* **26**, 193-199.

Bischof, J. and Driever, W. (2004). Regulation of hhex expression in the yolk syncytial layer, the potential Nieuwkoop center homolog in zebrafish. *Dev Biol* **276**, 552-62.

Bishop, A. L. and Hall, A. (2000). Rho GTPases and their effector proteins. *Biochem J* **348 Pt 2**, 241-55.

Bjornson, C. R., Griffin, K. J., Farr, G. H., 3rd, Terashima, A., Himeda, C., Kikuchi, Y. and Kimelman, D. (2005). Eomesodermin is a localized maternal determinant required for endoderm induction in zebrafish. *Dev Cell* **9**, 523-33.

Blader, P., Rastegar, S., Fischer, N. and Strahle, U. (1997). Cleavage of the BMP-4 antagonist chordin by zebrafish tolloid. *Science* **278**, 1937-40.

Blitzer, J. T. and Nusse, R. (2006). A critical role for endocytosis in Wnt signaling. *BMC Cell Biol* **7**, 28.

Bronner-Fraser, M., Wolf, J. J. and Murray, B. A. (1992). Effects of antibodies against N-cadherin and N-CAM on the cranial neural crest and neural tube. *Dev Biol* **153**, 291-301.

Brott, B. K. and Sokol, S. Y. (2002). Regulation of Wnt/LRP signaling by distinct domains of Dickkopf proteins. *Mol Cell Biol* **22**, 6100-10.

Bruce, A. E., Howley, C., Zhou, Y., Vickers, S. L., Silver, L. M., King, M. L. and Ho, R. K. (2003). The maternally expressed zebrafish T-box gene eomesodermin regulates organizer formation. *Development* **130**, 5503-17.

Brymora, A., Valova, V. A., Larsen, M. R., Roufogalis, B. D. and Robinson, P. J. (2001). The brain exocyst complex interacts with RalA in a GTP-dependent manner: identification of a novel mammalian Sec3 gene and a second Sec15 gene. *J Biol Chem* **276**, 29792-7.

Bucci, C., Lutcke, A., Steele-Mortimer, O., Olkkonen, V., Dupree, P., Chiariello, M., Bruni, C., Simons, K. and Zerial, M. (1995). Co-operaive regulation of endocytosis by three RAB5 isoforms. *FEBS Letters* **366**, 65-71.

Bucci, C., Parton, R. G., Mather, I. H., Stunnenberg, H., Simons, K., Hoflack, B. and Zerial, M. (1992). The small GTPase rab5 functions as a regulatory factor in the early endocytic pathway. *Cell* **70**, 715-28.

Bush, J., Franek, K., Daniel, J., Spiegelman, G. B., Weeks, G. and Cardelli, J. (1993). Cloning and characterization of five novel Dictyostelium discoideum rab-related genes. *Gene* **136**, 55-60.

Buznikov, G. A. and Ignat'Eva, G. M. (1958). [Hatching enzymes.]. *Usp Sovrem Biol* **46**, 337-56.

Campos, I. (2004). Genes Controlling Development: Roles for Rabs and Glis. In *Anatomy*, (ed., pp. 209. London: National Institute for Medical Research and University Collage London.

Camus, C., Hermann-Le Denmat, S. and Jacquet, M. (1995). Identification of guanine exchange factor key residues involved in exchange activity and Ras interaction. *Oncogene* **11**, 951-9.

Cao, X. and Barlowe, C. (2000). Asymmetric requirements for a Rab GTPase and SNARE proteins in fusion of COPII vesicles with acceptor membranes. *J Cell Biol* **149**, 55-66.

Casey, P. J. and Seabra, M. C. (1996). Protein prenyltransferases. *J Biol Chem* **271**, 5289-92.

Chandrasekhar, A., Warren, J. T., Jr., Takahashi, K., Schauerte, H. E., van Eeden, F. J., Haffter, P. and Kuwada, J. Y. (1998). Role of sonic hedgehog in branchiomotor neuron induction in zebrafish. *Mech Dev* **76**, 101-15.

Chavrier, P., Parton, R. G., Hauri, H. P., Simons, K. and Zerial, M. (1990). Localization of low molecular weight GTP binding proteins to exocytic and endocytic compartments. *Cell* **62**, 317-29.

Chavrier, P., Simons, K. and Zerial, M. (1992). The complexity of the Rab and Rho GTP-binding protein subfamilies revealed by a PCR cloning approach. *Gene* **112**, 261-4.

Chen, S. and Kimelman, D. (2000). The role of the yolk syncytial layer in germ layer patterning in zebrafish. *Development* **127**, 4681-9.

Chen, Y. and Scheller, R. (2001). SNARE-Mediated Membrane Fusion. *Nature Reviews Molecular Cell Biology* **2**, 98-106.

Chen, Y. and Schier, A. F. (2001). The zebrafish Nodal signal Squint functions as a morphogen. *Nature* **411**, 607-610.

Chen, Y. and Struhl, G. (1996). Dual roles for patched in sequestering and transducing Hedgehog. *Cell* **87**, 553-63.

Cheney, R. E. and Rodriguez, O. C. (2001). Cell biology. A switch to release the motor. *Science* **293**, 1263-4.

Cheng, J. C., Miller, A. L. and Webb, S. E. (2004). Organization and function of microfilaments during late epiboly in zebrafish embryos. *Dev Dyn* **231**, 313-23.

Chiariello, M., Bruni, B. and Bucci, C. (1999). The small GTPases Rab5a, Rab5b and Rab5c are differentially phosphorylated in vitro. *FEBA Letters* **453**, 20-24.
Child, C. M. (1915). Individuality in Organisms.
Child, C. M. (1941). Patterns and Problems of Development.
Christoforidis, S., McBride, H. M., Burgoyne, R. D. and Zerial, M. (1999a). The Rab5 effector EEA1 is a core component of endosome docking. *Nature* **397**, 621-5.
Christoforidis, S., Miaczynska, M., Ashman, K., Wilm, M., Zhao, L., Yip, S. C., Waterfield, M. D., Backer, J. M. and Zerial, M. (1999b). Phosphatidylinositol-3-OH kinases are Rab5 effectors. *Nat Cell Biol* **1**, 249-52.
Christoforidis, S. and Zerial, M. (2000). Purification and identification of novel Rab effectors using affinity chromatography. *Methods* **20**, 403-10.
Ciardiello, F., Dono, R., Kim, N., Persico, M. G. and Salomon, D. S. (1991). Expression of cripto, a novel gene of the epidermal growth factor gene family, leads to in vitro transformation of a normal mouse mammary epithelial cell line. *Cancer Res* **51**, 1051-4.
Clements, D., Friday, R. V. and Woodland, H. R. (1999). Mode of action of VegT in mesoderm and endoderm formation. *Development* **126**, 4903-11.
Clements, D. and Woodland, H. R. (2003). VegT induces endoderm by a self-limiting mechanism and by changing the competence of cells to respond to TGF-beta signals. *Dev Biol* **258**, 454-63.
Colicelli, J. (2004). Human RAS superfamily proteins and related GTPases. *Sci STKE* **2004**, RE13.
Cong, F., Schweizer, L. and Varmus, H. (2004). Wnt signals across the plasma membrane to activate the beta-catenin pathway by forming oligomers containing its receptors, Frizzled and LRP. *Development* **131**, 5103-15.
Connors, S. A., Trout, J., Ekker, M. and Mullins, M. C. (1999). The role of tolloid/mini fin in dorsoventral pattern formation of the zebrafish embryo. *Development* **126**, 3119-30.
Cooper, A. A., Gitler, A. D., Cashikar, A., Haynes, C. M., Hill, K. J., Bhullar, B., Liu, K., Xu, K., Strathearn, K. E., Liu, F. et al. (2006). Alpha-synuclein blocks ER-Golgi traffic and Rab1 rescues neuron loss in Parkinson's models. *Science* **313**, 324-8.
Costa, M. C., Mani, F., Santoro, W., Jr., Espreafico, E. M. and Larson, R. E. (1999). Brain myosin-V, a calmodulin-carrying myosin, binds to calmodulin-dependent protein kinase II and activates its kinase activity. *J Biol Chem* **274**, 15811-9.
Coutinho, P., Parsons, M. J., Thomas, K. A., Hirst, E. M., Saude, L., Campos, I., Williams, P. H. and Stemple, D. L. (2004). Differential requirements for COPI transport during vertebrate early development. *Dev Cell* **7**, 547-58.
Couve-Privat, S., Le Bret, M., Traiffort, E., Queille, S., Coulombe, J., Bouadjar, B., Avril, M. F., Ruat, M., Sarasin, A. and Daya-Grosjean, L. (2004). Functional analysis of novel sonic hedgehog gene mutations identified in Basal cell carcinomas from xeroderma pigmentosum patients. *Cancer Res* **64**, 3559-65.
Cremers, F. P., Molloy, C. M., van de Pol, D. J., van den Hurk, J. A., Bach, I., Geurts van Kessel, A. H. and Ropers, H. H. (1992). An autosomal homologue of the choroideremia gene colocalizes with the Usher syndrome type II locus on the distal part of chromosome 1q. *Hum Mol Genet* **1**, 71-5.
Cui, W. W., Low, S. E., Hirata, H., Saint-Amant, L., Geisler, R., Hume, R. I. and Kuwada, J. Y. (2005). The zebrafish shocked gene encodes a glycine

transporter and is essential for the function of early neural circuits in the CNS. *J Neurosci* **25**, 6610-20.
Curtis, L. M. and Gluck, S. (2005). Distribution of Rab GTPases in mouse kidney and comparison with vacuolar H+-ATPase. *Nephron Physiol* **100**, p31-42.
Daggett, D. F., Boyd, C. A., Gautier, P., Bryson-Richardson, R. J., Thisse, C., Thisse, B., Amacher, S. L. and Currie, P. D. (2004). Developmentally restricted actin-regulatory molecules control morphogenetic cell movements in the zebrafish gastrula. *Curr Biol* **14**, 1632-8.
de Larco, J. E. and Todaro, G. J. (1978). Growth factors from murine sarcoma virus-transformed cells. *Proc Natl Acad Sci U S A* **75**, 4001-5.
Denef, N., Neubuser, D., Perez, L. and Cohen, S. M. (2000). Hedgehog induces opposite changes in turnover and subcellular localization of patched and smoothened. *Cell* **102**, 521-31.
Derynck, R. and Miyazono, K. (2006). The TGF-β Family.
Dick, A., Hild, M., Bauer, H., Imai, Y., Maifeld, H., Schier, A. F., Talbot, W. S., Bouwmeester, T. and Hammerschmidt, M. (2000). Essential role of Bmp7 (snailhouse) and its prodomain in dorsoventral patterning of the zebrafish embryo. *Development* **127**, 343-54.
Dougan, S. T., Warga, R. M., Kane, D. A., Schier, A. F. and Talbot, W. S. (2003). The role of the zebrafish nodal-related genes squint and cyclops in patterning of mesendoderm. *Development* **130**, 1837-51.
Draper, B. W., Morcos, P. A. and Kimmel, C. B. (2001). Inhibition of zebrafish fgf8 pre-mRNA splicing with morpholino oligos: a quantifiable method for gene knockdown. *Genesis* **30**, 154-6.
Draper, B. W., Stock, D. W. and Kimmel, C. B. (2003). Zebrafish fgf24 functions with fgf8 to promote posterior mesodermal development. *Development* **130**, 4639-54.
Dubois, L., Lecourtois, M., Alexandre, C., Hirst, E. and Vincent, J. P. (2001). Regulated endocytic routing modulates wingless signaling in Drosophila embryos. *Cell* **105**, 613-24.
Dumas, J. J., Zhu, Z., Connolly, J. L. and Lambright, D. G. (1999). Structural basis of activation and GTP hydrolysis in Rab proteins. *Structure* **7**, 413-23.
Dutton, K. A., Pauliny, A., Lopes, S. S., Elworthy, S., Carney, T. J., Rauch, J., Geisler, R., Haffter, P. and Kelsh, R. N. (2001). Zebrafish colourless encodes sox10 and specifies non-ectomesenchymal neural crest fates. *Development* **128**, 4113-25.
Ebisawa, T., Fukuchi, M., Murakami, G., Chiba, T., Tanaka, K., Imamura, T. and Miyazono, K. (2001). Smurf1 interacts with transforming growth factor-beta type I receptor through Smad7 and induces receptor degradation. *J Biol Chem* **276**, 12477-80.
Echard, A., Jollivet, F., Martinez, O., Lacapere, J. J., Rousselet, A., Janoueix-Lerosey, I. and Goud, B. (1998). Interaction of a Golgi-associated kinesin-like protein with Rab6. *Science* **279**, 580-5.
Echard, A., Opdam, F. J., de Leeuw, H. J., Jollivet, F., Savelkoul, P., Hendriks, W., Voorberg, J., Goud, B. and Fransen, J. A. (2000). Alternative splicing of the human Rab6A gene generates two close but functionally different isoforms. *Mol Biol Cell* **11**, 3819-33.
Eggenschwiler, J., Espinoza and Anderson, K. (2001). Rab23 is an essential negative regulator of the mouse Sonic hedgehog signalling pathway. *Nature* **412**, 194 - 198.

Eggenschwiler, J. T. and Anderson, K. V. (2000). Dorsal and lateral fates in the mouse neural tube require the cell-autonomous activity of the open brain gene. *Dev Biol* **227**, 648-60.

Eggenschwiler, J. T., Bulgakov, O. V., Qin, J., Li, T. and Anderson, K. V. (2006). Mouse Rab23 regulates hedgehog signaling from smoothened to Gli proteins. *Dev Biol* **290**, 1-12.

Eisen, J. S. and Weston, J. A. (1993). Development of the neural crest in the zebrafish. *Dev Biol* **159**, 50-9.

Eldar, A., Dorfman, R., Weiss, D., Ashe, H., Shilo, B. Z. and Barkai, N. (2002). Robustness of the BMP morphogen gradient in Drosophila embryonic patterning. *Nature* **419**, 304-8.

Elde, N. C., Morgan, G., Winey, M., Sperling, L. and Turkewitz, A. P. (2005). Elucidation of clathrin-mediated endocytosis in tetrahymena reveals an evolutionarily convergent recruitment of dynamin. *PLoS Genet* **1**, e52.

Entchev, E. V. and Gonzalez-Gaitan, M. A. (2002). Morphogen gradient formation and vesicular trafficking. *Traffic* **3**, 98-109.

Entchev, E. V., Schwabedissen, A. and Gonzalez-Gaitan, M. (2000). Gradient formation of the TGF-beta homolog Dpp. *Cell* **103**, 981-91.

Erter, C. E., Wilm, T. P., Basler, N., Wright, C. V. and Solnica-Krezel, L. (2001). Wnt8 is required in lateral mesendodermal precursors for neural posteriorization in vivo. *Development* **128**, 3571-83.

Essner, J. J., Amack, J. D., Nyholm, M. K., Harris, E. B. and Yost, H. J. (2005). Kupffer's vesicle is a ciliated organ of asymmetry in the zebrafish embryo that initiates left-right development of the brain, heart and gut. *Development* **132**, 1247-60.

Evans, T. M., Ferguson, C., Wainwright, B. J., Parton, R. G. and Wicking, C. (2003). Rab23, a negative regulator of hedgehog signaling, localizes to the plasma membrane and the endocytic pathway. *Traffic* **4**, 869-84.

Fainsod, A., Deissler, K., Yelin, R., Marom, K., Epstein, M., Pillemer, G., Steinbeisser, H. and Blum, M. (1997). The dorsalizing and neural inducing gene follistatin is an antagonist of BMP-4. *Mech Dev* **63**, 39-50.

Fekany, K., Yamanaka, Y., Leung, T., Sirotkin, H. I., Topczewski, J., Gates, M. A., Hibi, M., Renucci, A., Stemple, D., Radbill, A. et al. (1999). The zebrafish bozozok locus encodes Dharma, a homeodomain protein essential for induction of gastrula organizer and dorsoanterior embryonic structures. *Development* **126**, 1427-38.

Feldman, B., Gates, M., Egan, E., Dougan, S., Rennebeck, G., Sirotkin, H., Schier, A. and Talbot, W. (1998). Zebrafish organizer development and germ-layer formation require nodal-related signals. *Nature* **395**, 181-185.

Finger, F. P., Hughes, T. E. and Novick, P. (1998). Sec3p is a spatial landmark for polarized secretion in budding yeast. *Cell* **92**, 559-71.

Fischer von Mollard, G., Mignery, G. A., Baumert, M., Perin, M. S., Hanson, T. J., Burger, P. M., Jahn, R. and Sudhof, T. C. (1990). rab3 is a small GTP-binding protein exclusively localized to synaptic vesicles. *Proc Natl Acad Sci U S A* **87**, 1988-92.

Fischer von Mollard, G., Stahl, B., Khokhlatchev, A., Sudhof, T. and R, J. (1994). Rab3C is a synaptic vesicle protein that dissociates from synaptic vesicles after stimulation of exocytosis. *J. Biol. Chem.* **269**, 10971-10974.

Fujii, R., Yamashita, S., Hibi, M. and Hirano, T. (2000). Asymmetric p38 activation in zebrafish: its possible role in symmetric and synchronous cleavage. *J Cell Biol* **150**, 1335-48.

Fujimoto, L. M., Roth, R., Heuser, J. E. and Schmid, S. L. (2000). Actin assembly plays a variable, but not obligatory role in receptor-mediated endocytosis in mammalian cells. *Traffic* **1**, 161-71.

Furthauer, M., Van Celst, J., Thisse, C. and Thisse, B. (2004). Fgf signalling controls the dorsoventral patterning of the zebrafish embryo. *Development* **131**, 2853-64.

Gallwitz, D., Donath, C. and Sander, C. (1983). A yeast gene encoding a protein homologous to the human c-has/bas proto-oncogene product. *Nature* **306**, 704-7.

Gardiner, M. R., Daggett, D. F., Zon, L. I. and Perkins, A. C. (2005). Zebrafish KLF4 is essential for anterior mesendoderm/pre-polster differentiation and hatching. *Dev Dyn* **234**, 992-6.

Garrett, M. D., Kabcenell, A. K., Zahner, J. E., Kaibuchi, K., Sasaki, T., Takai, Y., Cheney, C. M. and Novick, P. J. (1993). Interaction of Sec4 with GDI proteins from bovine brain, Drosophila melanogaster and Saccharomyces cerevisiae. Conservation of GDI membrane dissociation activity. *FEBS Lett* **331**, 233-8.

Gelbart, W. M. (1989). The decapentaplegic gene: a TGF-beta homologue controlling pattern formation in Drosophila. *Development* **107 Suppl**, 65-74.

Geng, X., Xiao, L., Lin, G. F., Hu, R., Wang, J. H., Rupp, R. A. and Ding, X. (2003). Lef/Tcf-dependent Wnt/beta-catenin signaling during Xenopus axis specification. *FEBS Lett* **547**, 1-6.

Geppert, M., Goda, Y., Stevens, C. F. and Sudhof, T. C. (1997). The small GTP-binding protein Rab3A regulates a late step in synaptic vesicle fusion. *Nature* **387**, 810-4.

Geyer, M., Schweins, T., Herrmann, C., Prisner, T., Wittinghofer, A. and Kalbitzer, H. R. (1996). Conformational transitions in p21ras and in its complexes with the effector protein Raf-RBD and the GTPase activating protein GAP. *Biochemistry* **35**, 10308-20.

Gibbs, D., Azarian, S. M., Lillo, C., Kitamoto, J., Klomp, A. E., Steel, K. P., Libby, R. T. and Williams, D. S. (2004). Role of myosin VIIa and Rab27a in the motility and localization of RPE melanosomes. *J Cell Sci* **117**, 6473-83.

Gilbert, S. F. (1997). CHAPTER 3 :: "REDISCOVERY" OF THE MORPHOGENETIC FIELD :: THE "RE-DISCOVERY" OF MORPHOGENIC FIELDS. In *Developmental Biology (DevBio.com)*, (ed.

Gimlich, R. L. and Gerhart, J. C. (1984). Early cellular interactions promote embryonic axis formation in Xenopus laevis. *Dev Biol* **104**, 117-30.

Goering, L. M., Hoshijima, K., Hug, B., Bisgrove, B., Kispert, A. and Grunwald, D. J. (2003). An interacting network of T-box genes directs gene expression and fate in the zebrafish mesoderm. *Proc Natl Acad Sci U S A* **100**, 9410-5.

Gonzalez-Gaitan, M., Capdevila, M. P. and Garcia-Bellido, A. (1994). Cell proliferation patterns in the wing imaginal disc of Drosophila. *Mech Dev* **46**, 183-200.

Gonzalez-Sancho, J. M., Aguilera, O., Garcia, J. M., Pendas-Franco, N., Pena, C., Cal, S., Garcia de Herreros, A., Bonilla, F. and Munoz, A. (2005). The Wnt antagonist DICKKOPF-1 gene is a downstream target of beta-catenin/TCF and is downregulated in human colon cancer. *Oncogene* **24**, 1098-103.

Gonzalez, F., Swales, L., Bejsovec, A., Skaer, H. and Martinez Arias, A. (1991). Secretion and movement of wingless protein in the epidermis of the Drosophila embryo. *Mech Dev* **35**, 43-54.

Gore, A. and Sampath, K. (2002). Localization of trascripts of the Zebrafish morphogen Squint is dependent on egg activation and the microtubule cytoskeleton. *Mechanisms in Development* **112**, 153-156.

Gore, A. V., Maegawa, S., Cheong, A., Gilligan, P. C., Weinberg, E. S. and Sampath, K. (2005). The zebrafish dorsal axis is apparent at the four-cell stage. *Nature* **438**, 1030-5.

Gorvel, J. P., Chavrier, P., Zerial, M. and Gruenberg, J. (1991). rab5 controls early endosome fusion in vitro. *Cell* **64**, 915-25.

Graff, J. M., Thies, R. S., Song, J. J., Celeste, A. J. and Melton, D. A. (1994). Studies with a Xenopus BMP receptor suggest that ventral mesoderm-inducing signals override dorsal signals in vivo. *Cell* **79**, 169-79.

Granato, M., van Eeden, F. J., Schach, U., Trowe, T., Brand, M., Furutani-Seiki, M., Haffter, P., Hammerschmidt, M., Heisenberg, C. P., Jiang, Y. J. et al. (1996). Genes controlling and mediating locomotion behavior of the zebrafish embryo and larva. *Development* **123**, 399-413.

Grant, K. A., Raible, D. W. and Piotrowski, T. (2005). Regulation of latent sensory hair cell precursors by glia in the zebrafish lateral line. *Neuron* **45**, 69-80.

Greco, V., Hannus, M. and Eaton, S. (2001). Argosomes: a potential vehicle for the spread of morphogens through epithelia. *Cell* **106**, 633-45.

Griffin, K. and Kimelman, D. (2003). Interplay between FGF, *one-eyed pinhead*, and T-box transcription factors during zebrafish development. *Developmental Biology* **264**, 456-466.

Griscelli, C., Durandy, A., Guy-Grand, D., Daguillard, F., Herzog, C. and Prunieras, M. (1978). A syndrome associating partial albinism and immunodeficiency. *Am J Med* **65**, 691-702.

Gritsman, K., Talbot, W. and Schier, A. (2000). Nodal signaling patterns the organizer. *Development* **127**, 921-932.

Gritsman, K., Zhang, J., Cheng, S., Heckscher, E., Talbot, W. S. and Schier, A. F. (1999). The EGF-CFC protein one-eyed pinhead is essential for nodal signaling. *Cell* **97**, 121-32.

Grosshans, B. L., Ortiz, D. and Novick, P. (2006). Rabs and their effectors: achieving specificity in membrane traffic. *Proc Natl Acad Sci U S A* **103**, 11821-7.

Gruenberg, J. and Howell, K. E. (1989). Membrane traffic in endocytosis: insights from cell-free assays. *Annu Rev Cell Biol* **5**, 453-81.

Guger, K. A. and Gumbiner, B. M. (1995). beta-Catenin has Wnt-like activity and mimics the Nieuwkoop signaling center in Xenopus dorsal-ventral patterning. *Dev Biol* **172**, 115-25.

Gunther, T., Struwe, M., Aguzzi, A. and Schughart, K. (1994). Open brain, a new mouse mutant with severe neural tube defects, shows altered gene expression patterns in the developing spinal cord. *Development* **120**, 3119-30.

Guo, A., Wang, T., Ng, E. L., Aulia, S., Chong, K. H., Teng, F. Y., Wang, Y. and Tang, B. L. (2006). Open brain gene product Rab23: expression pattern in the adult mouse brain and functional characterization. *J Neurosci Res* **83**, 1118-27.

Guo, W., Roth, D., Walch-Solimena, C. and Novick, P. (1999). The exocyst is an effector for Sec4p, targeting secretory vesicles to sites of exocytosis. *Embo J* **18**, 1071-80.

Gurdon, J. B., Fairman, S., Mohun, T. J. and Brennan, S. (1985). Activation of muscle-specific actin genes in Xenopus development by an induction between animal and vegetal cells of a blastula. *Cell* **41**, 913-22.

Gurdon, J. B., Harger, P., Mitchell, A. and Lemaire, P. (1994). Activin signalling and response to a morphogen gradient. *Nature* **371**, 487-92.

Gurkan, C., Lapp, H., Alory, C., Su, A. I., Hogenesch, J. B. and Balch, W. E. (2005). Large-scale profiling of Rab GTPase trafficking networks: the membrome. *Mol Biol Cell* **16**, 3847-64.

Haas, A. K., Fuchs, E., Kopajtich, R. and Barr, F. A. (2005). A GTPase-activating protein controls Rab5 function in endocytic trafficking. *Nat Cell Biol* **7**, 887-93.

Halloran, M. C. and Berndt, J. D. (2003). Current progress in neural crest cell motility and migration and future prospects for the zebrafish model system. *Dev Dyn* **228**, 497-513.

Hammer, J. and Wu, X. (2002). Rabs grab motors: defining the connections between Rab GTPases and motor proteins. *Current Opinion in Cell Biology* **14**, 69-75.

Hammerschmidt, M., Pelegri, F., Mullins, M. C., Kane, D. A., Brand, M., van Eeden, F. J., Furutani-Seiki, M., Granato, M., Haffter, P., Heisenberg, C. P. et al. (1996a). Mutations affecting morphogenesis during gastrulation and tail formation in the zebrafish, Danio rerio. *Development* **123**, 143-51.

Hammerschmidt, M., Serbedzija, G. N. and McMahon, A. P. (1996b). Genetic analysis of dorsoventral pattern formation in the zebrafish: requirement of a BMP-like ventralizing activity and its dorsal repressor. *Genes Dev* **10**, 2452-61.

Hashimoto, H., Itoh, M., Yamanaka, Y., Yamashita, S., Shimizu, T., Solnica-Krezel, L., Hibi, M. and Hirano, T. (2000). Zebrafish Dkk1 functions in forebrain specification and axial mesendoderm formation. *Dev Biol* **217**, 138-52.

Hatta, K., Kimmel, C., Ho, R. and Walker, C. (1991). The cyclops mutation blocks specification of the floor plate of the zebrafish central nervouse system. *Nature* **350**, 339-341.

Haubruck, H., Engelke, U., Mertins, P. and Gallwitz, D. (1990). Structural and functional analysis of ypt2, an essential ras-related gene in the fission yeast Schizosaccharomyces pombe encoding a Sec4 protein homologue. *Embo J* **9**, 1957-62.

Haubruck, H., Prange, R., Vorgias, C. and Gallwitz, D. (1989). The ras-related mouse ypt1 protein can functionally replace the YPT1 gene product in yeast. *Embo J* **8**, 1427-32.

Hawley, S. H., Wunnenberg-Stapleton, K., Hashimoto, C., Laurent, M. N., Watabe, T., Blumberg, B. W. and Cho, K. W. (1995). Disruption of BMP signals in embryonic Xenopus ectoderm leads to direct neural induction. *Genes Dev* **9**, 2923-35.

Haycraft, C. J., Banizs, B., Aydin-Son, Y., Zhang, Q., Michaud, E. J. and Yoder, B. K. (2005). Gli2 and Gli3 localize to cilia and require the intraflagellar transport protein polaris for processing and function. *PLoS Genet* **1**, e53.

Heisenberg, C. P., Tada, M., Rauch, G. J., Saude, L., Concha, M. L., Geisler, R., Stemple, D. L., Smith, J. C. and Wilson, S. W. (2000). Silberblick/Wnt11 mediates convergent extension movements during zebrafish gastrulation. *Nature* **405**, 76-81.

Heldin, C. H., Miyazono, K. and ten Dijke, P. (1997). TGF-beta signalling from cell membrane to nucleus through SMAD proteins. *Nature* **390**, 465-71.

Hikasa, H., Shibata, M., Hiratani, I. and Taira, M. (2002). The Xenopus receptor tyrosine kinase Xror2 modulates morphogenetic movements of the axial mesoderm and neuroectoderm via Wnt signaling. *Development* **129**, 5227-39.

Hild, M., Dick, A., Rauch, G. J., Meier, A., Bouwmeester, T., Haffter, P. and Hammerschmidt, M. (1999). The smad5 mutation somitabun blocks Bmp2b signaling during early dorsoventral patterning of the zebrafish embryo. *Development* **126**, 2149-59.

Hill, E., Clarke, M. and Barr, F. A. (2000). The Rab6-binding kinesin, Rab6-KIFL, is required for cytokinesis. *Embo J* **19**, 5711-9.

Hinck, L., Nelson, W. J. and Papkoff, J. (1994). Wnt-1 modulates cell-cell adhesion in mammalian cells by stabilizing beta-catenin binding to the cell adhesion protein cadherin. *J Cell Biol* **124**, 729-41.

Holloway, B., (2006 unpublished data). Betty boop, the Zebrafish Homologue of MAPKAPK2, Regulates Epiboly. *7th International meeting on Zebrafish development and genetics.*

Horowitz, J. M., Mikuckis, G. M. and Longshore, M. A. (1980). The response of single melanophores to extracellular and intracellular iontophoretic injection of melanocyte-stimulating hormone. *Endocrinology* **106**, 770-7.

Houart, C., Westerfield, M. and Wilson, S. W. (1998). A small population of anterior cells patterns the forebrain during zebrafish gastrulation. *Nature* **391**, 788-92.

Houlden, H., King, R. H., Muddle, J. R., Warner, T. T., Reilly, M. M., Orrell, R. W. and Ginsberg, L. (2004). A novel RAB7 mutation associated with ulcero-mutilating neuropathy. *Ann Neurol* **56**, 586-90.

Hsiung, F., Ramirez-Weber, F. A., Iwaki, D. D. and Kornberg, T. B. (2005). Dependence of Drosophila wing imaginal disc cytonemes on Decapentaplegic. *Nature* **437**, 560-3.

Hsu, H. J., Liang, M. R., Chen, C. T. and Chung, B. C. (2006). Pregnenolone stabilizes microtubules and promotes zebrafish embryonic cell movement. *Nature* **439**, 480-3.

Imai, Y., Gates, M. A., Melby, A. E., Kimelman, D., Schier, A. F. and Talbot, W. S. (2001). The homeobox genes vox and vent are redundant repressors of dorsal fates in zebrafish. *Development* **128**, 2407-20.

Inohaya, K., Yasumasu, S., Ishimaru, M., Ohyama, A., Iuchi, I. and Yamagami, K. (1995). Temporal and spatial patterns of gene expression for the hatching enzyme in the teleost embryo, Oryzias latipes. *Dev Biol* **171**, 374-85.

Inohaya, K., Yasumasu, S., Yasumasu, I., Iuchi, I. and Yamagami, K. (1999). Analysis of the origin and development of hatching gland cells by transplantation of the embryonic shield in the fish, Oryzias latipes. *Dev Growth Differ* **41**, 557-66.

Jesuthasan, S. and Stahle, U. (1997). Dynamic microtubules and specification of the zebrafish embryonic axis. *Curr Biol* **7**, 31-42.

Johnston, P. A., Archer, B. T., 3rd, Robinson, K., Mignery, G. A., Jahn, R. and Sudhof, T. C. (1991). rab3A attachment to the synaptic vesicle membrane mediated by a conserved polyisoprenylated carboxy-terminal sequence. *Neuron* **7**, 101-9.

Kane, D. A., Hammerschmidt, M., Mullins, M. C., Maischein, H. M., Brand, M., van Eeden, F. J., Furutani-Seiki, M., Granato, M., Haffter, P., Heisenberg, C. P. et al. (1996). The zebrafish epiboly mutants. *Development* **123**, 47-55.

Kane, D.A., Maischein, H.M., Brand, M., van Eeden, F.J., Furutani-Seiki, M., Granato, M., Haffter, P., Hammerschmidt, M., Heisenberg-, C.P., Jiang, Y.J.,

Kelsh, R.N., Mullins, M.C., Odenthal, J., Warga, R.M., and Nüsslein-Volhard, C. (1996b). The zebrafish early arrest mutants. *Development* **123**, 57-66.

Kane, D. A. and Kimmel, C. B. (1993). The zebrafish midblastula transition. *Development* **119**, 447-56.

Kane, D. A., McFarland, K. N. and Warga, R. M. (2005). Mutations in half baked/E-cadherin block cell behaviors that are necessary for teleost epiboly. *Development* **132**, 1105-16.

Kapfhamer, D., Valladares, O., Sun, Y., Nolan, P., Rux, J., Arnold, S., Veasey, S. and Bucan, M. (2002). Mutations in Rab3a alter circadian period and homeostatic response to sleep loss in the mouse. *Nature Genetics* **32**, 290-295.

Karcher, R. L., Roland, J. T., Zappacosta, F., Huddleston, M. J., Annan, R. S., Carr, S. A. and Gelfand, V. I. (2001). Cell cycle regulation of myosin-V by calcium/calmodulin-dependent protein kinase II. *Science* **293**, 1317-20.

Kawahara, A. and Dawid, I. B. (2000). Expression of the Kruppel-like zinc finger gene biklf during zebrafish development. *Mech Dev* **97**, 173-6.

Kawahara, A. and Dawid, I. B. (2001). Critical role of biklf in erythroid cell differentiation in zebrafish. *Curr Biol* **11**, 1353-7.

Kawahara, A., Wilm, T., Solnica-Krezel, L. and Dawid, I. B. (2000a). Antagonistic role of vega1 and bozozok/dharma homeobox genes in organizer formation. *Proc Natl Acad Sci U S A* **97**, 12121-6.

Kawahara, A., Wilm, T., Solnica-Krezel, L. and Dawid, I. B. (2000b). Functional interaction of vega2 and goosecoid homeobox genes in zebrafish. *Genesis* **28**, 58-67.

Kee, Y., Yoo, J. S., Hazuka, C. D., Peterson, K. E., Hsu, S. C. and Scheller, R. H. (1997). Subunit structure of the mammalian exocyst complex. *Proc Natl Acad Sci U S A* **94**, 14438-43.

Keller, R. E. and Trinkaus, J. P. (1987). Rearrangement of enveloping layer cells without disruption of the epithelial permeability barrier as a factor in Fundulus epiboly. *Dev Biol* **120**, 12-24.

Kelly, C., Chin, A. J., Leatherman, J. L., Kozlowski, D. J. and Weinberg, E. S. (2000). Maternally controlled (beta)-catenin-mediated signaling is required for organizer formation in the zebrafish. *Development* **127**, 3899-911.

Kelly, G. M., Erezyilmaz, D. F. and Moon, R. T. (1995). Induction of a secondary embryonic axis in zebrafish occurs following the overexpression of beta-catenin. *Mech Dev* **53**, 261-73.

Kelsh, R. N., Brand, M., Jiang, Y. J., Heisenberg, C. P., Lin, S., Haffter, P., Odenthal, J., Mullins, M. C., van Eeden, F. J., Furutani-Seiki, M. et al. (1996). Zebrafish pigmentation mutations and the processes of neural crest development. *Development* **123**, 369-89.

Kelsh, R. N. and Eisen, J. S. (2000). The zebrafish colourless gene regulates development of non-ectomesenchymal neural crest derivatives. *Development* **127**, 515-25.

Kerszberg, M. and Wolpert, L. (1998). Mechanisms for positional signalling by morphogen transport: a theoretical study. *J Theor Biol* **191**, 103-14.

Khosravi-Far, R., Lutz, R. J., Cox, A. D., Conroy, L., Bourne, J. R., Sinensky, M., Balch, W. E., Buss, J. E. and Der, C. J. (1991). Isoprenoid modification of rab proteins terminating in CC or CXC motifs. *Proc Natl Acad Sci U S A* **88**, 6264-8.

Kierszenbaum, A. (2000). Fusion of membranes during the acrosome reaction: a tale of two SNAREs. *Molecular Reproduction and Development* **57**, 309-10.

Kimelman, D. and Kirschner, M. (1987). Synergistic induction of mesoderm by FGF and TGF-beta and the identification of an mRNA coding for FGF in the early Xenopus embryo. *Cell* **51**, 869-77.
Kimmel, C., Ballard, W., Kimmel, S., Ullmann, B. and Schilling, T. (1995). Stages of Embryonic Development of the Zebrafish. *Developmental Dynamics* **203**, 253-310.
Kimmel, C. B., Kane, D. A., Walker, C., Warga, R. M. and Rothman, M. B. (1989). A mutation that changes cell movement and cell fate in the zebrafish embryo. *Nature* **337**, 358-62.
Kimmel, C. B. and Law, R. D. (1985). Cell lineage of zebrafish blastomeres. II. Formation of the yolk syncytial layer. *Dev Biol* **108**, 86-93.
Kimmel, C. B., Warga, R. M. and Schilling, T. F. (1990). Origin and organization of the zebrafish fate map. *Development* **108**, 581-94.
Kinsella, B. T. and Maltese, W. A. (1991). rab GTP-binding proteins implicated in vesicular transport are isoprenylated in vitro at cysteines within a novel carboxyl-terminal motif. *J Biol Chem* **266**, 8540-4.
Knecht, A. K., Good, P. J., Dawid, I. B. and Harland, R. M. (1995). Dorsal-ventral patterning and differentiation of noggin-induced neural tissue in the absence of mesoderm. *Development* **121**, 1927-35.
Kodjabachian, L., Dawid, I. B. and Toyama, R. (1999). Gastrulation in zebrafish: what mutants teach us. *Dev Biol* **213**, 231-45.
Koenig, B. B., Cook, J. S., Wolsing, D. H., Ting, J., Tiesman, J. P., Correa, P. E., Olson, C. A., Pecquet, A. L., Ventura, F., Grant, R. A. et al. (1994). Characterization and cloning of a receptor for BMP-2 and BMP-4 from NIH 3T3 cells. *Mol Cell Biol* **14**, 5961-74.
Kohler, K., Louvard, D. and Zahraoui, A. (2004). Rab13 regulates PKA signaling during tight junction assembly. *J Cell Biol* **165**, 175-80.
Kohler, K. and Zahraoui, A. (2005). Tight junction: a co-ordinator of cell signalling and membrane trafficking. *Biol Cell* **97**, 659-65.
Koos, D. S. and Ho, R. K. (1999). The nieuwkoid/dharma homeobox gene is essential for bmp2b repression in the zebrafish pregastrula. *Dev Biol* **215**, 190-207.
Kornbluth, S., Paulson, K. E. and Hanafusa, H. (1988). Novel tyrosine kinase identified by phosphotyrosine antibody screening of cDNA libraries. *Mol Cell Biol* **8**, 5541-4.
Lakadamyali, M., Rust, M. J. and Zhuang, X. (2006). Ligands for clathrin-mediated endocytosis are differentially sorted into distinct populations of early endosomes. *Cell* **124**, 997-1009.
Lamaze, C., Fujimoto, L. M., Yin, H. L. and Schmid, S. L. (1997). The actin cytoskeleton is required for receptor-mediated endocytosis in mammalian cells. *J Biol Chem* **272**, 20332-5.
Lamb, T. M. and Harland, R. M. (1995). Fibroblast growth factor is a direct neural inducer, which combined with noggin generates anterior-posterior neural pattern. *Development* **121**, 3627-36.
Lambert, J., Vancoillie, G. and Naeyaert, J. M. (1999). Molecular motors and their role in pigmentation. *Cell Mol Biol (Noisy-le-grand)* **45**, 905-18.
Lanzetti, L., Palamidessi, A., Areces, L., Scita, G. and Di Fiore, P. P. (2004). Rab5 is a signalling GTPase involved in actin remodelling by receptor tyrosine kinases. *Nature* **429**, 309-14.

Lanzetti, L., Rybin, V., Malabarba, M. G., Christoforidis, S., Scita, G., Zerial, M. and Di Fiore, P. P. (2000). The Eps8 protein coordinates EGF receptor signalling through Rac and trafficking through Rab5. *Nature* **408**, 374-7.
Lawrence, P. (2004). A Wigglesworth classic: how cells make patterns. *J Exp Biol* **207**, 192-3.
Lawrence, P. A. (2001). Morphogens: how big is the big picture? *Nat Cell Biol* **3**, E151-4.
Lazar, T., Gotte, M. and Gallwitz, D. (1997). Vesicular transport: how many Ypt/Rab-GTPases make a eukaryotic cell? *TIBS* **22**, 468-472.
Le Gallic, L. and Fort, P. (1997). Structure of the human ARHG locus encoding the Rho/Rac-like RhoG GTPase. *Genomics* **42**, 157-60.
Le, P. U. and Nabi, I. R. (2003). Distinct caveolae-mediated endocytic pathways target the Golgi apparatus and the endoplasmic reticulum. *J Cell Sci* **116**, 1059-71.
Le Roy, C. and Wrana, J. L. (2005). Clathrin- and non-clathrin-mediated endocytic regulation of cell signalling. *Nat Rev Mol Cell Biol* **6**, 112-26.
Lecuit, T., Brook, W. J., Ng, M., Calleja, M., Sun, H. and Cohen, S. M. (1996). Two distinct mechanisms for long-range patterning by Decapentaplegic in the Drosophila wing. *Nature* **381**, 387-93.
Lekven, A. C., Thorpe, C. J., Waxman, J. S. and Moon, R. T. (2001). Zebrafish wnt8 encodes two wnt8 proteins on a bicistronic transcript and is required for mesoderm and neurectoderm patterning. *Dev Cell* **1**, 103-14.
Lele, Z., Nowak, M. and Hammerschmidt, M. (2001). Zebrafish admp is required to restrict the size of the organizer and to promote posterior and ventral development. *Dev Dyn* **222**, 681-7.
Leung, K. F., Baron, R. and Seabra, M. C. (2006). Thematic review series: lipid posttranslational modifications. geranylgeranylation of Rab GTPases. *J Lipid Res* **47**, 467-75.
Leung, T., Soll, I., Arnold, S. J., Kemler, R. and Driever, W. (2003). Direct binding of Lef1 to sites in the boz promoter may mediate pre-midblastula-transition activation of boz expression. *Dev Dyn* **228**, 424-32.
Levi, V., Serpinskaya, A. S., Gratton, E. and Gelfand, V. (2006). Organelle transport along microtubules in Xenopus melanophores: evidence for cooperation between multiple motors. *Biophys J* **90**, 318-27.
Levina, S. and Gordon, R. (1983). Methionine enkephalin-induced changes in pigmentation of zebrafish (Cyprinidae, Brachydanio rerio) and related species and varieties, measured videodensitometrically. I. Zebrafish. *Gen Comp Endocrinol* **51**, 370-7.
Li, G. and Stahl, P. D. (1993). Structure-function relationship of the small GTPase rab5. *J Biol Chem* **268**, 24475-80.
Li, L., Mao, J., Sun, L., Liu, W. and Wu, D. (2002). Second cysteine-rich domain of Dickkopf-2 activates canonical Wnt signaling pathway via LRP-6 independently of dishevelled. *J Biol Chem* **277**, 5977-81.
Lin, H. Y., Wang, X. F., Ng-Eaton, E., Weinberg, R. A. and Lodish, H. F. (1992). Expression cloning of the TGF-beta type II receptor, a functional transmembrane serine/threonine kinase. *Cell* **68**, 775-85.
Lin, K., Wang, S., Julius, M. A., Kitajewski, J., Moos, M., Jr. and Luyten, F. P. (1997). The cysteine-rich frizzled domain of Frzb-1 is required and sufficient for modulation of Wnt signaling. *Proc Natl Acad Sci U S A* **94**, 11196-200.

Lippe, R., Horiuchi, H., Runge, A. and Zerial, M. (2001a). Expression, purification, and characterization of Rab5 effector complex, rabaptin-5/rabex-5. *Methods Enzymol* **329**, 132-45.

Lippe, R., Miaczynska, M., Rybin, V., Runge, A. and Zerial, M. (2001b). Functional synergy between Rab5 effector Rabaptin-5 and exchange factor Rabex-5 when physically associated in a complex. *Mol Biol Cell* **12**, 2219-28.

Lock, J. G. and Stow, J. L. (2005). Rab11 in recycling endosomes regulates the sorting and basolateral transport of E-cadherin. *Mol Biol Cell* **16**, 1744-55.

Loftus, S. K., Larson, D. M., Baxter, L. L., Antonellis, A., Chen, Y., Wu, X., Jiang, Y., Bittner, M., Hammer, J. A., 3rd and Pavan, W. J. (2002). Mutation of melanosome protein RAB38 in chocolate mice. *Proc Natl Acad Sci U S A* **99**, 4471-6.

Logan, D. W., Burn, S. F. and Jackson, I. J. (2006). Regulation of pigmentation in zebrafish melanophores. *Pigment Cell Res* **19**, 206-13.

Long, S., Ahmad, N. and Rebagliati, M. (2003). The zebrafish nodal-related gene southpaw is required for visceral and diencephalic left-right asymmetry. *Development* **130**, 2303-16.

Lopez-Schier, H. and Hudspeth, A. J. (2005). Supernumerary neuromasts in the posterior lateral line of zebrafish lacking peripheral glia. *Proc Natl Acad Sci U S A* **102**, 1496-501.

Lutcke, A., Jansson, S., Parton, R. G., Chavrier, P., Valencia, A., Huber, L. A., Lehtonen, E. and Zerial, M. (1993). Rab17, a novel small GTPase, is specific for epithelial cells and is induced during cell polarization. *J Cell Biol* **121**, 553-64.

Logan, D. W., Burn, S. F., and Jackson I. J. (2006). Regulation of pigmentation in zebrafish melanophores. *Pigment Cell Res* **19**, 206-13.

Lutcke, A., Parton, R. G., Murphy, C., Olkkonen, V. M., Dupree, P., Valencia, A., Simons, K. and Zerial, M. (1994). Cloning and subcellular localization of novel rab proteins reveals polarized and cell type-specific expression. *J Cell Sci* **107 (Pt 12)**, 3437-48.

Maciver, S. Myosin V, vol. 2006 (ed.

Mann, R. K. and Beachy, P. A. (2000). Cholesterol modification of proteins. *Biochim Biophys Acta* **1529**, 188-202.

Marois, E., Mahmoud, A. and Eaton, S. (2006). The endocytic pathway and formation of the Wingless morphogen gradient. *Development* **133**, 307-17.

Martin, E. (1998). Concise Colour Medical Dictionary, (ed. Oxford: Oxford University Press.

Martyn, U. and Schulte-Merker, S. (2003). The ventralized ogon mutant phenotype is caused by a mutation in the zebrafish homologue of Sizzled, a secreted Frizzled-related protein. *Dev Biol* **260**, 58-67.

Matesic, L. E., Yip, R., Reuss, A. E., Swing, D. A., O'Sullivan, T. N., Fletcher, C. F., Copeland, N. G. and Jenkins, N. A. (2001). Mutations in Mlph, encoding a member of the Rab effector family, cause the melanosome transport defects observed in leaden mice. *Proc Natl Acad Sci U S A* **98**, 10238-43.

Mathieu, J., Griffin, K., Herbomel, P., Dickmeis, T., Strahle, U., Kimelman, D., Rosa, F. M. and Peyrieras, N. (2004). Nodal and Fgf pathways interact through a positive regulatory loop and synergize to maintain mesodermal cell populations. *Development* **131**, 629-41.

May, S. R., Ashique, A. M., Karlen, M., Wang, B., Shen, Y., Zarbalis, K., Reiter, J., Ericson, J. and Peterson, A. S. (2005). Loss of the retrograde motor for IFT

disrupts localization of Smo to cilia and prevents the expression of both activator and repressor functions of Gli. *Dev Biol* **287**, 378-89.

McBride, H. M., Rybin, V., Murphy, C., Giner, A., Teasdale, R. and Zerial, M. (1999). Oligomeric complexes link Rab5 effectors with NSF and drive membrane fusion via interactions between EEA1 and syntaxin 13. *Cell* **98**, 377-86.

McDowell, N., Gurdon, J. B. and Grainger, D. J. (2001). Formation of a functional morphogen gradient by a passive process in tissue from the early Xenopus embryo. *Int J Dev Biol* **45**, 199-207.

McFarland, K. N., Warga, R. M. and Kane, D. A. (2005). Genetic locus half baked is necessary for morphogenesis of the ectoderm. *Dev Dyn* **233**, 390-406.

McLauchlan, H., Newell, J., Morrice, N., Osborne, A., West, M. and Smythe, E. (1998). A novel role for Rab5-GDI in ligand sequestration into clathrin-coated pits. *Curr Biol* **8**, 34-45.

Melby, A. E., Beach, C., Mullins, M. and Kimelman, D. (2000). Patterning the early zebrafish by the opposing actions of bozozok and vox/vent. *Dev Biol* **224**, 275-85.

Melton, D. A. (1987). Translocation of a localized maternal mRNA to the vegetal pole of Xenopus oocytes. *Nature* **328**, 80-2.

Menasche, G., Ho, C. H., Sanal, O., Feldmann, J., Tezcan, I., Ersoy, F., Houdusse, A., Fischer, A. and de Saint Basile, G. (2003). Griscelli syndrome restricted to hypopigmentation results from a melanophilin defect (GS3) or a MYO5A F-exon deletion (GS1). *J Clin Invest* **112**, 450-6.

Menasche, G., Pastural, E., Feldmann, J., Certain, S., Ersoy, F., Dupuis, S., Wulffraat, N., Bianchi, D., Fischer, A., Le Deist, F. et al. (2000). Mutations in RAB27A cause Griscelli syndrome associated with haemophagocytic syndrome. *Nat Genet* **25**, 173-6.

Mercer, J. A., Seperack, P. K., Strobel, M. C., Copeland, N. G. and Jenkins, N. A. (1991). Novel myosin heavy chain encoded by murine dilute coat colour locus. *Nature* **349**, 709-13.

Milburn, M. V., Tong, L., deVos, A. M., Brunger, A., Yamaizumi, Z., Nishimura, S. and Kim, S. H. (1990). Molecular switch for signal transduction: structural differences between active and inactive forms of protooncogenic ras proteins. *Science* **247**, 939-45.

Miller-Bertoglio, V., Carmany-Rampey, A., Furthauer, M., Gonzalez, E. M., Thisse, C., Thisse, B., Halpern, M. E. and Solnica-Krezel, L. (1999). Maternal and zygotic activity of the zebrafish ogon locus antagonizes BMP signaling. *Dev Biol* **214**, 72-86.

Milos, N., Dingle, A. D. and Milos, J. P. (1983). Dynamics of pigment pattern formation in the zebrafish, Brachydanio rerio. III. Effect of anteroposterior location of three-day lateral line melanophores on colonization by the second wave of melanophores. *J Exp Zool* **227**, 81-92.

Mintzer, K. A., Lee, M. A., Runke, G., Trout, J., Whitman, M. and Mullins, M. C. (2001). Lost-a-fin encodes a type I BMP receptor, Alk8, acting maternally and zygotically in dorsoventral pattern formation. *Development* **128**, 859-69.

Mizuno, T., Yamaha, M., Wakahara, A., Kuroiwa, A. and Takeda, H. (1996). Mesoderm induction in zebrafish. *Nature* **383**, 131-132.

Montero, J. A., Carvalho, L., Wilsch-Brauninger, M., Kilian, B., Mustafa, C. and Heisenberg, C. P. (2005). Shield formation at the onset of zebrafish gastrulation. *Development* **132**, 1187-98.

Moore, I., Schell, J. and Palme, K. (1995). Subclass-specific sequence motifs identified in Rab GTPases. *Trends Biochem Sci* **20**, 10-2.
Morgan, A. and Burgoyne, R. D. (1995). Is NSF a fusion protein? *Trends Cell Biol* **5**, 335-9.
Moskowitz, H. S., Heuser, J., McGraw, T. E. and Ryan, T. A. (2003). Targeted chemical disruption of clathrin function in living cells. *Mol Biol Cell* **14**, 4437-47.
Mruk, D. D., Lau, A. S. and Conway, A. M. (2005). Crosstalk between Rab GTPases and cell junctions. *Contraception* **72**, 280-90.
Murone, M., Rosenthal, A. and de Sauvage, F. J. (1999). Sonic hedgehog signaling by the patched-smoothened receptor complex. *Curr Biol* **9**, 76-84.
Nagashima, K., Torii, S., Yi, Z., Igarashi, M., Okamoto, K., Takeuchi, T. and Izumi, T. (2002). Melanophilin directly links Rab27a and myosin Va through its distinct coiled-coil regions. *FEBS Lett* **517**, 233-8.
Nakafuku, M., Nagamine, M., Ohtoshi, A., Tanaka, K., Toh-e, A. and Kaziro, Y. (1993). Suppression of oncogenic Ras by mutant neurofibromatosis type 1 genes with single amino acid substitutions. *Proc Natl Acad Sci U S A* **90**, 6706-10.
Nakagawa, S. and Takeichi, M. (1995). Neural crest cell-cell adhesion controlled by sequential and subpopulation-specific expression of novel cadherins. *Development* **121**, 1321-32.
Nakagawa, S. and Takeichi, M. (1998). Neural crest emigration from the neural tube depends on regulated cadherin expression. *Development* **125**, 2963-71.
Nakao, A., Afrakhte, M., Moren, A., Nakayama, T., Christian, J. L., Heuchel, R., Itoh, S., Kawabata, M., Heldin, N. E., Heldin, C. H. et al. (1997). Identification of Smad7, a TGFbeta-inducible antagonist of TGF-beta signalling. *Nature* **389**, 631-5.
Nakato, H., Futch, T. A. and Selleck, S. B. (1995). The division abnormally delayed (dally) gene: a putative integral membrane proteoglycan required for cell division patterning during postembryonic development of the nervous system in Drosophila. *Development* **121**, 3687-702.
Nakayama, T., Snyder, M. A., Grewal, S. S., Tsuneizumi, K., Tabata, T. and Christian, J. L. (1998). Xenopus Smad8 acts downstream of BMP-4 to modulate its activity during vertebrate embryonic patterning. *Development* **125**, 857-67.
Nasevicius, A. and Ekker, S. (2000). Effective targeted gene 'knockdown' in zebrafish. *Nature Genetics* **26**, 216-220.
Nelson, R. W. and Gumbiner, B. M. (1998). Beta-catenin directly induces expression of the Siamois gene, and can initiate signaling indirectly via a membrane-tethered form. *Ann N Y Acad Sci* **857**, 86-98.
Nicolson, T. (2005). The genetics of hearing and balance in zebrafish. *Annu Rev Genet* **39**, 9-22.
Nicolson, T., Rusch, A., Friedrich, R. W., Granato, M., Ruppersberg, J. P. and Nusslein-Volhard, C. (1998). Genetic analysis of vertebrate sensory hair cell mechanosensation: the zebrafish circler mutants. *Neuron* **20**, 271-83.
Nielsen, E., Christoforidis, S., Uttenweiler-Joseph, S., Miaczynska, M., Dewitte, F., Wilm, M., Hoflack, B. and Zerial, M. (2000). Rabenosyn-5, a novel Rab5 effector, is complexed with hVPS45 and recruited to endosomes through a FYVE finger domain. *J Cell Biol* **151**, 601-12.
Nielsen, E., Severin, F., Backer, J. M., Hyman, A. A. and Zerial, M. (1999). Rab5 regulates motility of early endosomes on microtubules. *Nat Cell Biol* **1**, 376-82.
Nojima, H., Shimizu, T., Kim, C. H., Yabe, T., Bae, Y. K., Muraoka, O., Hirata, T., Chitnis, A., Hirano, T. and Hibi, M. (2004). Genetic evidence for involvement

of maternally derived Wnt canonical signaling in dorsal determination in zebrafish. *Mech Dev* **121**, 371-86.

Nonet, M. L., Staunton, J. E., Kilgard, M. P., Fergestad, T., Hartwieg, E., Horvitz, H. R., Jorgensen, E. M. and Meyer, B. J. (1997). Caenorhabditis elegans rab-3 mutant synapses exhibit impaired function and are partially depleted of vesicles. *J Neurosci* **17**, 8061-73.

Nuoffer, C., Davidson, H. W., Matteson, J., Meinkoth, J. and Balch, W. E. (1994). A GDP-bound of rab1 inhibits protein export from the endoplasmic reticulum and transport between Golgi compartments. *J Cell Biol* **125**, 225-37.

Oates, A. C., Pratt, S. J., Vail, B., Yan, Y., Ho, R. K., Johnson, S. L., Postlethwait, J. H. and Zon, L. I. (2001). The zebrafish klf gene family. *Blood* **98**, 1792-801.

Odenthal, J., Rossnagel, K., Haffter, P., Kelsh, R. N., Vogelsang, E., Brand, M., van Eeden, F. J., Furutani-Seiki, M., Granato, M., Hammerschmidt, M. et al. (1996). Mutations affecting xanthophore pigmentation in the zebrafish, Danio rerio. *Development* **123**, 391-8.

Onichtchouk, D., Chen, Y. G., Dosch, R., Gawantka, V., Delius, H., Massague, J. and Niehrs, C. (1999). Silencing of TGF-beta signalling by the pseudoreceptor BAMBI. *Nature* **401**, 480-5.

Ono, F., Shcherbatko, A., Higashijima, S., Mandel, G. and Brehm, P. (2002). The Zebrafish motility mutant twitch once reveals new roles for rapsyn in synaptic function. *J Neurosci* **22**, 6491-8.

Oppenheimer, J. (1983). Thomas Hunt Morgan as an embryologist: The view from bryn mawr. *Amer. Zool* **23**, 845-854.

Osanai, K., Takahashi, K., Nakamura, K., Takahashi, M., Ishigaki, M., Sakuma, T., Toga, H., Suzuki, T. and Voelker, D. R. (2005). Expression and characterization of Rab38, a new member of the Rab small G protein family. *Biol Chem* **386**, 143-53.

Ossig, R., Laufer, W., Schmitt, H. D. and Gallwitz, D. (1995). Functionality and specific membrane localization of transport GTPases carrying C-terminal membrane anchors of synaptobrevin-like proteins. *Embo J* **14**, 3645-53.

Ostermeier, C. and Brunger, A. T. (1999) Structural basis of Rab effector specificity: crystal structure of the small G protein Rab3A complexed with the effector domain of rabphilin-3A.*Cell.* **96**, 363-74

Oyler, G. A., Higgins, G. A., Hart, R. A., Battenberg, E., Billingsley, M., Bloom, F. E. and Wilson, M. C. (1989). The identification of a novel synaptosomal-associated protein, SNAP-25, differentially expressed by neuronal subpopulations. *J Cell Biol* **109**, 3039-52.

Palokangas, H., Ying, M., Vaananen, K. and Saraste, J. (1998). Retrograde transport from the pre-Golgi intermediate compartment and the Golgi complex is affected by the vacuolar H+-ATPase inhibitor bafilomycin A1. *Mol Biol Cell* **9**, 3561-78.

Pan, J. Y. and Wessling-Resnick, M. (1998). GEF-mediated GDP/GTP exchange by monomeric GTPases: a regulatory role for Mg2+? *Bioessays* **20**, 516-21.

Papkoff, J., Rubinfeld, B., Schryver, B. and Polakis, P. (1996). Wnt-1 regulates free pools of catenins and stabilizes APC-catenin complexes. *Mol Cell Biol* **16**, 2128-34.

Parichy, D. M. (2003). Pigment patterns: fish in stripes and spots. *Curr Biol* **13**, R947-50.

Parichy, D. M., Rawls, J. F., Pratt, S. J., Whitfield, T. T. and Johnson, S. L. (1999). Zebrafish sparse corresponds to an orthologue of c-kit and is required for the morphogenesis of a subpopulation of melanocytes, but is not essential for hematopoiesis or primordial germ cell development. *Development* **126**, 3425-36.

Parsons, M., Pollard, S., Saude, L., Feldman, B., Coutinho, P., Hirst, E. and Stemple, D. (2002a). Zebrafish mutants identify an essential role for laminins in notochord formation. *Development* **129**, 3137-3146.

Parsons, M. J., Campos, I., Hirst, E. M. and Stemple, D. L. (2002b). Removal of dystroglycan causes severe muscular dystrophy in zebrafish embryos. *Development* **129**, 3505-12.

Pastural, E., Barrat, F. J., Dufourcq-Lagelouse, R., Certain, S., Sanal, O., Jabado, N., Seger, R., Griscelli, C., Fischer, A. and de Saint Basile, G. (1997). Griscelli disease maps to chromosome 15q21 and is associated with mutations in the myosin-Va gene. *Nat Genet* **16**, 289-92.

Pastural, E., Ersoy, F., Yalman, N., Wulffraat, N., Grillo, E., Ozkinay, F., Tezcan, I., Gedikoglu, G., Philippe, N., Fischer, A. et al. (2000). Two genes are responsible for Griscelli syndrome at the same 15q21 locus. *Genomics* **63**, 299-306.

Pavlos, N., Xu, J., Papadimitriou, J. and Zheng, M. (2001). Molecular cloning of the mouse homologue of Rab3c. *Journal of Molecular Endocrinology* **27**, 117-122.

Pelkmans, L., Fava, E., Grabner, H., Hannus, M., Habermann, B., Krausz, E. and Zerial, M. (2005). Genome-wide analysis of human kinases in clathrin- and caveolae/raft-mediated endocytosis. *Nature* **436**, 78-86.

Pellinen, T., Arjonen, A., Vuoriluoto, K., Kallio, K., Fransen, J. A. and Ivaska, J. (2006). Small GTPase Rab21 regulates cell adhesion and controls endosomal traffic of beta1-integrins. *J Cell Biol* **173**, 767-80.

Pepinsky, R. B., Zeng, C., Wen, D., Rayhorn, P., Baker, D. P., Williams, K. P., Bixler, S. A., Ambrose, C. M., Garber, E. A., Miatkowski, K. et al. (1998). Identification of a palmitic acid-modified form of human Sonic hedgehog. *J Biol Chem* **273**, 14037-45.

Pereira-Leal, J. and Seabra, M. (2000). The Mammalian Rab Family of Small GTPases: Definition of Family and SubfamilySequence Motifs Suggests a Mechanism for Functional Specificity in the Ras Superfamily. *Journal of Molecular Biology* **301**, 1077-1087.

Piccolo, S., Agius, E., Leyns, L., Bhattacharyya, S., Grunz, H., Bouwmeester, T. and De Robertis, E. M. (1999). The head inducer Cerberus is a multifunctional antagonist of Nodal, BMP and Wnt signals. *Nature* **397**, 707-10.

Piccolo, S., Sasai, Y., Lu, B. and De Robertis, E. M. (1996). Dorsoventral patterning in Xenopus: inhibition of ventral signals by direct binding of chordin to BMP-4. *Cell* **86**, 589-98.

Piek, E., Heldin, C. H. and Ten Dijke, P. (1999). Specificity, diversity, and regulation in TGF-beta superfamily signaling. *Faseb J* **13**, 2105-24.

Plutner, H., Cox, A. D., Pind, S., Khosravi-Far, R., Bourne, J. R., Schwaninger, R., Der, C. J. and Balch, W. E. (1991). Rab1b regulates vesicular transport between the endoplasmic reticulum and successive Golgi compartments. *J Cell Biol* **115**, 31-43.

Polo, S. and Di Fiore, P. P. (2006). Endocytosis conducts the cell signaling orchestra. *Cell* **124**, 897-900.

Poulain, M., Furthauer, M., Thisse, B., Thisse, C. and Lepage, T. (2006). Zebrafish endoderm formation is regulated by combinatorial Nodal, FGF and BMP signalling. *Development* **133**, 2189-200.

Price, A., Seals, D., Wickner, W. and Ungermann, C. (2000a). The docking stage of yeast vacuole fusion requires the transfer of proteins from a cis-SNARE complex to a Rab/Ypt protein. *J Cell Biol* **148**, 1231-8.

Price, A., Wickner, W. and Ungermann, C. (2000b). Proteins needed for vesicle budding from the Golgi complex are also required for the docking step of homotypic vacuole fusion. *J Cell Biol* **148**, 1223-29.

Pruyne, D. W., Schott, D. H. and Bretscher, A. (1998). Tropomyosin-containing actin cables direct the Myo2p-dependent polarized delivery of secretory vesicles in budding yeast. *J Cell Biol* **143**, 1931-45.

Pyati, U. J., Webb, A. E. and Kimelman, D. (2005). Transgenic zebrafish reveal stage-specific roles for Bmp signaling in ventral and posterior mesoderm development. *Development* **132**, 2333-43.

Raible, D. W., Wood, A., Hodsdon, W., Henion, P. D., Weston, J. A. and Eisen, J. S. (1992). Segregation and early dispersal of neural crest cells in the embryonic zebrafish. *Dev Dyn* **195**, 29-42.

Ramel, M. C., Buckles, G. R., Baker, K. D. and Lekven, A. C. (2005). WNT8 and BMP2B co-regulate non-axial mesoderm patterning during zebrafish gastrulation. *Dev Biol* **287**, 237-48.

Ramel, M. C. and Lekven, A. C. (2004). Repression of the vertebrate organizer by Wnt8 is mediated by Vent and Vox. *Development* **131**, 3991-4000.

Ramirez-Weber, F. A. and Kornberg, T. B. (1999). Cytonemes: cellular processes that project to the principal signaling center in Drosophila imaginal discs. *Cell* **97**, 599-607.

Rebagliati, M., Toyama, R., Haffterb, P. and Dawida, I. (1998). *cyclops* encodes a noda-related factor involved in midline signaling. *Proceedings of the National Academy of Sciences of the United States of America* **95**, 9932-9937.

Rebagliatia, M., Toyamaa, R., Frickeb, C., Haffterb, P. and Dawida, I. (1998). Zebrafish Nodal-Related Genes Are Implicated in Axial Patterning and Establishing Left–Right Asymmetry. *Developmental Biology* **199**, 261-272.

Reifers, F., Bohli, H., Walsh, E. C., Crossley, P. H., Stainier, D. Y. and Brand, M. (1998). Fgf8 is mutated in zebrafish acerebellar (ace) mutants and is required for maintenance of midbrain-hindbrain boundary development and somitogenesis. *Development* **125**, 2381-95.

Reissmann, E., Jornvall, H., Blokzijl, A., Andersson, O., Chang, C., Minchiotti, G., Persico, M. G., Ibanez, C. F. and Brivanlou, A. H. (2001). The orphan receptor ALK7 and the Activin receptor ALK4 mediate signaling by Nodal proteins during vertebrate development. *Genes Dev* **15**, 2010-22.

Rieder, S. E. and Emr, S. D. (1997). A novel RING finger protein complex essential for a late step in protein transport to the yeast vacuole. *Mol Biol Cell* **8**, 2307-27.

Riederer, M. A., Soldati, T., Shapiro, A. D., Lin, J. and Pfeffer, S. R. (1994). Lysosome biogenesis requires Rab9 function and receptor recycling from endosomes to the trans-Golgi network. *J Cell Biol* **125**, 573-82.

Rietveld, A., Neutz, S., Simons, K. and Eaton, S. (1999). Association of sterol- and glycosylphosphatidylinositol-linked proteins with Drosophila raft lipid microdomains. *J Biol Chem* **274**, 12049-54.

Rodionov, V. I., Hope, A. J., Svitkina, T. M. and Borisy, G. G. (1998). Functional coordination of microtubule-based and actin-based motility in melanophores. *Curr Biol* **8**, 165-8.

Rogers, S. L. and Gelfand, V. I. (1998). Myosin cooperates with microtubule motors during organelle transport in melanophores. *Curr Biol* **8**, 161-4.
Rothman, J. E. and Warren, G. (1994). Implications of the SNARE hypothesis for intracellular membrane topology and dynamics. *Curr Biol* **4**, 220-33.
Rybin, V., Ullrich, O., Rubino, M., Alexandrov, K., Simon, I., Seabra, M. C., Goody, R. and Zerial, M. (1996). GTPase activity of Rab5 acts as a timer for endocytic membrane fusion. *Nature* **383**, 266-9.
Sacher, M., Jiang, Y., Barrowman, J., Scarpa, A., Burston, J., Zhang, L., Schieltz, D., Yates, J. R., 3rd, Abeliovich, H. and Ferro-Novick, S. (1998). TRAPP, a highly conserved novel complex on the cis-Golgi that mediates vesicle docking and fusion. *Embo J* **17**, 2494-503.
Sakuma, R., Ohnishi Yi, Y., Meno, C., Fujii, H., Juan, H., Takeuchi, J., Ogura, T., Li, E., Miyazono, K. and Hamada, H. (2002). Inhibition of Nodal signalling by Lefty mediated through interaction with common receptors and efficient diffusion. *Genes Cells* **7**, 401-12.
Salminen, A. and Novick, P. J. (1987). A ras-like protein is required for a post-Golgi event in yeast secretion. *Cell* **49**, 527-38.
Sampath, K., Rubinstein, A., Cheng, A., Liang, J., Fekany, K., Solnica-Krezel, L., Korzh, V., Halpern, M. and Wright, C. (1998). Induction of the zebrafish ventral brain and floorplate requires cyclops/nodal signalling. *Nature* **395**, 185-189.
Sannerud, R., Saraste, J. and Goud, B. (2003). Retrograde traffic in the biosynthetic-secretory route: pathways and machinery. *Curr Opin Cell Biol* **15**, 438-45.
Sanson, B., Alexandre, C., Fascetti, N. and Vincent, J. P. (1999). Engrailed and hedgehog make the range of Wingless asymmetric in Drosophila embryos. *Cell* **98**, 207-16.
Sasaki, T., Kaibuchi, K., Kabcenell, A. K., Novick, P. J. and Takai, Y. (1991). A mammalian inhibitory GDP/GTP exchange protein (GDP dissociation inhibitor) for smg p25A is active on the yeast SEC4 protein. *Mol Cell Biol* **11**, 2909-12.
Schier, A. and Talbot, W. (2001). Nodal signaling and the zebrafish organizer. *Int.J.Dev.Biol* **45**, 289-297.
Schier, A. F. and Talbot, W. S. (2005). Molecular Genetics of Axis Formation in Zebrafish. *Annu Rev Genet.*
Schimmoller, F., Simon, I. and Pfeffer, S. R. (1998). Rab GTPases, directors of vesicle docking. *J Biol Chem* **273**, 22161-4.
Schmid, B., Furthauer, M., Connors, S. A., Trout, J., Thisse, B., Thisse, C. and Mullins, M. C. (2000). Equivalent genetic roles for bmp7/snailhouse and bmp2b/swirl in dorsoventral pattern formation. *Development* **127**, 957-67.
Schmidt, A. and Hall, A. (2002). Guanine nucleotide exchange factors for Rho GTPases: turning on the switch. *Genes Dev* **16**, 1587-609.
Schmitt, H. D., Puzicha, M. and Gallwitz, D. (1988). Study of a temperature-sensitive mutant of the ras-related YPT1 gene product in yeast suggests a role in the regulation of intracellular calcium. *Cell* **53**, 635-47.
Schmitt, H. D., Wagner, P., Pfaff, E. and Gallwitz, D. (1986). The ras-related YPT1 gene product in yeast: a GTP-binding protein that might be involved in microtubule organization. *Cell* **47**, 401-12.
Schneider, S., Steinbeisser, H., Warga, R. M. and Hausen, P. (1996). Beta-catenin translocation into nuclei demarcates the dorsalizing centers in frog and fish embryos. *Mech Dev* **57**, 191-8.

Scholpp, S. and Brand, M. (2004). Endocytosis controls spreading and effective signaling range of Fgf8 protein. *Curr Biol* **14**, 1834-41.
Schott, D., Ho, J., Pruyne, D. and Bretscher, A. (1999). The COOH-terminal domain of Myo2p, a yeast myosin V, has a direct role in secretory vesicle targeting. *J Cell Biol* **147**, 791-808.
Schulte-Merker, S., Lee, K. J., McMahon, A. P. and Hammerschmidt, M. (1997). The zebrafish organizer requires chordino. *Nature* **387**, 862-3.
Scott, M. (2001). Signalling and endocytosis: Wnt breaks down on back roads. *Nat Cell Biol* **3**, E185-6.
Seabra, M., Mules, E. and Hume, A. (2002). Rab GTPases, intracellular traffic and disease. *Trends In Molecular Medicine* **8**, 23-26.
Seabra, M. C. and Wasmeier, C. (2004). Controlling the location and activation of Rab GTPases. *Curr Opin Cell Biol* **16**, 451-7.
Seals, D. F., Eitzen, G., Margolis, N., Wickner, W. T. and Price, A. (2000). A Ypt/Rab effector complex containing the Sec1 homolog Vps33p is required for homotypic vacuole fusion. *Proc Natl Acad Sci U S A* **97**, 9402-7.
Sepich, D. S., Myers, D. C., Short, R., Topczewski, J., Marlow, F. and Solnica-Krezel, L. (2000). Role of the zebrafish trilobite locus in gastrulation movements of convergence and extension. *Genesis* **27**, 159-73.
Seto, E. S. and Bellen, H. J. (2006). Internalization is required for proper Wingless signaling in Drosophila melanogaster. *J Cell Biol* **173**, 95-106.
Settleman, J., Albright, C. F., Foster, L. C. and Weinberg, R. A. (1992). Association between GTPase activators for Rho and Ras families. *Nature* **359**, 153-4.
Sheldahl, L. C., Park, M., Malbon, C. C. and Moon, R. T. (1999). Protein kinase C is differentially stimulated by Wnt and Frizzled homologs in a G-protein-dependent manner. *Curr Biol* **9**, 695-8.
Shimizu, T., Bae, Y. K., Muraoka, O. and Hibi, M. (2005a). Interaction of Wnt and caudal-related genes in zebrafish posterior body formation. *Dev Biol* **279**, 125-41.
Shimizu, T., Yabe, T., Muraoka, O., Yonemura, S., Aramaki, S., Hatta, K., Bae, Y. K., Nojima, H. and Hibi, M. (2005b). E-cadherin is required for gastrulation cell movements in zebrafish. *Mech Dev* **122**, 747-63.
Shimizu, T., Yamanaka, Y., Nojima, H., Yabe, T., Hibi, M. and Hirano, T. (2002). A novel repressor-type homeobox gene, ved, is involved in dharma/bozozok-mediated dorsal organizer formation in zebrafish. *Mech Dev* **118**, 125-38.
Singer-Kruger, B., Stenmark, H., Dusterhoft, A., Philippsen, P., Yoo, J. S., Gallwitz, D. and Zerial, M. (1994). Role of three rab5-like GTPases, Ypt51p, Ypt52p, and Ypt53p, in the endocytic and vacuolar protein sorting pathways of yeast. *J Cell Biol* **125**, 283-98.
Singer-Kruger, B., Stenmark, H. and Zerial, M. (1995). Yeast Ypt51p and mammalian Rab5: counterparts with similar function in the early endocytic pathway *J Cell Sci* **108**, 3509-3521.
Sivars, U., Aivazian, D. and Pfeffer, S. R. (2003). Yip3 catalyses the dissociation of endosomal Rab-GDI complexes. *Nature* **425**, 856-9.
Skold, H. N., Norstrom, E. and Wallin, M. (2002). Regulatory control of both microtubule- and actin-dependent fish melanosome movement. *Pigment Cell Res* **15**, 357-66.
Slack, J. M. (1994). Developmental biology. How to make the gradient. *Nature* **371**, 477-8.

Smith, W. C. and Harland, R. M. (1991). Injected Xwnt-8 RNA acts early in Xenopus embryos to promote formation of a vegetal dorsalizing center. *Cell* **67**, 753-65.

Sollner, C., Burghammer, M., Busch-Nentwich, E., Berger, J., Schwarz, H., Riekel, C. and Nicolson, T. (2003). Control of crystal size and lattice formation by starmaker in otolith biomineralization. *Science* **302**, 282-6.

Sollner, T., Whiteheart, S. W., Brunner, M., Erdjument-Bromage, H., Geromanos, S., Tempst, P. and Rothman, J. E. (1993). SNAP receptors implicated in vesicle targeting and fusion. *Nature* **362**, 318-24.

Solnica-Krezel, L. and Driever, W. (1994). Microtubule arrays of the zebrafish yolk cell: organization and function during epiboly. *Development* **120**, 2443-55.

Solnica-Krezel, L. and Driever, W. (2001). The role of the homeodomain protein Bozozok in zebrafish axis formation. *Int J Dev Biol* **45**, 299-310.

Solnica-Krezel, L., Stemple, D. L., Mountcastle-Shah, E., Rangini, Z., Neuhauss, S. C., Malicki, J., Schier, A. F., Stainier, D. Y., Zwartkruis, F., Abdelilah, S. et al. (1996). Mutations affecting cell fates and cellular rearrangements during gastrulation in zebrafish. *Development* **123**, 67-80.

Southard-Smith, E. M., Kos, L. and Pavan, W. J. (1998). Sox10 mutation disrupts neural crest development in Dom Hirschsprung mouse model. *Nat Genet* **18**, 60-4.

Spemann, H. and Mangold, H. (1924). On the induction of embryonic structures by implantation of organizers of different species. *Wilhelm Roux Arch Entw Mech* **100**, 599-638.

Starr, C. J., Kappler, J. A., Chan, D. K., Kollmar, R. and Hudspeth, A. J. (2004). Mutation of the zebrafish choroideremia gene encoding Rab escort protein 1 devastates hair cells. *Proc Natl Acad Sci U S A* **101**, 2572-7.

Stenmark, H. and Aasland, R. (1999). FYVE-finger proteins--effectors of an inositol lipid. *J Cell Sci* **112 (Pt 23)**, 4175-83.

Stenmark, H., Aasland, R., Toh, B. H. and D'Arrigo, A. (1996). Endosomal localization of the autoantigen EEA1 is mediated by a zinc-binding FYVE finger. *J Biol Chem* **271**, 24048-54.

Stenmark, H., Valencia, A., Martinez, O., Ullrich, O., Goud, B. and Zerial, M. (1994). Distinct structural elements of rab5 define its functional specificity. *Embo J* **13**, 575-83.

Stenmark, H., Vitale, G., Ullrich, O. and Zerial, M. (1995). Rabaptin-5 is a direct effector of the small GTPase Rab5 in endocytic membrane fusion. *Cell* **83**, 423-32.

Strigini, M. and Cohen, S. M. (2000). Wingless gradient formation in the Drosophila wing. *Curr Biol* **10**, 293-300.

Sun, Z., Jin, P., Tian, T., Gu, Y., Chen, Y. G. and Meng, A. (2006). Activation and roles of ALK4/ALK7-mediated maternal TGFbeta signals in zebrafish embryo. *Biochem Biophys Res Commun* **345**, 694-703.

Suzuki, A., Thies, R. S., Yamaji, N., Song, J. J., Wozney, J. M., Murakami, K. and Ueno, N. (1994). A truncated bone morphogenetic protein receptor affects dorsal-ventral patterning in the early Xenopus embryo. *Proc Natl Acad Sci U S A* **91**, 10255-9.

Suzuki, T., Miyamura, Y., Inagaki, K. and Tomita, Y. (2003). Characterization of the human RAB38 and RAB7 genes: exclusion of new major pathological loci for Japanese OCA. *J Dermatol Sci* **32**, 131-6.

Takei, K., McPherson, P. S., Schmid, S. L. and De Camilli, P. (1995). Tubular membrane invaginations coated by dynamin rings are induced by GTP-gamma S in nerve terminals. *Nature* **374**, 186-90.

Tall, G. G., Hama, H., DeWald, D. B. and Horazdovsky, B. F. (1999). The phosphatidylinositol 3-phosphate binding protein Vac1p interacts with a Rab GTPase and a Sec1p homologue to facilitate vesicle-mediated vacuolar protein sorting. *Mol Biol Cell* **10**, 1873-89.

Tao, Q., Yokota, C., Puck, H., Kofron, M., Birsoy, B., Yan, D., Asashima, M., Wylie, C. C., Lin, X. and Heasman, J. (2005). Maternal wnt11 activates the canonical wnt signaling pathway required for axis formation in Xenopus embryos. *Cell* **120**, 857-71.

Teleman, A. and Cohen, S. (2000). Dpp Gradient Formation in the Drosophila Wing Imaginal Disc. *Cell* **103**, 971-980.

ten Dijke, P., Yamashita, H., Ichijo, H., Franzen, P., Laiho, M., Miyazono, K. and Heldin, C. H. (1994). Characterization of type I receptors for transforming growth factor-beta and activin. *Science* **264**, 101-4.

TerBush, D. R., Maurice, T., Roth, D. and Novick, P. (1996). The Exocyst is a multiprotein complex required for exocytosis in Saccharomyces cerevisiae. *Embo J* **15**, 6483-94.

Thoma, N. H., Iakovenko, A., Goody, R. S. and Alexandrov, K. (2001a). Phosphoisoprenoids modulate association of Rab geranylgeranyltransferase with REP-1. *J Biol Chem* **276**, 48637-43.

Thoma, N. H., Iakovenko, A., Kalinin, A., Waldmann, H., Goody, R. S. and Alexandrov, K. (2001b). Allosteric regulation of substrate binding and product release in geranylgeranyltransferase type II. *Biochemistry* **40**, 268-74.

Thoma, N. H., Niculae, A., Goody, R. S. and Alexandrov, K. (2001c). Double prenylation by RabGGTase can proceed without dissociation of the mono-prenylated intermediate. *J Biol Chem* **276**, 48631-6.

Tickle, C., Summerbell, D. and Wolpert, L. (1975). Positional signalling and specification of digits in chick limb morphogenesis. *Nature* **254**, 199-202.

Tisdale, E. J., Bourne, J. R., Khosravi-Far, R., Der, C. J. and Balch, W. E. (1992). GTP-binding mutants of rab1 and rab2 are potent inhibitors of vesicular transport from the endoplasmic reticulum to the Golgi complex. *J Cell Biol* **119**, 749-61.

Topczewski, J., Sepich, D. S., Myers, D. C., Walker, C., Amores, A., Lele, Z., Hammerschmidt, M., Postlethwait, J. and Solnica-Krezel, L. (2001). The zebrafish glypican knypek controls cell polarity during gastrulation movements of convergent extension. *Dev Cell* **1**, 251-64.

Touchot, N., Chardin, P. and Tavitian, A. (1987). Four additional members of the ras gene superfamily isolated by an oligonucleotide strategy: molecular cloning of YPT-related cDNAs from a rat brain library. *Proc Natl Acad Sci U S A* **84**, 8210-4.

Trimble, W. S., Cowan, D. M. and Scheller, R. H. (1988). VAMP-1: a synaptic vesicle-associated integral membrane protein. *Proc Natl Acad Sci U S A* **85**, 4538-42.

Trinh, L. A., Meyer, D. and Stainier, D. Y. (2003). The Mix family homeodomain gene bonnie and clyde functions with other components of the Nodal signaling pathway to regulate neural patterning in zebrafish. *Development* **130**, 4989-98.

Trinkaus, J. P. (1963). The cellular basis of Fundulus epiboly. Adhesivity of blastula and gastrula cells in culture. *Dev Biol* **7**, 513-32.

Trinkaus, J. P. (1984). Mechanism of Fundulus epiboly - a current view. *Amer. Zool* **24**, 673-688.

Tsikolia, N. (2006). The role and limits of a gradient based explanation of morphogenesis: a theoretical consideration. *Int J Dev Biol* **50**, 333-40.

Tsukazaki, T., Chiang, T. A., Davison, A. F., Attisano, L. and Wrana, J. L. (1998). SARA, a FYVE domain protein that recruits Smad2 to the TGFbeta receptor. *Cell* **95**, 779-91.

Ullrich, O., Reinsch, S., Urbe, S., Zerial, M. and Parton, R. G. (1996). Rab11 regulates recycling through the pericentriolar recycling endosome. *J Cell Biol* **135**, 913-24.

Ulrich, F., Concha, M. L., Heid, P. J., Voss, E., Witzel, S., Roehl, H., Tada, M., Wilson, S. W., Adams, R. J., Soll, D. R. et al. (2003). Slb/Wnt11 controls hypoblast cell migration and morphogenesis at the onset of zebrafish gastrulation. *Development* **130**, 5375-84.

Ulrich, F., Krieg, M., Schotz, E. M., Link, V., Castanon, I., Schnabel, V., Taubenberger, A., Mueller, D., Puech, P. H. and Heisenberg, C. P. (2005). Wnt11 functions in gastrulation by controlling cell cohesion through Rab5c and E-cadherin. *Dev Cell* **9**, 555-64.

Vagner, S., Galy, B. and Pyronnet, S. (2001). Irresistible IRES. Attracting the translation machinery to internal ribosome entry sites. *EMBO Rep* **2**, 893-8.

Valencia, A., Chardin, P., Wittinghofer, A. and Sander, C. (1991). The ras protein family: evolutionary tree and role of conserved amino acids. *Biochemistry* **30**, 4637-48.

Verhoeven, K., De Jonghe, P., Coen, K., Verpoorten, N., Auer-Grumbach, M., Kwon, J. M., FitzPatrick, D., Schmedding, E., De Vriendt, E., Jacobs, A. et al. (2003). Mutations in the small GTP-ase late endosomal protein RAB7 cause Charcot-Marie-Tooth type 2B neuropathy. *Am J Hum Genet* **72**, 722-7.

Wagner, D. S., Dosch, R., Mintzer, K. A., Wiemelt, A. P. and Mullins, M. C. (2004). Maternal control of development at the midblastula transition and beyond: mutants from the zebrafish II. *Dev Cell* **6**, 781-90.

Wagner, D. S. and Mullins, M. C. (2002). Modulation of BMP activity in dorsal-ventral pattern formation by the chordin and ogon antagonists. *Dev Biol* **245**, 109-23.

Wallingford, J. B., Rowning, B. A., Vogeli, K. M., Rothbacher, U., Fraser, S. E. and Harland, R. M. (2000). Dishevelled controls cell polarity during Xenopus gastrulation. *Nature* **405**, 81-5.

Wang, W., Sacher, M. and Ferro-Novick, S. (2000). TRAPP stimulates guanine nucleotide exchange on Ypt1p. *J Cell Biol* **151**, 289-96.

Wang, Y., Ng, E. L. and Tang, B. L. (2006). Rab23: what exactly does it traffic? *Traffic* **7**, 746-50.

Warga, R. M. and Kimmel, C. B. (1990). Cell movements during epiboly and gastrulation in zebrafish. *Development* **108**, 569-80.

Weigmann, K. and Cohen, S. M. (1999). Lineage-tracing cells born in different domains along the PD axis of the developing Drosophila leg. *Development* **126**, 3823-30.

Wennerberg, K., Rossman, K. L. and Der, C. J. (2005). The Ras superfamily at a glance. *J Cell Sci* **118**, 843-6.

Westerfield, M. (2000). The zebrafish book. A guide for the laboratory use of zebrafish (Danio rerio). 4th ed., Univ. of Oregon Press, Eugene.

Whitman, M. (2001). Nodal Signaling in Early Vertabrate Embryos: Themes and Variations. *Developmental Call* **1**, 605-617.

Wichmann, H., Hengst, L. and Gallwitz, D. (1992). Endocytosis in yeast: evidence for the involvement of a small GTP-binding protein (Ypt7p). *Cell* **71**, 1131-42.

Wiederkehr, A., De Craene, J. O., Ferro-Novick, S. and Novick, P. (2004). Functional specialization within a vesicle tethering complex: bypass of a subset of exocyst deletion mutants by Sec1p or Sec4p. *J Cell Biol* **167**, 875-87.

Williams, P. H., Hagemann, A., Gonzalez-Gaitan, M. and Smith, J. C. (2004). Visualizing long-range movement of the morphogen Xnr2 in the Xenopus embryo. *Curr Biol* **14**, 1916-23.

Willot, V., Mathieu, J., Lu, Y., Schmid, B., Sidi, S., Yan, Y. L., Postlethwait, J. H., Mullins, M., Rosa, F. and Peyrieras, N. (2002). Cooperative action of ADMP- and BMP-mediated pathways in regulating cell fates in the zebrafish gastrula. *Dev Biol* **241**, 59-78.

Wilson, D. B. and Wilson, M. P. (1992). Identification and subcellular localization of human rab5b, a new member of the ras-related superfamily of GTPases. *J Clin Invest* **89**, 996-1005.

Wilson, S. M., Yip, R., Swing, D. A., O'Sullivan, T. N., Zhang, Y., Novak, E. K., Swank, R. T., Russell, L. B., Copeland, N. G. and Jenkins, N. A. (2000). A mutation in Rab27a causes the vesicle transport defects observed in ashen mice. *Proc Natl Acad Sci U S A* **97**, 7933-8.

Wolpert, L. (1996). One hundred years of positional information. *Trends Genet* **12**, 359-64.

Wu, S. K., Zeng, K., Wilson, I. A. and Balch, W. E. (1996). Structural insights into the function of the Rab GDI superfamily. *Trends Biochem Sci* **21**, 472-6.

Wu, X., Bowers, B., Rao, K., Wei, Q. and Hammer, J. A., 3rd. (1998). Visualization of melanosome dynamics within wild-type and dilute melanocytes suggests a paradigm for myosin V function In vivo. *J Cell Biol* **143**, 1899-918.

Wu, X., Bowers, B., Wei, Q., Kocher, B. and Hammer, J. A., 3rd. (1997). Myosin V associates with melanosomes in mouse melanocytes: evidence that myosin V is an organelle motor. *J Cell Sci* **110 (Pt 7)**, 847-59.

Wylie, C., Kofron, M., Payne, C., Anderson, R., Hosobuchi, M., Joseph, E. and Heasman, J. (1996). Maternal beta-catenin establishes a 'dorsal signal' in early Xenopus embryos. *Development* **122**, 2987-96.

Xu, X. Z., Wes, P. D., Chen, H., Li, H. S., Yu, M., Morgan, S., Liu, Y. and Montell, C. (1998). Retinal targets for calmodulin include proteins implicated in synaptic transmission. *J Biol Chem* **273**, 31297-307.

Yabe, T., Shimizu, T., Muraoka, O., Bae, Y. K., Hirata, T., Nojima, H., Kawakami, A., Hirano, T. and Hibi, M. (2003). Ogon/Secreted Frizzled functions as a negative feedback regulator of Bmp signaling. *Development* **130**, 2705-16.

Yang-Snyder, J., Miller, J. R., Brown, J. D., Lai, C. J. and Moon, R. T. (1996). A frizzled homolog functions in a vertebrate Wnt signaling pathway. *Curr Biol* **6**, 1302-6.

Yang, C. T., Sengelmann, R. D. and Johnson, S. L. (2004). Larval melanocyte regeneration following laser ablation in zebrafish. *J Invest Dermatol* **123**, 924-9.

Yisraeli, J. K. and Melton, D. A. (1988). The material mRNA Vg1 is correctly localized following injection into Xenopus oocytes. *Nature* **336**, 592-5.

Yucel, G. and Small, S. (2006). Morphogens: precise outputs from a variable gradient. *Curr Biol* **16**, R29-31.

Zalik, S. E., Lewandowski, E., Kam, Z. and Geiger, B. (1999). Cell adhesion and the actin cytoskeleton of the enveloping layer in the zebrafish embryo during epiboly. *Biochem Cell Biol* **77**, 527-42.

Zerial, M. and McBride, H. (2001). Rab Proteins as Membrane Organizers. *Nature Reviews Molecular Cell Biology* **2**, 107-119.

Zhang, J., Houston, D. W., King, M. L., Payne, C., Wylie, C. and Heasman, J. (1998). The role of maternal VegT in establishing the primary germ layers in Xenopus embryos. *Cell* **94**, 515-24.

Zhang, J. and King, M. L. (1996). Xenopus VegT RNA is localized to the vegetal cortex during oogenesis and encodes a novel T-box transcription factor involved in mesodermal patterning. *Development* **122**, 4119-29.

Zhang, Y., Chang, C., Gehling, D. J., Hemmati-Brivanlou, A. and Derynck, R. (2001). Regulation of Smad degradation and activity by Smurf2, an E3 ubiquitin ligase. *Proc Natl Acad Sci U S A* **98**, 974-9.

Zhang, Y., Musci, T. and Derynck, R. (1997). The tumor suppressor Smad4/DPC 4 as a central mediator of Smad function. *Curr Biol* **7**, 270-6.

Zhou, X., Sasaki, H., Lowe, L., Hogan, B. L. and Kuehn, M. R. (1993). Nodal is a novel TGF-beta-like gene expressed in the mouse node during gastrulation. *Nature* **361**, 543-7.